Surface tension effects in condensation heat transfer: Condensation on wire-wrapped tubes and Marangoni condensation of mixtures

A thesis submitted by

Takahiro Murase

in part fulfilment of the requirements for
the degree of

Doctor of Philosophy

in the
Department of Engineering
Queen Mary, University of London
Mile End Road
London, E1 4NS
UK

2006

Abstract

Enhancement of condensation heat transfer by wrapping of fine wires on a condenser tube and Marangoni condensation of binary mixtures have been studied.

For wire-wrapped tubes enhancement is due to modification of the profile of the condensate surface which leads to axially-directed pressure gradients and local thinning of the condensate film. Approximate theories do not agree well with limited available data prior to the present work.

A systematic experimental investigation has been conducted using three fluids with widely different properties. Five wire diameters and a range of winding pitch have been used. Maximum heat-transfer enhancement ratios of 3.7, 2.2 and 2.3 for R-113, ethylene glycol and steam respectively were obtained. The effect of inundation for steam condensation on wire-wrapped tubes has also been investigated.

Extensive data exist for Marangoni condensation of steam-ethanol mixtures on *small plane vertical surfaces*. Here the practically more relevant case of a *horizontal tube* has been studied. Apparent differences between the vertical plate and horizontal tube data are shown to be due to circumferential variation of tube surface temperature. Enhancement ratios up to around 3.7 have been obtained with as little as 0.05% mass fraction of ethanol in the boiler feed.

For wire-wrapped tube and Marangoni condensation, a copper condenser tube (outside diameter 12.2 mm) fitted with four embedded wall thermocouples was cooled internally by water using a wide range of flow rates. The coolant temperature rise was measured to within 0.01 K using a ten-junction thermopile while the coolant temperature rise ranges were 0.11 to 0.77 K, 0.89 to 9.28 K and 1.00 to 6.98 K for the wire-wrap tests with R-113, ethylene glycol and steam respectively and 1.24 to 29.1 K for Marangoni condensation. The effect on the boiler performance for water-ethanol mixtures has also been investigated.

Acknowledgement

I would like to express my greatest appreciation to Professor J.W. Rose for his supervision, detailed guidance and many helpful advices for my work, experiments and writing and, before everything else, giving me this special opportunity to study at Queen Mary. I also would like to give my special thanks to Dr. H.S. Wang and Dr. A. Briggs for many helps, discussions and advices.

I would like to express my special appreciation to Professor Y. Utaka in Yokohama National University for his generous advices and discussion, and especially for giving me this precious opportunity to study at Queen Mary. Thanks must also go to colleagues in Utaka Lab, in particular Dr. S. Wang for his helps for the Marangoni condensation investigation.

I would like to give my gratitude to Professor Crooks and Secretary of Department of Engineering, Mrs. J. Hefford for their kindness and many helps. I also greatly appreciate the technicians of the Mechanical Engineering Department, in particular to Mr. H. Gray and Mr. M. Collins for their kindness, and great jobs and wonderful ideas for the test apparatuses.

I extend my gratitude to colleagues at Queen Mary, Srinivas, Su and Satesh, friends in London, Bobby, Aran and Cherie and MARDI members in Japan for their friendship and encouragement. I also would like to express my thanks to all people who I met during this four years in London for their helps to the improvement of my English ability. In particular, I would like to say thanks to Wayne and Taishi as both best friends in London.

Finally, I would like to give my thanks to my family, 'Oyaji', Shouji and 'Ofukuro', Kimiko, younger brother and sisters, Yoshitake, Hisako and Tomoko for their financial support, greatest encouragement and warmest kindness in the world.

List of publications

Briggs, A., Wang, H.S., Murase, T. and Rose, J.W., 2003, Heat transfer measurements for condensation of steam on a horizontal wire-wrapped tube, *Journal of Enhanced Heat Transfer*, vol. 10, no. 4, pp. 355-362

Briggs, A., Wang, H.S., Murase, T. and Rose, J.W., 2003, Enhanced condensation of CFC113 on a horizontal wire-wrapped tube, *Proceedings of 4th Int. Conf. Compact Heat Exchangers and Enhancement Tech. for the Process Industries*, Crete Island, Greece, pp. 357-360

Murase, T., Briggs, A., Wang, H.S. and Rose, J.W., 2005, Condensation on a horizontal wire-wrapped tube, *6th World Conf. on Exp. Heat transfer, Fluid Mechanics, and Thermodynamics*, Matsushima, Miyagi, Japan.

Murase, T., Briggs, A., Wang, H.S. and Rose, J.W., 2005, Condensation on a horizontal wire-wrapped tube, *Transactions of the ASME Journal of Heat Transfer*, vol. 127, no. 11, pp. 1207-1213

Murase, T., Wang, H.S. and Rose, J.W., 2005, Marangoni condensation of steam-ethanol mixtures on a horizontal tube, *Transactions of the ASME Journal of Heat Transfer*, to be submitted

Murase, T., Wang, H.S. and Rose, J.W., 2005, Inundation effect on condensation on horizontal wire-wrapped tubes, *International Journal of Heat and Mass Transfer*, to be submitted

List of contents

Nomenclature

A	constant defined in Eq. (E-1)
A_1	defined in Eq. (2-21)
A_2	defined in Eq. (4-26)
A_{ts}	cross-sectional area of test chamber
a_1	constant defined in Eq. (4-34)
a_2	constant defined in Eq. (4-34)
a_3	constant defined in Eq. (4-34)
B	constant defined in Eqs. (2-8) and (4-22)
B^*	constant defined in Eqs. (2-7) and (4-21)
b	interfin space
C	ethanol mass fraction
C_g	mass fraction of non-condensing gases in test section
C_{iL}	initial ethanol liquid mass fraction as prepared at atmospheric (room) temperature
C_{iv}	corresponding value of ethanol vapour mass fraction to initial ethanol liquid mass fraction as prepared at atmospheric temperature under equilibrium relation
C_L	equilibrium ethanol liquid mass fraction
C_{loss}	constant defined in Eq. (4-14)
C_p	specific isobaric heat capacity of condensate or liquid
C_{pc}	specific isobaric heat capacity of coolant
C_v	equilibrium ethanol vapour mass fraction
d	outside diameter of tube
d_i	inside diameter of tube
$d_{i,sb}$	inside diameter of sheath for heater
d_{sb}	outside diameter of sheath for heater
d_{tc}	pitch diameter of embedded thermocouples in test condenser tube, or in sheath for heater
d_{tip}	diameter of finned tube at fin tip

d_{ts}	diameter of test chamber
d_w	wire diameter
E	thermo-e.m.f.
E_{Iin}	thermo-e.m.f. reading for electric current input to heater
E_{in}	thermo-e.m.f. reading using inlet thermocouple
E_m	defined in Eq. (4-7)
E_{Vin}	thermo-e.m.f. reading for voltage input to heater
F	defined in Eq. (2-5)
Gr_d	dimensionless parameter defined in Eq. (5-12)
g	specific force of gravity
H_1	level of liquid in chamber-side of manometer
H_2	level of liquid in atmosphere-side of manometer
h	fin height
h_{fg}	specific enthalpy of evaporation
I_{in}	actual electric current input to heater
K	experimentally determined constant defined in Eq. (2-26)
k	thermal conductivity of condensate or liquid
k_w	thermal conductivity of test tube
l	active heat-transfer length of test tube, i.e. length exposed externally to condensing vapour and internally to coolant
l_{sb}	active heat-transfer length of sheath for heater
N	number of tubes from the top in vertical column
Nu	average Nusselt number
Nu^*	dimensionless parameter defined in Eq. (5-11)
n	constant defined in Eq. (2-7)
$\tilde{M}_g$	molar mass of non-condensing gases
$\tilde{M}_{tf}$	molar mass of test fluid
m	constant defined in Eq. (2-43)
$\dot{m}_{cond}$	condensation rate
$\dot{m}_{cond,N}$	condensation rate for N^{th} tube in column
$\dot{m}_{inun}$	inundation rate

$\dot{m}_{\text{inun},N}$	inundation rate for N^{th} tube in column
$\dot{m}_{\text{v}}$	vapour mass flow rate approaching test tube
P	pressure in condensate film
P_{atm}	atmospheric pressure
P_{B}	reading of pressure by barometer
Pr	Prandtl number
P_{sat}	saturation pressure of test fluid
$P_{\text{sat}}(T_{\text{v}})$	saturation pressure of test fluid at T_{v}
P_{v}	vapour pressure in test section
p	wire pitch of winding
Q	total heat-transfer rate through test tube
Q_{b}	input power to boiler
Q_{in}	input power to heater
Q_{loss}	heat loss from apparatus between boiler inlet and test section, defined in Eq. (4-14)
Q_N	condensate heat-transfer rate of N^{th} tube from the top in column
q	heat flux, based on area of smooth tube with diameter equal to d
q^*	heat flux for boiling experiments, based on outside diameter of sheath for heater, d_{sb}
q_{Ma}	heat flux for Marangoni condensation
$q_{\text{Ro,wa}}$	heat flux calculated by Rose (1984) theory for water
q_{zero}	heat flux obtained without inundation
$\tilde{Re}$	two-phase Reynolds number, defined in Eq. (2-3)
R_i	resistance of i^{th} heater
r_{s}	radius of curvature of condensate surface
s	length of thin film between adjacent wires
s_{o}	distance of thin film along tube surface between adjacent turns of wire at the top of tube, defined in Eq. (2-34)
T	thermodynamic temperature
T^*_{inun}	inundation supply temperature
T_{atm}	ambient temperature
T_{B}	reading of temperature near barometer

$T_{c,in}$	inlet temperature of coolant to test tube
$T_{c,out}$	outlet temperature of coolant from test tube
T_{cond}	condensate temperature
T_L	liquid temperature
T_r	temperature of condensate returning to boiler
T_{ref}	reference temperature, defined in Eq. (4-23)
T_{ref}^*	reference temperature, defined in Eq. (5-14)
T_s	saturation temperature of test fluid
T_v	vapour temperature in test section
T_w	wall temperature
$T_{w,i}$	reading temperature measured by i^{th} thermocouple in test condenser tube, or in sheath for heater
T_w(lowest)	wall surface temperature measured by thermocouple embedded in tube at angular position of -157.5° measured from the top of tube
T_w(top)	estimated outside wall temperature at the top of tube
T_{wo}	average outside wall temperature
$T_{wo,i}$	outside wall surface temperature of test condenser tube, or sheath for heater, at angular position corresponding to i^{th} thermocouple
T_y	temperature distribution in condensate film at coordinate y
t	fin thickness
u_y	velocity of condensate flow at coordinate y
u_∞	free-stream vapour velocity
U_v	vapour velocity
$\dot{V}_c$	volume flow rate of coolant through test tube
V_i	potential difference across terminals of i^{th} heater
V_{in}	actual voltage input to heater
x	linear dimension along liquid-vapour interface
$\tilde{x}$	ethanol liquid mole fraction
y	coordinate in outward normal direction measured from tube surface
z	coordinate in direction of tube axis measured from mid-point between wires, or defined in Eq. (2-31)
z_o	value of dimensionless film thickness at the top of tube, defined in Eq. (2-32)

Greek letters

α	average vapour-side, heat-transfer coefficient, (q / (T_v - T_{wo}))
α_f	average vapour-side, heat-transfer coefficient in flooded region
α_N	heat-transfer coefficient of N^{th} tube from the top in column
$\bar{\alpha}_N$	arithmetic average of heat-transfer coefficients for each tube in column of N tubes
α_{top}	average vapour-side, heat-transfer coefficient of the top tube in vertical column (without inundation)
α_{zero}	average vapour-side, heat-transfer coefficient obtained without inundation
α_u	average vapour-side, heat-transfer coefficient in unflooded region
β	fin tip half-angle
γ	volume coefficient of expansion
ΔE	thermo-e.m.f. reading using ten-junction thermopile
$\Delta E_{friction}$	thermo-e.m.f. reading using ten-junction thermopile due to dissipate temperature rise of coolant in test tube and mixing chambers, defined in Eq. (C-1)
ΔT	vapour-to-surface temperature difference, ($T_v - T_{wo}$)
ΔT^*	liquid-to-surface temperature difference, ($T_{wo} - T_L$)
ΔT_c	coolant temperature rise due to condensation
ΔT_p	equilibrium temperature difference between vapour and liquid lines at the same vapour composition
ΔT_{top}	vapour-to-surface temperature difference at the top of tube
δ	condensate film thickness
ε_{Ma}	enhancement ratio for Marangoni condensation, i.e. ratio of heat flux or vapour-side, heat-transfer coefficient for steam-ethanol mixtures divided by the same quantity for pure steam at the same vapour-to-surface temperature difference
ε_q	enhancement ratio, i.e. ratio of vapour-side, heat-transfer coefficient or vapour-to-surface temperature difference for enhanced tube divided by the same quantity for smooth tube at the same heat flux

$\varepsilon_{\Delta T}$	enhancement ratio, i.e. ratio of heat flux or vapour-side, heat-transfer coefficient for enhanced tube divided by the same quantity for smooth tube at the same vapour-to-surface temperature difference
λ	defined in Eq. (C-1)
μ	dynamic viscosity of condensate or liquid
ρ	density of condensate or liquid
ρ_c	density of coolant
ρ_{tf}	density of test fluid
ρ_v	density of vapour
σ	surface tension
ϕ	angle measured from the top of tube
ϕ_f	condensate retention angle / flooding angle measured from the top of horizontal finned tube

Subscripts

0	top of tube
c	coolant
fin	finned tube
g	non-condensing gas
L	liquid
Ma	Marangoni condensation
Nu	Nusselt (1916) theory
Ro	Rose (1984) theory
sb	sheath for boiling experiments
smooth	smooth tube
tc	thermocouple
top	top tube in vertical column
v	vapour
wa	water
wire	wire-wrapped tube
zero	without inundation

List of figures

Chapter 2 Page

Appendixes Page

List of tables

Chapter 5

Appendix

Chapter 1
Introduction

1.1 Condensation on wire-wrapped tubes

To improve the heat-transfer performance of condensers consisting of smooth tubes, wrapping the tubes with fine wires is a simple and cheap technique. Several earlier workers have investigated condensation heat transfer on such tubes and strived to make theoretical models. However, the phenomenon is yet to be well understood due to a small number of experimental data and incomplete theoretical investigations; the latter is due to the complexity of the three-dimensional flow of the condensate film affected by surface tension and condensate surface curvature.

For a single, horizontal, wire-wrapped tube, a few heat-transfer measurements were made for condensation of R-11 and ethanol by Fujii et al. (1985) and for steam by Sethumadhavan and Rao (1985) and Marto et al. (1987). In these experiments, wire diameter and pitch of winding were varied and optimum combination of those was seemed to exist for each fluid. Neither available theoretical approaches by Fujii et al. (1985) nor Rose (2002) is in wholly satisfactory agreement with these experimental data.

A few investigations have been conducted to study the effect of inundation (condensate from high tubes in a tube bank falling on lower tubes) on wire-wrapped tubes. These indicated that the effect of condensate inundation on wire-wrapped tubes is less significant than that for smooth tubes due to the fact that the wires, in the same way as fins, prevent lateral spreading of condensate along the tube so that the space between columns of falling condensate is not affected and these parts of lower tubes behave like the top tube. However, the report by Brower (1985) and Marto (1986) that the performance of wire-wrapped tubes is less degraded by inundation than low integral-finned tubes during steam condensation is unexplained.

New accurate experimental data are of vital importance to the development of a successful model. In the present investigation, experiments have been conducted for

condensation on a wire-wrapped tube with three different fluids, R-113, ethylene glycol and steam to cover a wider range of fluid properties, especially surface tension. The copper test condenser tube had an outside diameter of 12.2 mm and was fitted with four embedded wall thermocouples enabling direct measurement for wall temperatures. Steel wires having diameters of 0.2, 0.35, 0.4, 0.75 and 1.0 mm were wound on the outside surface of the test tube with pitches of the winding ranging from values a little larger than the wire diameter in each wire diameter up to 6.0 mm. The cooling water temperature rise, from which the heat-transfer rate to the test tube was calculated, was measured using a ten-junction thermopile. Care was taken to ensure adequate mixing and isothermal immersion of the leads in the vicinity of the junctions of thermocouples. The heat flux was found from the coolant flow rate and the coolant water temperature rise. A small predetermined correction for the dissipative temperature rise of the cooling water in the tube and mixing boxes was incorporated in the calculation of the heat-transfer rate. The surface temperature was taken as the arithmetic average of the temperatures indicated by the embedded thermocouples with a small correction for the depth of the thermocouples below the condensing surface.

Experiments have also been conducted to study the effect of condensate inundation during condensation of steam on smooth, wire-wrapped and finned tubes to judge the credibility of the report of Brower (1985) and Marto (1986). The same copper condenser tube was used. A wire having a wire diameter of 1.6 mm with pitches from 4 to 16 mm was tested. The integral-finned tube had an outside diameter at fin root of 12.7 mm with a fin thickness, fin height and interfin space of 0.5, 1.59 and 1.5 mm respectively. Care was also taken to correctly set and control of artificial inundation liquid temperature and to avoid the presence of air in the test section.

1.2 Marangoni condensation of steam-ethanol mixtures

Another means of achieving enhanced heat-transfer performance for condensation may also be obtained in some cases by adding a small amount of second fluid. In general, the condensation heat-transfer coefficient of vapour mixtures is smaller than that of a pure or single-constituent fluid. Degradation of the heat-transfer coefficient due to species diffusion in the vapour phase is considerable resulting in increase in size of heat exchangers.

Adding a small amount of ethanol to water, however, has been found to give significant enhancement of condensation heat transfer because this combination can lead a pseudo-dropwise condensation mode of a condensate film. This can occur when the more volatile constituent has the lower surface tension. The explanation for this behaviour, given by Hijikata et al. (1996), lies in the fact that in these circumstances the condensate film is potentially unstable. The valley of the condensate film has lower surface temperature (nearer to the surface temperature), which, assuming equilibrium at the interface, gives higher ethanol mass fraction in the liquid. The crest has higher surface temperature (nearer to vapour temperature), which gives lower ethanol mass fraction and hence higher water mass fraction (see equilibrium diagram, Fig. 2.22). Because water has the higher surface tension this generates a gradient of the surface tension towards the crest and the film thickness in the valley becomes even thinner. This mode of condensation of mixtures such as steam-ethanol, is called Marangoni condensation. Very thin condensate film regions cause reduction of vapour-side, heat-transfer resistance.

Several workers made efforts to clarify Marangoni condensation of steam-ethanol mixtures, e.g. Fujii et al. (1989, 1993) for a horizontal tube, Hashimoto et al. (1994) for a vertical tube and Hijikata et al. (1996) for a horizontal flat plate. These experiments were conducted with the full range of ethanol mass fractions, indicating that the appearances of the condensate film was dependent on ethanol mass fraction and condensation heat transfer differs from that for pure steam. Some heat-transfer enhancements were reported.

Utaka and co-workers have more recently found that the heat-transfer

enhancement and the appearance of the condensate film for Marangoni condensation on a short vertical heat-transfer surface was not only dependent on the mixture composition but also vapour-to-surface temperature difference, vapour velocity and distance from the top on a condensing surface. Marangoni condensation was also found to be very sensitive to the presence in the vapour of non-condensing gas.

The present investigation provides new data for Marangoni condensation on a horizontal smooth tube. The same apparatus was used and the same procedures were followed as for the wire-wrapped tube investigation. By varying coolant flow rates, various vapour-to-surface temperature differences from 2 to 50 K were obtained and data, in the form of heat flux, vapour-to-surface temperature difference and heat-transfer coefficient were obtained. Referring to experimental data of Utaka and co-workers, ethanol concentrations in water were 0.05%, 0.1%, 0.5% and 1.0% by mass fraction as prepared at atmospheric temperature. Also by adjusting the boiler heater powers, the vapour velocity over the condenser tube was varied from 0.15 to 0.75 m/s.

Interesting as the phenomenon of Marangoni condensation of steam-ethanol binary mixture may be, it remains at present largely of academic interest although possible applications have been cited, for even power generation. In the last case, boiling of water-ethanol binary mixtures requires investigation. It is known that boiling heat-transfer coefficients for binary mixtures are lower than those of pure components due to the mass-transfer resistance in the vicinity of the heat-transfer surface. A few experiments have been conducted for nucleate boiling of water-ethanol mixtures in the past. No experimental data using low ethanol liquid mass fractions, i.e. less than 1%, which gives the high condensation heat transfer, has been found in the literature. Therefore, new data for nucleate boiling of water-ethanol mixtures with the low ethanol liquid mass fractions has also been obtained in the present investigation.

Chapter 2
Literature survey

2.1 Introduction

The following survey gives an overview of the current state of knowledge for two condensation phenomena, primarily for condensation on wire-wrapped tubes and also for Marangoni or pseudo-dropwise condensation, which can occur with certain binary mixtures, such as steam-ethanol and steam-ammonia. Before discussing condensation heat transfer on wire-wrapped tubes, the related topic of condensation on low integral-finned tubes is first surveyed. The possibility that water-ethanol mixtures could be used to enhance the performance of power plant condensers draws attention to the effects of such mixtures on the boiling process and brief consideration of this topic is also included.

The present survey consists of four sections: condensation on low integral-finned tubes, condensation on wire-wrapped tubes, Marangoni condensation of mixtures (primarily steam-ethanol mixtures) and boiling of water-ethanol mixtures. Before surveying above topics, fundamental theories for condensation on a horizontal tube are briefly outlined.

Theory of film condensation on a horizontal tube

The starting point and comparison reference for all condensation investigations is the well-established and well-verified theory of Nusselt (1916) for laminar film condensation on smooth isothermal surfaces. The key approximations, now well verified by more elaborate numerical studies made possible by the advent of computers, are that inertia and convection terms are small in the equations of conservation of momentum and energy in the condensate film. The Nusselt result for a horizontal condenser tube may be expressed:

$$Nu = 0.728\left\{\frac{\rho(\rho-\rho_v)gh_{fg}d^3}{\mu k\Delta T}\right\}^{1/4} \tag{2-1}$$

where Nu is the average Nusselt number, ρ and ρ_v are the densities of condensate and vapour respectively, g is the specific force of gravity, h_{fg} is the specific enthalpy of evaporation, d is the outside diameter of the condenser tube, μ is the viscosity of condensate, k is the thermal conductivity of condensate and ΔT is the vapour-to-surface temperature difference.

With the simplification of adopting the infinite condensation rate asymptotic expression for the condensate surface shear stress, Shekriladze and Gomelauri (1966) theoretically analyzed the problem of condensation of a vapour flowing normal to a horizontal smooth tube while neglecting the pressure gradient in the momentum balance and assuming potential flow outside the vapour boundary layer around the tube; these simplifications avoid the problem of vapour boundary layer separation. At high condensation rates, when gravity was omitted, the average Nusselt number was expressed:

$$Nu\tilde{R}e^{-1/2} = 0.9 \tag{2-2}$$

where

$$\tilde{R}e = \frac{u_\infty \rho d}{\mu} \tag{2-3}$$

is the two-phase Reynolds number and u_∞ is the free-stream vapour velocity. To include the effect of gravity, Shekriladze and Gomelauri (1966) proposed a simple interpolation formula, which approximately satisfies Eq. (2-2) at high vapour velocity and Eq. (2-1) at low vapour velocity:

$$Nu\tilde{R}e^{-1/2} = 0.644\left\{1+\left(1+1.69F\right)^{1/2}\right\}^{1/2} \tag{2-4}$$

where

$$F = \frac{\mu h_{fg} g d}{k \Delta T u_\infty^2} \tag{2-5}$$

The largest error in $Nu\tilde{R}e^{-1/2}$ predicted by Eq. (2-4) when compared with the numerical solutions was 2%.

Rose (1984) later showed that the numerical solutions of Shekriladze and Gomelauri (1966) could be more accurately represented by:

$$Nu\tilde{R}e^{-1/2} = \frac{0.9 + 0.728F^{1/2}}{\left(1 + 3.44F^{1/2} + F\right)^{1/4}} \tag{2-6}$$

which satisfies the zero and infinite velocity asymptotes ($F \rightarrow \infty$, $F \rightarrow 0$) and gives values of $Nu\tilde{R}e^{-1/2}$ within 0.4% of the numerically obtained values for all F.

2.2 Condensation on low integral-finned tubes

2.2.1 Introduction

This section describes experimental and theoretical investigations concerning condensation heat transfer on low integral-finned tubes. This topic has been studied much more intensively than the closely related problem of condensation on wire-wrapped tubes and provides general background to the phenomena involved. The survey is divided into three parts: experimental investigations on vapour-side, heat-transfer performance; studies of condensate retention between fins and at the fin roots; and theoretical models to predict the heat-transfer performance.

The presence of fins on a condenser tube affects condensation heat transfer in three ways: firstly the fins provide additional heat-transfer surface as in single phase heat transfer; secondly a surface tension-induced pressure gradient in the condensate film assists drainage from parts of the surface and thereby enhances the heat transfer by reducing the condensate film thickness; and lastly condensate retention between fins at the lower part of the condenser tube due to surface tension leads to deterioration of heat transfer. The term 'low integral-finned' is used to indicate that the fin height is small in comparison with the tube diameter. For refrigerants, heat-transfer enhancement ratios (i.e. ratio of heat flux or heat-transfer coefficient for a low integral-finned tube, based on a smooth-tube area of fin root diameter, to the corresponding value for a smooth tube at the same vapour-to-surface temperature difference, $\varepsilon_{\Delta T}$) of around 8 and higher have been measured. The presence of fins on the surface of a condenser tube leads to sharp changes in condensate surface curvature, especially near the tip and root of a fin. This, together with the tubes own curvature, introduces considerable theoretical complexity through the appearance of a surface curvature term in the momentum balance equation for the condensate film.

Experimental and theoretical investigations over the past twenty years or so have led to good understanding of condensation heat transfer on horizontal low integral-finned tubes.

2.2.2 Experimental investigations

A large number of experimental investigations have been conducted. Earlier experimental investigations include Beatty and Katz (1948), Karkhu and Borokhov (1971), Mills et al. (1975) and Carnavos (1980). Experimental accuracy in some cases is questionable but the investigations suggest that integral-finned tubes give good enhancement in comparison with a smooth tube. Recent studies are chronologically summarized in Table 2.1.

Earlier methods used to evaluate the vapour-side, heat-transfer coefficient were by means of subtraction of a predetermined coolant-side resistance and a tube wall thermal resistance from measured overall resistance and 'modified Wilson plots'. Recently, more accurate results, described in more detail below, have been obtained by measurement of the temperature of the tube surface using embedded thermocouples. Fin height, h, fin thickness, t, interfin space, b and fin shape have been systematically varied using several fluids with widely different properties. Masuda and Rose (1985, 1988), Wanniarachchi et al. (1986), Briggs et al. (1992) have shown that vapour-side, heat-transfer enhancement ratios of 2 to 3 can be obtained for steam and around 7 to 9 for refrigerants. Higher enhancement ratios were obtained with lower surface tension fluids and there was an optimum interfin space which depends strongly on fluid properties, notably surface tension, and more weakly on the other geometric variables. Dependence on thermal conductivity of a condenser tube material has also been investigated for tubes of copper, brass, bronze, aluminium, copper-nickel and stainless steal by Briggs et al. (1995) and Das et al. (1995). As anticipated copper tubes, with fin efficiency near unity, gave the highest enhancement ratio.

The effect of vapour approach velocity for forced-convection condensation has also been studied by Michael et al. (1989), Bella et al. (1993), Cavallini et al. (1995), Namasivayam and Briggs (2004a, 2004b). The fluids used were steam, R-11, R-113 and ethylene glycol. It was found that the heat transfer increased with increasing vapour velocity and the relative effect of vapour velocity for low integral-finned tubes was less than for smooth tubes. The effect of vapour velocity on the very thin film on the fin surface and interfin tube space due to surface tension generated

pressure gradients is much less than that on the relatively thick film on a smooth tube.

Relation between heat flux and vapour-to-surface temperature difference

It was found by Yau et al. (1985) that their results for steam condensation on low integral-finned tubes were closely fitted by the following equation:

$$q = B^* \Delta T^n \tag{2-7}$$

where q is the heat flux and B^* and n are constants found from experimental data. Values of n of between 0.64 and 0.86 were found for the tubes tested in Yau et al. (1985), but the data could generally be satisfactory represented with n forced to 0.75 (as in the Nusselt (1916) theory for smooth tubes) in all cases.

Subsequently, Masuda and Rose (1985) found that for ethylene glycol it was necessary to take account of fluid property variation, especially viscosity, using the following Nusselt (1916) type equation:

$$q = B\left\{\frac{\rho(\rho-\rho_v)gh_{fg}k^3}{\mu d}\right\}^{1/4} \Delta T^{3/4} \tag{2-8}$$

where B is the constant found from the experimental data. Masuda and Rose (1988) showed that Eq. (2-8) represented experimental data of steam, R-113 and ethylene glycol for both smooth and finned tubes very well. The fact that both smooth and finned tube data are represented by Eq. (2-8) has the advantage, as discussed below, that the enhancement ratio is essentially independent of ΔT and q.

Heat-transfer enhancement ratio

It is convenient to express the performance of low integral-finned tubes using an enhancement ratio defined as the vapour-side, heat-transfer coefficient or heat flux on a low integral-finned tube divided by that for a smooth tube at the same vapour-

to-surface temperature difference, both based on the smooth-tube area. From Eq. (2-8) the enhancement ratio is given by:

$$\varepsilon_{\Delta T} = \frac{\text{(low integral-finned tube)}}{\text{(smooth tube)}} = \left(\frac{\alpha_{\text{fin}}}{\alpha_{\text{smooth}}}\right)_{\Delta T} = \left(\frac{q_{\text{fin}}}{q_{\text{smooth}}}\right)_{\Delta T} = \frac{B_{\text{fin}}}{B_{\text{smooth}}} \tag{2-9}$$

The fact that the dependence of q on ΔT is the same for the smooth and finned tubes means that $\varepsilon_{\Delta T}$ does not depend on ΔT.

In the same manner, an enhancement ratio at the same heat flux is given by:

$$\varepsilon_q = \frac{\text{(low integral-finned tube)}}{\text{(smooth tube)}} = \left(\frac{\alpha_{\text{fin}}}{\alpha_{\text{smooth}}}\right)_q = \left(\frac{\Delta T_{\text{smooth}}}{\Delta T_{\text{fin}}}\right)_q \tag{2-10}$$

where ε_q does not depend on q. It follows that

$$\varepsilon_{\Delta T} = \left(\varepsilon_q\right)^{3/4} \tag{2-11}$$

2.2.3 Theoretical investigations

A number of theoretical approaches to predict condensation heat transfer on horizontal integral-finned tubes have been conducted. The important condensate drainage mechanisms are gravity, surface tension and vapour shear, the last being small for low vapour velocity.

The important effect of surface tension, neglected in the earliest approach of Beaty and Katz (1948), has been taken into account in more recent analyses. Surface tension causes a pressure gradient in the condensate film which draws condensate to the centre of the fin tips and to the fin roots resulting in thinner condensate film near the corner of the fin tips and in the interfin spaces near the fin roots at the upper part

of a condenser tube. The capillary effect also leads to condensate retention between fins at the lower part of the tube. Thus, surface tension has both beneficial and detrimental effects on heat transfer, both of which also have relevance to condensation on wire-wrapped tubes.

Condensate retention on horizontal finned tubes

In the same way that it is drawn up a capillary tube liquid is held between fins when a horizontal finned tube is wetted or the lower part is immersed in liquid. This is due to the pressure drop across the curved meniscus at the liquid surface which is balanced by the gravity force across the supported liquid column. This phenomenon is known as liquid 'retention', 'hold up', or 'flooding'. Earlier studies, for instance Katz et al. (1946), Taborek (1974), Rudy and Webb (1981), found the following results: firstly the entire interfin spaces around the tube could be filled with liquid in some circumstances; secondly the retention was strongly dependent on σ/ρ, i.e. a ratio of liquid surface tension to liquid density and h/b, i.e. a ratio of fin height to interfin space; and lastly the so-called 'retention' angle, i.e. an angle, measured from the top of the tube to the position, at which the whole of the interfin spaces is completely filled with liquid ('flooded'), was observed to be almost the same for both static (without condensation) and dynamic (with condensation) measurements.

The first detailed analysis for this problem was by Honda et al. (1983), who gave an expression for the retention angle, ϕ_f, for a trapezoidal-section low-finned tube by applying a force balance between gravity and surface tension acting on a liquid interface with approximations for the meniscus profile and radius of curvature of the interface. Honda et al. (1983) obtained

$$\phi_f = \cos^{-1}\left(\frac{4\sigma\cos\beta}{\rho g b d_{tip}} - 1\right) \qquad (2\text{-}12)$$

where d_{tip} is the tube diameter at the fin tip, β is the fin tip half-angle and b is the interfin space at the fin tip. Eq. (2-12) is valid when

$$h \geq \frac{b(1-\sin\beta)}{2\cos\beta} \tag{2-13}$$

and when

$$\frac{\sigma\cos\beta}{\rho g b d_{tip}} > 0.5 \tag{2-14}$$

the interfin space is fully flooded ($\phi_f = 0$).

In the case for rectangular-section fins $\beta = 0$ so that

$$\phi_f = \cos^{-1}\left(\frac{4\sigma}{\rho g b d_{tip}} - 1\right) \tag{2-15}$$

which is valid when

$$h \geq \frac{b}{2} \tag{2-16}$$

Essentially the same result as Eq. (2-15) has also been obtained independently by Owen et al. (1983) and Rudy and Webb (1985). The predictions have been well verified experimentally by several investigators, e.g. Katz et al. (1946), Rudy and Webb (1981), Yau et al. (1985).

Masuda and Rose (1987) gave the most thorough treatment of the condensate retention problem which included capillary retained liquid at the fin roots over the whole tube surface. Masuda and Rose (1987) showed that the condensate was not only retained on the lower part of the tube surface, i.e. 'flooded' area, but also on part of the upper surface previously regarded as 'unflooded'. This took the form of a 'wedge' between the fins in the interfin spaces as shown in Fig. 2.1(a). Figs. 2.1(b) and 2.1(c) which show radial sections of the liquid profiles between fins at various circumferential positions, compare the behaviour with closely spaced fins ($b < 2h$, Fig. 2.1(b)) to widely spaced fins ($b > 2h$, Fig. 2.1(c)).

Prediction of condensation heat transfer on low integral-finned tubes

The earliest theoretical investigation of condensation heat transfer on low integral-finned tubes was by Beatty and Katz (1948), who ignored the effect of surface tension. Their model treated both the fin flanks and the cylindrical interfin spaces using the Nusselt (1916) approach with condensate flow on the vertical and cylindrical surfaces controlled by gravity and viscosity. Despite the neglect of the effect of surface tension, their model was in good agreement with their experimental data for a low fin-density tube when using low surface tension fluids. This may now be seen to be fortuitous and due to the two opposing effects of surface tension approximately cancelling each other in this case.

When considering condensation on a vertical fluted tube Gregorig (1954) drew attention to the pressure gradient resulting from surface tension in the presence of condensate surface curvature, which for the two-dimensional case gives:

$$\frac{dP}{dx} = \sigma \frac{d(1/r_s)}{dx} \qquad (2\text{-}17)$$

where P is the pressure in the condensate film, r_s is the radius of curvature of a condensate surface and x is the linear dimension along the liquid-vapour interface. For finned tubes, this effect causes flow away from or toward the positions of highest curvature i.e. the fin tip and root respectively.

Honda and Nozu (1987) have given the most complete solution for this problem. The key feature of their analysis was the inclusion of the pressure gradient term, resulting from surface tension in the presence of surface curvature, in the momentum balance equations for the condensate film. The effect of condensate retention was also taken into account. Comparisons of the predictions of their model with experimental data with various test fluids showed agreement in most cases within $\pm$ 20%.

Rose (1994) used a semi-empirical approach utilising dimensional analysis and incorporated the essential mechanisms of the Honda and Nozu (1987) approach.

This resulted in an algebraic expression for the enhancement ratio in good agreement with the Honda and Nozu (1987) solution and with experimental data. Data for steam condensing on brass and bronze tubes, however, had less good agreement with the model, suggesting that 'fin efficiency' may be important for condensation on low-thermal-conductivity tubes. Briggs and Rose (1994) went on to modify the model of Rose (1994) by including the effect of conduction in the fins. With this correction, the data for steam condensing on the brass and bronze tubes were in better agreement without significantly affecting the results of the other (copper tube) data.

2.2.4 Conclusion

Condensation heat transfer on low integral-finned tubes is affected by several parameters, namely fin geometry (fin height, fin thickness, interfin space and shape) and tube material, fluid properties and vapour velocity. A sufficient number of reliable experimental data have been obtained, indicating enhancement ratios up to around 9 for lower surface tension fluids and optimum fin geometry. Several theoretical investigations have also been carried out. The condensate retention angle is well predicted by the investigations such as those of Honda et al. (1983) and Masuda and Rose (1987). Detailed analyses by Honda and Nozu (1987) and Rose (1994) have given good theoretical predictions for the heat transfer.

2.3 Condensation on wire-wrapped tubes

2.3.1 Introduction

This section describes experimental and theoretical investigations concerning condensation heat transfer on wire-wrapped tubes. The survey is divided into two parts: investigations for single wire-wrapped tubes and condensate inundation effect on horizontal wire-wrapped tubes. The first section deals with experimental investigations for vapour-side, heat-transfer performance and theoretical models to predict the heat-transfer performance. In the second section, studies for condensate inundation on smooth and low integral-finned tubes are first briefed, followed by investigations for inundation on wire-wrapped tubes paying attention to treatment of artificial inundation liquid in simulated inundation experiments.

2.3.2 Single wire-wrapped tubes

(1) Introduction

The wire wrap does not act in precisely the same way as fins and the wire need not have high thermal conductivity due to negligible contact area between the wire and the tube, which is essentially along a line. Enhancement is due only to thinning of the film between adjacent turns of the wire caused by the surface tension induced pressure gradient in the condensate film. The pressure gradient results from the fact that the interface curvature is higher nearer the wire and causes axial flow of condensate towards the wire. Several earlier workers have investigated this simple and cheap method of enhancing condensation heat transfer. However, the number of experimental investigations is few, mainly by Fujii et al. (1985) with R-11 and ethanol, Sethumadhavan and Rao (1985) and Marto et al. (1987) with steam. Theoretical investigations have also been attempted by Fujii et al. (1985), Marto et al. (1987) and Rose (2002).

(2) Experimental investigations

Thomas (1967) found that loosely attached vertical wires on a vertical condenser tube gave enhancement for steam condensation. An aluminium condenser tube of an outside diameter of 12.7 mm and a length of 1079.5 mm, and wires made of either stainless steel or aluminium, having diameters of 0.79 mm and 1.57 mm were used. The wires were stretched along the tube parallel to the axis and spot-welded at both ends and the number of the wires was varied from 3 to 12. One spirally wire-wrapped tube with four wires having pitch of 101.6 mm for each wire was also tested. It was not clearly stated which wire was used for each tube. The Wilson plot method was employed to obtain vapour-side, heat-transfer coefficients. Enhancement ratios (not clearly defined) of up to 4.5 were reported for the vertical tube with 8 wires, while around 2.4 was reported for the wire-wrapped tube at a heat flux of about 60 kW/m^2.

In performance tests on a compact heat exchanger for Ocean Thermal Energy Conversion (OTEC) application, Thomas et al. (1977) reported data for condensation of ammonia on an internally enhanced (axial fins) externally wire-wrapped tube. Based on the Wilson plot calculation Thomas et al. (1977) reported that the vapour-side, heat-transfer coefficient was around twice the value predicted by the Nusselt (1916) theory for a smooth tube. It was not clear which parameter was the same for the two cases e.g. temperature difference, heat flux, coolant-side flow rate. Thomas et al. (1977) acknowledged that their Wilson plot calculation was susceptible to large error.

Rifert et al. (1984) performed experiments for ammonia condensation on a horizontal wire-wrapped steel tube at a vapour pressure of around 1 MPa (vapour temperature at 26 C^o). The tube had an outside diameter of 10 mm and 1.5 mm diameter steel wire was spirally welded to the outside surface of the tube with pitches of 4, 8 and 16 mm. Data were obtained at vapour velocities between 0.02 and 0.03 m/s and heat fluxes between 5 and 50 kW/m^2. Vapour-side, heat-transfer coefficients were obtained by subtracting a predetermined coolant-side resistance from measured overall resistance. It was found the wire wrap enhanced heat transfer by up to 100%. A pitch of 8 mm gave the highest enhancement while

smaller enhancements were reported for pitches of 4 and 16 mm.

Fujii et al. (1985) conducted experiments for film condensation on a horizontal wire-wrapped tube using R-11 and ethanol. The tests were conducted at low vapour velocity. The horizontal copper test tube had an outside diameter of 18 mm and an active heat-transfer length of 385 mm. Data were obtained for a wire diameter of 0.3 mm with wire pitches of 0.5, 1.0 and 2.0 mm for R-11, and wire diameters of 0.1, 0.2 and 0.3 mm with a wire pitch of 1.0 mm (the material and method of attachment were not given). Volume averaged temperature of the test tube was measured by means of the variation of the electrical resistance. The enhancement ratio was defined as the ratio of the Nusselt number for a wire-wrapped tube to that for a smooth tube, the latter was obtained using Eq. (2-1). The enhancement ratio was essentially independent of vapour-to-surface temperature difference. Figs. 2.2(a) and 2.2(b) show plots of enhancement ratio against wire pitch-to-diameter ratio for R-11 and ethanol respectively. For condensation of R-11 at the fixed wire diameter, the smallest pitch gave the highest enhancement ratio. For condensation of ethanol at the fixed pitch, the largest wire diameter gave the highest heat transfer. For both fluids, maximum enhancement ratios were obtained using a wire diameter of 0.3 mm with a pitch of 0.5 mm. Fujii et al. (1985) concluded that the optimum wire pitch-to-diameter ratio was around 2 for both fluids. The highest enhancement ratios measured were approximately 3.4 and 2.8 for R-11 and ethanol respectively.

Marto et al. (1987) performed experiments for steam at atmospheric pressure and under vacuum conditions (absolute pressure ~85 mmHg) with vapour velocities of 1 and 2 m/s respectively. The test tube had an outside diameter of 19 mm and an active heat-transfer length of 133.4 mm. Three different wire diameters of 0.5, 1.0 and 1.6 mm were used and for each wire diameter, three different nominal spacings of 1, 2 and 3 mm were used (the corresponding pitches are the spacing plus the wire diameter). Overall heat-transfer rates were calculated using an energy balance for the coolant through the test tube, from which vapour-side, heat-transfer coefficients were obtained using the modified Wilson plot method. Heat-transfer coefficients for the smooth tube lay about 30% above the Nusselt (1916) prediction due to the downward vapour velocity. Fig. 2.3 shows the enhancement ratio at the same vapour-to-surface temperature difference, plotted against the wire pitch-to-diameter

ratio. It was not clearly stated but presumably the enhancement ratio was defined as a ratio of heat-transfer coefficient for the wire-wrapped tube to that for the smooth tube at the same vapour-to-surface temperature difference. For both pressures, the enhancement ratio increased with increasing wire pitch-to-diameter ratio to a maximum of 1.8 for a wire diameter of 0.5 mm with a pitch of 3.6 mm at atmospheric pressure. Lower values were obtained under vacuum conditions. The optimum wire pitch-to-diameter ratio was found to be between 5 and 7.

Sethumadhavan and Rao (1985) investigated condensation of steam on a horizontal wire-wrapped tube at atmospheric pressure. Copper wires of three different diameters 0.71, 1.5 and 3.0 mm with relatively large pitches from 7.5 to 30.0 mm were tested. Overall heat-transfer rates were calculated using the energy balance for the coolant through the test tube and wall temperatures were directly measured by a digital temperature indicator which was not clearly described. Figs. 2.4 and 2.5 show the variation of enhancement ratio with pitch of winding and with wire diameter respectively. The enhancement ratios plotted were defined as the ratio of vapour-side, heat-transfer coefficient for wire-wrapped tubes to that for a smooth tube at the same heat flux. For fixed pitch, the enhancement ratio was higher for the larger wire diameter. For the small diameter wires the enhancement ratio was highest at the lowest pitch used. The maximum enhancement ratio obtained was around 1.45 using the wire combinations of a wire diameter of 1.5 mm with a pitch of 7.5 mm and a wire diameter of 3.0 mm with a pitch of 15 mm. Sethumadhavan and Rao (1985) indicated that an optimum wire combination might exist at a smaller pitch, i.e. a pitch less than 7.5 mm, the smallest used in this investigation. As found in the present work peak enhancement ratios for smaller wire diameters occur at winding pitches smaller than those used in this investigation.

Golubnichniy et al. (1991) investigated the enhancement of condensation of nitrogen dioxide on a horizontal wire-wrapped tube at pressures between 0.15 and 0.35 MPa. The tube outside diameter was 22 mm. Stainless steel wires of 0.5 and 1 mm were welded with wire spacings (not clearly defined) of 1, 1.5, 5 and 9 mm. The heat flux varied from 28 to 130 kW/m^2. Some enhancement of the heat transfer was mentioned but no detailed data were reported.

(3) Theoretical investigations

An approximate approach to an analysis of condensation on a horizontal wire-wrapped tube was first proposed by Fujii et al. (1985), which is outlined below with minor changes in notation. Fig. 2.6 shows their coordinate system. By applying the conservation equations, together with the Nusselt (1916) approximations and including the surface tension-generated axial pressure gradient, they obtained the following differential equation for the condensate film thickness, δ.

$$\rho g z \frac{\partial}{\partial \phi}\left(\delta^3 \sin\phi\right) - \frac{d}{2}\frac{\partial}{\partial z}\left(\delta^3 \frac{\partial P}{\partial z}\right) = \frac{3}{2}\frac{\mu k d \Delta T z}{\rho h_{fg} \delta} \qquad (2\text{-}18)$$

where z is the coordinate in the direction of the tube axis measured from a mid-point between wires.

An essential feature of the approach was the simplification achieved when solving Eq. (2-18) by a major assumption for axial distribution of film thickness along the condenser tube. As shown in Fig. 2.7 the film thickness and the pressure in the condensate film were considered essentially constant over a range of z equal to the pitch of the wire winding minus the wire diameter. No heat transfer was assumed to occur beneath the wire. With the symmetry condition $\partial P/\partial z = 0$ at z = 0, Eq. (2-18) was integrated, to give:

$$\delta \frac{\mathrm{d}}{\mathrm{d}\phi}(\delta^3 \sin\phi) - \frac{4 d \sigma}{\rho g s^2 r_s}\delta^4 = \frac{3}{2}\left(\frac{\mu k d \Delta T}{\rho^2 g h_{fg}}\right) \qquad (2\text{-}19)$$

where s is the axial length of the thin film along the condenser tube between adjacent turns of the wires.

Eq. (2-19) was solved for the condensate film thickness with r_s and s taken to be constant around the tube and the enhancement ratio for the same vapour-to-surface temperature difference was expressed by:

$$\frac{Nu}{Nu_{\text{smooth}}} = (s/p)\frac{F_2(A_1)}{F_2(0)} \tag{2-20}$$

where

$$A_1 = \frac{4\sigma d}{\rho g s^2 r_s} \tag{2-21}$$

$$F_1(\phi, A_1) = \frac{(\tan(\phi/2))^{A_1/3}(\sin\phi)^{1/3}}{\left\{\int_0^{\pi}(\tan(\phi/2))^{4A_1/3}(\sin\phi)^{1/3}\mathrm{d}\phi\right\}^{1/4}} \tag{2-22}$$

$$F_2(A_1) = \frac{1}{\pi}\int_0^{\pi} F_1(\phi, A_1)\mathrm{d}\phi \tag{2-23}$$

and Nu_{smooth} is the average Nusselt number for a smooth tube, p is the wire pitch and ϕ is the angle measured from the top of the tube. When $A_1 > 15$, which occurs for organic fluids, it was found that Eq. (2-20) can be simplified as:

$$\frac{Nu}{Nu_{\text{smooth}}} = (s/p)\left\{\frac{4(1+A_1)}{3}\right\}^{1/4} \tag{2-24}$$

s was taken as:

$$s = p - d_w \tag{2-25}$$

r_s was assumed to be a function of $\sigma/\rho g$ and wire diameter, d_w, given by the following form:

$$r_s = \frac{K(2\sigma/\rho g)^{3/2}}{d_w^2} \tag{2-26}$$

where K was a dimensionless constant, which was determined by fitting the

experimental data of Fujii et al. (1985) for R-11 and ethanol. A value of 0.03 was selected as giving the best overall representation of the data (see Fig. 2.2).

Apart from the method of handling the transverse pressure gradient several features of this analysis may be questioned, namely, s and r_s taken as constant and given by Eqs. (2-25) and (2-26), the fact that the quantity of A_1 given by Eq. (2-21) is often less than 15 and, perhaps more importantly, Eq. (2-26) as pointed out by Murase et al. (2005), with $K = 0.03$, is incompatible with the assumed geometry (see Fig. 2.6) in many cases as illustrated in Fig. 2.8.

Marto et al. (1987) found that the model of Fuji et al. (1985) overestimated their heat-transfer data for steam condensation. This was attributed to condensate retention between adjacent wires on the lower part of the tube in the same manner as occurs for condensation on integral-finned tubes. Marto et al. (1987) attempted to modify the theory of Fujii et al. (1985) to include condensate retention. It was noted, however, that for wire-wrapped tubes there was no abrupt, well-defined, condensate retention location as found with low integral-finned tubes. Marto et al. (1987) performed static measurements of retention angles for each of the wire-wrapped tubes tested. It was found that the condensate between the wires appeared to exhibit a parabolic-shaped profile and no clear retention angle could be seen. A modification to the Rudy and Webb (1985) retention equation for low-finned tubes was made so as to fit approximately their observations.

By using the approach of Fujii et al. (1985) for the 'unflooded' region together with their approximate retention equation and one-dimensional conduction in the condensate in the 'flooded' region below the retention position, the average heat-transfer coefficient for the entire tube, α, was obtained:

$$\alpha = \alpha_u \frac{\phi_f}{\pi} + \alpha_f \left(1 - \frac{\phi_f}{\pi}\right) \tag{2-27}$$

where α_u and α_f are the average heat-transfer coefficients in the 'unflooded' and 'flooded' regions respectively. Fig. 2.3 compares their experimental results for steam condensation with the model of Fujii et al. (1985) with $K = 0.03$ and lines calculated

using the modified model with $K = 0.02$. It is seen that the modified model was able to bring the calculated enhancement ratios into closer accord with their steam data. They did not, however, examine the consequence of their modification for comparison with the earlier data of Fujii et al. (1985) for R-11 and ethanol.

Rose (2002) analysed the problem, based on the model of Fujii et al. (1985) while including effects of condensate retention. It was noted that the condensate surface profile must vary continuously along the tube surface. The approach of Masuda and Rose (1987) for condensation on low integral-finned tubes was used to determine the configuration of the retained condensate over the whole tube surface. Fig. 2.9 illustrates a wire-wrapped tube and the general appearance of liquid retained by surface tension forces at different positions around the tube. This gave

$$r_s = \frac{2\sigma}{\rho g d(1+\cos\phi)} \tag{2-28}$$

$$s = p - 4\left[\frac{d_w \sigma}{\rho g d(1+\cos\phi)}\right]^{1/2} \tag{2-29}$$

Eq. (2-19) of Fujii et al. (1985) was written by Rose (2002) as:

$$\sin\phi \frac{dz}{d\phi} = 2 - \frac{4}{3} z\cos\phi - \frac{16}{3}\left(\frac{\sigma d}{\rho g s^2 r_s}\right) z \tag{2-30}$$

where

$$z = \frac{\rho^2 g h_{fg}}{\mu k d \Delta T}\delta^4 \tag{2-31}$$

It is readily seen from Eq. (2-30) that the value of z at $\phi = 0$ is given by:

$$z_0 = \frac{3}{2\left[1+\left(4d^2/s_0^2\right)\right]} \tag{2-32}$$

as found by Fujii et al. (1985). (The subscript 0 denotes the top of the tube.)

In principle, Eq. (2-30), with r_s and s from Eqs. (2-28) and (2-29) and the boundary condition of Eq. (2-32), could be solved numerically for z in the range of ϕ from 0 to ϕ_f. With neglect of heat transfer over the curved part of the condensate surface and beneath the wire, the following expression for the enhancement ratio was obtained:

$$\varepsilon_{\Delta T} = \frac{z_0^{-1/4}}{2.287p}\left[p\phi_f - 4\left(\frac{2d_w\sigma}{\rho g d}\right)^{1/2} \ln\left\{\tan\left(\frac{\phi_f}{4}+\frac{\pi}{4}\right)\right\}\right] \tag{2-33}$$

where

$$s_0 = p - 4\left[\frac{d_w\sigma}{2\rho g d}\right]^{1/2} \tag{2-34}$$

$$\phi_f = \cos^{-1}\left(\frac{16 d_w\sigma}{\rho g d p^2} - 1\right) \tag{2-35}$$

Figs. 2.10 and 2.11 show the comparison between the earlier experimental data of Marto et al. (1987) for steam at atmospheric and low pressures respectively, and calculated enhancement ratio using Eqs. (2-32) to (2-35). It is seen from the figures that, while agreement was not perfect, the theoretical model gave values of the right order of magnitude and follows the same general trends (dependence of enhancement ratio on pitch, wire diameter and pressure).

Figs. 2.12 and 2.13 show the comparison with the experimental data of Fujii et al. (1985) for R-11 and ethanol and the model of Rose (2002). The experimental trends differed from those found by Marto et al. (1987) and the theoretical lines intersect the data. Evidently further accurate measurements and detailed appraisal of the theory are needed.

(4) Summary

From the few experimental studies conducted to date clear evidence of significant heat-transfer enhancement by the wire wrap can be seen. Values of maximum enhancement ratio between around 1.3 and 3.5 have been found, the value increasing with decreasing surface tension of the fluid. No firm conclusions can yet be drawn for optimum geometric variables for given fluid properties. More extensive systematic experimental investigation is needed.

Theoretical studies of this problem are all based on the original approximate solution of Fujii et al. (1985). Neither the original theory nor subsequent modifications are in wholly satisfactory agreement with the experimental data available.

2.3.3 Condensate inundation

(1) Introduction

Inundation is a term applied to tube banks and denotes the effect on the performance of a given tube or row of tubes of condensate falling from higher tubes in the bank. For low downward vapour velocity, the condensate inundation rate is dependent only on the condensation rate on the upper rows. The condensate thickness around the lower tubes should, therefore, increase due to inundation and consequently heat transfer should decrease. In addition, with increase in inundation, the appearance of inundation varies from droplets to columns and sheets as shown in Fig. 2.14.

Experimental work has been conducted using small tube banks which require high vapour generation capacity and by artificial inundation using a single tube or a column of tubes with additional simulated condensate supplied to the uppermost tube. It is difficult to isolate the effect of inundation in a tube bank due to the inevitable simultaneous effect of vapour shear. Measurements with low vapour velocity may, on the other hand, give significant accumulation of non-condensing gas, especially on lower rows.

Experiments with artificial inundation also encounter difficulties. Firstly much attention must be paid to inundation supply temperature. Too high an inundation temperature causes additional convective heat transfer which results in apparently higher vapour-side, heat-transfer coefficients. Too low an inundation temperature causes reduction of the apparent heat-transfer coefficient. It is also necessary to consider heat transfer to and condensation on condensate falling between tubes. Finally correspondence between an artificial inundation rate and equivalent tube depth in an actual tube bank needs careful consideration.

A large number of investigations have been made in studying condensate inundation primarily on smooth tubes. Experimental data for condensation on banks of integral-finned tubes are recently becoming available. To date few and conflicting data are available for inundation of wire-wrapped tubes.

(2) Inundation on smooth tubes

This problem was first analysed for smooth tubes by Nusselt (1916), who considered an in-line column of horizontal tubes with the same surface temperature. Condensate flowed from one tube to the one below as a continuous laminar sheet which is uniform along the length of the tubes as shown in Fig. 2.14 (c). The result is given by:

$$\bar{\alpha}_N = 0.728\left\{\frac{\rho(\rho-\rho_v)gh_{fg}k^3}{N\mu d\Delta T}\right\}^{1/4} \tag{2-36}$$

where $\bar{\alpha}_N$ is the arithmetic average of heat-transfer coefficients for each tube in a column of N tubes. From Eq. (2-36),

$$\bar{\alpha}_N/\alpha_{top} = \frac{\sum_{i=1}^{N}\left(\alpha_i/\alpha_{top}\right)}{N} = N^{-1/4} \tag{2-37}$$

and α_{top} is the heat-transfer coefficient for the top tube in the column and α_N is the heat-transfer coefficient of the N^{th} tube from the top in the column. From Eq. (2-37):

$$\alpha_N/\alpha_{top} = N^{3/4} - (N-1)^{3/4} \tag{2-38}$$

Several experimental investigations have been made for the effect of condensate inundation on smooth tube banks (e.g. Marto and Wanniarachchi (1984) for steam, Kutateladze, S.S. et al. (1985) for R-12, Honda et al. (1991) for R-113). These generally suggested that the Nusselt (1916) model was over conservative i.e. significantly exaggerated the detrimental effect of condensate inundation on the performance of lower tubes in the tube bank. A commonly used correlation is that due to Kern (1950) who modified the Nusselt (1916) equation. Taking account of the splashing of the condensate as it drips over successive rows of tubes, based on experience of operating condensers, consequently the following expression was obtained:

$$\bar{\alpha}_N / \alpha_{top} = N^{-1/6} \tag{2-39}$$

which gives

$$\alpha_N / \alpha_{top} = N^{5/6} - (N-1)^{5/6} \tag{2-40}$$

Fig. 2.15 shows a broad schematic comparison between experimental and theoretical studies for condensate inundation on smooth tubes depicted by Marto (1984). In the figure, the Eissenberg (1972) result which was based on a side drainage model for a staggered smooth tube bank (see Fig. 2.14(d)) is included. Based on the Eissenberg (1972) result, Marto (1984) gives:

$$\bar{\alpha}_N / \alpha_{top} = 0.6 + 0.42 N^{-1/4} \tag{2-41}$$

which gives

$$\alpha_N / \alpha_{top} = 0.6 + 0.42 \left\{ N^{3/4} - (N-1)^{3/4} \right\} \tag{2-42}$$

The Eissenberg (1972) result predicts a much smaller dependence on row number than the Nusselt (1916) and Kern (1950) equations, due to the drainage models (less area covered by inundation liquid). Inundation data are widely scattered due to the many parameters involved, such as tube bank geometry (i.e. in-line or staggered), tube vertical spacing, surface tension of condensate, heat flux and local vapour velocity. In addition, the presence of non-condensing gas, partial dropwise condensation, insufficient amounts of steam reaching lower tubes in the bank, and inaccurate heat-transfer measurement no doubt play a role.

Finally it is not generally clear what is meant by heat-transfer coefficient for a column or bank of tubes, since in practice the tube wall temperature and heat flux are both different at different depths.

(3) Inundation on finned tubes

Several investigators have found that the effect of condensate inundation is much less severe for low integral-finned tubes (e.g. Webb and Murawski (1990) for R-11, Honda et al. (1991, 1992, 1996, 2002, and 2003) for R-113, R-123, R-134a and R-407c). This has been explained by Honda et al. (1989) by the fact that the fins suppress lateral spreading of condensate along the tube so that the interfin spaces between columns of falling condensate are not affected and these parts of lower tubes behave like the top tube as shown in Fig. 2.16.

Results of Leicy (1999) demonstrated the importance of the inundation temperature control. Leicy (1999) simulated an in-line column of finned tubes using the artificial inundation method with steam and R-113. Inundation was supplied from an inundation supply tube onto a test tube via a dummy non-active tube located in the middle position between the inundation supply and test tubes. The inundation supply temperature was set to Eq. (D-4) at the inlet of the inundation supply tube. It was reported that for steam vapour-side, heat-transfer coefficient increased with increase in inundation rate, which is unrealistic. This was thought to be due to the convective heat transfer resulting from higher inundation temperature due to additional condensation on the falling condensate between the supply and test tubes. For R-113, heat-transfer coefficient was observed to decrease with increase in inundation rate. Leicy (1999) attributed this to the fact that the specific heat capacity of liquid R-113 is around one fourth of that for steam so that the effect of the additional heat transfer was less severe.

(4) Inundation on wire-wrapped tubes

Rifert et al. (1984) conducted experiments for ammonia condensation with inundation on a horizontal wire-wrapped tube. The tube, wire diameter and pitches used were the same for the single tube investigation, described in Section 2.3.2 (2). The test tube was placed below a condenser tube bank (which the authors did not clearly describe) and condensate for inundation onto the test tube was generated by the upper tubes. Data taken at a constant heat flux of 12 kW/m^2 were reported. It

was found that heat-transfer coefficients for the wire-wrapped tubes were higher than the smooth tube at all inundation rates tested. The highest heat-transfer coefficients under inundation were obtained for the wire-wrapped tube with 8 mm pitch. This was 60% to 100% higher than for the smooth tube.

Marto and Wanniarachchi (1984) investigated steam condensation with inundation. Five wire-wrapped horizontal titanium tubes were set in a vertical in-line column with distance between adjacent tube surfaces of 8 mm. The tubes had an outside diameter of 16 mm and an active heat-transfer length of 305 mm. Helically-corrugated ('roped') tube with a single groove (8 mm pitch) was also tested with and without wire wrap. 1.58 mm wire was wrapped on the smooth tube with pitches of 4, 8 and 16 mm, and on the roped tube along the groove. All the experiments were conducted at atmospheric pressure with a constant coolant velocity of 1.56 m/s for each of the five tubes. Vapour velocity was about 0.5 to 1.0 m/s. A perforated inundation supply tube was located above the column of the five active tubes to supply artificial inundation. It was not clearly stated which value was used for the inundation supply temperature. The average amount of condensate generated by the five active tubes (and artificial inundation liquid for tests with inundation) for one (inundation) condition was used to determine the rate of flow of the water into the inundation supply tube for the next inundation condition. By repeating this procedure, up to 30 tubes were simulated. Heat-transfer measurements were performed for each of the five active tubes. The vapour-side, heat-transfer coefficients were determined using the modified Wilson plot method. It should be noted that Marto and Wanniarachchi (1984) stated the inundation temperature control was poor, it was not possible to maintain a constant temperature, nor was it quickly adjustable. This is critical for the reliability of their heat-transfer results.

Table 2.2 shows the top tube results (i.e. without inundation) for different tubes at the same coolant and vapour velocities. The ratio, $\alpha_{top} / \alpha_{Nu}$, was denoted heat-transfer enhancement in comparison with the Nusselt (1916) theory for a smooth tube at the same heat flux which included enhancement due both to the wire wrap and vapour shear. The relatively low enhancement for the enhanced tubes was obtained as shown in Table 2.2. Enhancement ratio at the same heat flux of around 1.7 has been observed by Marto et al. (1987) using a 19 mm outside diameter tube

with the same wire diameter and with pitches of about 3.6 and 4.6. Ratios of around 1.2 have been found in the present investigation using a 12.2 mm diameter tube (see Section 4.2.4 (1)). Therefore, the presence of significant amount of air in the test section in this investigation is strongly suspected.

Marto and Wanniarachchi (1984) indicated that their experimental data for columns of horizontal smooth and wire-wrapped tubes could be well represented by the following equation:

$$\bar{\alpha}_N / \alpha_{top} = N^{-m} \qquad (2\text{-}43)$$

where m is a constant found from experimental data. This is the same form of expression as the Nusselt (1916) and Kern (1950) equations (Eqs. (2-37) and (2-39) respectively). Values of constant m in Eq. (2-43) found with their data are shown in Table 2.3. The smooth tube results were in close accord with the Kern (1950) equation. The roped tube was found to be slightly less affected by inundation than the smooth tube. Although the reduction in the detrimental effect of inundation was observed for the wire-wrapped tubes tested, the presence of air and the lack of inundation temperature control could be critical for the reliability of these data.

Brower (1985) extended the experiments of Marto and Wanniarachchi (1984) using the same apparatus for different wire diameters and pitches. Wire was also wrapped on the inundation supply tube. All the experiments were conducted at atmospheric pressure with the constant coolant velocity of around 1.55 m/s. Vapour velocity was between 1.4 and 2.1 m/s. Wire diameters and pitches of winding used are shown in Table 2.4. No improvement of the inundation temperature control nor special attention to eliminate non-condensing gas (air) were mentioned.

The presence of air in the test section is also suspected from the results of Brower (1985) obtained without inundation for smooth and wire-wrapped tubes. Fig. 2.17 shows comparison between Brower (1985) data for the smooth tube without inundation and earlier theoretical results of Nusselt (1916) and Rose (1984), based on Eqs. (2-1) and (2-6) respectively. The data were significantly lower than the Rose (1984) prediction. Table 2.4 shows data for the top tube of a column of

smooth and wire-wrapped tubes. The definition of the enhancement ratio was not clearly stated but was presumably the same as defined in Marto and Wanniarachchi (1984). As later shown in Figs. 4.14 and 4.22 (in Chapter 4), the enhancement ratios of Brower (1985) were seen to be significantly lower than those of Marto et al. (1987) and the present data. In Table 2.4 $\left(\alpha_{\text{top}}/\alpha_{\text{Nu}}\right)_q$ for the smooth tube shows 19% higher than the Nusselt (1916) theory. This enhancement was due to the effect of vapour shear. This indicates that $\left(\alpha_{\text{top}}/\alpha_{\text{Nu}}\right)_q$ for the wire-wrapped tubes due solely to the wire wrap is expected to become further lower.

Inundation data of Brower (1985) are shown in Table 2.5. It was indicated that vapour-side, heat-transfer performance of a smooth tube column was considerably improved by winding wire on the smooth tubes. The optimum pitches to give the highest, average, vapour-side, heat-transfer coefficient for 30 tubes were found to be 4, 4 and 8 mm for 0.5, 1.0 and 1.6 mm wire diameters respectively. However, data $\left(\bar{\alpha}_N/\alpha_{\text{top}}\right)$ for a wire diameter of 1.6 mm with a pitch of 8 mm (see Fig. 2.18) appeared to be more than unity for first several numbers of tubes (improvement of the heat transfer on lower row tubes in a column by inundation) which is unlikely realistic. Brower (1985) gave no explanation for this phenomenon. This is thought by the present author to be likely due to the presence of air affecting the top tube measurement. The more than unity behaviour of $\left(\bar{\alpha}_N/\alpha_{\text{top}}\right)$ was likely resulting from the low heat-transfer coefficient for the top tube.

In a review paper Marto (1986) reported that for steam condensation the effect of inundation was very weak for a column of horizontal wire-wrapped tubes which were better in this respect than low-finned tubes (see Fig. 2.19). In the figure, the wire-wrapped tube data cited were those of Brower (1985), which are suspected by the present author to be affected by the presence of air. No detailed information was given for the finned tube data. When the major component of the condensing side resistance is due to air, presumably approximately the same for all tubes, any effect of inundation is masked when plotting normalized heat-transfer coefficients.

Memory et al. (1992) measured condensation heat transfer with inundation on a

vertical in-line column of four horizontal wire-wrapped, roped tubes using R-113 at atmospheric pressure. The copper-nickel tubes having an active heat-transfer length of 1.2 m and an average outside diameter of 15.8 mm formed a vertical column, with distance between adjacent tube surfaces of around 20 mm. The tubes had a groove pitch of 9.27 mm and a groove depth of 0.33 mm. Stainless-steel wire was wrapped in the shallow grooves. Wire diameters used were 0.74, 1.24 and 1.72 mm. Smooth tubes having an outside diameter of 15.9 mm were also tested. Care was taken to avoid the presence of air in the test section by running a vacuum pump during experiments while the vapour temperature was maintained at 47.5 °C (1 atm). Measurements were performed at various coolant velocities from 0.2 to 1.2 m/s (each tube in the column had the same coolant velocity). Vapour-side, heat-transfer coefficients were obtained using the modified Wilson plot method. It was found that for the top tube (without inundation) with a coolant velocity of 1.2 m/s, the vapour-side, heat-transfer coefficient for a wire-wrapped roped tube with a wire diameter of 1.24 mm gave the highest enhancement which was 60% more than given by the Nusselt (1916) theory. $\bar{\alpha}_N/\alpha_{top}$ decreased with increasing number of tubes, in close accord with the Eissenberg (1972) equation (Eq. (2-41)). The values of constant m in Eq. (2-43) at a coolant velocity of 1.2 m/s were found to be 0.113, 0.146 and 0.075 for smooth, roped and wire-wrapped roped tubes respectively. Even for the small number of tubes, reduction in the detrimental effect of inundation by wire wrapping was clearly confirmed.

(5) Summary

It is clear that the effect of condensate inundation on both wire-wrapped and finned tubes is less significant than that for smooth tubes. This is understandable on the bases of the explanation given by Honda et al. (1989). However, the report by Brower (1985) and Marto (1986) that wire-wrapped tubes perform better than low integral-finned tubes during steam condensation is unexplained and seems unlikely. It seems probable that these data were vitiated by the presence of air in the steam and failure to control inundation supply temperature.

2.3.4 Conclusion

It has been found that an enhancement of heat transfer can be obtained by wire-wrapping of condenser tubes. The enhancement varies with wire diameter, pitch of winding and fluid properties. Optimum combinations of the geometric parameters seem to exist for each fluid. For low surface-tension fluids, higher enhancement ratios have been found for larger wire diameter. For a high surface-tension fluid, smaller wire diameter appears to provide higher enhancement. However, available data are insufficient to establish a reliable correlation.

The presence of the curvature term in the momentum balance for the condensate film gives rise to significant complication in the theory and no complete solution of the problem has been published to date. An approximate approach by Fujii et al. (1985) involved some empiricism backed by experiments for R-11 and ethanol, and naturally the final result was in broad agreement with their data for these fluids. Later measurements by Marto et al. (1987) for steam did not agree with the approximate theory. Moreover, the deficiency for the treatment of the condensate film of Fujii et al. (1985) was pointed out by Murase et al. (2005). Rose (2002) has more recently amended the approximate theory to take account of condensate retention. The modified theory then involves no empiricism and is in general agreement with the steam data of Marto et al. (1987), but does not predict the whole of the available data satisfactorily.

It has been established that the effect of condensate inundation on both wire-wrapped and finned tubes is less significant than that for smooth tubes due to the fact that the wires, in the same way as fins, prevent lateral spreading of condensate along the tube so that the space between columns of falling condensate are not affected and these parts of lower tubes behave like the top tube. In experiments with artificial inundation liquid, much attention needs to be paid to inundation temperature control, which may cause additional heat transfer. The report by Marto (1986) referring to measurements by Brower (1985) suggested that wire-wrapped tubes perform better than low integral-finned tubes under inundation conditions for steam condensation. However these data may be unreliable due to the presence of air in the test section and lack of inundation temperature control.

2.4 Marangoni condensation of mixtures

2.4.1 Introduction

This section describes experimental investigations of Marangoni or pseudo-dropwise condensation of vapour mixtures, such as steam-ethanol and steam-ammonia. The survey is divided into two parts: investigations for Marangoni condensation of mixtures and boiling of water-ethanol mixtures. In the first section, the mechanism of a pseudo-dropwise mode is explained, followed by experimental investigations, mainly for recent extensive investigations by Utaka and co-workers using steam-ethanol mixtures condensing on small vertical flat plates. In the second section nucleate boiling of pure and binary mixtures is briefly outlined.

2.4.2 Marangoni condensation of mixtures

(1) Introduction

Condensation of vapour mixtures has been widely studied for many years. In most cases the focus has been on the diffusion process in the vapour phase which results in the so-called mass-transfer resistance and deterioration of the heat transfer. The vapour phase convection with diffusion process in forced and free convection of binary mixtures is now well understood (see, for instance, Fujii (1991)). During condensation of mixtures, the more volatile constituent accumulates near the condensate-vapour interface and forms a composition boundary layer across which there exists a difference between the bulk vapour and the equilibrium composition adjacent to the interface. This results in a temperature drop in the vapour boundary layer and consequent reduction in the temperature difference across the condensate film, which reduces the heat transfer.

For certain binary mixtures, e.g. steam-ethanol, steam-methanol and steam-ammonia, for a fully wetted surface a mode of condensation whose appearance resembles that of dropwise condensation of a pure vapour, was first observed by Mirkovich and Missen (1961). Ford and Missen (1968) indicated that this

Marangoni or pseudo-dropwise condensation may occur when the more volatile constituent has the smaller surface tension, such as for a steam-ethanol mixture, which is also so-called a 'positive' mixture. Since then, further investigations concerning such mixtures have been conducted, e.g. Fujii et al. (1989, 1993) for a horizontal tube, Hashimoto et al. (1994) for a vertical tube and Hijikata et al. (1996) for a horizontal flat plate. Fig. 2.20 shows photographs of Marangoni condensation of steam-ethanol mixtures with ethanol vapour mass fractions of 7% and 52% on a short vertical flat plate (20 mm height), from Utaka et al. (1998). This results in the reduction of the condensate resistance by thinning parts of the film and enhances the heat transfer.

Owing to the complexity of the phenomenon a theory of Marangoni condensation is yet to be established. However, the mechanism of developing the droplets has been explained by Hijikata et al. (1996) who pointed out that, in certain circumstances, a binary condensate film could be unstable. The model for instability and growing process of the condensate film during Marangoni condensation is illustrated in Fig. 2.21. Referring to Fig. 2.21 and considering condensation of a steam-ethanol mixture, for any small irregularity of the condensate film surface the condensate surface temperature will be relatively low (nearer the surface temperature) in the valley and relatively high (nearer the vapour temperature) near the crest. Thus, from the equilibrium diagram (see Fig. 2.22) the ethanol concentration in the liquid will be higher in the valley and lower at the crest. Consequently the water concentration will be higher at the crest and lower in the valley. Since water has the higher surface tension the surface tension for the condensate film will be lower in the valley and higher at the crest. The gradient of surface tension increasing from valley to crest (as indicated by the arrows in Fig. 2.21) tends to magnify the irregularity and leads to instability of the film. When the pseudo-dropwise condensation mode occurs, the effect of composition on surface tension presumably outweighs the effect of temperature (generally lower surface tension at higher temperature for fixed composition) and the pressure gradient resulting from change of interface curvature.

(2) Experimental investigations

Wallace and Davison (1938) performed experiments on condensation of steam-ethanol mixtures on a horizontal brass tube. The vapour-side, heat-transfer coefficient for the mixtures was found to be smaller than that for pure steam for all of the ethanol concentrations tested. No visual observation for the test tube surface was made. Observations of condensation modes were made by Mirkovich and Missen (1961, 1963) using organic binary mixtures, such as n-pentane-methanol and n-pentane-methylene dichloride, and by Ford and Missen (1968) and Ford and McAleer (1971) using binary mixtures, such as water-ethanol, water-methanol and water-acetone. The former investigations showed streakwise or pseudo-dropwise appearance at lower n-pentane fraction and at low temperature difference between the bulk vapour and heat-transfer surface, and gave higher heat transfer. The latter visually observed that during the pseudo-dropwise condensation mode the entire heat-transfer surface was covered by a liquid film at all times. (During dropwise condensation of *pure* fluids, in general, the heat-transfer surface is non-wetted between droplets.)

Recently, Fujii et al. (1989) conducted experiments for condensation of steam-ethanol mixtures on a horizontal copper tube. The tube had an outside diameter of 18.0 mm and an active heat-transfer length of 385 mm. The experiments were conducted at absolute pressures between 3 to 20 kPa and vapour-to-surface temperature differences varied from 2 to 20 K. A full range of ethanol mass fractions was tested from pure steam to pure ethanol and visual observations of the appearance of the condensate film were made. The condensation modes were classified as drop, streak, ring and smooth film, as shown in Table 2.6. During the pseudo-dropwise condensation, heat transfer, when neglecting diffusion resistance in the vapour phase, was found to be improved. However, heat-transfer coefficients between the bulk vapour and the heat-transfer surface, i.e. when including diffusion resistance in the vapour phase, were observed to be lower than the Nusselt (1916) theory for pure steam at all the vapour-to-surface temperature differences tested. Fujii et al. (1989) found that heat-transfer enhancement resulting from changes in condensation modes by vapour compositions but did not mention the dependence of the condensation mode on heat flux or vapour-to-surface temperature difference.

Fujii et al. (1993) extended the experiments of Fujii et al. (1989) using 9.5 and 18 mm outside diameter tubes for water-ethanol mixtures as well as water-methanol, water-n-propanol, methanol-ethanol and methanol-n-propanol. For the water-ethanol, water-methanol and water-n-propanol mixtures, the condensation modes could also be classified as drop, streak, ring, smooth film and wavy film. Fig. 2.22 shows photographs of the condensate film for water-ethanol mixtures with different ethanol vapour mass fractions using the 9.5 mm outside diameter tube, taken from the side and top of the tube. The condensation mode was found to be dependent on vapour composition, vapour pressure and heat flux, and gave different heat-transfer enhancements. For water-ethanol mixtures, the heat-transfer coefficient excluding the diffusion resistance was found to be larger than the Nusselt (1916) theory for pure water by 6 to 7 times for drop, 2 to 3 times for streak, 1.6 to 2 times for ring and 1.3 to 2 for wavy film, while that for smooth film was in good agreement with the Nusselt (1916) theory. Similar enhancements were observed for water-methanol and water-n-propanol mixtures. For methanol-ethanol and methanol-n-propanol mixtures, only the continuous film mode was observed and the heat-transfer coefficients were well predicted by the Nusselt (1916) theory. No heat-transfer data including the diffusion resistance was reported.

Hashimoto et al. (1994) conducted experiments on a vertical copper tube using water-ethanol mixtures with various ethanol mass fractions. The tube had an outside diameter of 30 mm and an active heat-transfer length of 90 mm. The experiments were performed at around atmospheric pressure with various vapour-to-surface temperature differences. Similar condensate flow patterns to those found by Fujii et al. (1989, 1993) were observed. Heat-transfer coefficient for the vertical tube was also found to be higher than the Nusselt (1916) theory by up to 3 times (excluding the diffusion resistance), when condensation mode appeared to be a pseudo-dropwise mode, while those for smooth film were in good agreement with the Nusselt (1916) theory.

Hijikata et al. (1996) observed the condensate film appearance during condensation of steam-ethanol mixtures on a horizontal copper surface at an absolute pressure of 135 mmHg. The heat-transfer surface having a diameter of 30 mm was periodically wiped by a sweeper to remove the condensate. Four main

points were noted: firstly the droplets 'floated' on a thin condensate film which always existed on the heat-transfer surface (as also observed by the earlier investigators); secondly the droplets move more frequently on the horizontal surface in comparison with dropwise condensation of pure steam; thirdly drop formation always began at the same points where small scratches existed; and lastly the diameter of the droplets formed on the surface during the pseudo-dropwise condensation mode was around 0.5 mm after wiping, which they suggested was roughly 20 times larger than for dropwise condensation of pure steam.

For condensation of steam-ammonia mixtures, several experimental investigations have been conducted on horizontal tubes by Goto et al. (1995), Morrison and Deans (1997) and Philpott and Deans (2004). Goto et al. (1995) found that the vapour-side, heat-transfer coefficients of the mixtures (including the diffusion resistance) were lower than those for each pure component and appearance of three types of condensate film were observed, described as smooth film, stationary ringwise film and turbulent ringwise film. Similar appearances were observed by Morrison and Deans (1997), who noted that the condensation mode was dependent on the vapour composition. Morrison and Deans (1997) and Philpott and Deans (2004) reported vapour-side, heat-transfer coefficient (including the diffusion resistance) up to 34% higher with ammonia vapour mass fraction of 0.9% in comparison with the Nusselt (1916) theory for steam condensation calculated using the same saturation temperature of the steam-ammonia vapour and the measured tube wall temperature.

For condensation of steam-methylamine mixtures Morrison and Deans (1998) reported the highest heat-transfer coefficient (including the diffusion resistance) around 130% higher than the Nusselt (1916) value for pure steam with methylamine vapour mass fraction of 0.2% at a vapour-to-surface temperature difference of 6.4 K, when the condensate film appeared to be a pseudo-dropwise condensation mode.

(3) Investigations by Utaka and co-workers

Most recently Utaka and co-workers have studied this phenomenon extensively

using vertical flat plates. The dependence of the vapour-side, heat-transfer coefficient on vapour composition (Utaka and Wang (2004)), vapour-to-surface temperature difference, distance from the top on a condensing surface (Utaka and Terachi (1995)), vertically downward vapour velocity (Utaka and Kobayashi (2003)) and the effect of non-condensing gas (Utaka and Wang (2005)) have been systematically investigated. Utaka and Nishikawa (2002) used a laser light absorption technique to measure the condensate film thickness over time at a given location on a heat-transfer surface during condensation of steam-ethanol mixtures. It was confirmed that a film with thickness of at least 1 μm was always present.

Figs. 2.23 and 2.24 show the dependence of heat flux and heat-transfer coefficient (including the vapour phase diffusion resistance) on vapour-to-surface temperature difference for different vapour compositions with vertically downward vapour velocities of 0.4 m/s and 0.7 m/s, from Utaka and Wang (2002, 2001), respectively. A short vertical flat plate having a width of 10 mm and a length of 20 mm was used. It is seen that the heat flux and heat-transfer coefficient first increase and subsequently decrease with increasing vapour-to-surface temperature difference. Lower ethanol mass fraction mixtures give higher enhancement for both heat flux and heat-transfer coefficient. The general behaviours of the $q - \Delta T$ and $\alpha - \Delta T$ curves were explained by Utaka et al. (1995) as follows. Referring to Fig. 2.25, which is schematically drawn experimental data for Marangoni condensation on a vertical flat plate with one ethanol mass fraction mixture, the heat-transfer coefficient was very low in the region from the points A' to B' due to the large diffusion resistance in the vapour phase, i.e. low heat flux and large temperature drop across the diffusion layer, even when the appearance of the condensate film showed a pseudo-dropwise mode. A (small) decrease in the diffusion resistance began at the point B', as the surface temperature of the condensate film reaches the minimum value (equilibrium liquid temperature at the given ethanol mass fraction) and the composition of the condensate surface becomes equivalent to that of the bulk vapour. The reduction of the heat-transfer resistance in the condensate film due to the pseudo-dropwise mode which also contributes to reducing the diffusion layer by generating turbulence resulted in the steep increase in the heat-transfer coefficient to the point C'. It was noted that the vapour-to-surface temperature difference of the point B' coincided with the vapour and liquid

equilibrium temperature difference, ΔT_p (see Fig. 2.22), for the given vapour composition. After reaching a maximum at the point D', the heat-transfer coefficient then decreased as the condensation mode progressed to smooth film with increase in vapour-to-surface temperature difference at around the point E'. In conclusion, Marangoni condensation heat transfer was mainly determined by the diffusion resistance in the vapour side as well as the condensate film resistance in the liquid side (the condensation mode).

Fig. 2.26 shows the variation of enhancement ratio (ratio of heat-transfer coefficient for steam-ethanol mixtures to that for pure steam at the same vapour-to-surface temperature difference including diffusion resistance in the vapour phase) with vapour-to-surface temperature difference for different ethanol vapour mass fractions at a vapour velocity of 0.4 m/s, from Utaka and Wang (2004). The enhancement ratio exceeds unity over almost the entire range of vapour-to-surface temperature difference for ethanol vapour mass fractions of less than 6%. For ethanol vapour mass fractions higher than 12%, the heat-transfer coefficient was first lower than that for pure steam at low vapour-to-surface temperature difference and subsequently exceeded the pure steam with increase in the temperature difference. This behaviour was explained by Utaka and Wang (2004) to be due to diffusion resistance in the vapour phase, which is proportional to ethanol vapour mass fraction.

Fig. 2.27 shows the variation of the peak enhancement ratio with ethanol vapour mass fraction from Utaka and Wang (2004). An ethanol vapour mass fraction of approximately 1% gave the highest heat-transfer enhancement ratios for both vapour velocities of 0.4 m/s and 1.5 m/s. It was found that under optimum conditions, i.e. low ethanol vapour mass fraction with high vapour velocity, the enhancement ratio of up to 8 or more (including diffusion resistance in the vapour phase) could be observed. Very low ethanol vapour mass fractions of 0.05% and 0.1% (the corresponding equilibrium ethanol liquid mass fractions were approximately 0.005% and 0.01% respectively) gave the enhancement ratios of from 3.5 to 5.5 at a vapour velocity of 0.4 m/s at the relatively small temperature difference range of approximately 3 to 5 K. Utaka and Wang (2004) noted that the addition of a very small amount of ethanol in water would be very effective to promote condensation

heat transfer.

Utaka and Terachi (1995) found the dependence of Marangoni condensation heat transfer on the distance from the top on a relatively long vertical flat plate (30 mm width and 71 mm length). The following was pointed out: firstly the condensation mode varied at the higher and lower surface positions; secondly values of heat flux and heat-transfer coefficient decrease with increase in the distance from the top especially at the peaks of heat flux and heat-transfer coefficient due to a large amount of condensate generated at the higher surface position, which thickens the condensate film at the lower surface position; and lastly the ethanol vapour mass fraction in the vicinity of the heat-transfer surface increases with increase in the distance from the top since less volatile constituent (steam) could preferentially condensate at the higher position.

Fig. 2.28 shows the dependence of vertically downward vapour velocity on Marangoni condensation on the short vertical flat plate for ethanol vapour mass fractions of 9%, 32% and 53%, from Utaka and Kobayashi (2001). Regardless of the ethanol vapour mass fractions, the heat-transfer coefficient increased with increase in the vapour velocity over the entire range of vapour-to-surface temperature difference. This was considered to be due to reduction in the diffusion resistance by reducing the build up of the more volatile constituent (i.e. ethanol) in the vicinity of the interface.

Figs. 2.29 and 2.30 show the dependence on non-condensing gas (nitrogen) concentration with a vapour velocity of 0.5 m/s for ethanol vapour mass fractions of 1% and 45% respectively, both from Utaka and Wang (2005). A short vertical flat plate having a width of 10 mm and a length of 20 mm was used. The data for the smallest mass fraction of non-condensing gas were measured with the vapour loop sealed off from the atmosphere and the non-condensing gas in the vapour loop continuously extracted using a vacuum pump (while maintaining pressure in the test section a little above atmospheric pressure). Those for the second smallest were obtained with the vapour loop open to the atmosphere. For other data, nitrogen vapour mass fractions were varied by injecting the gas into the apparatus. A strong effect of nitrogen concentration on both peaks of heat flux and heat-transfer

coefficient (at the middle range of vapour-to-surface temperature difference) was found particularly at lower ethanol vapour mass fraction and when the appearance of the condensate film showed a pseudo-dropwise condensation mode. A smaller influence of nitrogen gas was observed at low vapour-to-surface temperature difference. This was explained by Utaka and Wang (2005) on the basis that at the low temperature difference the heat transfer was much affected by diffusion resistance in the vapour phase even without non-condensing gas so that the additional effect of the nitrogen gas is not significant.

(4) Summary

Significant condensation heat-transfer enhancement has been found by adding ethanol in water for both horizontal smooth tubes and short vertical flat plates. Values of maximum enhancement ratio (in comparison with pure steam condensation) of up to 8 have been found using low ethanol mass fraction and with high vapour velocity. These enhancements include the detrimental effect of diffusion resistance in the vapour phase. No systematic experiments using the more practically relevant geometry of a horizontal tube and covering a wide range of vapour-to-surface temperature difference with relatively small ethanol vapour mass fractions have been made to date.

2.4.3 Boiling of water-ethanol mixtures

Owing to its possible use in improving the performance of power plant condensers, the effect of the small amount of ethanol in the boiler is of interest.

Fig. 2.31 shows the typical boiling curve for a pure fluid, i.e. dependence of boiling heat flux, q^*, on the wall superheat on a surface submerged in a pool of liquid. The wall superheat, ΔT^*, is defined as the difference between the wall temperature and the saturation temperature of the liquid at the system pressure, i.e. liquid-to-surface temperature difference. Referring to Fig. 2.32, the mode of heat transfer shifts from natural convection through various regimes ultimately to film boiling. Nucleate boiling heat transfer is affected by heater geometry, surface conditions (roughness, wettability and chemical contamination), system pressure, gravity and fluid properties.

For nucleate boiling of mixtures, as a bubble grows on a heat-transfer surface, the more volatile constituent (i.e. ethanol for the case of a water-ethanol mixture) evaporates preferentially at the liquid-vapour interface, establishing a composition gradient in the liquid surrounding the interface. This additional mass-transfer resistance along with the associated increase in interface temperature causes deterioration in the boiling heat transfer of mixtures.

Ali and Thome (1984) investigated boiling of water-ethanol mixtures on an enhanced boiling surface, so-called 'high flux'. The surface structure is the porous metallic matrix produced by sintering or brazing small particles to the case surface (see for details Bergles (2003)). Tests were done at atmospheric pressure and for the full range of ethanol mole fractions. The results are shown in Fig. 2.32, where ethanol liquid mole fractions are shown in the legend. Focusing on low ethanol liquid mole fractions from 5% to 45% in the figure, deterioration in the boiling heat flux of the mixtures is seen in comparison with pure water results. The heat flux for pure water is seen to be higher than those for the mixtures of from 5% to 45% at low liquid-to-surface temperature difference. With increase in liquid-to-surface temperature difference the heat flux for 15% to 45% mixtures exceeds those for pure water. The heat flux for 5% mixtures is seen to be lower than those for pure water

over the range of vapour-to-surface temperature difference. (The corresponding ethanol liquid mass fraction is approximately 12%.)

Fujita and Tsutsui (1994) investigated boiling of water-ethanol mixtures on a horizontal circular copper plate for a full range of ethanol fractions with a wide range of heat flux. The results are shown in Fig. 2.33, where $\tilde{x}$ is the ethanol liquid mole fraction. Deterioration in the boiling heat transfer is also seen on the horizontal plate. The boiling heat flux for mixtures is seen to be lower than those for pure water. The minimum ethanol liquid mole fraction tested was 7% (the corresponding ethanol liquid mass fraction is approximately 16%), whose heat flux is also seen to be lower than those for pure water over the range of liquid-to-surface temperature difference.

Summary

Apparent reduction of boiling heat transfer by adding ethanol in water has been observed on an enhanced heat-transfer surface and a horizontal flat plate. This has been considered to be due to the additional mass-transfer caused by a composition gradient between the vicinity of a heat-transfer surface and bulk liquid. Although the full range of liquid compositions has been investigated for nucleate boiling of water-ethanol mixtures, no experimental data using low ethanol liquid mass fractions, i.e. less than 1%, which gives the high condensation heat transfer, is available.

2.4.4 Conclusion

Marangoni or pseudo-dropwise condensation may be observed for binary mixtures where the more volatile constituent has the lower surface tension, such as water-ethanol and water-ammonia. Although the pseudo-dropwise condensation mode was first observed more than 30 years ago, the heat-transfer enhancement has not been reported until recently. A series of investigations using steam-ethanol mixtures and short vertical flat plates by Utaka and co-workers has revealed Marangoni condensation heat transfer to be dependent on vapour composition, vapour velocity, vapour-to-surface temperature difference, distance from the top on a condensing surface and the presence of non-condensing gas. The nature of Marangoni condensation on a short vertical flat plate was found to involve not only the diffusion resistance in the vapour phase but also the changes in the mode of condensation, i.e. film, streak and pseudo-drop. Higher enhancement ratios can be obtained using low ethanol vapour mass fraction, i.e. less than 6% (giving corresponding room temperature liquid composition of approximately 0.5%), at low vapour-to-surface temperature difference, and with higher vapour velocity. Under an optimum condition the enhancement of heat-transfer coefficient (including diffusion resistance in the vapour phase) up to 8 has been observed. For horizontal tubes with low ethanol mass fractions, no systematic investigation has been conducted to date.

For nucleate boiling of water-ethanol mixtures with low ethanol liquid mole fraction, earlier investigations have generally shown that addition of ethanol in water gives lower boiling heat flux than those for pure water. However, no data exists for extremely low ethanol mass fractions, i.e. less than 1%, which gives strong enchantment for condensation heat transfer.

Table 2.1 Earlier experimental investigations for condensation on low integral-finned tubes.

Reference	Test fluid	Tube tested		Fin geometry				Method of determination of surface temperature	Vapour approach velocity / (m/s)	Experimental conditions	Enhancement	Primary objective	Comment
		Diameter / mm, Active length, l / mm	Material	Height h / mm	Thickness t / mm	Interfin space b / mm	Fin shape						
Honda et al. (1983)	R-113 methanol	i.d. 14.1 - 15.5 o.d. 18.7 - 19.4 l = 170 - 433	Copper	0.92 - 1.46	0.11 - 0.27	0.39 - 0.71	Rectangular Trapezoidal	Surface thermocouples	Near stationary	Vapour pressure was above atmospheric	Best $\varepsilon_{\Delta T}$ 8.8 / R-113 5.3 / methanol at ΔT = 5 K	Effect of an attached porous drainage strip	Theoretical analysis and measurement of condensate retention were presented.
Yau et al. (1985)	steam	i.d. 9.78 o.d. 12.7 l = 102	Copper	1.6	0.5	0.5 - 20	Rectangular	Subtraction of resistances*	0.5, 0.7, 1.1	Near atmospheric pressure	Best $\varepsilon_{\Delta T}$ = 3.6 with b = 1.5 mm	Effect of interfin space on heat-transfer performance	Retention effect was experimentally confirmed.
Masuda and Rose (1985)	R-113 E-G**	i.d. 9.78 o.d. 12.7 l = 102	Copper	1.59	0.5	0.25 - 20	Rectangular	modified Wilson plot	0.28 / R-113 0.36 / E-G**	Little above atmospheric	Best $\varepsilon_{\Delta T}$ 7.5 / R-113 5.2 / E-G**	Effect of interfin space	Continued work of Yau et al. (1985) with different fluids.
Wanniarachchi et al. (1986)	steam	i.d. 12.7 o.d. 19.1 l = 133.4	Copper	1	0.5	1.5	Rectangular Triangular Trapezoidal Parabolic	modified Wilson plot	2 / 85 mmHg 1 / 760 mmHg	Atmospheric and vacuum conditions, i.e. 85 mmHg	Best ε_q (parabolic fin tube) 4.1 / 6.2 (760 / 85 mmHg)	Experimental study on effect of fin shape and pressure	ε_q was evaluated at q = 0.25 / 0.75 (MW/m2) (760 / 85 mmHg).
Michael et al. (1989)	steam R-113	i.d. 12.7 o.d. 19.1 l = 135	Copper	1	1	0.25, 1.5, 4.0	Rectangular	Subtraction of resistances*	0.4 - 1.9 (R-113) 4.8 - 31.5 (steam)	near-atmospheric / (R-113) 11.6 kPa / (steam)	4 / 2 (R-113 / steam) at lower vapour velocity, 3.2 / 1.4 at the highest vapour velocity	Effect of vapour shear stress	Effect of vapour velocity was less than on smooth tubes.

Table 2.1 (continued).

Reference	Test fluid	Tube tested: Diameter / mm, Active length, l / mm	Tube tested: Material	Fin geometry: Height h / mm	Fin geometry: Thickness t / mm	Fin geometry: Interfin space b / mm	Fin geometry: Fin shape	Method of determination of surface temperature	Vapour approach velocity / (m/s)	Experimental conditions	Enhancement	Primary objective	Comment
Marto et al. (1990)	R-113	i.d. 12.7 o.d. 21.1 - 23.1 l = 133	Copper	0.5 - 2.0	0.5 - 1.0	0.25 - 4.0	Rectangular		0.4	Slightly above atmospheric pressure	Best $\varepsilon_{\Delta T}$ = 7.0 with h = 1.0 mm, t = 0.5 mm, b = 0.25 mm	Report of experimental results for R-113	Continued work of Marto et al. (1986) 24 finned tubes were tested.
Sukhatme et al. (1990)	R-11	i.d. 15.5 - 15.7 o.d. 23.5 - 25.0 l = 500	Copper	0.29 - 1.22	0.25 - 0.93	0.06 - 0.46	Trapezoidal	Surface thermocouples		Vapour pressure 150 - 250 (kN/m^2)	Best $\varepsilon_{\Delta T}$ = 10.3 with h = 1.22 mm, t = 0.52 mm, b = 0.19 mm	Report of experimental results and comparison with theory.	Data of 9 finned tubes were presented together with 3 specially enhanced tubes
Wang et al. (1990)	R-113			1.3	0.3	0.7		Surface thermocouples	Near stationary	T_s was set at 50 ℃	α_m = around 10 (kW/m^2)	Circumferential distributions of ΔT, q and α of horizontal finned tubes	13 tubes including Thermoexcel-C and R-tube were tested.
Briggs et al. (1992)	steam R-113 E-G**	o.d. 12.7 l = 102	Copper	1.59	0.5	0.5, 1.0, 1.5	Rectangular	Surface thermocouples	0.72 / steam 0.28 / R-113 0.42 / E-G**	100 kPa	$\varepsilon_{\Delta T}$ 2.5 - 3.0 / steam 5.2 - 6.8 / R-113 4.2 - 4.8 / E-G**	Report of accurate experimental results and comparison with theory.	Comparison between direct measurement, subtraction and modified Wilson plot.
	steam R-113	o.d. 19.1 l = 150	Copper	1	1	0.5, 1.0, 1.5	Rectangular	Surface thermocouples	0.8 - 1.2 / steam 0.4 - 1.5 / R-113	100 kPa	$\varepsilon_{\Delta T}$ 2.5 - 3.4 / steam 3.8 - 5.0 / R-113		
Bella et al. (1993)	R-11 R-113	i.d.10.00 o.d. 15.00 l = 150	Copper	0.7	0.22	0.53	Trapezoidal	Surface thermocouples	1.9 - 26.1 / R-11 2.5 - 29.5 / R-113	109 - 198 kPa (R-11) 104 - 125 kPa (R-113)	At the highest U_v 50 % higher than a quiescent vapour case	Effect of vapour shear stress	

Table 2.1 (continued).

Reference	Test fluid	Tube tested: Diameter / mm, Active length, l / mm	Tube tested: Material	Fin geometry: Height h / mm	Fin geometry: Thickness t / mm	Fin geometry: Interfin space b / mm	Fin geometry: Fin shape	Method of determination of surface temperature	Vapour approach velocity / (m/s)	Experimental conditions	Enhancement	Primary objective	Comment
Cavallini et al. (1995)	R-11 R-113	i.d.10.00 o.d. 14.60 or 12.80 l = 150	Copper	0.6, 1.5	(Fin pitch = 0.50)		Rectangular	Surface thermocouples	0.6 - 37.9	111 - 190 kPa	At the highest U_v 70 - 80 % higher than a quiescent vapour case	Effect of vapour shear stress	Flooding angle was only slightly affected by vapour shear stress
Briggs et al. (1995)	steam R-113	i.d. 9.78 o.d. 12.7 l = 100	Copper Brass Bronze	0.5 - 1.6	0.25 - 0.75	1	Rectangular	Subtraction of resistances* (R-113 on bronze tubes), modified Wilson plot (others)	< 0.7 / steam < 0.2 / R-113	Little above atmospheric	$\varepsilon_{\Delta T}$ (steam, R-113) 2.6, 6.5 / Copper 2.0, 6.1 / Brass 1.7, 5.4 / Bronze	Effects of tube material, fin height and fin thickness	4 tubes for each material were tested
Das et al. (1995)	steam	i.d. 12.3 - 13.1 o.d. 13.6 - 14.2 l = 133.4	Copper Aluminium Cu-Ni*** SS****	0.4 - 1.51	1	1.5	Rectangular	modified Wilson plot	2 / vacuum 1 / atmospheric conditions	Atmospheric and vacuum conditions, i.e. 8.3 - 10.3 kPa	Best $\varepsilon_{\Delta T}$ = 2.5 with h = 1.4 mm for a copper tube	Effect of thermal conductivity of tube and pressure	Effect of thermal conductivity was revealed as follows (in order of high performance) Cu > Al > Cu-Ni[(2)] > SS[(3)]
Briggs and Rose (1995)	steam R-113	o.d. 18.8 - 19.4 l = 150	Copper	0.87 - 1.55	0.33 - 1.25	0.19 - 0.97	Trapezoidal	modified Wilson plot	1.2 / steam 0.4 / R-113	Little above atmospheric	$\varepsilon_{\Delta T}$ 2.5 - 3.3 / steam 3.0 - 7.7 / R-113	Accurate experimental data	7 commercially manufactured integral-fin tubes together with 2 Y- and 3 T- profile ones were tested.

Table 2.1 (continued).

Reference	Test fluid	Tube tested: Diameter / mm, Active length, l / mm	Tube tested: Material	Fin geometry: Height h / mm	Fin geometry: Thickness t / mm	Fin geometry: Interfin space b / mm	Fin geometry: Fin shape	Method of determination of surface temperature	Vapour approach velocity / (m/s)	Experimental conditions	Enhancement	Primary objective	Comment
Cheng et al. (1996)	R-22	i.d. 14.6, 13.7 o.d. 18.8		1.3, 1.42	0.17, 0.15	0.8, 0.46	Trapezoidal	Wilson plot	< 0.1	1.32, 1.47, 1.62 MPa	The lower pressure, the higher HTC	Further experimental results	4 popular enhanced surface tubes were also tested.
Jung et al. (1999)	R-11 R-12 R-123 R-134a	o.d. 18.9 l = 290	Copper	1.21	0.58	0.4	Trapezoidal	Surface thermocouples	Near stationary	T_s was set at 39 ℃	$\varepsilon_{\Delta T}$ 5.1 - 5.3 / R-11 6.0 - 6.3 / R-12 5.2 - 5.8 / R-123 4.9 - 5.1 / R-134a	Further experimental results of R-123 and R134a for alternative to R-11 and R-12	One Turbo-C tube was tested, having higher heat-transfer performance.
Kumar et al. (2000)	R-134a	o.d. 22.3 - 23.6 l = 417	Copper	0.6 - 0.8	0.43 - 0.94	0.1	Trapezoidal	Surface thermocouples	Near stationary	T_s was set at 312.4 ± 0.5 K	Best $\varepsilon_{\Delta T}$ = 5.6 with b = 0.69 mm	Experimental results with R-134a as a replacement for R-12	4 finned tubes were tested.
Namasivayam and Briggs (2004)	steam	i.d. 9.4 o.d. 12.7 l = 70	Copper	1.6	0.25	0.25, 0.5, 1.0, 1.5, 2.0	Rectangular	Subtraction of resistances* (using an instrumented smooth tube)	2.3 - 10.2	Little above atmospheric	Best $\varepsilon_{\Delta T}$ 2.5 / 1.6 with lowest / highest vapour velocity	Experimental data for forced-convection condensation of steam	5 finned tubes were tested.
Namasivayam and Briggs (2004)	E-G**	i.d. 9.4 o.d. 12.7 l = 70	Copper	1.6	0.25	0.25, 0.5, 1.0, 1.5, 2.0	Rectangular	Subtraction of resistances* (using an instrumented smooth tube)	11 - 22	approximately 15 kPa	Best $\varepsilon_{\Delta T}$ 2.5 / 2.7 with lowest / highest vapour velocity	Experimental data for forced-convection condensation of ethylene glycol	9 finned tubes were tested.

* Subtraction of resistances using predetermined coolant-side correlation

** Ethylene glycol

*** Copper-Nickel

**** Stainless steel

Table 2.2 Results for top tube of vertical in-line column of tubes tested and comparison with Nusselt (1916) theory, based on Marto and Wanniarachchi (1984) (Wire diameter 1.58 mm, coolant velocity 1.56 m/s, vapour velocity 0.5 to 1.0m/s.)

Tube		ΔT / K	α_{top} / (kW/m^{2}K)	$\left(\frac{\alpha_{top}}{\alpha_{Nu}}\right)_q$
smooth		21.2	11.1	1.02
smooth + wire (p / mm)	4	26.3	10.3	0.94
	8	24.7	11.3	1.05
	16	23.2	12.3	1.15
roped		29.5	11.4	1.16
roped + wire (p / mm)	8	32.6	9.9	0.99

Table 2.3 Values of constant m in Eq. (2-43) under inundation for different tubes tested during steam condensation, based on Marto and Wanniarachchi (1984). (Wire diameter 1.58 mm, coolant velocity 1.56 m/s, vapour velocity 0.5 to 1.0 m/s.)

Tube		m
smooth		0.154
smooth + wire (p / mm)	4	0.059
	8	0.039
	16	0.102
roped		0.183
roped + wire (p / mm)	8	0.039

Table 2.4 Top tube data for smooth and wire-wrapped tube columns (without inundation) during steam condensation, based on Brower (1985). (Coolant velocity 1.55 m/s, vapour velocity 1.4 to 2.1 m/s.)

Tube	Wire diameter / (mm)	Wire pitch / (mm)	α_{top} / (kW/m^{2}K)	$\left(\frac{\alpha_{top}}{\alpha_{Nu}}\right)_q$
smooth	0	0	12.6	1.19
	0.5	2.0	13.9	1.29
	0.5	4.0	15.8	1.50
	1.01	4.0	13.4	1.27
wire-	1.01	6.0	13.3	1.25
wrapped	1.01	8.0	12.9	1.22
	1.58	4.0	10.4	0.95
	1.58	7.6	11.4	1.05
	1.58	16.0	12.3	1.15

Table 2.5 Values of constant m in Eq. (2-43) under inundation for wire combinations tested during steam condensation, based on Brower (1985). (Coolant velocity 1.55 m/s, vapour velocity 1.4 to 2.1 m/s.)

Tube	Wire diameter / (mm)	Wire pitch / (mm)	m
smooth	0	0	0.183
	0.5	2.0	0.061
	0.5	4.0	0.082
	1.01	4.0	0.024
wire-	1.01	6.0	0.034
wrapped	1.01	8.0	0.055
	1.58	4.0	0.017
	1.58	7.6	0.012
	1.58	16.0	0.097

Table 2.6 Relation between condensate film appearance and ethanol vapour mass fraction during condensation of steam-ethanol mixtures, based on Fujii et al. (1989).

Ethanol vapour mass fraction range	Condensation mode
0	smooth-film
0.02 – 0.20	smooth-film
0.20 – 0.40	drop
0.52 – 0.65	drop and streak
0.75 – 0.78	ring
0.85	smooth-film
1	smooth-film

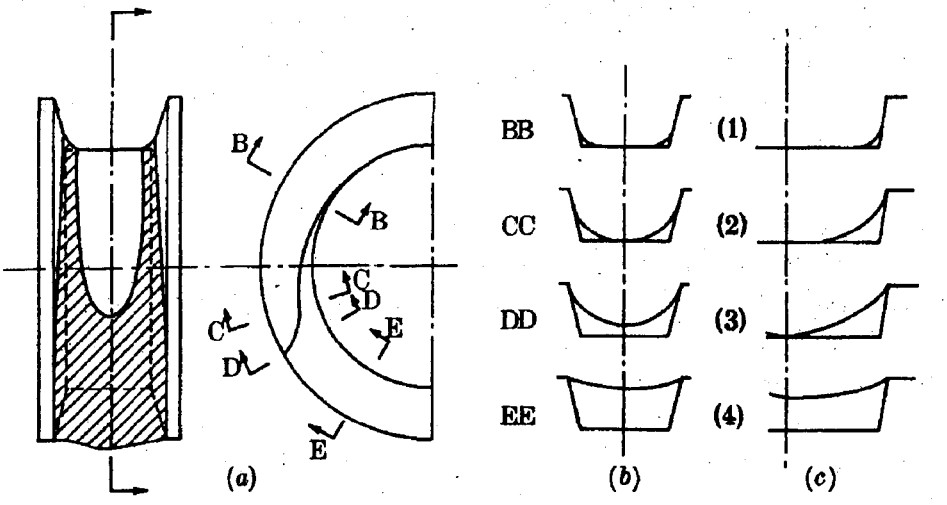

Fig. 2.1. Configuration of retained liquid for low integral-finned tubes by Masuda and Rose (1987).

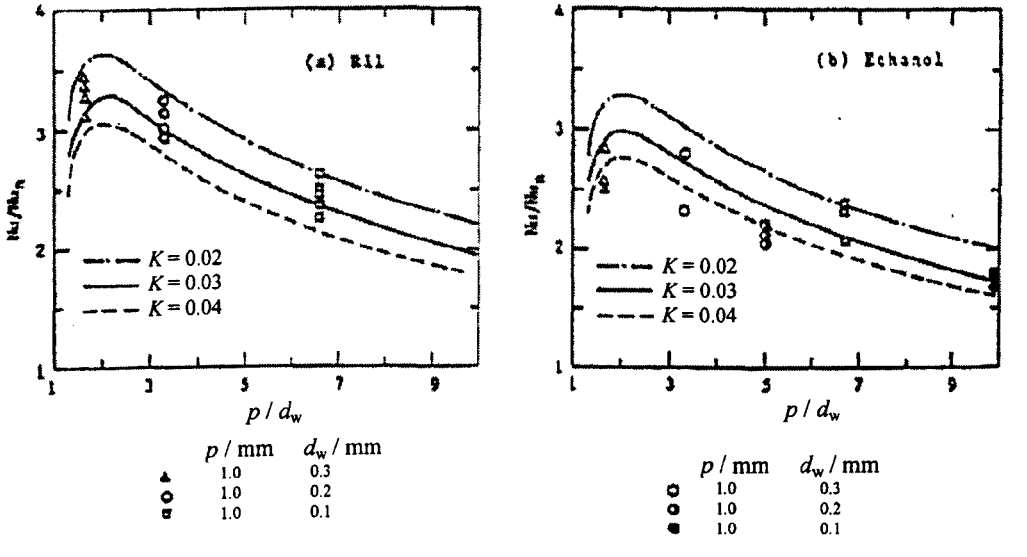

Fig. 2.2. Relation between heat-transfer enhancement ratio and wire pitch-to-diameter ratio, based on Fujii et al. (1985). (Lines were calculated using Eqs. (2-22) and (2-25) to (2-27) with dimensionless constants, K.)

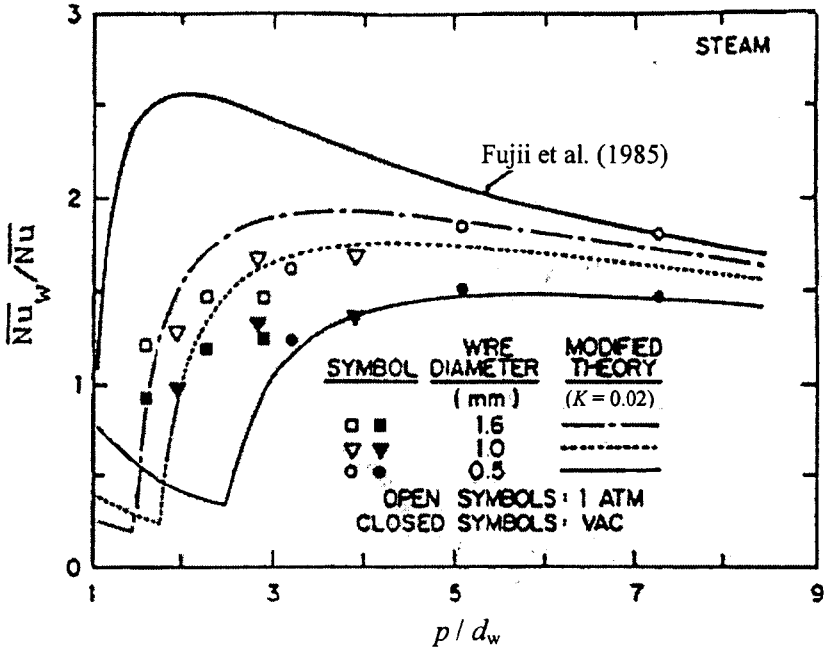

Fig. 2.3. Relation between enhancement ratio and wire pitch-to-diameter ratio, based on modified model of Marto et al. (1987) with K = 0.02. (Line for Fujii et al. (1985) was calculated with K = 0.03.)

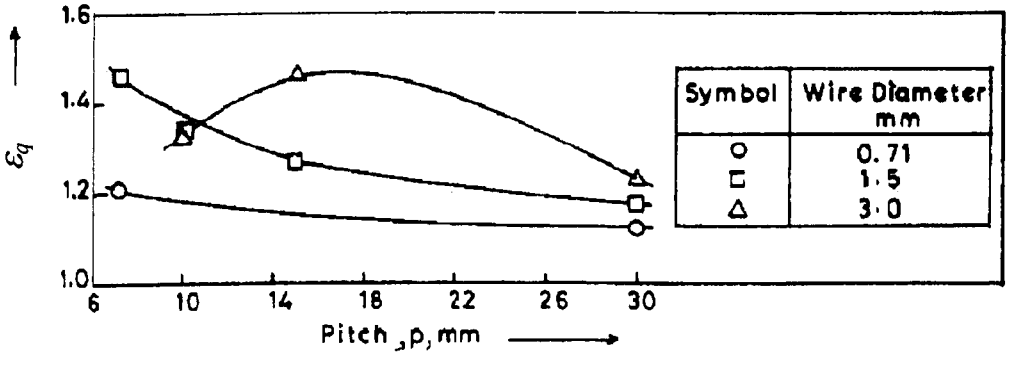

Fig. 2.4. Relation between enhancement ratio and wire pitch, based on Sethumadhavan and Rao (1985).

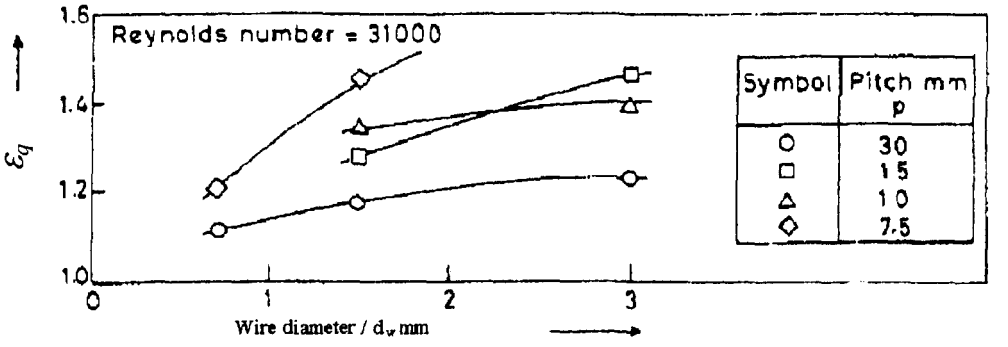

Fig. 2.5. Relation between enhancement ratio and wire diameter, based on Sethumadhavan and Rao (1985).

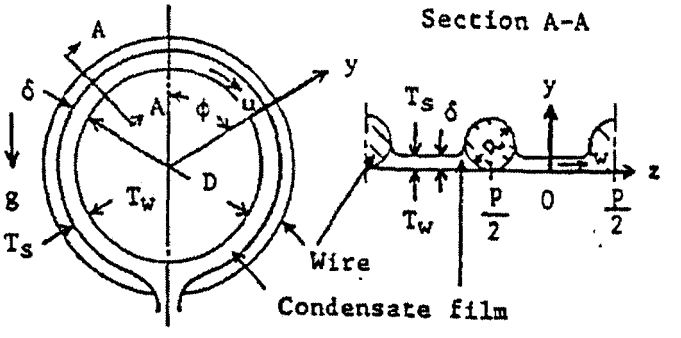

Fig. 2.6. Simplified model of condensate film by Fujii et al. (1985).

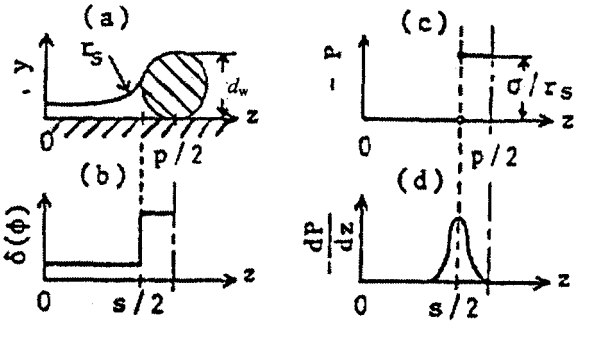

Fig. 2.7. Physical coordinates for model of Fujii et al. (1985).

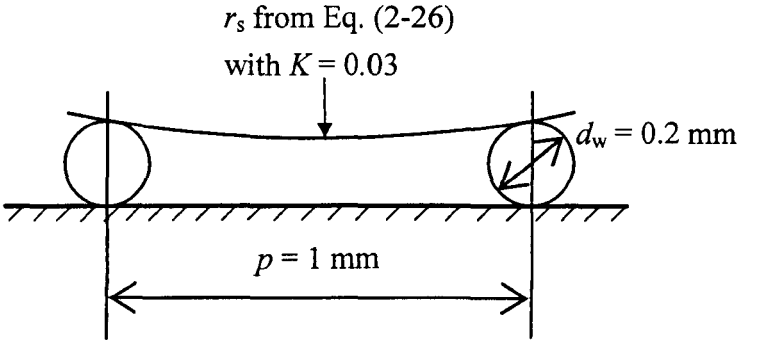

Fig. 2.8. Example of geometry incompatibility in Fujii et al. (1985) theory (R-11, d = 18 mm, saturation pressure 1.02 bar, saturation temperature 24 °C), from Murase et al. (2005).

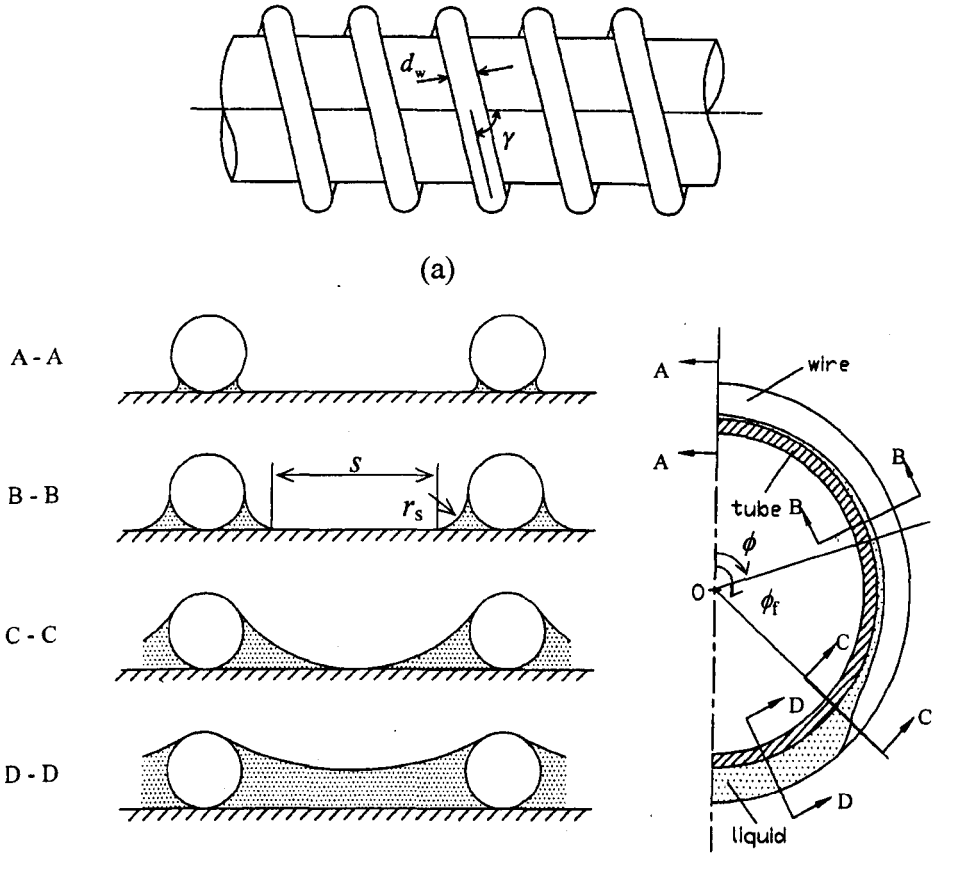

Fig. 2.9. Model and coordinate for wire-wrapped tube and capillary retention by Rose (2002).

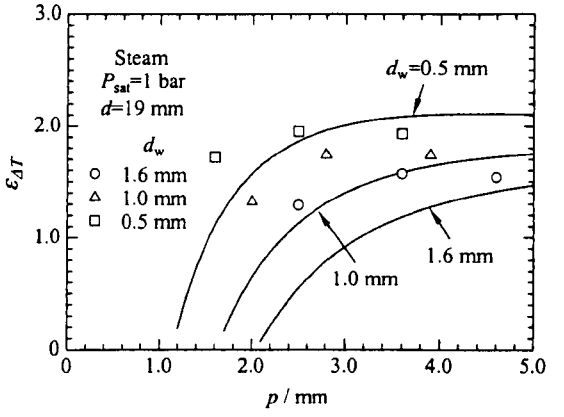

Fig. 2.10. Comparison of model of Rose (2002) with atmospheric pressure steam data of Marto et al. (1987) for dependence of enhancement ratio on pitch, from Rose (2002).

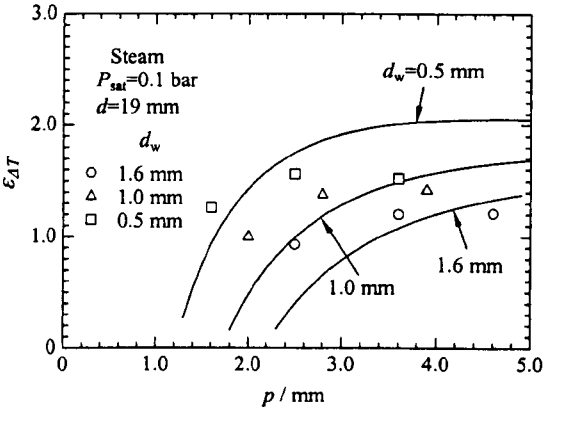

Fig. 2.11. Comparison of model of Rose (2002) with low pressure steam data of Marto et al. (1987) for dependence of enhancement ratio on pitch, from Rose (2002).

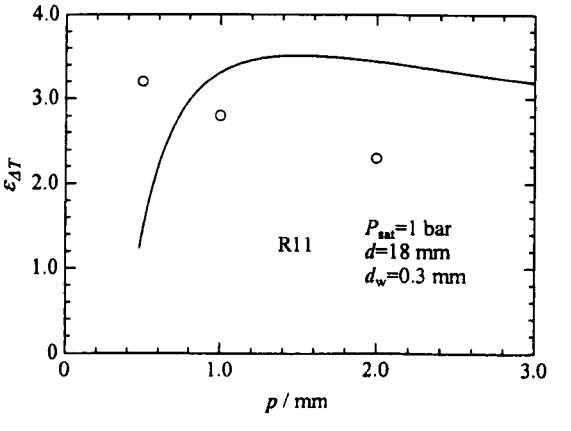

Fig. 2.12. Comparison of model of Rose (2002) with R-11 data of Fujii et al. (1985) for dependence of enhancement ratio on pitch, from Rose (2002).

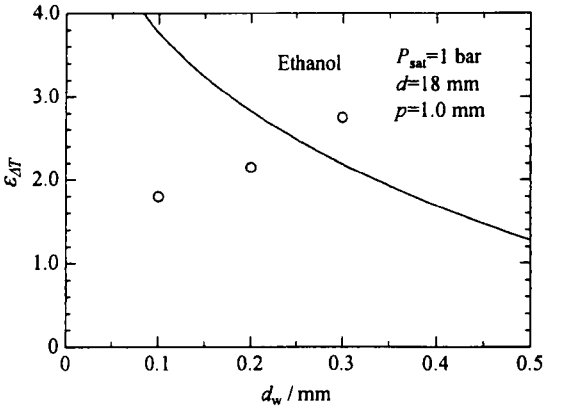

Fig. 2.13. Comparison of model of Rose (2002) with R-11 data of Fujii et al. (1985) for dependence of enhancement ratio on wire diameter, from Rose (2002).

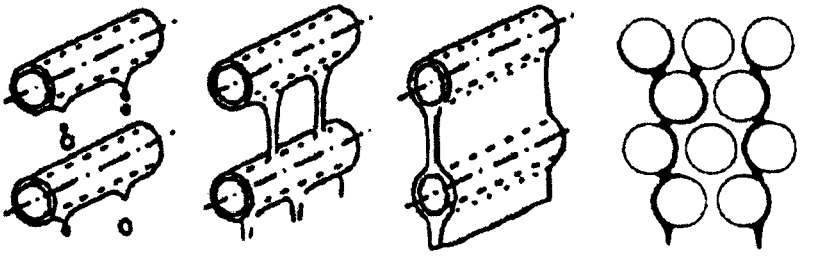

(a) (b) (c) (d)

Fig. 2.14. Schematic representations of condensate drainage in-line horizontal smooth tube bank, (a), (b) and (c), from Honda (1997), and in staggered horizontal smooth tube bank, (d), based on Marto (1984).

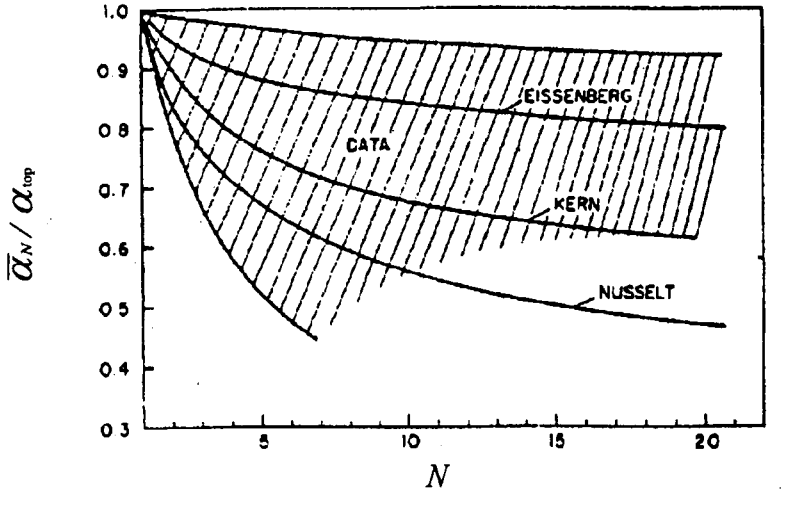

Fig. 2.15. Schematic representation of uncertainty between theory and experiment during condensation with inundation, from Marto (1984).

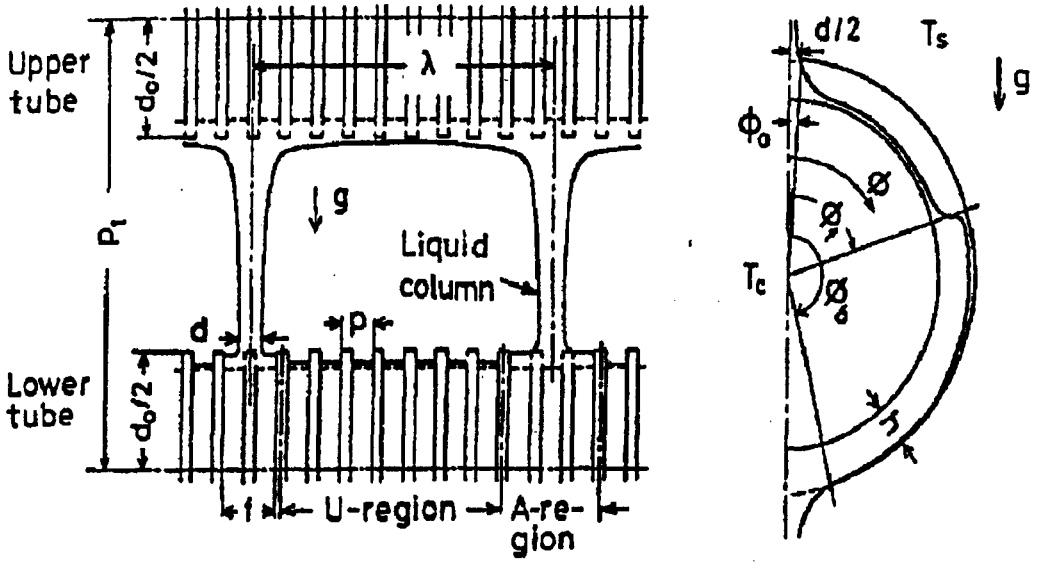

Fig. 2.16. Model of condensate drainage in column of horizontal finned tubes, from Honda et al. (1989).

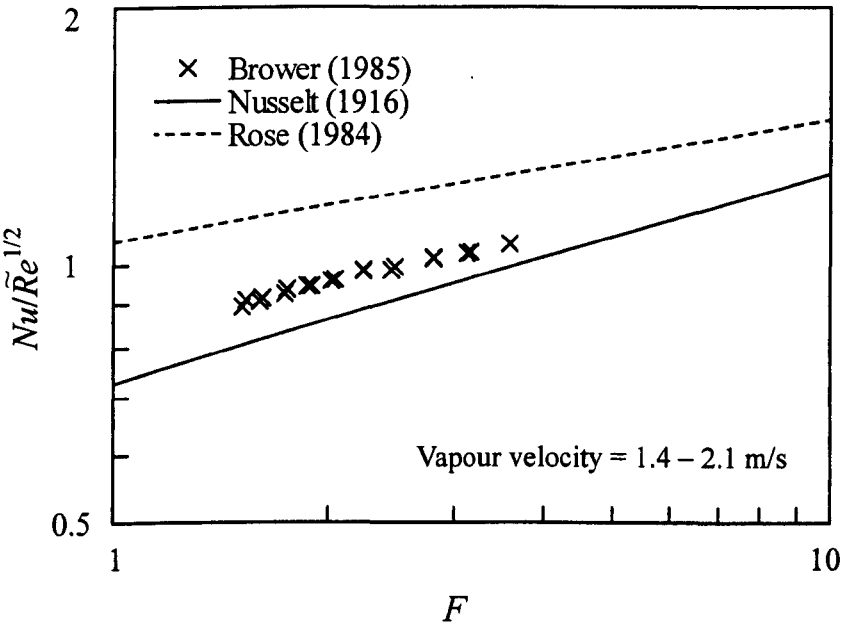

Fig. 2.17. Comparison of Brower (1985) data for top tube of smooth tube column with Rose (1984) and Nusselt (1916) prediction, based on Brower (1985).

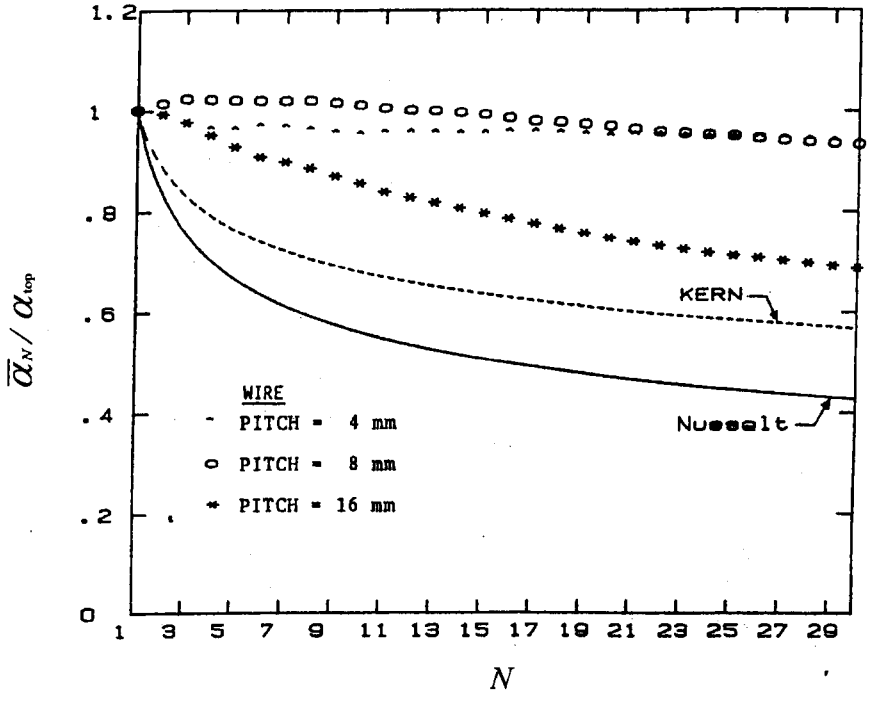

Fig. 2.18. Experimental data for condensate inundation effect on wire-wrapped tube column for wire diameter of 1.6 mm with different pitches, based on Brower (1985).

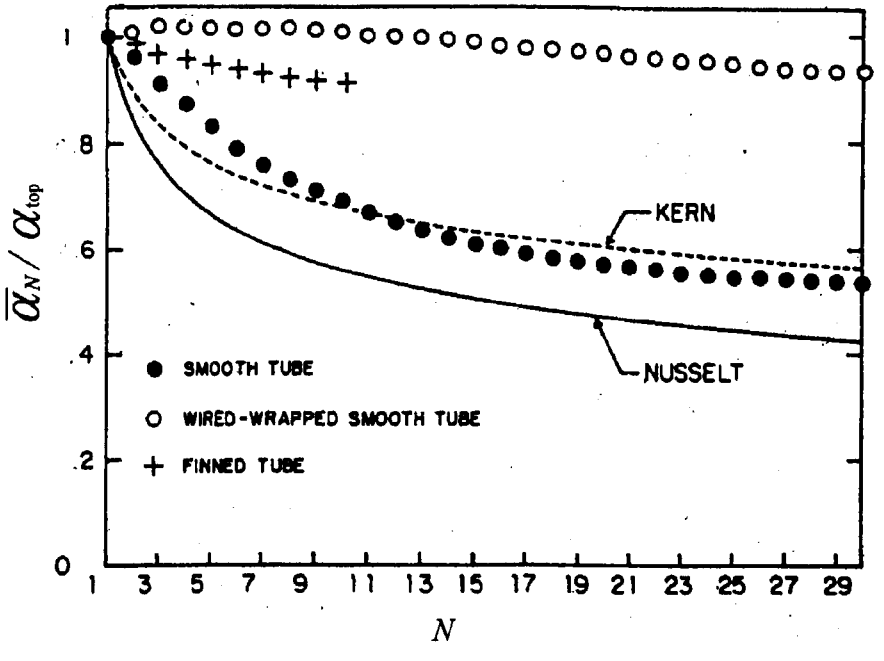

Fig. 2.19. Comparison for effect of condensate inundation during steam condensation on columns of smooth, finned and wire-wrapped tubes, based on Marto (1986).

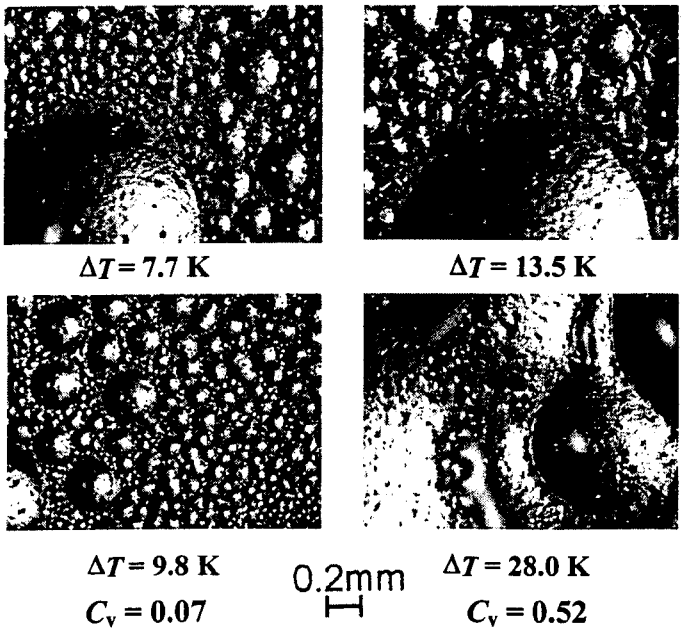

Fig. 2.20. Appearance of condensate film on vertical flat plate during condensation of steam-ethanol mixtures, based on Utaka et al. (1998). C_v denotes ethanol vapour mass fraction.

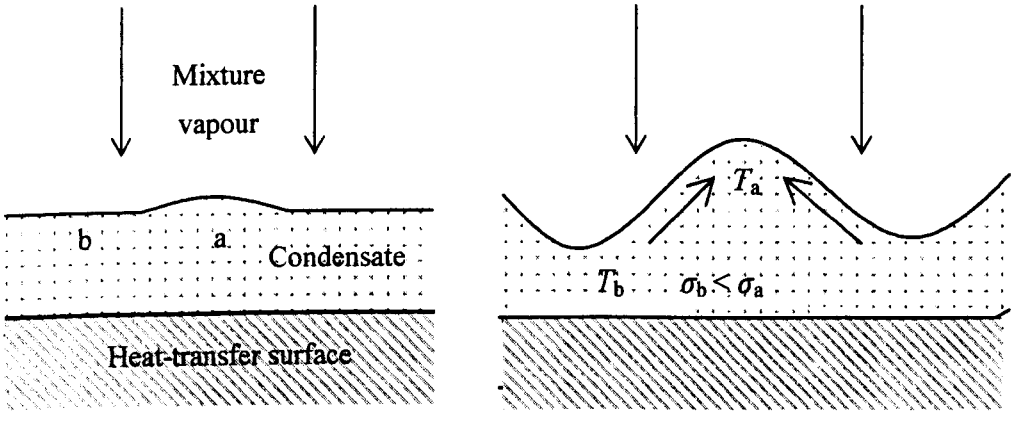

Fig. 2.21. Model of developing pseudo-dropwise condensation mode during Marangoni condensation of mixtures. σ denotes surface tension.

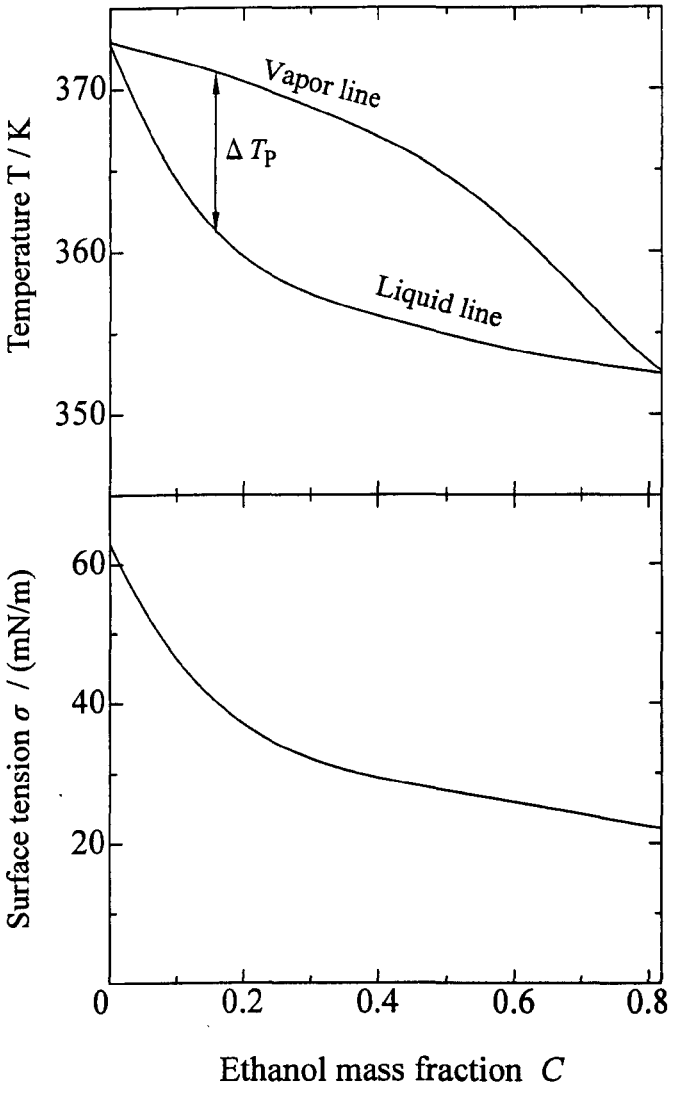

Fig. 2.22. Vapour-liquid equilibrium phase diagram and variation of surface tension of water-ethanol mixture, from Wang (2002). ΔT_p is the temperature difference between vapour and liquid lines at the same mixture composition under phase equilibrium.

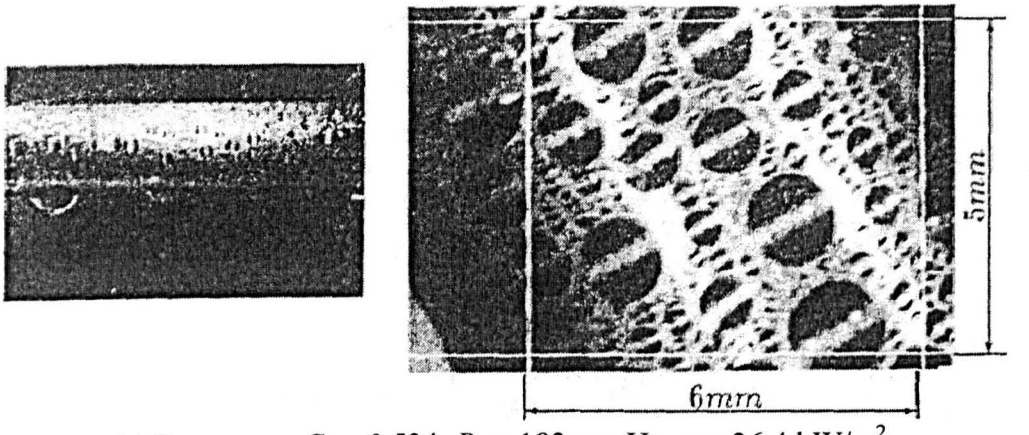

(a) Drop: $C_v = 0.534$, $P_v = 183$ mmHg, $q = 36.4$ kW/m^2

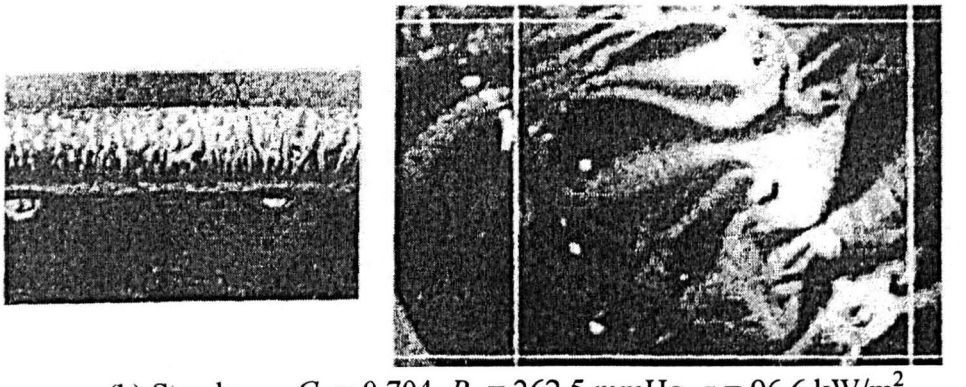

(b) Streak: $C_v = 0.704$, $P_v = 262.5$ mmHg, $q = 96.6$ kW/m^2

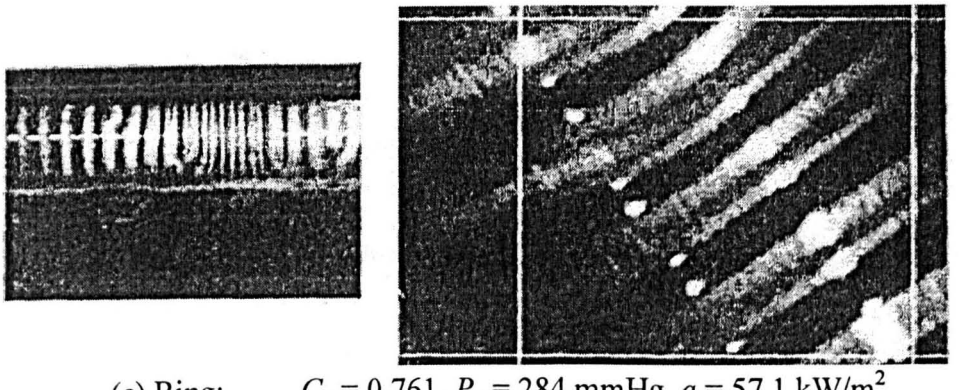

(c) Ring: $C_v = 0.761$, $P_v = 284$ mmHg, $q = 57.1$ kW/m^2

Fig. 2.23. Appearance of condensate film on smooth horizontal tube during condensation of steam-ethanol mixtures, based on Fujii et al. (1993). C_v denotes ethanol vapour mass fraction.

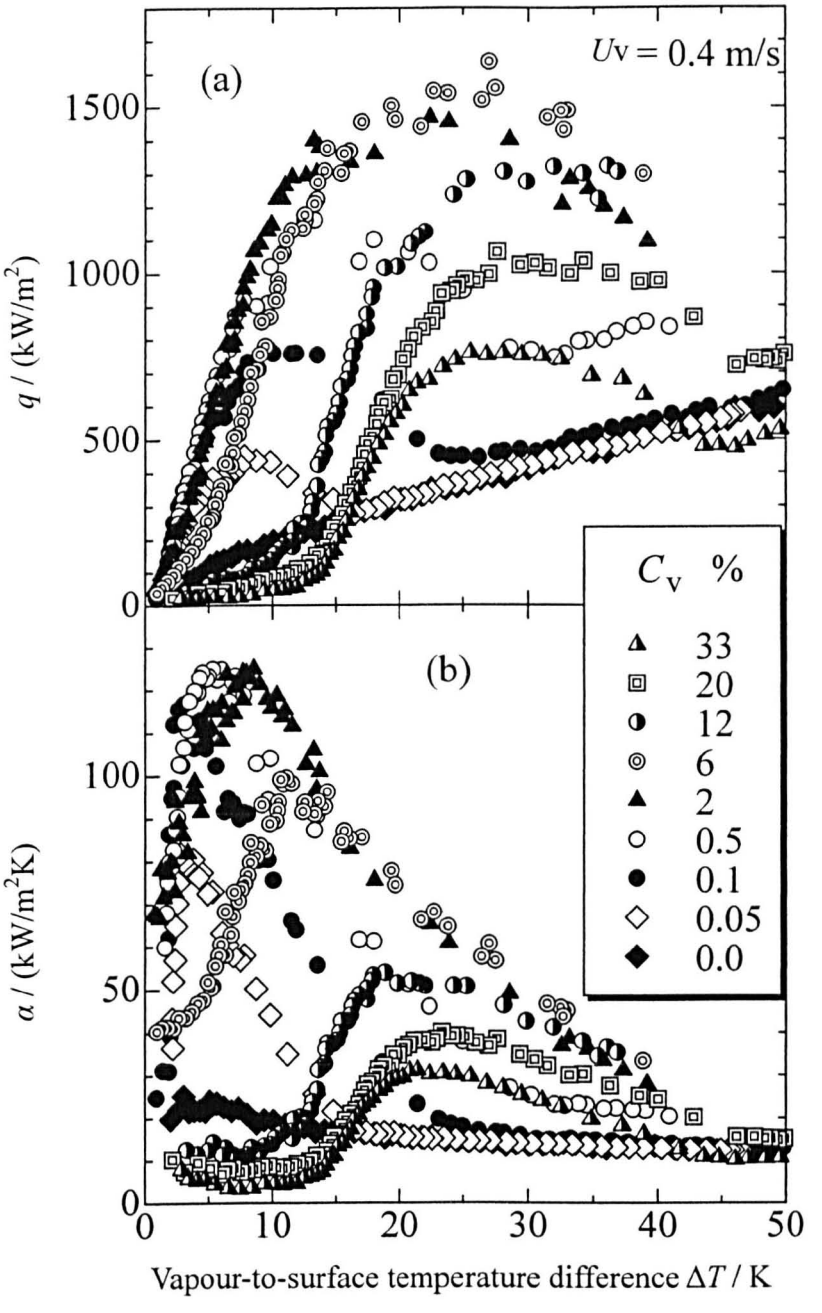

Fig. 2.24. Condensation of steam-ethanol mixtures on vertical flat plate for various ethanol vapour mass fractions at 0.4 m/s vapour velocity, based on Utaka and Wang (2004). C_v denotes ethanol vapour mass fraction.

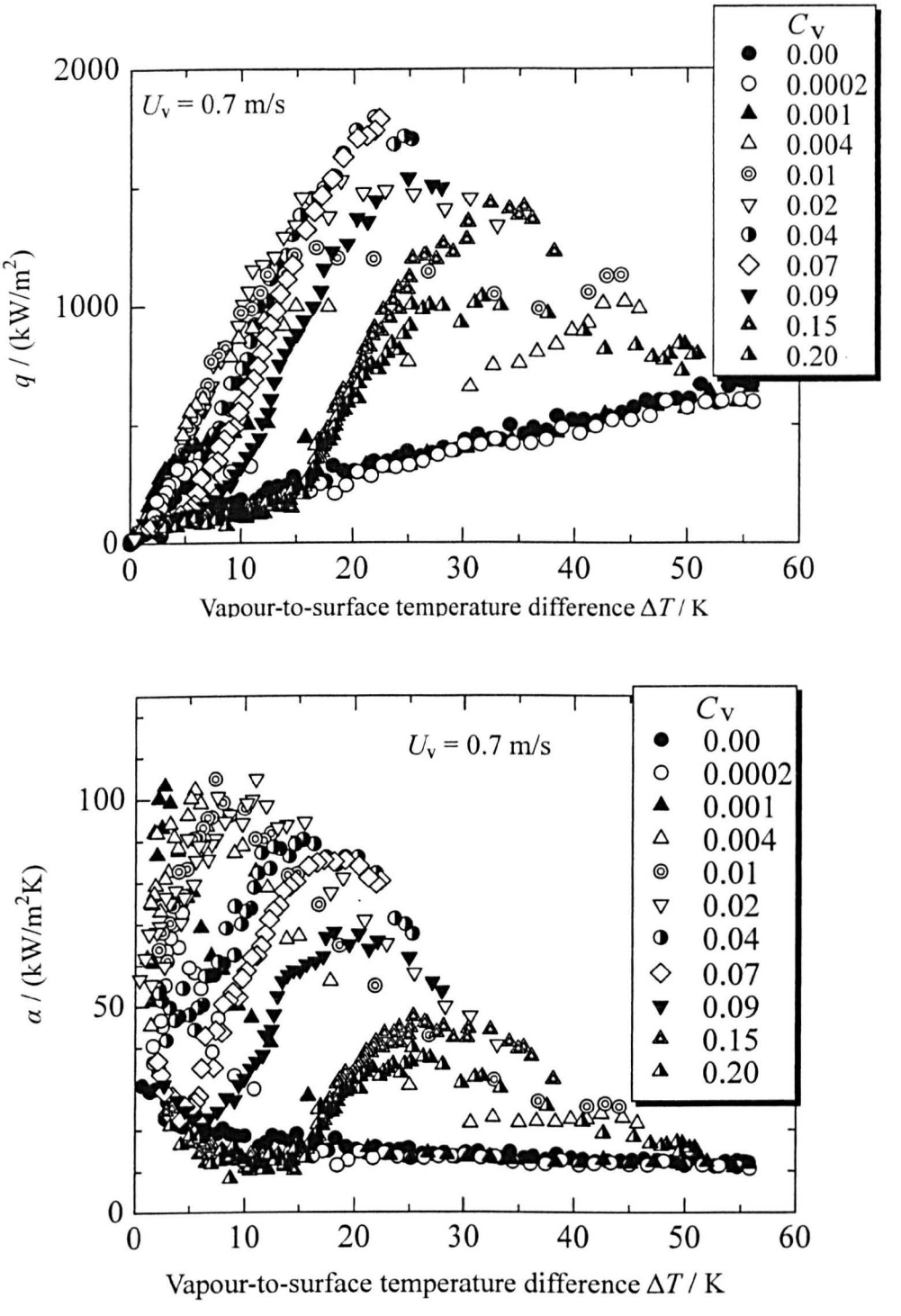

Fig. 2.25. Condensation of steam-ethanol mixtures on vertical flat plate for various ethanol vapour mass fractions at 0.7 m/s vapour velocity, based on Utaka and Wang (2001). C_v denotes ethanol vapour mass fraction.

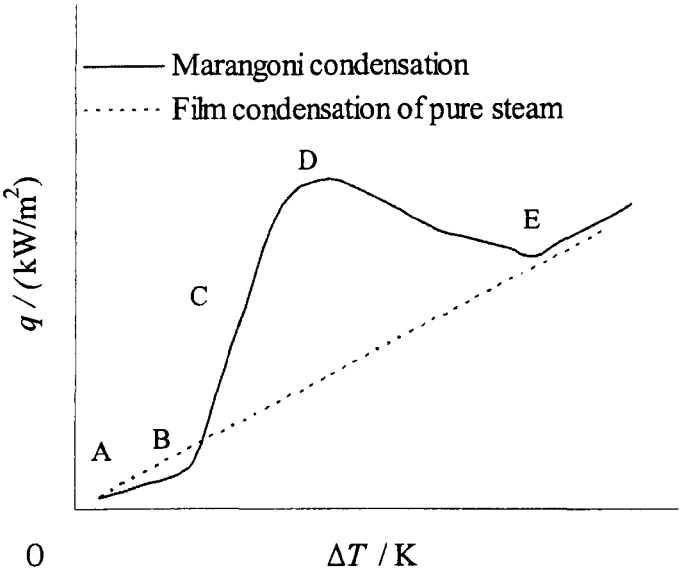

(a) Heat flux

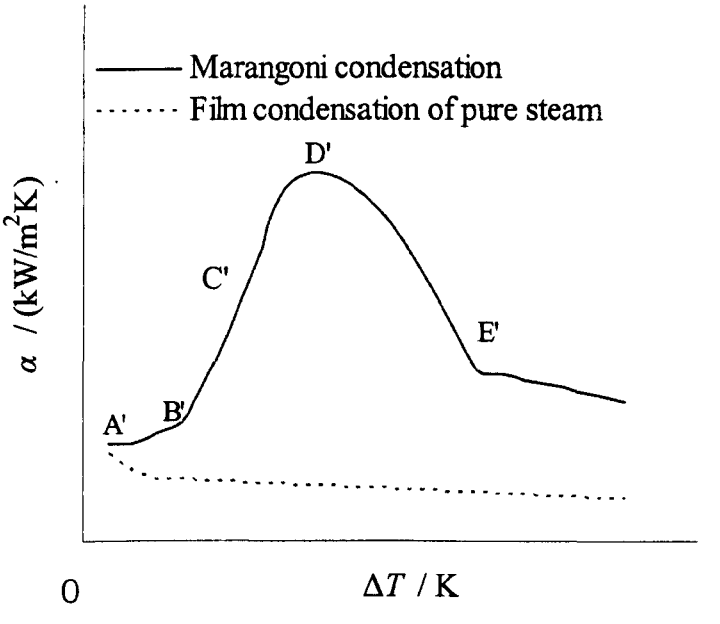

(b) Heat-transfer coefficient

Fig. 2.26. Comparison of typical experimental data between Marangoni condensation of steam-ethanol mixtures and condensation of pure steam on vertical flat plate, based on experimental data of Utaka and co-workers.

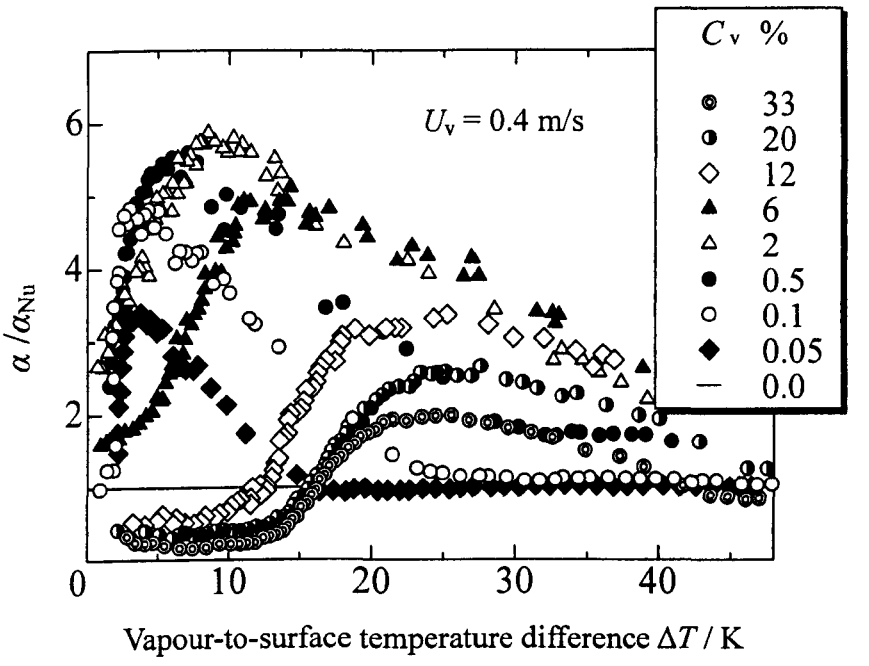

Fig. 2.27. Heat-transfer enhancement ratio during Marangoni condensation on vertical flat plate (steam-ethanol mixtures / pure steam), based on Utaka and Wang (2004). C_v denotes ethanol vapour mass fraction.

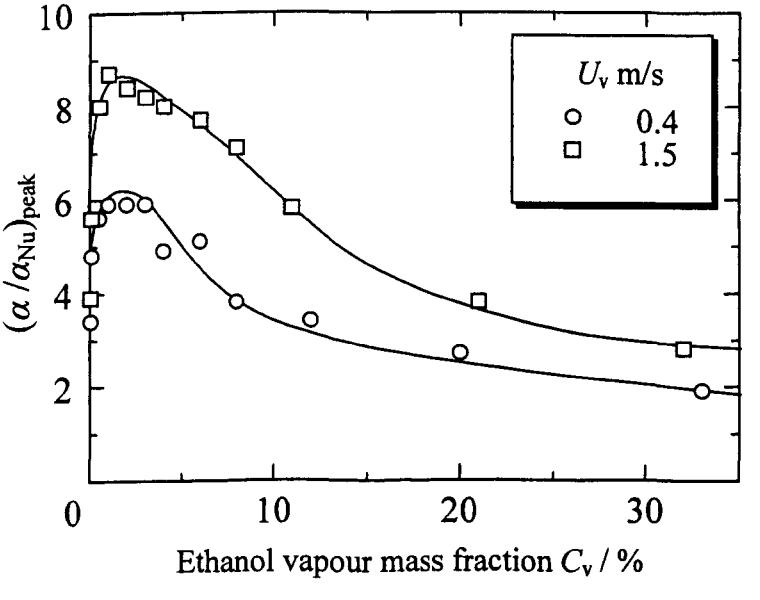

Fig. 2.28. Variation of peak enhancement ratio for ethanol vapour mass fraction, based on Utaka and Wang (2004).

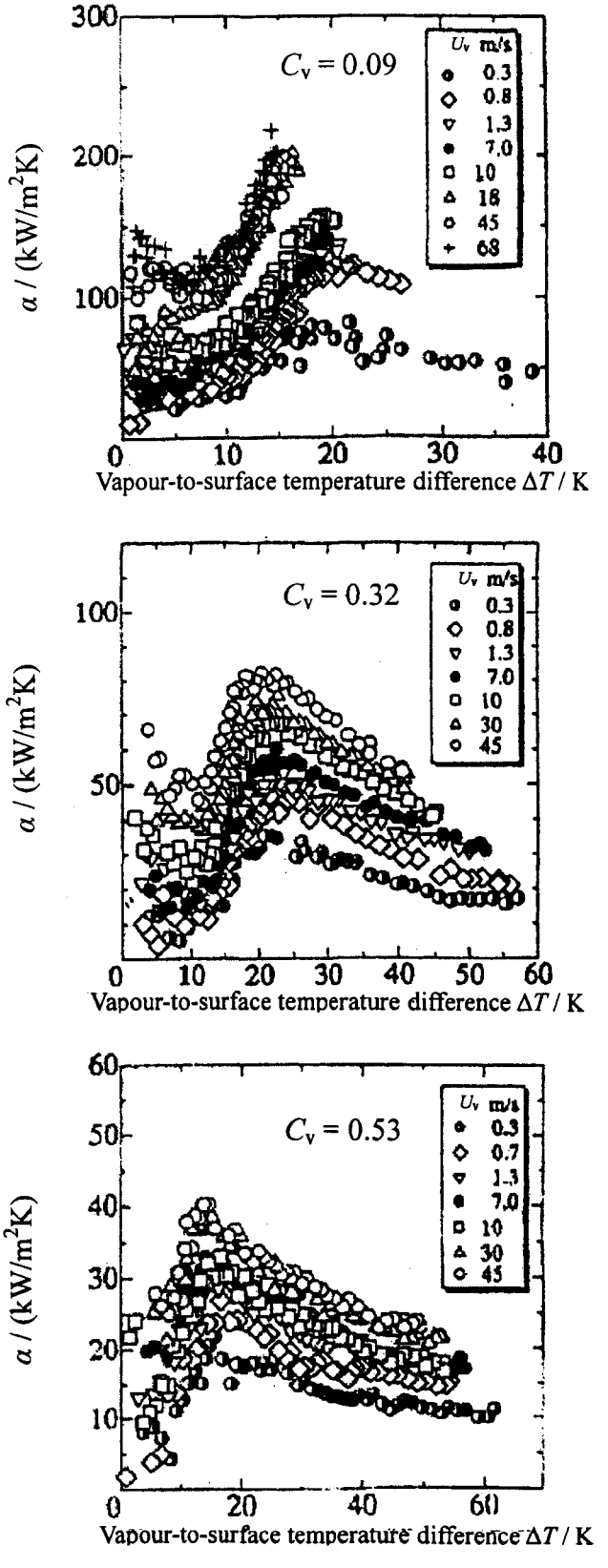

Fig. 2.29. Dependence of vertically downward vapour velocity on Marangoni condensation heat transfer of steam-ethanol mixtures at fixed ethanol vapour mass fraction, based on Utaka and Kobayashi (2003). C_v denotes ethanol vapour mass fraction.

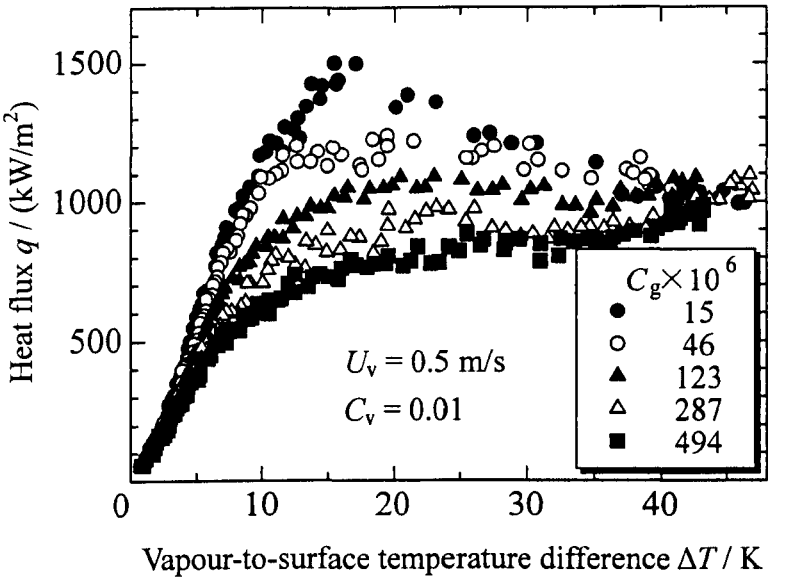

(a) Heat flux

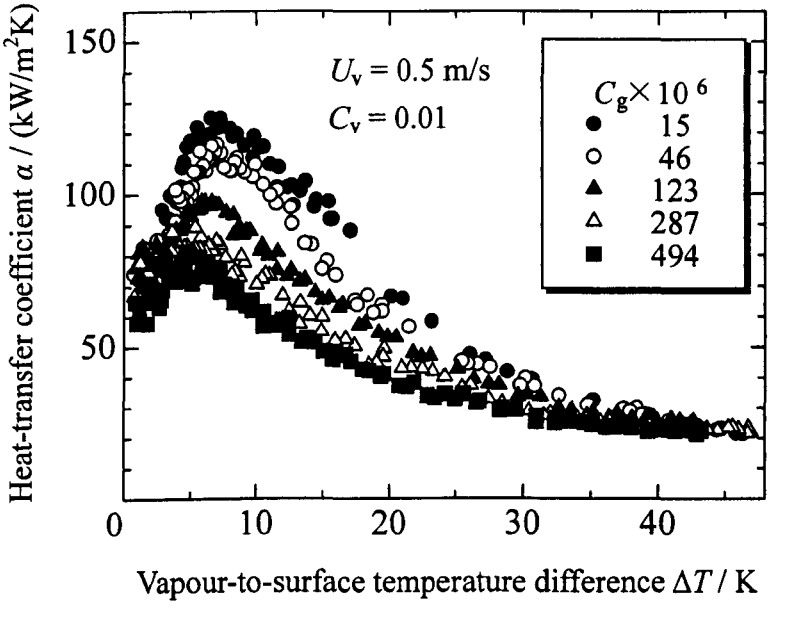

(b) Heat-transfer coefficient

Fig. 2.30. Dependence of non-condensing gas on Marangoni condensation heat transfer of steam-ethanol mixtures (U_v = 0.5 m/s, C_v = 0.01), based on Utaka and Wang (2005). C_v and C_g denote mass fractions of ethanol vapour and non-condensing (nitrogen) gas respectively.

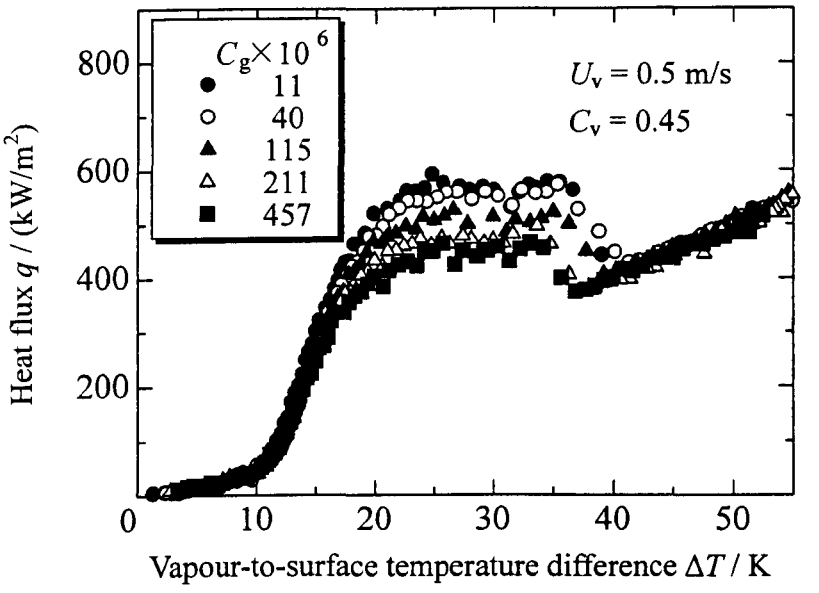

(a) Heat flux

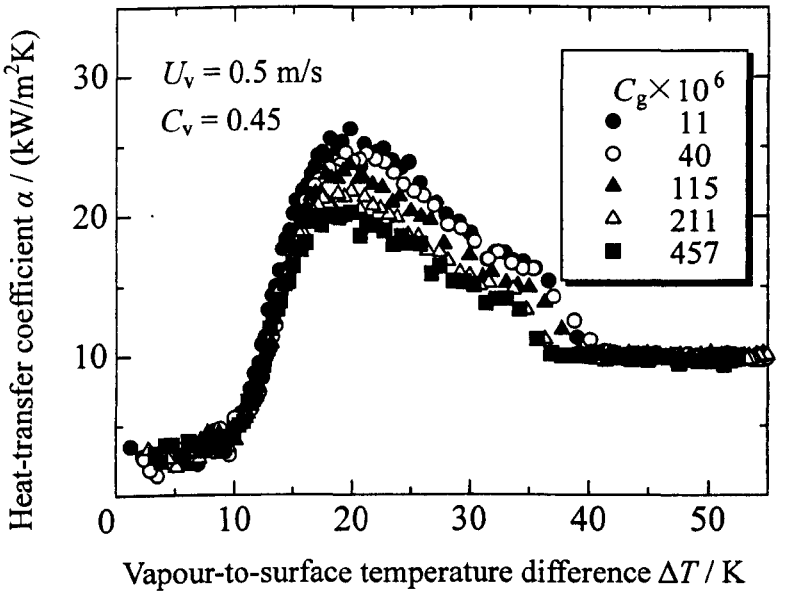

(b) Heat-transfer coefficient

Fig. 2.31. Dependence of non-condensing gas on Marangoni condensation heat transfer of steam-ethanol mixtures (U_v = 0.5 m/s, C_v = 0.45), based on Utaka and Wang (2005). C_v and C_g denote mass fractions of ethanol vapour and non-condensing (nitrogen) gas respectively.

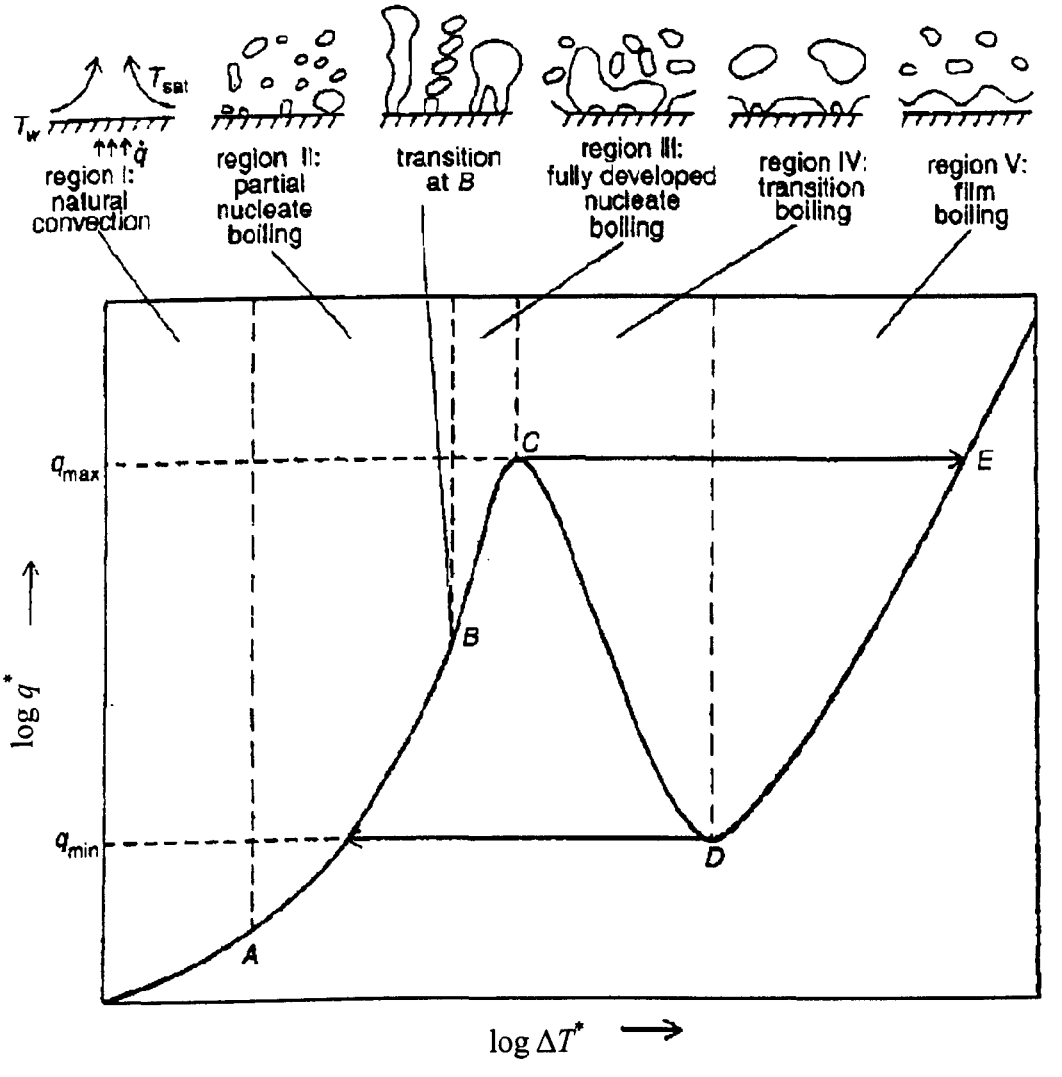

Fig. 2.32. Typical boiling curve for pure fluid, dependence of boiling heat flux on liquid-to-surface temperature difference and boiling process, based on Vijay (1999).

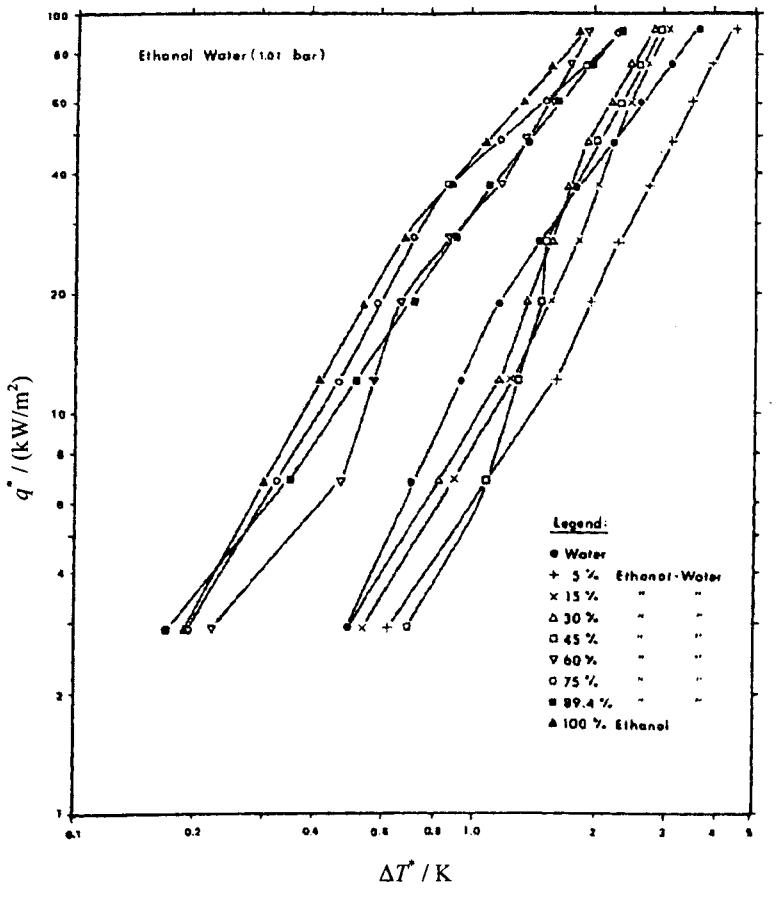

Fig. 2.33. Relation between boiling heat flux and liquid-to-surface temperature difference during nucleate boiling of water-ethanol mixtures on enhanced heat-transfer surface, base on Ali and Thome (1984).

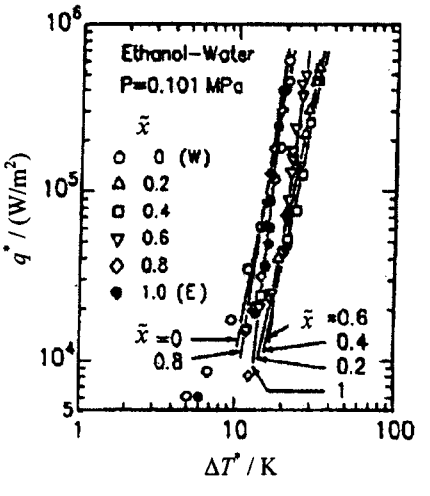

Fig. 2.34. Relation between boiling heat flux and liquid-to-surface temperature difference during nucleate boiling of water-ethanol mixtures on horizontal copper plate, based on Fujita and Tsutsui (1994). $\tilde{x}$ denotes the ethanol liquid mole fraction.

Chapter 3

Aim and scope of the present investigation

3.1 Condensation on wire-wrapped tubes

The phenomenon of condensation heat transfer on a wire-wrapped tube is not fully understood. This is due to the limited quantities of experimental data and lack of satisfactory theoretical analysis. Earlier investigations indicated that for fixed tube and wire diameters there is an optimum pitch of winding. Only a few and conflicting data are available for condensation of steam with inundation on wire-wrapped tubes. It has been reported that wire-wrapped tubes perform better than low integral-finned tubes under inundation conditions for steam condensation; this seems unlikely and at least unexpected. The aims of the present investigation are:

1. to provide new, accurate data for condensation heat transfer on a wire-wrapped tube with three test fluids, steam, R-113 and ethylene glycol, so as to cover a wider range of fluid properties.

2. to establish optimum combinations of wire diameter and pitch of winding.

3. to compare the new data with existing theories.

4. to provide new, accurate data for condensation of steam with inundation on smooth, wire-wrapped and low integral-finned tubes using artificial (simulated) inundation.

3.2 Marangoni condensation of steam-ethanol mixtures

No systematic experimental investigation has been conducted for Marangoni condensation of steam-ethanol binary mixtures on a horizontal tube covering a wide range of the vapour-to-surface temperature difference. Referring to the experimental data of Utaka and co-workers for a small vertical heat-transfer surface, low ethanol vapour mass fractions gave high condensation heat-transfer enhancement. In case small amounts of ethanol might in future be used in power plant to enhance the condenser performance it was thought desirable to also investigate the effect of small concentrations of ethanol on the boiler performance. The aims of the present investigation are:

1. to provide new data for Marangoni condensation of steam-ethanol mixtures on a horizontal tube with small ethanol mass fractions and vapour velocities covering a wide range of vapour-to-surface temperature difference.

2. to compare the effect of the heat-transfer surface geometry difference (horizontal tube versus vertical plate).

3. to provide new data for nucleate boiling of water-ethanol mixtures with small ethanol mass fractions.

Chapter 4

Condensation on wire-wrapped tubes

4.1 Single tube investigation

To provide new, accurate data for condensation heat transfer on a wire-wrapped tube, experiments were conducted using three test fluids, R-113, ethylene glycol and steam, so as to cover a wider range of fluid properties. Fluid, wire diameter and pitch of winding were varied systematically.

4.1.1 Apparatus and instrumentation

The stainless-steel test apparatus, shown schematically in Fig. 4.1, consisted of a loop, with test vapour (R-113, ethylene glycol or steam) generated in an electrically-heated boiler (maximum power about 12 kW). A sight glass was fitted to the boiler to indicate the liquid level. The vapour was directed vertically downward through a calming section before flowing over the horizontal, water-cooled, test condenser tube. A glass manometer filled with the test liquid was used to measure test section gauge pressure. Details of the test section are shown in Fig. 4.2. Nylon bushes were located at both inlet and exit of the test tube to insulate the test tube from the body of the test section and from the environment. A PTFE (polytetrafluoroethylene) mixing chamber was located immediately after the exit nylon bush to ensure good mixing and sufficient isothermal immersion of the thermocouple leads in the vicinity of the junctions. Excess vapour was condensed in two auxiliary condensers below the test section and all condensate was returned to the boiler by gravity. Coolant was supplied via a float-type flow meter to the test tube and to the auxiliary condensers. The test apparatus between the boiler and the test section was thermally well insulated.

K-type (nickel-chromium/nickel-aluminium) thermocouples and thermopile were used for temperature measurements. All thermocouples were calibrated in a high precision constant temperature bath against a platinum resistance thermometer.

The calibration procedure is described in Appendix B. The coolant temperature rise through the test tube was measured both by thermocouples at the inlet of the test tube and the exit of the mixing chamber and more accurately using a ten-junction thermopile. The wiring arrangement of the ten-junction thermopile is shown in Fig. 4.3. The thermocouple reference and lead junctions were immersed in an ice bath (see Fig. 4.4), and connected via a selector switch to a digital voltmeter (Agilant 34401 with the resolution of 1 μV).

All experiments were performed using the same copper tube (12.2 mm outside diameter, 8.35 mm inside diameter and 275 mm total length) which was fitted with four embedded wall thermocouples located as shown in Fig. 4.5. Four equi-spaced slots, 0.5 mm square, were machined axially along the outer surface. Thermocouples were inserted in the slots and their junctions soldered midway along the tube. Close-fitting copper strips were soldered in the grooves over the thermocouple leads and the outer surface turned smooth. The tubes were then thinly copper plated. When inserted in the test section, the tubes were oriented so that the positions of the thermocouples were at angles of 22.5°, 112.5°, -157.5° and -67.5° measured from the top of the tube. For the unwrapped tube tests a 100 mm length of tube was exposed to the condensing vapour and 90 mm for the wire-wrapped tube. This difference of active heat-transfer length was due to stainless-steel collars required to fix the wire at both ends of the test tube. PTFE sleeves were inserted at both ends of the tube so that the cooled length of the tube was the same as that exposed to vapour in both cases. Steel wires having diameters of 0.2, 0.35, 0.4, 0.75 and 1.0 mm were wound, in turn, tightly (but not soldered) on the outside surface with winding pitches ranging from values a little larger than the wire diameter in each case up to 6.0 mm for R-113 and steam and up to 4.5 mm for ethylene glycol. Uniformity of the spacing was judged by eye. Photographs of wire-wrapped tubes tested are shown in Fig. 4.6.

To ensure filmwise condensation the following procedure were always done before installation of the test tube. The tube and nylon bushes were first wiped using a clean cloth and rinsed with distilled water. They were then cleaned by immersing for a few minutes in the following mixture:

2000 ml	distilled water (H_2O)
100 ml	sulphuric acid (H_2SO_4)
200 g	sodium dichromate ($Na_2Cr_2O_7$)

While immersed, the tube was agitated to ensure that all air bubbles were removed so that the solution came into contact with all parts of the tube and wire surfaces. The tube was then rinsed with distilled water and dried by air blown from an airline fitted with an oil filter. Finally, the tube and the bushes were rinsed with the operating fluid and carefully installed in the test section.

4.1.2 Experimental procedure

Prior to measurements, in the case of experiments with steam, vapour was vented to atmosphere through the manometer for at least 5 minutes to eliminate air from the apparatus. For other fluids, the apparatus was left for a longer time (more than an hour) to eliminate air in the test section. Also the number of operative boiler heaters was varied so as to vary the vapour approach velocity over the test tube and no change of surface temperature was confirmed. By varying the coolant flow rate, heat flux and vapour-to-surface temperature difference were varied. Normally it took about 7 minutes for the condition in the test section to become steady after varying the coolant flow rate. At first the coolant flow rate was set to the maximum at around 20 l/min, and was subsequently reduced in steps to 3 l/min. The experiments were then repeated in ascending order of the coolant flow rate.

During experiments, the ambient temperature and pressure, test section gauge pressure, coolant flow rate, vapour temperature in the test section, coolant inlet and exit temperatures, coolant temperature rise, test tube wall temperatures and condensate temperature returning to the boiler were measured. Visual observations of the condenser tube were also made through the Pyrex glass window in the test section to confirm filmwise condensation. When necessary, a hot air blower was used on the outside surface to clear condensate from the window for the observation. This is the most important during steam condensation which is more susceptible to dropwise condensation due to impurities. Filmwise condensation was observed on

all occasions.

4.1.3 Determination of experimental parameters

The atmospheric pressure, P_{atm} in mmHg, was measured by Fortin barometer located in the laboratory. The manufacturer tabulated values for the temperature correction were given to within 0.025 mmHg by the following equation:

$$P_{atm} = P_B - \left[0.015 + \left(1.6229T_B - 0.01188\right) \times 10^{-4} P_B\right] \quad (4\text{-}1)$$

where T_B is the reading of absolute temperature measured by a thermometer fitted on the barometer in K and P_B is the pressure given by the barometer in mmHg.

The vapour pressure in the test section, P_v, was obtained using the atmospheric pressure and gauge pressure measured using the manometer filled with test fluid used:

$$P_v = P_{atm} + g\rho_{tf}\left(H_2 - H_1\right) \quad (4\text{-}2)$$

where ρ_{tf} is the density of the test fluid (in the manometer) and H_1 and H_2 are the levels of the fluid in the chamber-side and atmosphere-side of manometer respectively.

The input power to the boiler, Q_b, was obtained using the following equation:

$$Q_b = \sum_{i=1}^{4}\left(\frac{V_i^2}{R_i}\right) \quad (4\text{-}3)$$

where V_i is the potential difference across the terminals of i^{th} heater, and R_i is the resistance of i^{th} heater as shown in Table 4.1.

Temperatures were measured by K-type thermocouples. The details for the

calibration procedure are reported in Appendix B. The calibration data were fitted by the following equation:

$$T = 273.15 + 2.563\times10^{-2}E - 4.066\times10^{-7}E^2 - 6.973\times10^{-12}E^3 + 1.325\times10^{-14}E^4 - 9.704\times10^{-19}E^5 \quad (4\text{-}4)$$

where E is the thermo-e.m.f. in μV and T is the thermodynamic temperature in K.

The coolant temperature rise was measured by two separate methods, namely using separate thermocouples and using the ten-junction thermopile, as described in Section 4.1.1. In the both methods a small predetermined correction (dependent on coolant flow rate) for the dissipative temperature rise of the coolant in the tube and mixing chamber was incorporated in the calculation. Determination of the dissipative temperature rise is described in Appendix C. The coolant temperature rise due to condensation using the ten-junction thermopile, ΔT_c, is then given by:

$$\Delta T_c = \frac{(\Delta E - \Delta E_{\text{friction}})}{10} \times \left(\frac{dT}{dE}\right)_{E=E_m} \quad (4\text{-}5)$$

where ΔE is the thermo-e.m.f. reading using the ten-junction thermopile, $\Delta E_{\text{friction}}$ is given in terms of the coolant flow rate by Eq. (C-1) and $\left(\frac{dT}{dE}\right)_{E=E_m}$ is obtained by differentiating Eq. (4-4), i.e.

$$\left(\frac{dT}{dE}\right)_{E=E_m} = 0.02563 - 4.066\times10^{-7}\times2E_m - 6.973\times10^{-12}\times3E_m^2 + 1.325\times10^{-14}\times4E_m^3 - 9.704\times10^{-19}\times5E_m^4 \quad (4\text{-}6)$$

and

$$E_m = E_{in} + \frac{1}{2}\times\frac{(\Delta E - \Delta E_{\text{friction}})}{10} \quad (4\text{-}7)$$

E_{in} is the thermo-e.m.f. reading using the thermocouple at the inlet. Agreement

between ΔT_c and $T_{c,out} - T_{c,in}$ were always better than 0.2 K. ($T_{c,in}$ and $T_{c,out}$ are the inlet and exit temperature of coolant of the test tube respectively.)

The heat-transfer rate through the tube, Q, was calculated using:

$$Q = \rho_c \dot{V}_c C_{pc} \Delta T_c \tag{4-8}$$

where ρ_c is the density of the coolant, $\dot{V}_c$ is the volume flow rate of the coolant through the test tube, C_{pc} is the specific isobaric heat capacity of the coolant; all properties were calculated at the temperature of $(T_{c,in} + \frac{1}{2}\Delta T_c)$.

The heat flux based on the outside diameter, d, of the test tube, q, was calculated from:

$$q = \frac{Q}{\pi d l} \tag{4-9}$$

where l is the active heat-transfer length, i.e. length of the test tube exposed to the condensing vapour and internally to the coolant.

The wall temperatures were measured directly by four thermocouples embedded in the tube wall. Correction for the depth of the thermocouples below the condensing surface was incorporated in the calculation for the temperatures by assuming uniform radial heat conduction in the wall. The local outside wall surface temperature can be obtained by the following equation:

$$T_{wo,i} = T_{w,i} + \frac{Q}{2\pi k_w l} \ln\left(\frac{d}{d_{tc}}\right) \tag{4-10}$$

where $T_{wo,i}$ is the outside wall surface temperature of the tube at an angular position corresponding to the i^{th} thermocouple, $T_{w,i}$ is the temperature measured by i^{th} thermocouple, d_{tc} is the pitch diameter of thermocouple junctions in the test tube

(see Fig. 4.5) and k_w is the thermal conductivity of the tube material. Because k_w is dependent on temperature, an iteration scheme was employed with k_w initially evaluated at T_{wo}, and continued until convergence to 0.0001 K. The average outside wall temperature, T_{wo}, was taken as the arithmetic average of the four local outside wall temperatures. The vapour-to-surface temperature difference is given by:

$$\Delta T = T_v - T_{wo} \tag{4-11}$$

where T_v is the observed vapour temperature.

The vapour-side, heat-transfer coefficient, α, was then obtained using Eqs. (4-9) and (4-11):

$$\alpha = \frac{q}{\Delta T} \tag{4-12}$$

The vapour mass flow rate in the test section approaching the condenser tube was calculated from the input power to the boiler by applying a steady-flow energy balance between the boiler inlet (temperature of condensate returning to the boiler) and the test section (immediately before the test tube). Neglecting gravity and kinetic energy, this gives:

$$Q_b - Q_{loss} = \dot{m}_v \left[C_p \left(T_v - T_r \right) + h_{fg} \right] \tag{4-13}$$

where $\dot{m}_v$ is the vapour mass flow rate approaching the test tube, C_p is the specific isobaric heat capacity of the test fluid, T_r is the temperature of the condensate returning to the boiler and Q_{loss} is the (small) heat loss rate from the apparatus between the boiler inlet and the test section. The heat loss was established in preliminary tests by Huang (1995), in which the minimum power required to provide vapour at the test section was determined. The heat loss rate was then expressed by the following equation:

$$Q_{loss} = C_{loss} \left(T_v - T_{atm} \right) \tag{4-14}$$

where T_{atm} is the ambient temperature and C_{loss} was found to be 5.97 W/K.

Thus the vapour mass flow rate can be expressed as:

$$\dot{m}_v = \frac{Q_b - Q_{loss}}{C_p(T_v - T_r) + h_{fg}} \tag{4-15}$$

The vapour approach velocity to the test tube, U_v, is given by:

$$U_v = \frac{\dot{m}_v}{\rho_v A_{ts}} \tag{4-16}$$

where A_{ts} is the cross-sectional area of the test chamber:

$$A_{ts} = d_{ts}^2 \pi / 4 \tag{4-17}$$

and d_{ts} is the diameter of the test chamber, 117 mm.

The mass fraction of non-condensing gases, C_g, in the test section was estimated by assuming saturation conditions in the test section for an ideal-gas mixture which gives:

$$C_g = \frac{P_v - P_{sat}(T_v)}{P_v - \left(1 - \frac{\tilde{M}_{tf}}{\tilde{M}_g}\right) P_{sat}(T_v)} \tag{4-18}$$

where $P_{sat}(T_v)$ is the saturation pressure of the test fluid at observed T_v, and $\tilde{M}_{tf}$ and $\tilde{M}_g$ are the molar masses of the test fluid and non-condensing gas respectively. In the present investigation, the non-condensing gas was regarded as air, with molar mass 28.96 g/mol.

4.1.4 Results and discussion

All experiments were done at a little above atmospheric pressure. Vapour approach velocity to the test tube was approximately 0.23 m/s for R-113, 0.41 m/s for ethylene glycol and 0.57 m/s for steam. The coolant inlet temperature was always around 20 °C and the variation during one experiment was less than 1 K. The range of coolant temperature rise was between about 0.1 and 0.8 K for R-113, between about 1 and 9 K for ethylene glycol and between about 1 and 7 K for steam. The ranges of heat flux and vapour-to-surface temperature difference, and vapour approach velocity for each test fluid during experiments are summarized in Table 4.2.

Figs. 4.7, 4.8 and 4.9 show relations between heat flux and vapour-to-surface temperature difference for R-113, ethylene glycol and steam respectively. The figures also include some earlier experimental and theoretical results. Smooth tube data of Briggs et al. (1992) are included as their experiments were conducted using the same apparatus as that used in the present investigation. The solid line represents the Nusselt (1916) equation, which may be written as:

$$q_{Nu} = 0.728\left\{\frac{\rho(\rho-\rho_v)gh_{fg}k^3}{\mu d}\right\}^{1/4}\Delta T^{3/4} \qquad (4\text{-}19)$$

and the dot-and-dashed line is that of Rose (1984), which included the effect of vapour shear (see Section 2.1), and may be written as:

$$q_{Ro} = \left[\frac{0.9+0.728F^{1/2}}{\left(1+3.44F^{1/2}+F\right)^{1/4}}\right]\left(\frac{k\Delta T}{d}\right)\tilde{Re}^{1/2} \qquad (4\text{-}20)$$

where $\tilde{Re}$ and F are given by Eqs. (2-3) and (2-5) respectively. The vapour velocities employed in $\tilde{Re}$ and F are 0.23, 0.41 and 0.57 m/s for R-113, ethylene glycol and steam respectively. The smooth tube data were seen to lie above the Nusselt (1916) line for all three fluids due to the effect of vapour shear. In this respect the Rose (1984) lines are in closer agreement with the data. Good agreement

between the present smooth tube data and the data of Briggs et al. (1992) are seen for all test fluids.

As described in Section 2.2.2, in earlier experiments using steam and refrigerants for low integral-finned tubes, e.g. Yau et al. (1985) and Masuda and Rose (1985), it has been found that the heat flux varies approximately as the $^3/_4$ power of the vapour-to-surface temperature difference as in the Nusselt (1916) smooth-tube case. This has the advantage that the enhancement ratio obtained by fitting the data by a Nusselt-type expression is independent of temperature difference or heat flux. Sets of data for steam and refrigerants were satisfactorily fitted with:

$$q = B^* \Delta T^{3/4} \tag{4-21}$$

In the case of ethylene glycol some of the data were not well represented by Eq. (4-21) and it was better to fit the data incorporating fluid properties as in the Nusselt (1916) theory with:

$$q = B\left\{\frac{\rho(\rho-\rho_v)gh_{fg}k^3}{\mu d}\right\}^{1/4} \Delta T^{3/4} \tag{4-22}$$

The same was found in the present investigation for wire-wrapped tubes. For example, sets of the present data for all three fluids between using Eqs. (4-21) and (4-22) are shown in Fig. 4.10. For R-113 and steam the fits obtained when using Eqs. (4-21) and (4-22) do not differ substantially but Eq. (4-22) is evidently more satisfactory for ethylene glycol. Eq. (4-22) has been used for all data in the present investigation and the properties, with the exception of h_{fg}, taken at reference temperature:

$$T_{ref} = \frac{1}{3}T_v + \frac{2}{3}T_{wo} \tag{4-23}$$

while h_{fg} was evaluated at T_v. Values of constant B found are shown in the legends in

Figs. 4.7, 4.8 and 4.9. It is seen from the figures that Eq. (4-22) gives a satisfactory fit in all cases. This also has the advantage for wire-wrapped tubes that the enhancement ratio obtained by fitting the data by Eq. (4-22) is independent of temperature difference or heat flux.

The enhancement ratio is given by:

$$\varepsilon_{\Delta T} = \frac{\text{(wire-wrapped tube)}}{\text{(smooth tube)}} = \frac{B_{\text{wire}}}{B_{\text{smooth}}} \tag{4-24}$$

where B_{wire} and B_{smooth} are found from the curve fits for wire-wrapped and smooth tube data respectively using Eq. (4-22). Table 4.3 shows a summary of values of constant B and enhancement ratio $\varepsilon_{\Delta T}$ for each wire combination (diameter and pitch) tested. It is noted that the enhancement ratio given by Eq. (4-24) is based on the same vapour approach velocity for both smooth and wire-wrapped tubes, indicating the enhancement is due solely to the wire wrap.

Figs. 4.11, 4.12 and 4.13 show enhancement ratios plotted against pitch of winding for each wire diameter for R-113, ethylene glycol and steam respectively, together with earlier theoretical results of Fujii et al. (1985) and Rose (2002) and experimental data of Fujii et al. (1985) for R-11.

The predictive equations for enhancement ratio by Fujii et al. (1985) are given by Eqs. (2-24) to (2-26) with K = 0.03. The equation of Fujii et al. (1985) can be simplified to the following forms:

$$\varepsilon_{\Delta T} = \frac{p - d_w}{0.9p}\left\{\frac{4(1+A_2)}{3}\right\}^{1/4} \tag{4-25}$$

where

$$A_2 = \frac{\sqrt{2}}{0.03}\frac{dd_w^2}{(p-d_w)^2}\sqrt{\frac{\rho g}{\sigma}} \tag{4-26}$$

The results of Rose (2002) are given by Eqs. (2-32) to (2-35).

Discussion of results for R-113

For R-113 as shown in Fig. 4.11, the present data appear to exhibit somewhat unique behaviour. For wire diameters of 0.2, 0.35, 0.4 and 1.0 mm, the enhancement ratios increase with decreasing pitch of winding. When sufficiently small values of pitch can be obtained (limiting value is d_w), the enhancement ratio first increases with decreasing pitch and appears to begin to fall with further decrease in pitch. The highest enhancement ratio in the present investigation of 3.7 was obtained using a wire diameter of 0.35 mm with a pitch of 0.8 mm. The general trend for R-113 is that combinations of smaller wire diameter with smaller pitch provide better enhancement.

For R-113 the present enhancement ratios are generally closer to the theoretical result of Fujii et al. (1985). This may be attributable to the fact that data for fluids with similar properties were used by Fujii et al. (1985) to determine the empirical constant in their model. The modified model of Rose (2002) underpredicts the enhancement ratio at small pitches and overpredicts at large pitches for all wire diameters tested. It is recalled from Chapter 2 that the Fujii et al. (1985) model incorporated the approximation that the condensate film thickness was uniform laterally along the tube surface between wires. This approximation, necessary to make the problem more tractable, was retained in the Rose (2002) modification of the Fujii et al. (1985) approach. This may be a fundamental flaw in both models.

For a wire diameter of 0.35 mm, the experimental data of Fujii et al. (1985) for condensation of R-11 on an 18 mm diameter tube with a wire diameter of 0.3 mm are included. In view of the different fluid and tube and wire diameters it would appear that the present and the earlier data are in broad agreement.

Discussion of results for ethylene glycol

For ethylene glycol as shown in Fig. 4.12, for the smallest wire diameter of 0.2 mm and larger wire diameters of 0.75 and 1.0 mm, the enhancement ratios

appear to have weak dependence on pitch of winding. For wire diameters of 0.35 and 0.4 mm, the enhancement ratio increases with decrease in pitch. The highest enhancement ratio of 2.2 was obtained using a wire diameter of 0.35 mm with a pitch of 1.0 mm. Dependence of enhancement on wire pitch is generally less than for R-113. For wire diameters of 0.35 and 0.4 mm the dependence of enhancement on pitch appears larger with smaller pitch giving better enhancement.

Neither theoretical result is in good agreement with the present data. In the case of smaller wire diameters of 0.2, 0.35 and 0.4 mm, the data are closer to the line given by the Fujii et al. (1985) equation, while the Rose (2002) equation underpredicts the data at small pitches and overpredicts at large pitches. For larger wire diameters of 0.75 and 1.0 mm, the present data lie between the two models.

Discussion of results for steam

For steam as shown in Fig. 4.13, for larger wire diameters of 0.4, 0.75 and 1.0 mm, the enhancement ratio first increases with decreasing pitch and subsequently decreases. In the case of a wire diameter of 0.35 mm, with further decrease in pitch, the enhancement ratio surprisingly apparently rises again. In the case of wire diameters of 0.2 and 0.35 mm, there is evidence that a maximum has been reached at the smallest pitch used. The highest enhancement ratios are found for smaller wire diameters with the smallest pitch tested: 2.2 for a wire diameter of 0.2 mm with a pitch of about 0.8 mm; and 2.3 for a wire diameter of 0.35 mm with a pitch of 0.8 mm. The general trend for steam condensation is also that combinations of smaller wire diameter with smaller pitch provide better enhancement.

The Fujii et al. (1985) equation is apparently in quite good agreement with the steam data for the smallest wire diameter but overpredicts the data for larger wire diameters. The modified approach of Rose (2002) generally underpredicts the data except for the smallest wire diameter with larger pitches.

In Fig. 4.14, comparison is made with data of Marto et al. (1987) and Brower (1985) for enhancement ratio at the same heat flux. For the latter case, the data for the top tube of a column of horizontal tubes whose enhancement was due both to the

wire wrap and vapour shear (see Section 2.3.3 (4)) are given. For a wire diameter of 0.4 mm, the data for a wire diameter of 0.5 mm from both investigations are compared. Bearing in mind differences in tube and wire dimensions, the present data are in broad agreement with those of Marto et al. (1987). The data of Brower (1985) are noticeably lower for a wire diameter of 0.4 mm. For a wire diameter of 1.0 mm, the data of Brower (1985) would become further lower if the enhancement due to vapour shear had been extracted.

Table 4.4 shows the ratio of pitch to wire diameter giving the highest enhancement ratio for each wire diameter. For R-113 using wire diameters of 0.2 and 0.35 mm, the highest enhancement ratios are given with the smallest pitch tested, indicating that smaller pitch may give better enhancement ratio. For the other fluids, the optimum wire pitch giving the highest enhancement ratio seems to be within the test range. From an engineering view point it can be said that wire wrapping on a smooth tube with ratios of pitch to wire diameter of approximately 2, 3 and 5 give the highest enhancement ratios, i.e. up to 3.7, 2.2 and 2.3 for R-113, ethylene glycol and steam, respectively.

4.2 Condensate inundation investigation

In order to check the data of Brower (1985) and Marto (1986) which showed that wire-wrapped tubes performed better than integral-finned tubes (see Section 2.3.3 (4)), inundation measurements were also performed for steam. For this purpose, the apparatus used for the single wire-wrapped tube investigation was slightly modified and heat-transfer measurements were done at as close as possible to be experimental conditions of Brower (1985).

4.2.1 Apparatus and instrumentation

The modified apparatus is shown schematically in Fig. 4.15. The test fluid, i.e. water, from the boiler was pumped to the inundation supply tube via the inundation cooler and flow meter. Fig. 4.16 shows detail of the modified test section, which consists of three vertically in-line horizontal tubes, namely the inundation supply tube, the inundation distribution tube and the test condenser tube. The artificial inundation liquid flowed into the inundation supply tube from both ends as shown in Fig. 4.17, and was then directed from holes located at the bottom of the inundation supply tube onto the inundation distribution tube and subsequently onto the test tube. For the inundation distribution tube only one wire-wrapped was used for convenience. The inundation liquid and condensate returned to the boiler by gravity. Inundation supply temperatures were measured at the inlet of the inundation supply tube and inside the inundation distribution tube. The latter value was used for subsequent data reduction.

Preliminary tests to establish uniform inundation flow were first conducted without condensation. Inundation supply, inundation distribution and plain tubes were vertically located in line and water flowed into the inundation supply tube from both ends via a flow meter. Inundation flow rates up to 1.5 l/min were tested. The surface distance between the inundation distribution tube and the test tube was 10 mm. An attempt was made by trial and error to establish optimum diameter and spacing of holes in the bottom of the inundation supply tube, and of the depth of cutting and wire pitches for the inundation distribution tube to achieve uniform

inundation. Fig. 4.18 shows photographs of the flow during the preliminary tests. Uniform flow distribution (judged by eye) was established in a range of flow rates up to 0.8 l/min, which is equivalent to the inundation from approximately 30 tubes calculated by the Nusselt (1916) theory for a single smooth horizontal tube at a heat flux of 300 kW/m^2. Uniformity of flow was strongly dependent on the inclination of the inundation distribution tube. For higher flow rates, water was overconcentrated in the centre of the inundation distribution tube leading to excessive inundation flow at that location (see for instance Fig. 4.18 (d)). From the preliminary tests, the specifications for the tubes were then determined as indicated below.

The brass inundation supply tube had an outside diameter of 12.7 mm, an inside diameter of 10.2 mm and a total length of 400 mm (see Fig. 4.19). Eight 1.0 mm diameter holes were located along the bottom of the tube at intervals of 10 mm except that the centremost two holes were spaced at 20 mm, to avoid the excessive inundation flow at the centre. Both sides of the tube were sealed with o-rings.

The inundation distribution tube was designed in order to distribute uniform inundation liquid over the test condenser tube. Since the inclination of the tube was vital for uniform inundation distribution, provision was made for external level adjustment. Details of the inundation distribution tube are given in Fig. 4.20. Wire having a diameter of 1.27 mm was wrapped with a pitch of winding of about 10 mm. For convenience the same distribution tube was used for all tubes tested.

Three condenser tubes were tested, namely smooth, wire-wrapped and low integral-finned tubes. The smooth and wire-wrapped tubes were the same as used in the single tube investigation. For the wire-wrapped tubes a wire diameter of 1.6 mm with pitches of 4, 8 and 16 mm were used for comparison with Brower (1985). The low integral-finned tube was made of copper, having an outside diameter at fin root of 12.7 mm, an active heat-transfer length of 100 mm with a fin thickness, fin height and interfin space of 0.5, 1.59 and 1.5 mm respectively, as used by Briggs et al. (1992) and, when used as a single tube without inundation, gave the highest heat-transfer enhancement ratio of 3 for steam. The same cleaning procedure for the test tube described in Section 4.1.1 before installation was always followed to ensure filmwise condensation.

4.2.2 Experimental procedure

The smooth tube was first tested both with and without inundation followed by tests with the wire-wrapped and finned tubes. Care was taken to avoid the presence of non-condensing gas in the test section by venting steam from the test apparatus for more than 5 minutes in the beginning of experiments. For experiments without inundation the same experimental procedure was used as in the single tube investigation. For experiments with inundation, flow rates and temperatures of inundation liquid were additionally adjusted and measured.

By varying inundation flow rates, a column of about 30 vertically in-line horizontal tubes could be simulated. An interval of at least 7 minutes was taken to achieve steady conditions after varying the inundation flow rate. The inundation flow rate was first set to zero (no inundation), and subsequently increased in steps up to 0.8 l/min or until a rate at which uniform inundation distribution along the test tube could not be maintained. By adjusting the flow control valve for the inundation coolant (see Fig. 4.15), the inundation supply temperature was set to the desired values, as close as possible to the temperature calculated using the following equation (the derivation of the equation is described in Appendix D):

$$T^{*}_{inun} = \frac{5}{8}T_{v} + \frac{3}{8}T_{wo} \qquad (4\text{-}27)$$

This is the mean condensate temperature at which condensate would leave a tube according to the Nusselt (1916) theory. Vapour and wall temperatures substituted into Eq. (4-27) were values measured at the previous lower inundation rate. For instance, for the first inundation flow rate the inundation supply temperature calculated using vapour and wall temperatures observed under no inundation at the same coolant flow rate. Vapour and wall temperatures measured for the subsequent inundation flow rates were then substituted into Eq. (4-27) for the next higher inundation flow rate.

4.2.3 Determination of experimental parameters

Heat flux, vapour-to-surface temperature difference, vapour approach velocity to the test tube, temperatures (wall, vapour, coolant-in, coolant-out, coolant temperature difference, return condensate and inundation supply) and pressures (atmospheric and test section gauge) were observed as in the single tube investigation (see Section 4.1.3).

4.2.4 Results and discussion

(1) Results without inundation

All experiments were done at around atmospheric pressure with a vapour approach velocity to the test tube of approximately 0.56 m/s. The coolant inlet temperature was always around 10 °C and the variation during one experiment was less than 1 K. The range of coolant temperature rises was between about 1.9 and 46.5 K for the smooth tube (a wider range of coolant flow rates was tested), between about 1.6 and 8.7 K for the wire-wrapped tubes and between 2.9 and 11.6 K for the finned tube. The ranges of heat flux and vapour-to-surface temperature difference during experiments are summarized in Table 4.5.

Fig. 4.21 shows the relation between heat flux and vapour-to-surface temperature difference for the smooth, wire-wrapped and finned tubes. Also included are lines of the Nusselt (1916) theory given by Eq. (4-19), the Rose (1984) theory given by Eq. (4-20) and the curve fit using Eq. (4-22). The present smooth tube data are in good agreement with the Rose (1984) equation, which takes account of vapour shear. For the wire-wrapped tube (d_w = 1.6 mm), no significant difference among the results for different wire pitches is seen. For the finned tube, for which measurements were performed using almost the same range of coolant flow rates, the results show much lower vapour-to-surface temperature differences and higher heat fluxes indicating significantly higher enhancement.

Table 4.6 gives values of the constant B found by the curve fitting the data using Eq. (4-22) and enhancement ratios for the smooth, wire-wrapped and finned tubes.

The smooth data are also based on the latest measurements using the modified test apparatus. For the wire-wrapped tube, no significant dependence of enhancement ratio on pitch is seen. Fig. 4.22 shows comparison of enhancement ratio at the same heat flux for a wire diameter of 1.6 mm with earlier experimental data of Marto et al. (1987) who used a 19 mm diameter tube and Brower (1985) who used a 16 mm diameter tube. In the case of the Brower (1985) data, these are for the top tube of a column of horizontal tubes and the enhancement ratio includes the effect of vapour shear (see Section 2.3.3 (4)). The relatively large difference between the present data and those of Marto et al. (1987) may in part be due to difference in tube diameter. The data of Brower (1985) are significantly lower even including the effect of vapour shear; presence of air during the heat-transfer measurements is suspected in this case.

(2) Results with inundation

All experiments were done at around atmospheric pressure with a vapour approach velocity to the test tube of approximately 0.56 m/s at a coolant flow rate of 2.0 l/min which gave a heat flux of approximately 300 kW/m^2 for the smooth tube. The coolant inlet temperature was always around 10 °C and the variation during one experiment was less than 1 K. The ranges of heat flux, vapour-to-surface temperature difference, and temperature and flow rate of artificial inundation liquid during experiments are summarized in Table 4.7.

Visual observations

As observed in the preliminary tests, the appearance of inundation from the inundation distribution tube onto the test tube changed from discrete drops (Fig. 4.18(a)) to columns (Fig. 4.18(c)) with increase in inundation.

For the smooth tube case, at lower inundation rate up to 0.2 l/min, the discrete drops fell onto random locations along the tube. For the middle range of the inundation rates tested, i.e. 0.3 to 0.6 l/min, the appearance was seen both as discrete drops and broken columns randomly located along the tube. For the higher inundation rates, several columns were established and occasionally the columns

were broken and re-appeared at different locations along the tube.

Similar observations with increase in inundation were seen for the wire-wrapped tubes. Photographs of the wire-wrapped tube with a pitch of 4 mm under different inundation rates are shown in Fig. 4.23. When broken columns appeared at the middle range of the inundation rates or higher, the inundation seemed occasionally attracted laterally onto the wire on the test tube. It is interesting to note that once columns appeared they tended to stay at the same locations. This difference from the smooth tube case may be due to the surface distance between the inundation distribution tube and the test tube. The presence of the wire (d_w = 1.6 mm) on the test tube made the distance shorter, for instance the distance between the edge of the wires on the inundation distribution tube and the test tube was 7.1 mm and that for the smooth tube case is 8.7 mm, so that inundation columns are relatively more stable than the otherwise.

For the finned tube, the observed trends were similar to the visual observations for the wire-wrapped tubes. The area affected by inundation was observed to be slightly smaller than for the wire-wrapped tubes. This is thought to be due to the interfin space of the finned tube tested, i.e. 1.5 mm, in comparison with the spacing between adjacent turns of wire for the wire-wrapped tubes tested, which ranges from 2.4 to 14.4 mm.

Fig. 4.24 shows photographs indicating the difference of inundation for the smooth, wire-wrapped and finned tubes. For the smooth tube, the inundation spreads along the tube. For the enhanced tubes the inundation flows straight down and most of the heat-transfer surfaces are not affected by the inundation.

Heat-transfer results

Figs. 4.25 and 4.26 show the dependence of heat flux and heat-transfer coefficient, respectively, on inundation rate during steam condensation on the smooth tube at a coolant flow rate of 2.0 l/min. It is seen that the heat flux decreases with increase in inundation, while the vapour-to-surface temperature difference

increases. This is due to the condensate film being thickened by inundation. As a result the heat-transfer coefficient decreases with increase in inundation.

Figs. 4.27 and 4.28 show the dependence of heat flux and heat-transfer coefficient, respectively, on inundation rate for the wire-wrapped tubes at a coolant flow rate of 2.0 l/min. The heat flux decreases with increase in inundation and the fall is seen to be less for smaller pitch of winding. This is thought to be due to the difference of the spacing between adjacent turns of the wire. The length affected by inundation spacing is approximately p minus d_w, the value of which is smaller for smaller pitch for constant wire diameter. The vapour-to-surface temperature difference increases with inundation and the increase is less for smaller pitch. As a result the heat-transfer coefficient falls less for smaller pitch.

Figs. 4.29 and 4.30 show the dependence of heat flux and heat-transfer coefficient, respectively, on inundation rate for the finned tube at a coolant flow rate of 2.0 l/min. The open points were observed at inundation supply temperatures calculated using Eq. (4-27). The data appear to exhibit somewhat unrealistic behaviour for the heat-transfer coefficient, which increases with increase in inundation. This is thought to be due to the fact that the inundation temperature given by Eq. (2-27), which is based on the assumption of an isothermal tube wall (see Appendix D), may be too high. The additional heat transfer due to cooling of the inundation liquid as it flows over the test condenser tube would have a stronger effect on the finned tube for which the vapour-to-surface temperature difference is much smaller and the heat-transfer surface temperature higher than for the wire-wrapped and smooth tubes. Further data for the finned tube was then taken using a lower inundation temperature, arbitrarily taken as:

$$T^*_{inun} = \frac{5}{8}T_v + \frac{3}{8}T_w(\text{lowest}) \qquad (4\text{-}28)$$

where T_w(lowest) is the surface temperature indicated by the thermocouple at the lowest part of the tube (-157.5° from the top of the tube, see Fig. 4.5). The results using Eq. (4-28) are also shown in Figs. 4.29 and 4.30 by closed points. The data are lower and more reasonable for both heat flux and heat-transfer coefficient. The data

show a very slight decrease in heat flux with increase in inundation. Extremely low influence of inundation on the finned tube is seen. In subsequent comparisons the finned tube data are those using Eq. (4-28) to determine the inundation temperature. Time did not permit repetition of the measurements at inundation supply temperature calculated using Eq. (4-28) for smooth and wire-wrapped tubes which are less sensitive to the inundation temperature.

Fig. 4.31 shows variations of heat flux inundation ratio, i.e. heat flux with inundation divided by that without inundation (q_{zero} denotes the heat flux obtained without inundation) at the same coolant flow rate and the same vapour approach velocity, on inundation rate for the smooth, wire-wrapped and finned tubes. Fig. 4.32 shows those for heat-transfer coefficient inundation ratio (α_{zero} denotes the heat-transfer coefficient obtained without inundation). It is seen that the effect of inundation is less severe for the wire-wrapped tubes than the smooth tube. This, together with the visual observations (see Fig. 4.24) indicated that the wire also plays a role in preventing from inundation spreading along the tube as explained by Honda et al. (1989) for finned tubes. The finned tube data are seen to lie above the wire-wrapped tubes, i.e. are less affected by inundation. This is due both to more effective suppression of lateral spreading of condensate and may also be due to the additional heat transfer due to cooling of the inundation liquid as described above.

Discussion of inundation supply temperature

It has been found from the finned tube results that care must be taken to determine the inundation supply temperature for heat-transfer measurements with artificial inundation. These tests illustrate the sensitivity of measurements to inundation temperature for the case of highly enhanced tubes. The effect is found to be much smaller for wire-wrapped and smooth tubes. Memory and Rose (1991) observed that the tube wall surface temperature distribution could be closely represented using a cosine curve. The actual surface temperature approximation to a cosine distribution is discussed in Appendix E. Referring to Appendix D, using a cosine distribution of surface temperature yields the following equation for the mean temperature of condensate draining from a tube:

$$T^*_{inun} = \frac{5}{8}T_v + \frac{3}{8}T_{wo}(1-A) \qquad (4\text{-}29)$$

where A is a constant found from the temperature distribution (see Table. E.1 in Appendix E). Eq. (4-29) should be a better expression for the inundation supply temperature for the present investigation. Time did not permit repeating of experiments using Eq. (4-29) to determine the inundation supply temperature.

Estimation of effective number of tubes in a simulated column

In Brower (1985), the inundation rate was set equal to the measured amount of condensate generated by the five active test condenser tubes. Increase in the artificial inundation rate was used to simulate a column of up to 30 tubes. In the present investigation, only one active test condenser tube was used. The experimental procedure was described in Section 4.2.2 and the estimation of the effective tube number (depth in simulated bank) is given below.

Consider condensation on an in-line column of tubes. Assuming all condensate flowed from one tube to the one below in the column, the inundation rates, $\dot{m}_{inun,N}$, and condensation rate, $\dot{m}_{cond,N}$, for the N^{th} tube from the top are given by:

$$\begin{aligned}
\dot{m}_{inun,1} &= 0 \\
\dot{m}_{inun,2} &= \dot{m}_{cond,1} \\
\dot{m}_{inun,3} &= \dot{m}_{cond,2} + \dot{m}_{cond,1} \\
\dot{m}_{inun,4} &= \dot{m}_{cond,3} + \dot{m}_{cond,2} + \dot{m}_{cond,1} \\
&\vdots
\end{aligned} \qquad (4\text{-}30)$$

In general,

$$\dot{m}_{inun,1} = 0 \qquad (4\text{-}31)$$

$$\dot{m}_{inun,N} = \sum_{1}^{N-1} \dot{m}_{cond,i} \quad (N \geq 2) \qquad (4\text{-}32)$$

$\dot{m}_{cond,N}$ (without inundation for the first tube and with inundation for other tubes) is obtained from the condensation heat-transfer rate Q_N

$$\dot{m}_{cond,N} = Q_N / h_{fg} \tag{4-33}$$

To find the effective tube number form the observed inundation rate, $\dot{m}_{inun}$, and condensation rate, $\dot{m}_{cond}$, $\dot{m}_{cond}$ is plotted against $\dot{m}_{inun}$, as shown in Fig. 4.33. As may be seen the data are well fitted by the equation:

$$\dot{m}_{cond} = a_1 + a_2 \dot{m}_{inun}^{a_3} \tag{4-34}$$

where a_1, a_2 and a_3 were found by minimization of the sum of squares of residuals of $\dot{m}_{cond}$. An iteration procedure (e.g. 'solver' in Microsoft Excel) was used to determine the value of the non-linear constant a_3. For each a_3, the linear constants a_1 and a_2 are readily found by 'least squares'. Calculated values of the constants for each tube tested are shown in Table 4.8.

$\dot{m}_{cond,1}$ was measured without inundation ($\dot{m}_{inun} = 0$). From Eq. (4-30) $\dot{m}_{inun,2} = \dot{m}_{cond,1}$, then $\dot{m}_{cond,2}$, the condensation rate under inundation rate of $\dot{m}_{inun,2}$, can be calculated by Eq. (4-34) (see Fig. 4.34)

$$\dot{m}_{cond,2} = a_1 + a_2 \dot{m}_{inun,2}^{a_3} \tag{4-35}$$

and subsequently $\dot{m}_{inun,3} = \dot{m}_{cond,2} + \dot{m}_{cond,1}$. Repeating this procedure gives the estimated inundation rate for the N^{th} tube in the simulated column and thus the relation between inundation rate and the effective tube number, as shown in Fig. 4.35. Due to the difference of heat-transfer enhancement for each tube tested, the estimated depth of a tube in a column is different for each tube at the same inundation rate. This is least for the finned tube for which the condensation rate on a given tube is highest.

Comparison with earlier results

To compare with earlier theoretical and experimental results, the present results are arranged in the form of inundation ratios α_N/α_{top} and $\bar{\alpha}_N/\alpha_{top}$ against N. Neglecting the fact that the tube wall temperature is different at different depths in a tube column, $\bar{\alpha}_N$ is obtained by arithmetically averaging observed vapour-side, heat-transfer coefficients.

Fig. 4.36 shows comparison of the present smooth tube data with earlier theoretical results in terms of a ratio α_N/α_{top} plotted against N. The solid line represents the Nusselt (1916) equation, Eq. (2-37), the dot-and-dashed line is the Kern (1950) equation, Eq. (2-39) and the two-dots-and-dashed line is the Eissenberg (1972) equation, Eq. (2-41). The present data are in best agreement with Kern (1950).

Fig. 4.37 shows the present smooth tube data compared with data of Brower (1985) using a 16 mm diameter tube for $\bar{\alpha}_N/\alpha_{top}$ plotted against N. The present data are higher than the data of Brower (1985). The difference is thought to be due to test section geometry (e.g. tube diameter, the number of active tubes).

Fig. 4.38 shows comparison of the present data for wire-wrapped tubes with those of Brower (1985) in terms of a ratio $\bar{\alpha}_N/\alpha_{top}$ plotted against N. For a wire pitch of 16 mm, the present data are seen to be higher than the data of Brower (1985), which is thought to be due to the difference in geometry in the same manner as for the smooth tube. The effect of air on a tube column is thought to be higher for higher rows in the column. The presence of air during tests could result in the ratio $\bar{\alpha}_N/\alpha_{top}$ being higher as described in Section 2.3.3 (4). In this regard, for wire pitches of 4 and 8 mm, the present data are seen to be lower than those of Brower (1985). The surprising behaviour of a ratio $\bar{\alpha}_N/\alpha_{top}$ more than unity of Brower (1985) for 8 mm pitch is not observed in the present investigation. This indicates the data of Brower (1985) was likely affected by air.

Table 4.8 gives values of the constant m found by the curve fitting the data with Eq. (2-43) for the smooth, wire-wrapped and finned tubes. The detrimental effect of inundation was found to be least for the low integral-finned tube. Wire wrap was also found to be effective to reduce the detrimental effect, which was found to be dependent on wire pitch.

4.3 Conclusions

The main objective of the investigation of condensation on wire-wrapped tubes was to obtain new accurate data using R-113, ethylene glycol and steam with systematic change of wire diameter and pitch combinations, so as to obtain the optimum geometry for a range of fluid properties, especially surface tension. All measurements were made using relatively low vapour velocity at a little above atmospheric pressure with a range of coolant flow rates. A total of 993 data points has been obtained.

It has been found that data, in the form of heat flux and vapour-to-surface temperature difference, for all cases are well represented by an equation of the form:

$$q = B\left\{\frac{\rho(\rho-\rho_v)gh_{fg}k^3}{\mu d}\right\}^{1/4}\Delta T^{3/4} \qquad (4\text{-}36)$$

in the same manner as for condensation on smooth and low integral-finned tubes. This also has the advantage that the enhancement ratio obtained by fitting the data by Eq. (4-36) is independent of temperature difference or heat flux.

The enhancement ratio was generally higher for lower surface tension fluid. It has been found that wire wrapping on a smooth tube with ratios of pitch to wire diameter of approximately 2, 3 and 5 give the highest enhancement ratios for R-113, ethylene glycol and steam respectively. The optimum wire-pitch combination has been found to be a wire diameter of 0.35 mm with a pitch of around 0.8 mm, which gives the enhancement ratio of 3.7, 2.2 and 2.3 for R-113, ethylene glycol and steam respectively.

Deficiencies of existing theoretical results have been highlighted. The validity of the treatment of the condensate film in the model of Fujii et al. (1985) remains to be established. Further, the assumption of uniform condensate fillet radius at the wire is incorrect and, with the empirical equation for fillet radius, is incompatible in many cases with the assumed geometry of the condensate film. The modification by Rose

(2002) removes the incompatibility and empiricism from the Fujii et al. (1985) model but probably significantly underestimates the heat transfer by taking those parts of the surface where the condensate surface is curved to be adiabatic. Neither result gives satisfactory agreement with the data taken as a whole. It is considered that this new data base will contribute significantly to the eventual solution of the problem.

Data for condensation of steam with inundation on smooth, wire-wrapped and low integral-finned tubes have been successfully obtained by modifying the test apparatus used in the single wire-wrapped tube investigation. Measurements were made at around atmospheric pressure with a coolant flow rate of 2.0 m/s and a vapour velocity of 0.56 m/s using artificial inundation at temperature adjusted to:

$$T^*_{inun} = \frac{5}{8}T_v + \frac{3}{8}T_{wo} \qquad (4\text{-}37)$$

The estimation of effective numbers of tubes in a simulated column has been successfully addressed. The importance of the inundation supply temperature has also been clarified, namely too low or high inundation supply temperatures cause corresponding changes in convective heat transfer between the artificial inundation and condenser tube wall, whose effect is significant for the case of highly enhanced tubes. Taking account of the circumferential wall temperature distribution, the following expression may be better used:

$$T^*_{inun} = \frac{5}{8}T_v + \frac{3}{8}T_{wo}(1-A) \qquad (4\text{-}38)$$

where A is a constant in the cosine fit to the circumferential surface temperature distribution.

It has been found that the detrimental effect of condensate inundation decreases in order from low integral-finned to wire-wrapped to smooth tubes. The report of Brower (1985) and Marto (1986) of the superiority of wire-wrapped tubes has been found to be incorrect.

Table 4.1 Resistances of boiler heaters.

Heater	Electric resistance / Ω
1	19.1
2	17.7
3	16.8
4	18.5

Table 4.2 Summary of ranges of experimental parameters for condensation on smooth and wire-wrapped tubes for each test fluid.

	U_v / m/s	q / (kW/m^2)	ΔT / K
R-113			
smooth	0.23	25 – 35	21 – 26
wire-wrapped		40 – 95	15 – 25
ethylene glycol			
smooth	0.41	280 – 300	110 – 160
wire-wrapped		320 – 600	110 – 160
steam			
smooth	0.57	100 – 450	5 – 40
wire-wrapped		300 – 900	15 – 58

Table 4.3 Values of constant B in Eq. (4-22) and enhancement ratio $\varepsilon_{\Delta T}$ given by Eq. (4-24) for each wire combination tested.

Fluid	d_w / mm	p / mm	B	$\varepsilon_{\Delta T}$
R-113	smooth tube		0.758	1.0
	0.2	0.5	2.43	3.21
		0.75	2.31	3.04
		1.0	1.69	2.23
		1.5	1.65	2.17
		2.5	1.52	2.00
		3.5	1.33	1.76
		4.5	1.27	1.67
		6.0	1.16	1.54
R-113	0.35	0.8	2.79	3.68
		1.0	2.28	3.01
		1.2	2.36	3.11
		1.5	2.10	2.77
		2.5	1.87	2.46
		3.5	1.54	2.03
		4.5	1.36	1.80
		6.0	1.29	1.70
R-113	0.4	0.7	2.35	3.10
		1.0	1.98	2.61
		1.5	1.98	2.62
		2.0	1.94	2.56
		2.5	1.87	2.47
		3.5	1.68	2.22
		4.5	1.43	1.89
		6.0	1.30	1.71

Table 4.3 (continue).

Fluid	d_w / mm	p / mm	B	$\varepsilon_{\Delta T}$
R-113	0.75	1.0	1.77	2.34
		1.5	1.84	2.42
		1.7	2.05	2.71
		2.0	1.95	2.57
		2.5	1.92	2.54
		3.0	1.79	2.37
		3.5	1.57	2.08
		4.0	1.56	2.06
		2.5	1.47	1.94
		6.0	1.34	1.77
R-113	1.0	1.5	2.22	2.92
		2.5	2.04	2.70
		3.5	1.82	2.40
		4.5	1.47	1.94
		6.0	1.37	1.81
ethylene glycol	smooth tube		0.763	1.0
	0.2	0.5	1.19	1.55
		1.0	1.22	1.59
		2.0	1.05	1.37
		4.0	0.92	1.21
	0.35	0.8	1.62	2.13
		1.0	1.65	2.16
		1.5	1.46	1.92
		2.5	1.19	1.55
		4.0	1.02	1.34

Table 4.3 (continue).

Fluid	d_w / mm	p / mm	B	$\varepsilon_{\Delta T}$
ethylene glycol	0.4	1.0	1.53	2.01
		1.5	1.33	1.74
		2.5	1.17	1.53
		4.0	1.01	1.32
	0.75	1.0	1.24	1.63
		1.5	1.26	1.65
		2.5	1.21	1.58
		4.0	1.18	1.54
	1.0	1.5	1.12	1.46
		2.5	1.23	1.61
		3.5	1.22	1.60
		4.5	1.22	1.60
steam	smooth tube		0.842	1.0
	0.2	0.5	1.47	1.76
		0.5	1.83	2.18
		0.75	1.69	2.01
		1.0	1.47	1.76
		1.5	1.31	1.57
		2.5	1.28	1.53
		3.5	1.16	1.38
		4.5	1.05	1.25
		6.0	1.02	1.22

Table 4.3 (continue).

Fluid	d_w / mm	p / mm	B	$\varepsilon_{\Delta T}$
steam	0.35	0.7	1.94	2.32
		1.0	1.47	1.76
		1.5	1.47	1.76
		2.0	1.71	2.04
		4.5	1.50	1.80
		6.0	1.21	1.45
steam	0.4	1.0	1.14	1.37
		1.5	1.19	1.42
		2.0	1.61	1.92
		2.5	1.57	1.88
		3.5	1.47	1.76
		4.5	1.40	1.67
		6.0	1.33	1.59
steam	0.75	1.5	0.67	0.80
		2.5	1.08	1.29
		3.5	1.46	1.74
		4.5	1.50	1.80
		6.0	1.23	1.47
steam	1.0	1.5	0.67	0.81
		2.5	0.89	1.06
		3.5	1.10	1.31
		4.5	1.26	1.51
		6.0	1.07	1.27

Table 4.4 Ratio of pitch to wire diameter giving the highest enhancement ratio. (* the smallest pitch tested.)

a) R-113

d_w / mm	p / d_w	$\varepsilon_{\Delta T}$ (highest)
0.2	2.5*	3.21
0.35	2.3*	3.68
0.4	1.8*	3.10
0.75	2.3	2.71
1.0	1.5*	2.92

b) ethylene glycol

d_w / mm	p / d_w	$\varepsilon_{\Delta T}$ (highest)
0.2	5.0	1.55
0.35	2.3*	2.13
0.35	2.9	2.16
0.4	2.5*	2.01
0.75	2.0	1.65
1.0	2.5	1.61

c) steam

d_w / mm	p / d_w	$\varepsilon_{\Delta T}$ (highest)
0.2	2.5*	2.18
0.2	3.8	2.01
0.35	2.0*	2.32
0.35	5.7	2.04
0.4	5.0	1.92
0.75	4.7	1.75
0.75	6.0	1.80
1.0	4.5	1.51

Table 4.5 Summary of ranges of observed experimental parameters for steam condensation without inundation on smooth, wire-wrapped and low integral-finned tubes. (Vapour approach velocity 0.56 m/s.)

Tube / mm	q / (kW/m^2)	ΔT / K
smooth (d = 12.2, l = 100)	170 – 560	10 – 60
wire-wrapped (d = 12.2, l = 90, d_w = 1.6)	330 – 640	22 – 55
low integral-finned (d = 12.7, l = 100, h = 1.6, t = 0.5, s = 1.5)	350 – 1000	7 – 28

Table 4.6 Values of constant B in Eq. (4-22) and enhancement ratios for steam condensation without inundation on smooth, wire-wrapped and low integral-finned tubes.

Tube		B	$\varepsilon_{\Delta T}$
smooth		0.813	1.0
wire-wrapped (p / mm)	4	0.946	1.16
	8	0.936	1.15
	16	0.960	1.18
low finned		2.40	2.95

Table 4.7 Summary of ranges of experimental parameters for steam condensation with inundation. (Vapour approach velocity 0.56 m/s, coolant flow rate 2.0 l/min.)

Tube		T^*_{inun} / °C	$\dot{m}_{inun}$ / (g/s)	q / (kW/m^2)	ΔT / K
smooth		86.7 – 90.7	0 – 14.5	220 – 300	24.2 – 33.7
wire-wrapped (p / mm)	4	91.3 – 92.0	0 – 13.0	325– 365	22.0 – 24.3
	8	90.1 – 91.1	0 – 13.4	300 - 350	24.9 – 27.5
	16	89.1 – 91.8	0 – 12.9	275 – 350	22.8 – 30.1
low finned		92.6 – 94.5	0 – 11.5	365 – 375	6.9 – 7.2

Table 4.8 Values of constants a_1, a_2 and a_3 in Eq. (4-34) found to fit relation between observed condensate and inundation rates for each test tube. (Vapour approach velocity 0.56 m/s, coolant flow rate 2.0 l/min.)

Tube		a_1	a_2	a_3
smooth		0.5116	-0.0548	0.3483
wire-wrapped (p / mm)	4	0.5522	-0.0140	0.4472
	8	0.5274	-0.0120	0.6440
	16	0.5290	-0.0257	0.5608
low finned		0.6703	-0.0037	0.7737

Table 4.9 Values of constant m in Eq. (2-43) for steam condensation with inundation on smooth, wire-wrapped and low integral-finned tubes.

Tube		m
smooth		0.1247
wire-wrapped (p / mm)	4	0.0223
	8	0.0249
	16	0.0765
low finned		0.0009

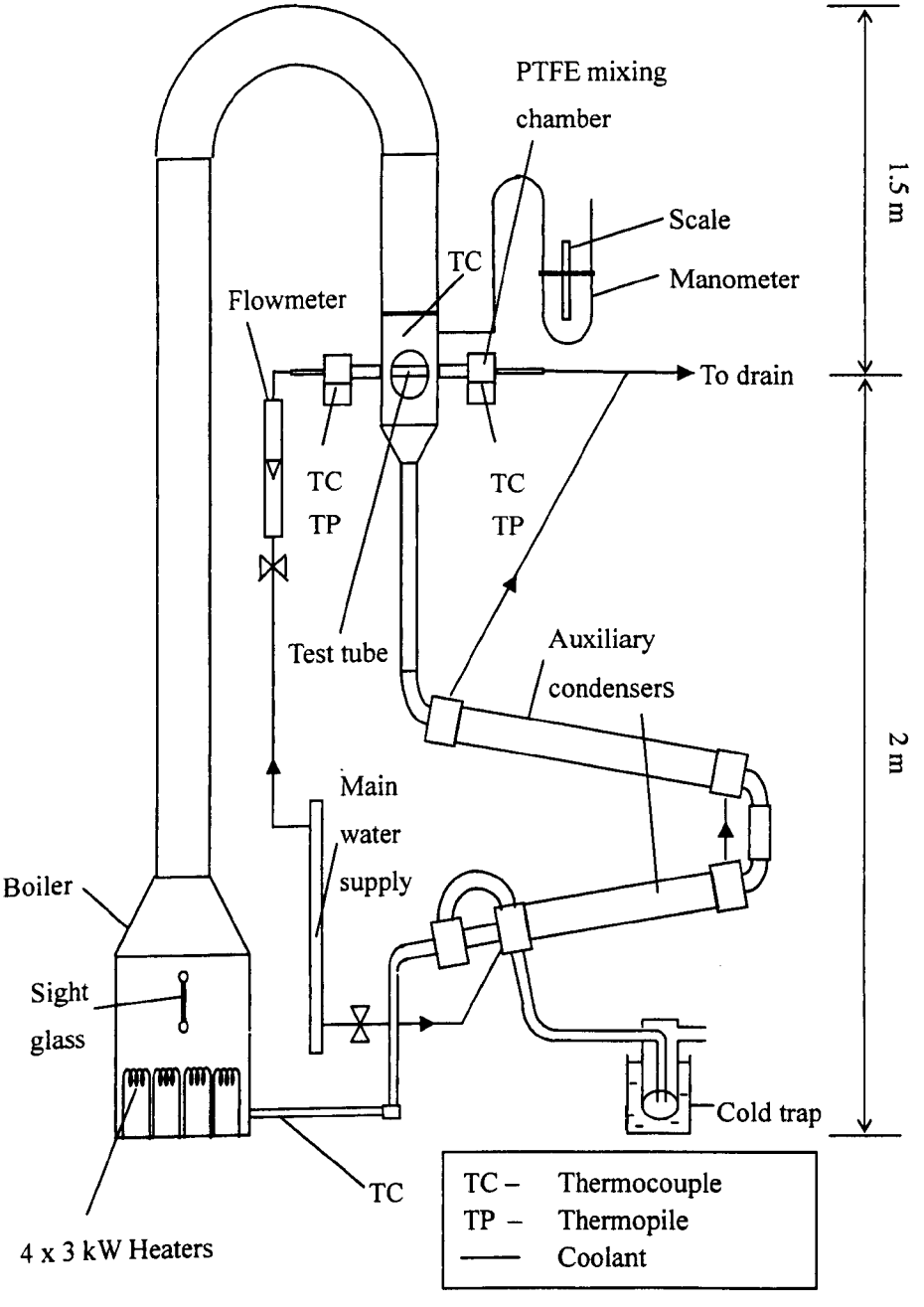

Fig. 4.1. Test apparatus used for condensation investigations.

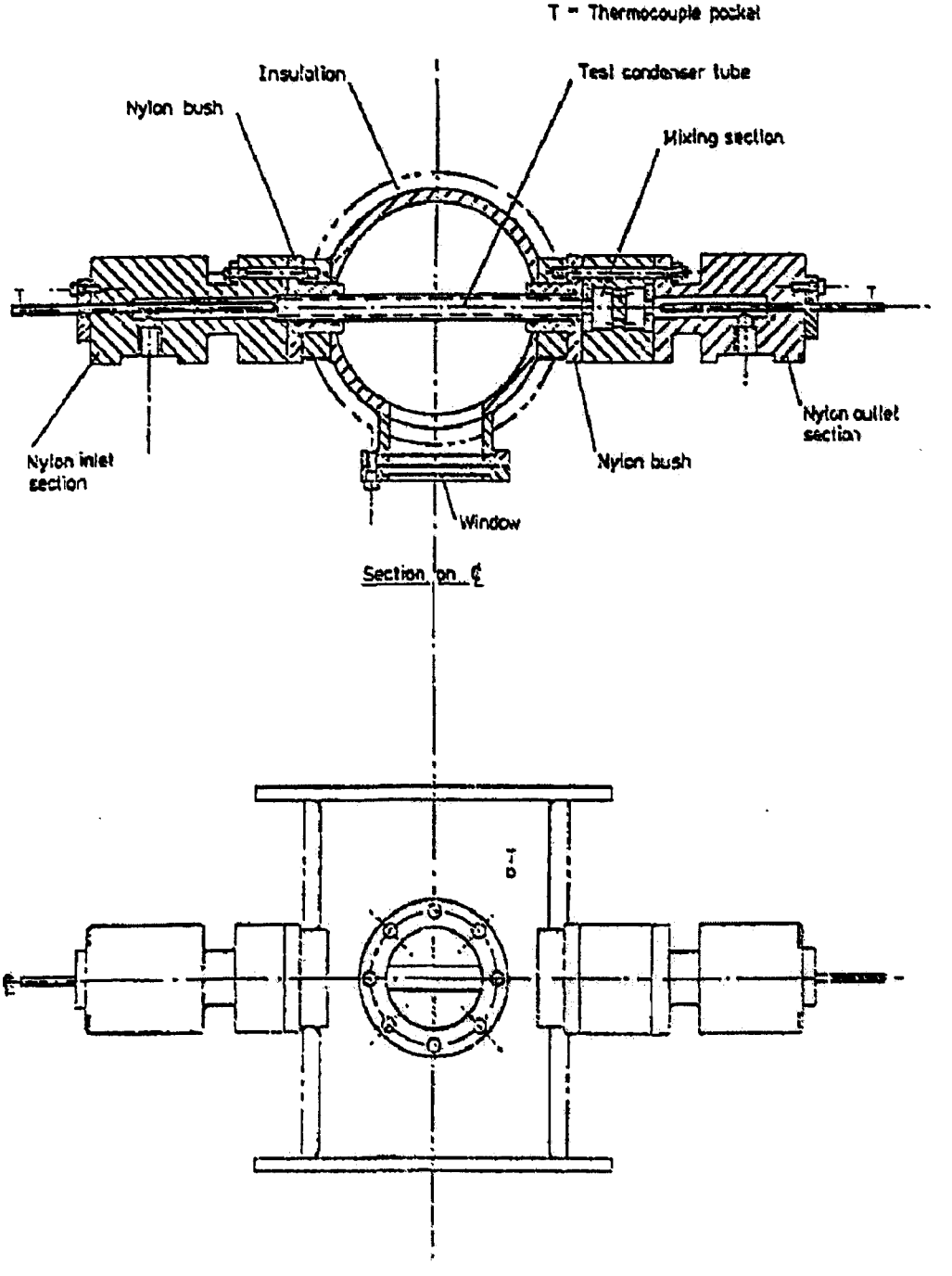

Fig. 4.2. Detail of test section, reproduced from Masuda (1985).

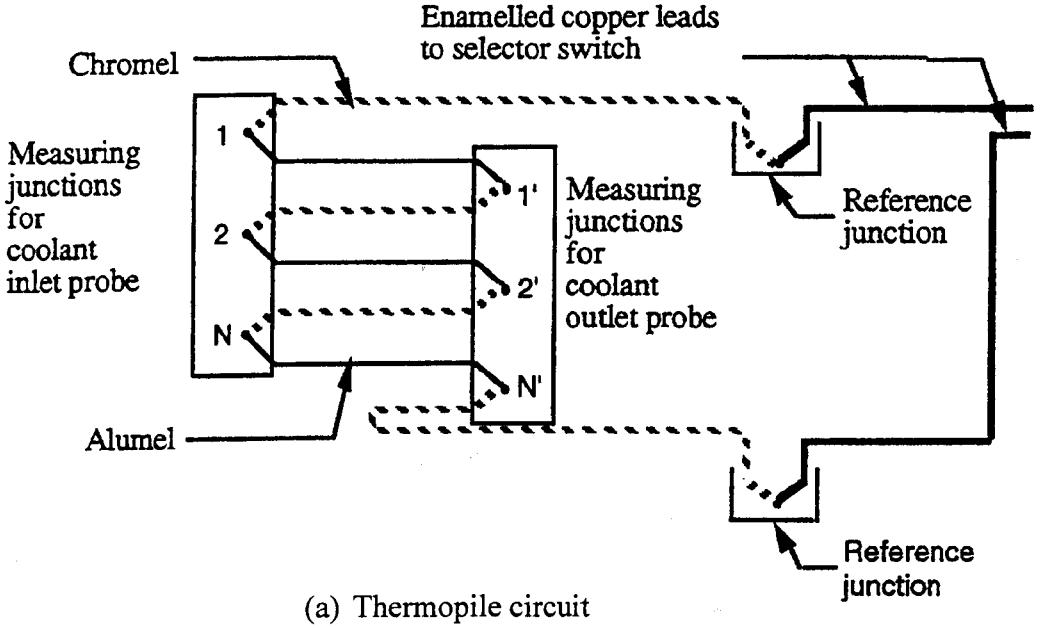

(a) Thermopile circuit
(Two junctions shown)

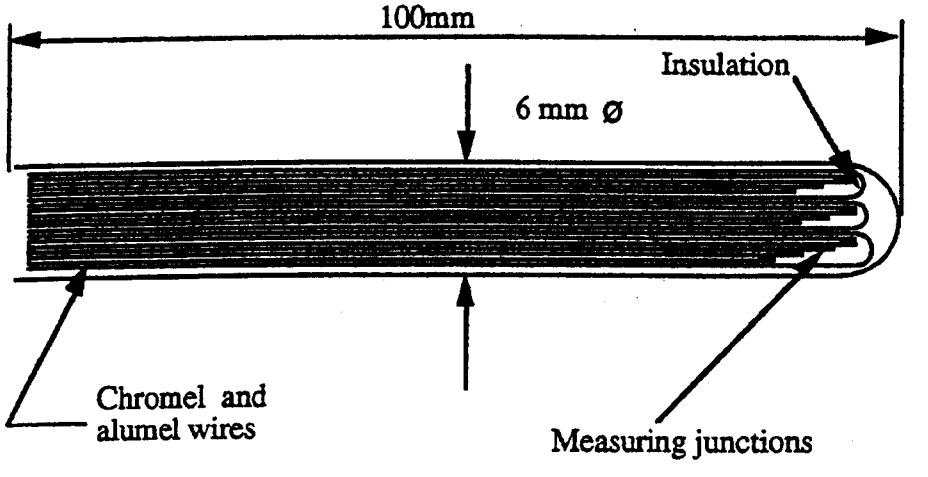

(b) Thermopile pocket
(Three junctions shown)

Fig. 4.3. Ten-junction thermopile, reproduced from Leicy (1999).
(A few junctions shown).

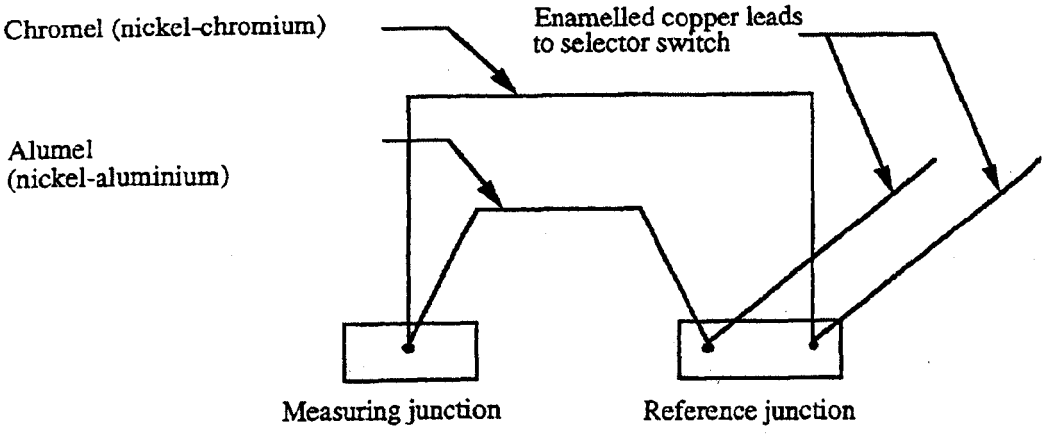

(a) Thermocouple connection

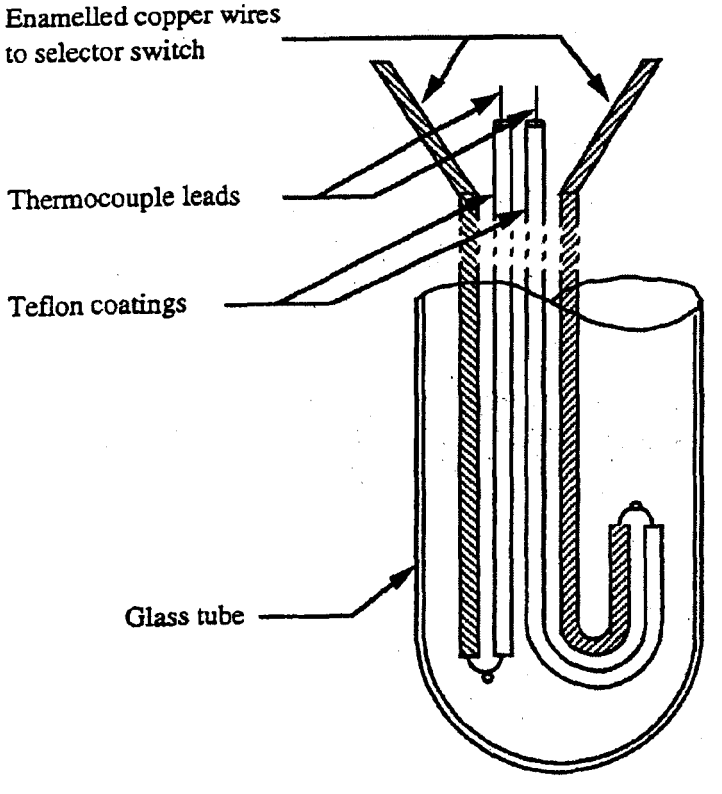

(b) Thermocouple reference junction

Fig. 4.4. Single junction thermocouple, reproduced from Leicy (1999). (Glass tube inside diameter 10 mm, length immersed in ice 250 mm).

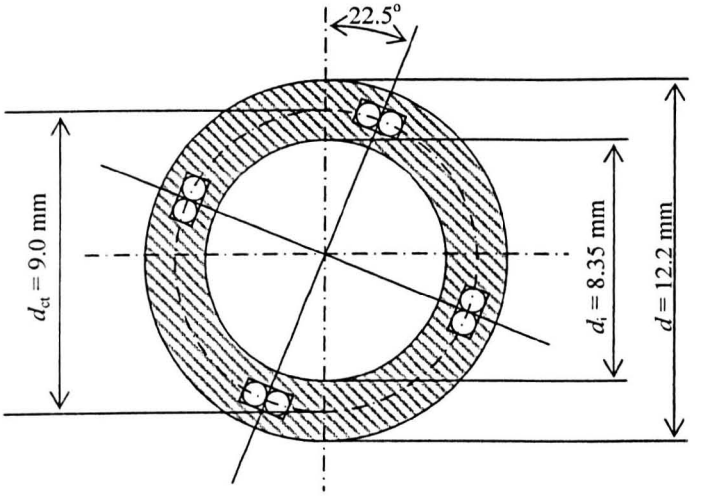

Fig. 4.5. Location of thermocouples in test tube wall.

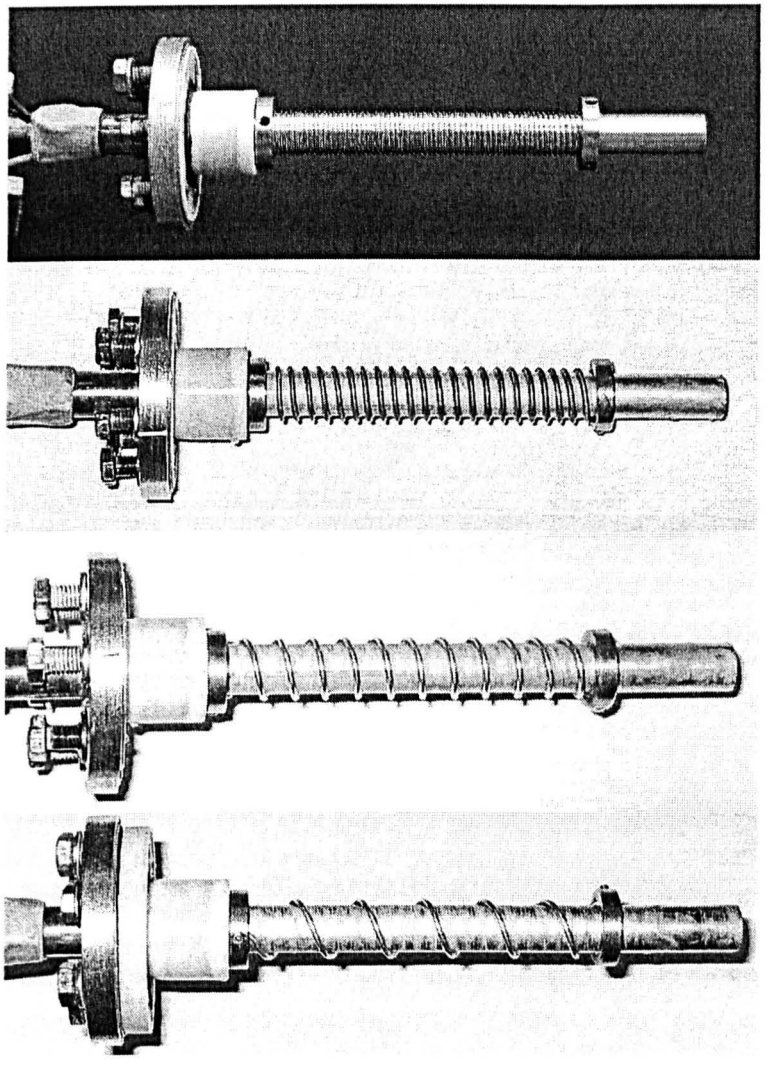

Fig. 4.6. Photographs of wire-wrapped tubes tested.

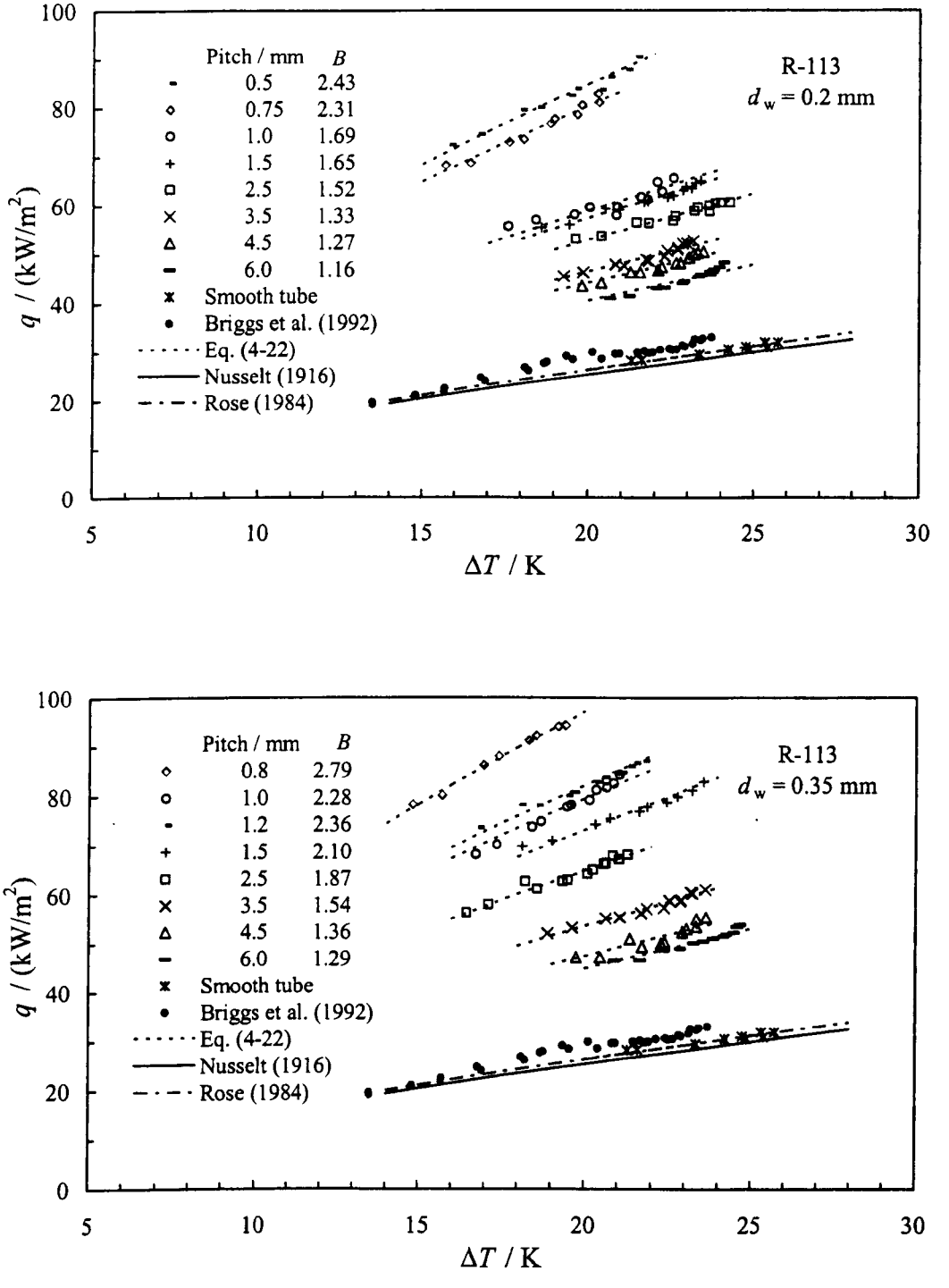

Fig. 4.7. Dependence of heat flux on vapour-to-surface temperature difference for condensation of R-113. (B is 0.758 for smooth tube, vapour approach velocity 0.23 m/s).

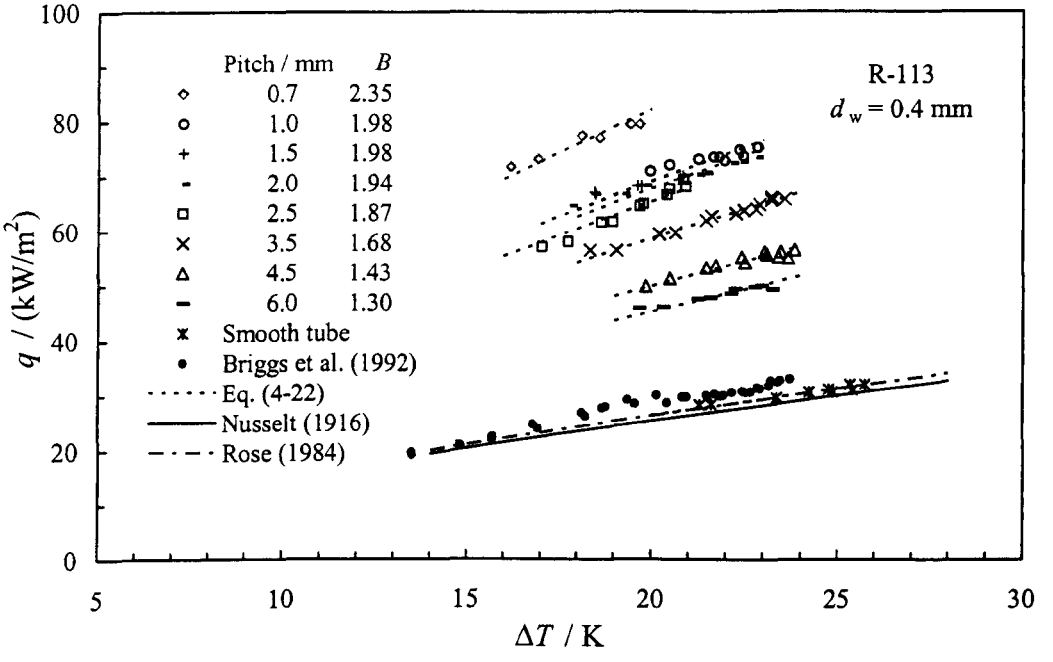

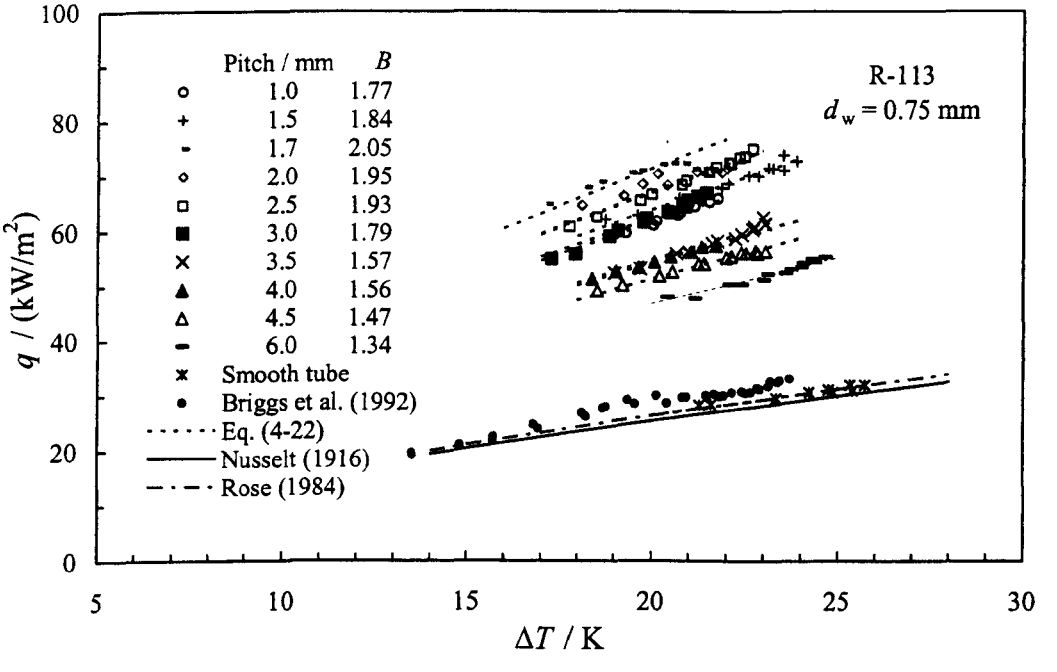

Fig. 4.7. (continued).

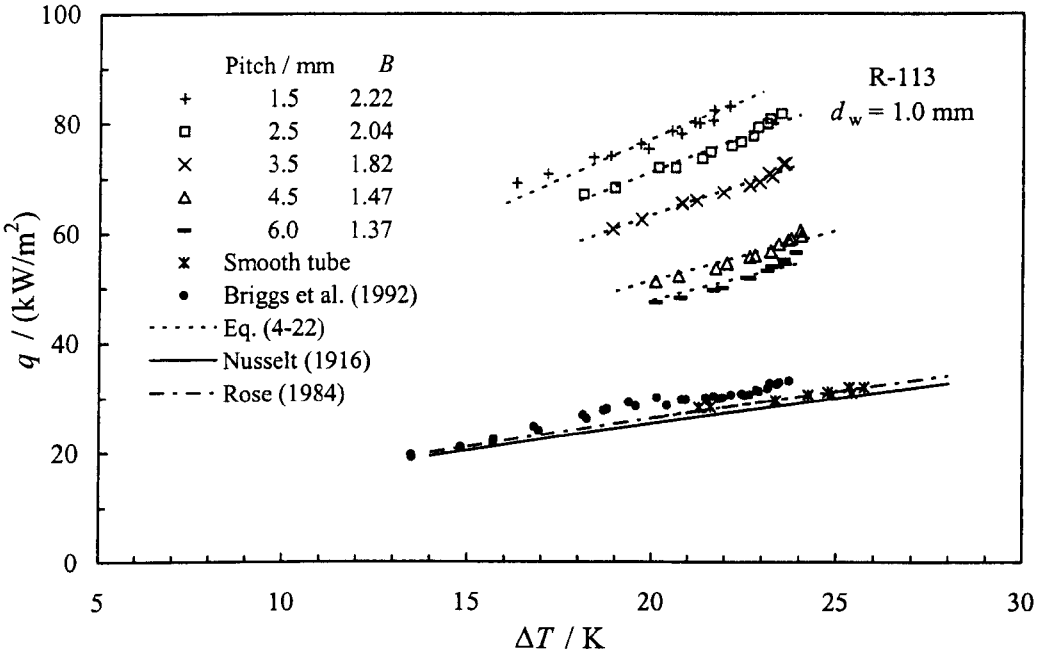

Fig. 4.7. (continued).

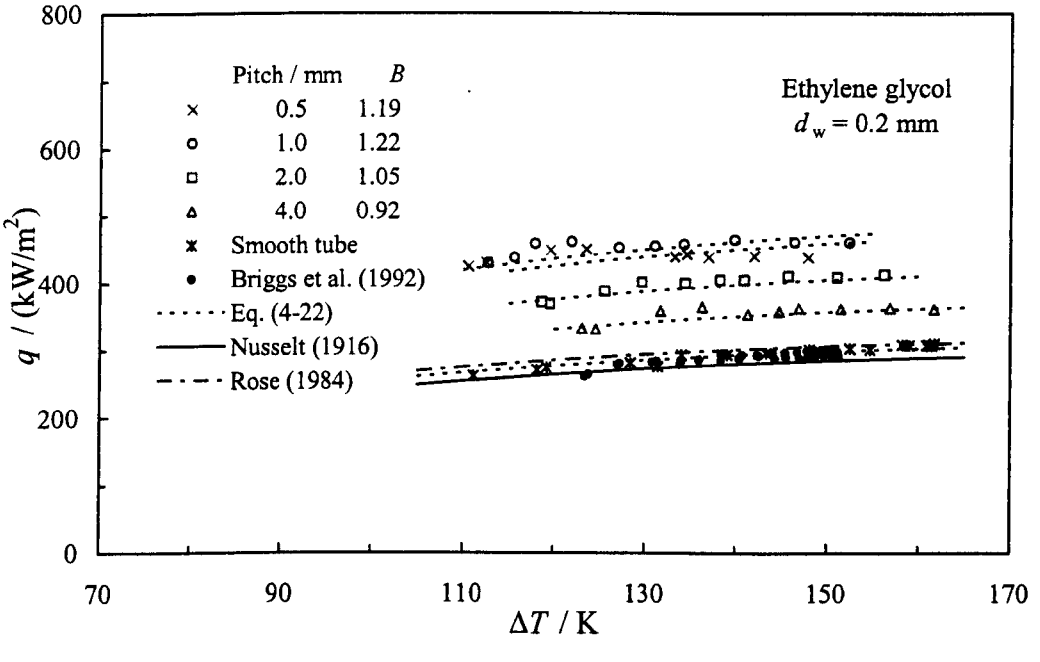

Fig. 4.8. Dependence of heat flux on vapour-to-surface temperature difference for condensation of ethylene glycol. (B is 0.763 for smooth tube, vapour approach velocity 0.41 m/s).

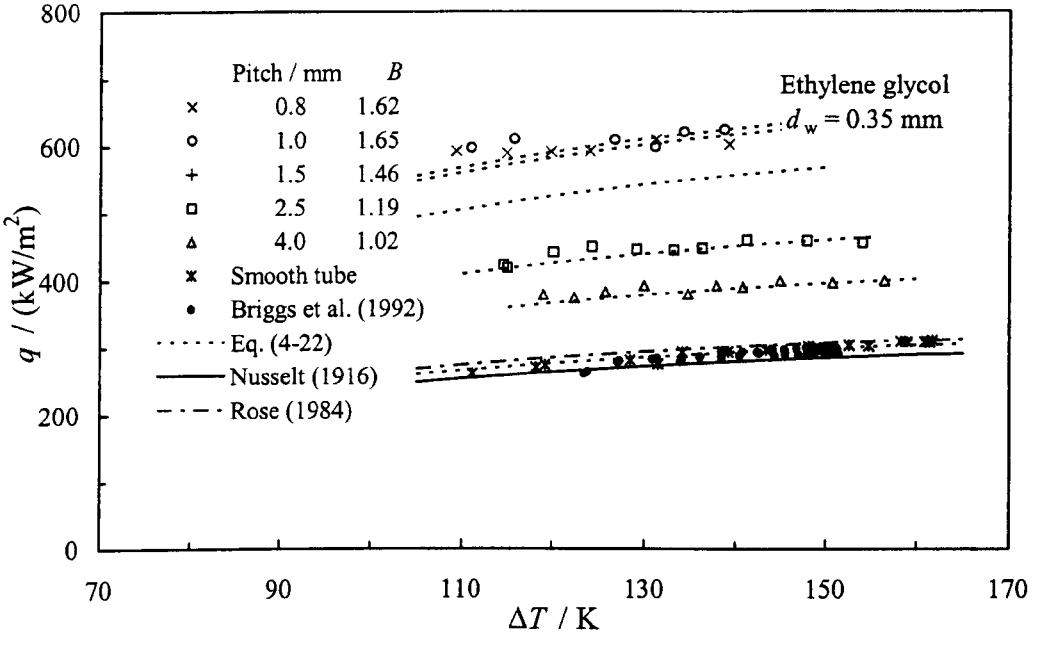

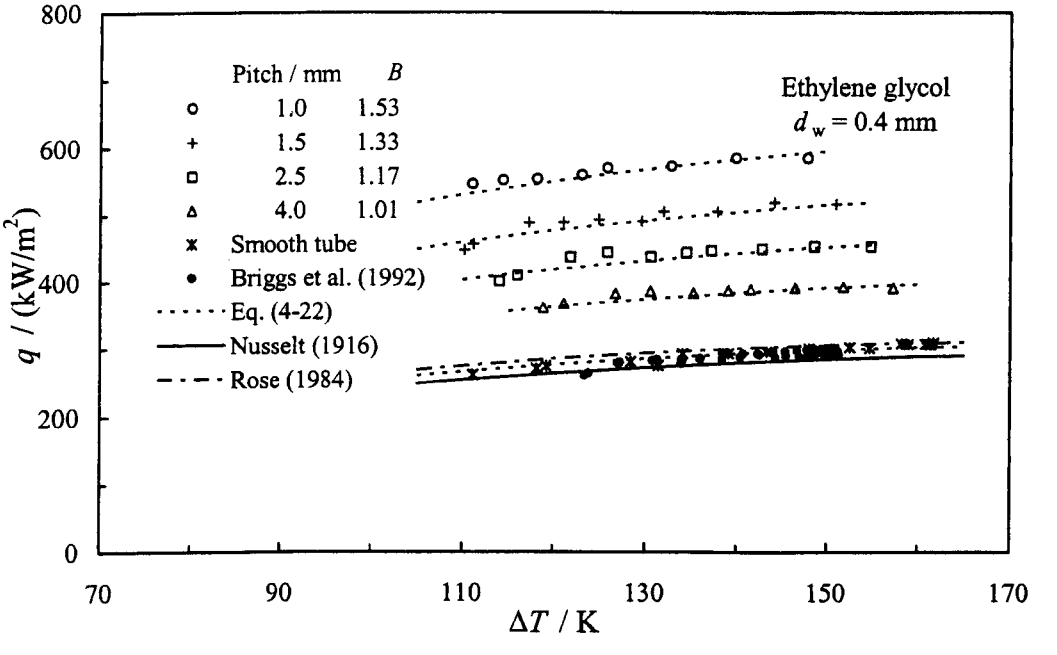

Fig. 4.8. (continued).

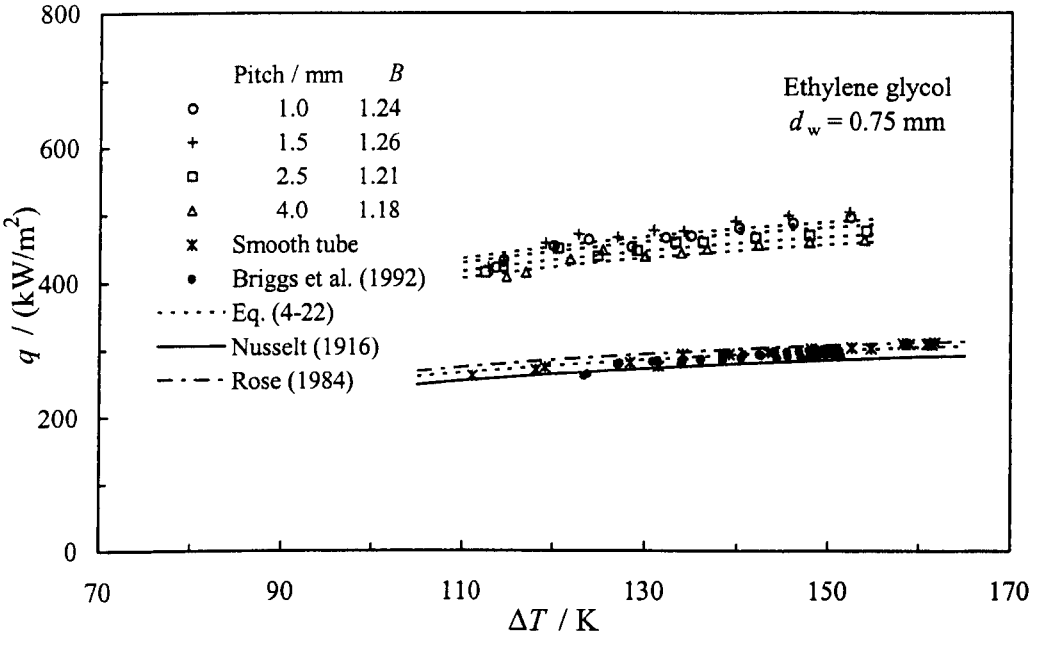

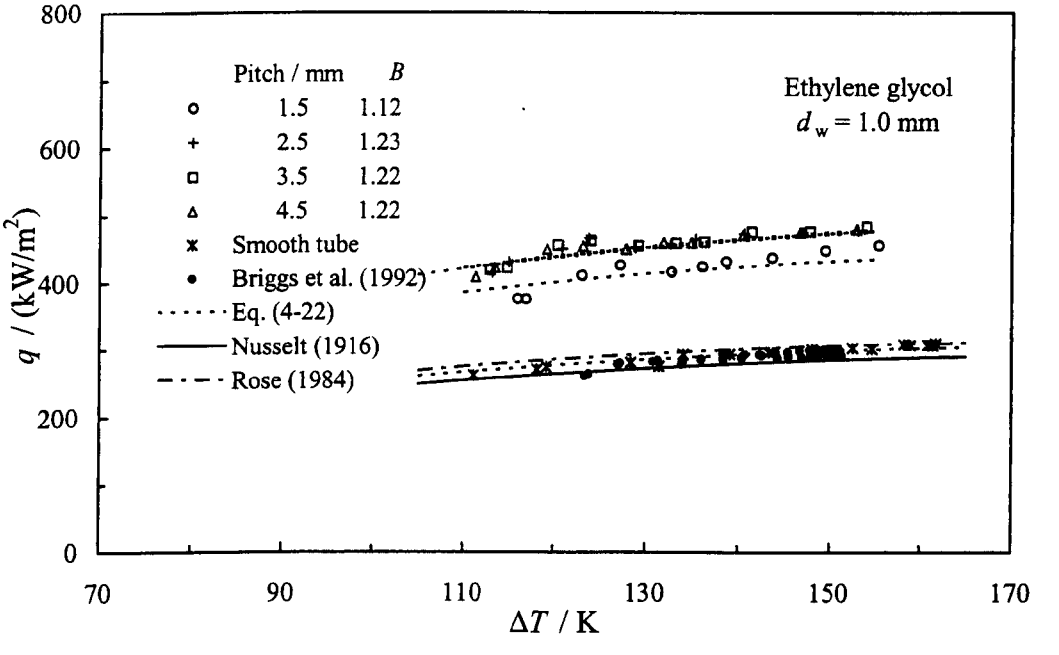

Fig. 4.8. (continued).

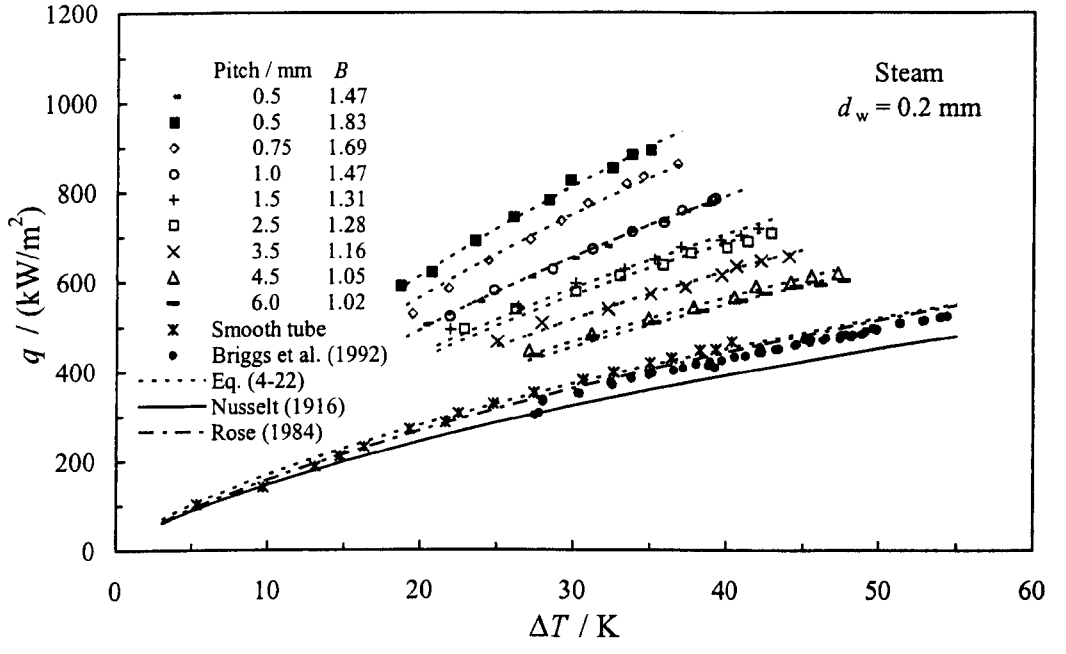

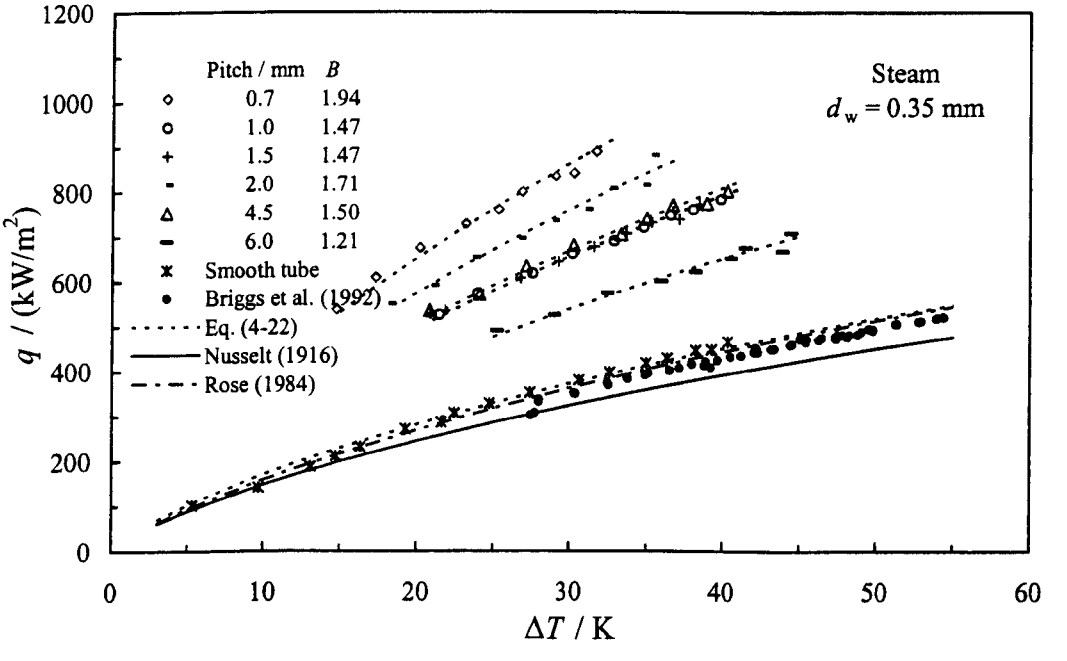

Fig. 4.9. Dependence of heat flux on vapour-to-surface temperature difference for condensation of steam. (B is 0.837 for smooth tube, vapour approach velocity 0.57 m/s).

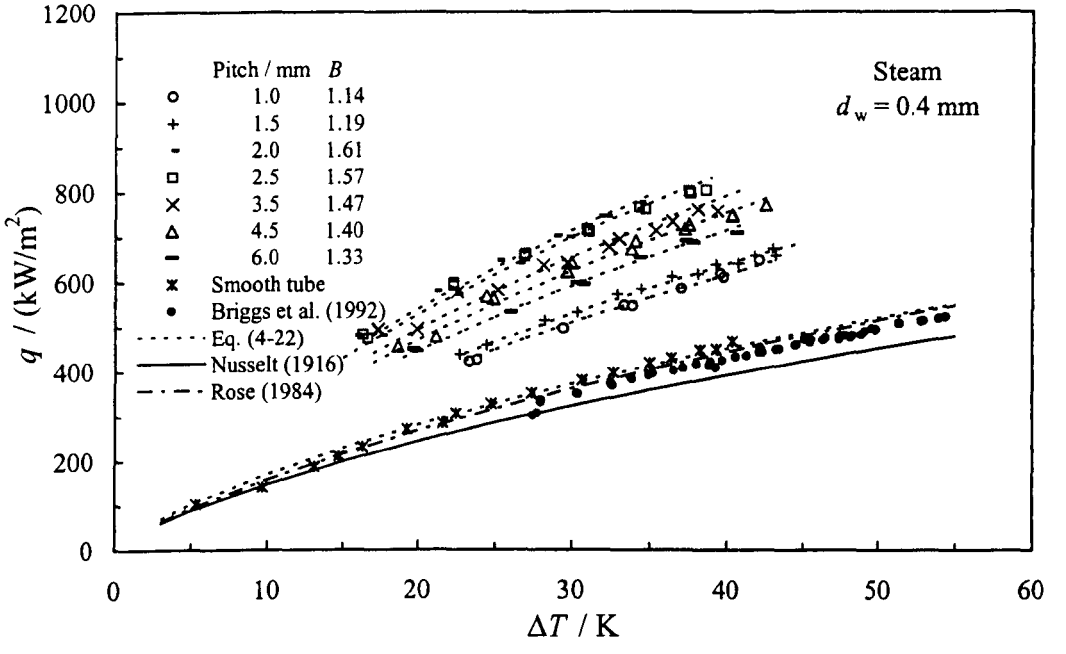

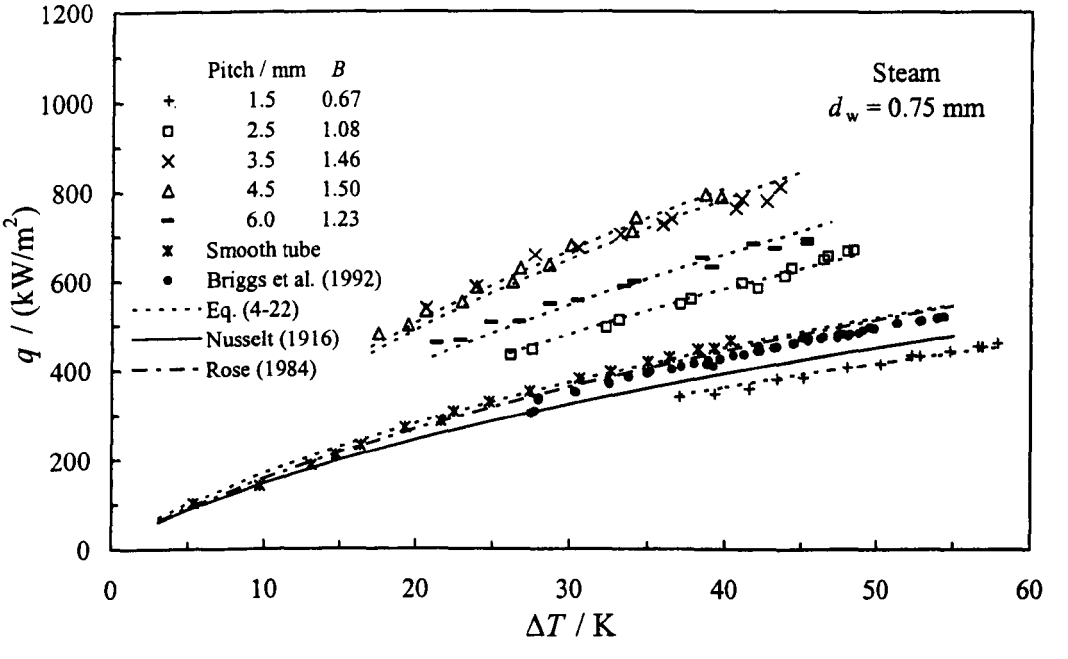

Fig. 4.9. (continued).

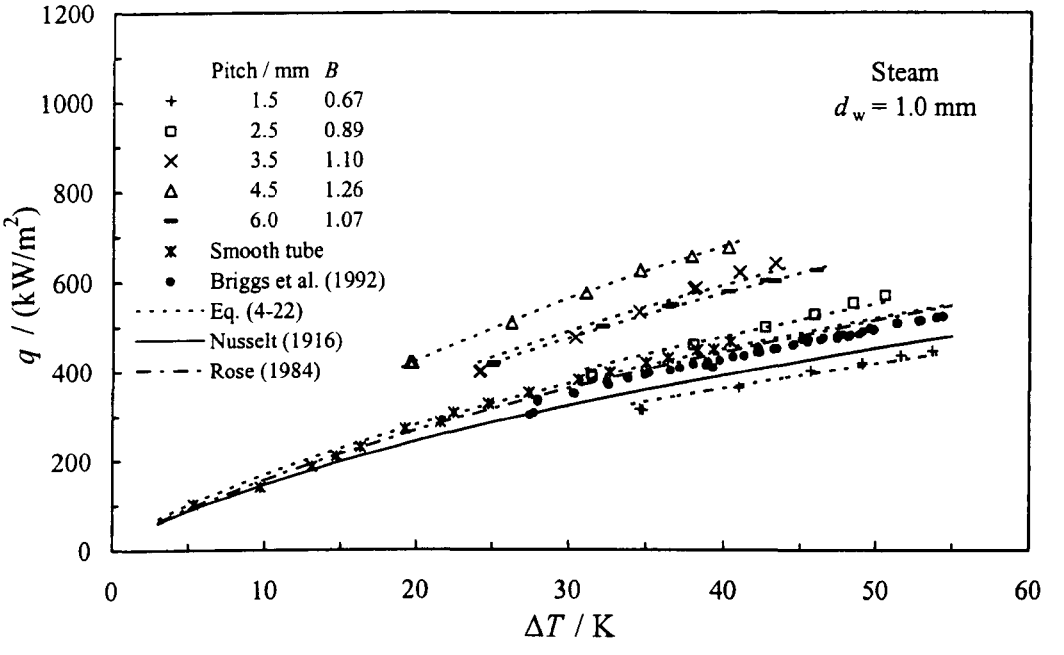

Fig. 4.9. (continued).

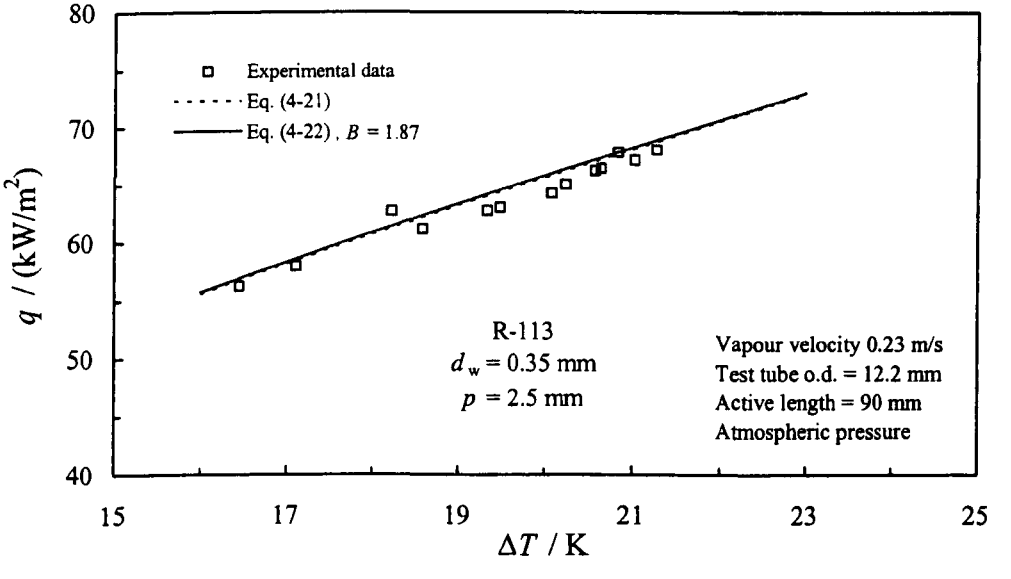

Fig. 4.10. Effect of variable properties on curve fit.

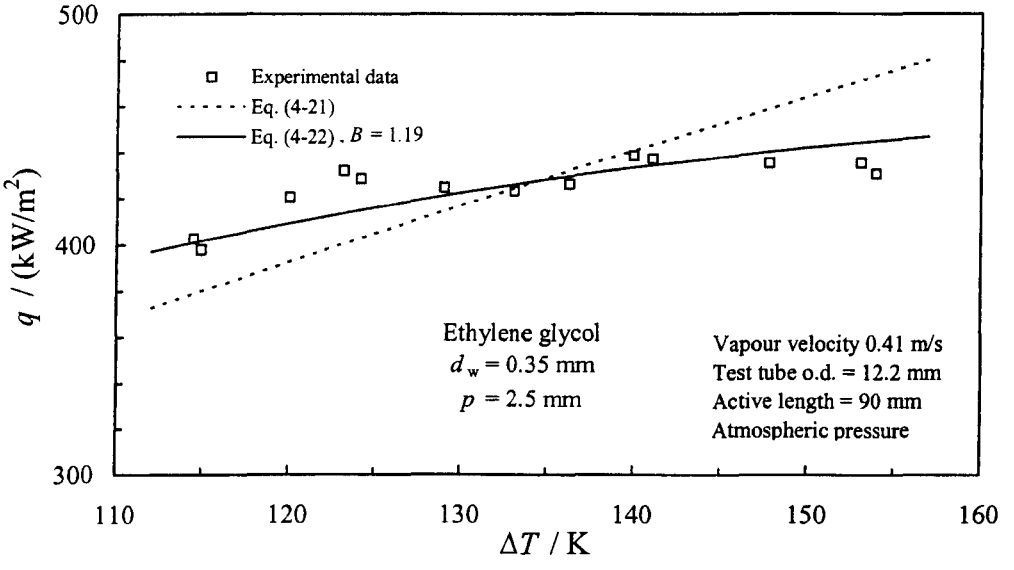

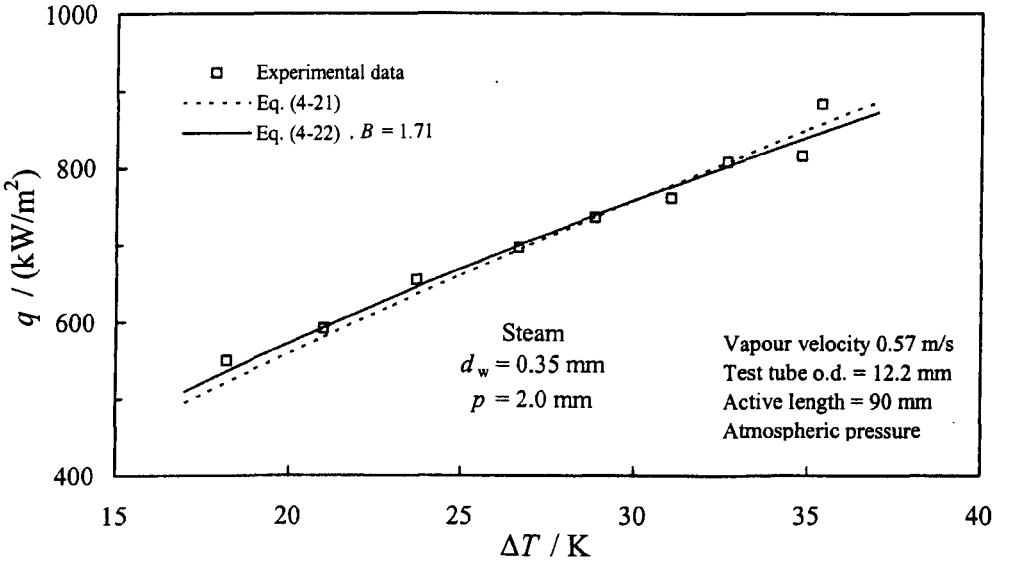

Fig. 4.10. (continued).

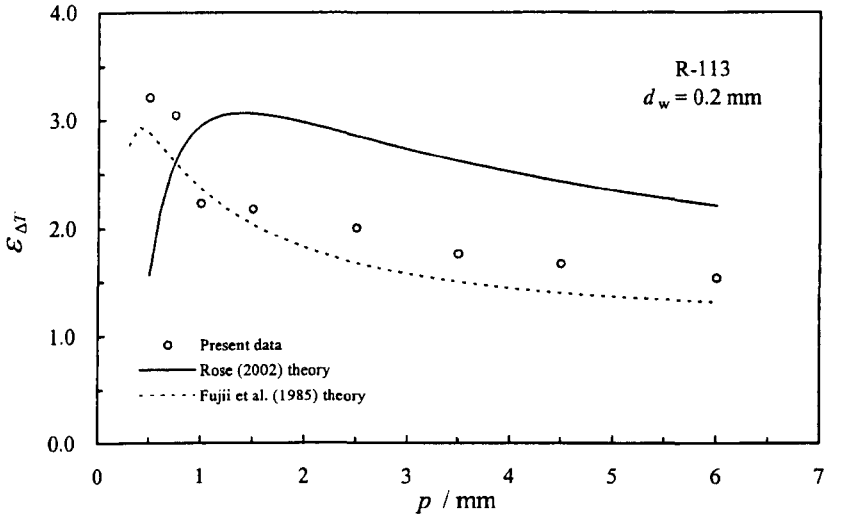

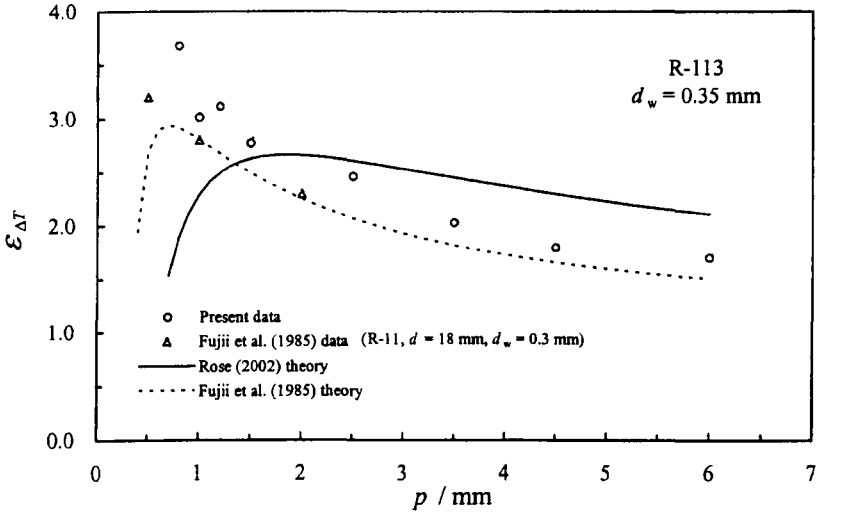

Fig. 4.11. Dependence of enhancement ratio on wire pitch for condensation of R-113. (B is 0.758 for smooth tube, vapour approach velocity 0.23 m/s).

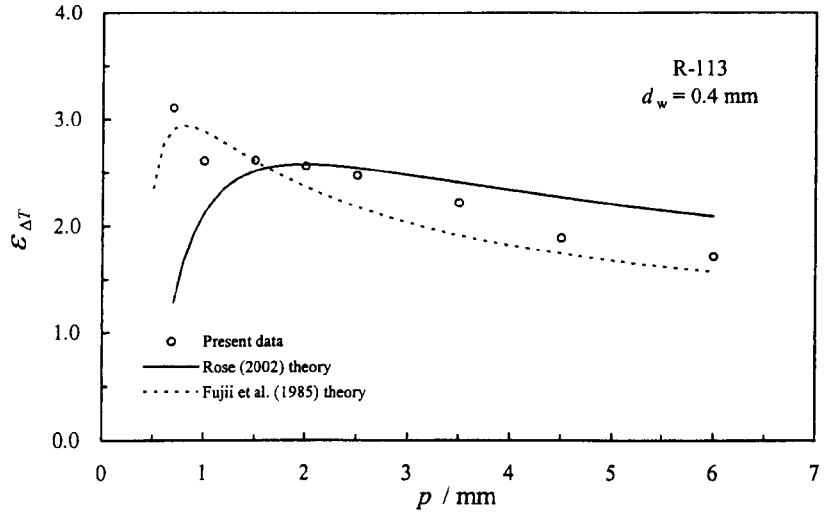

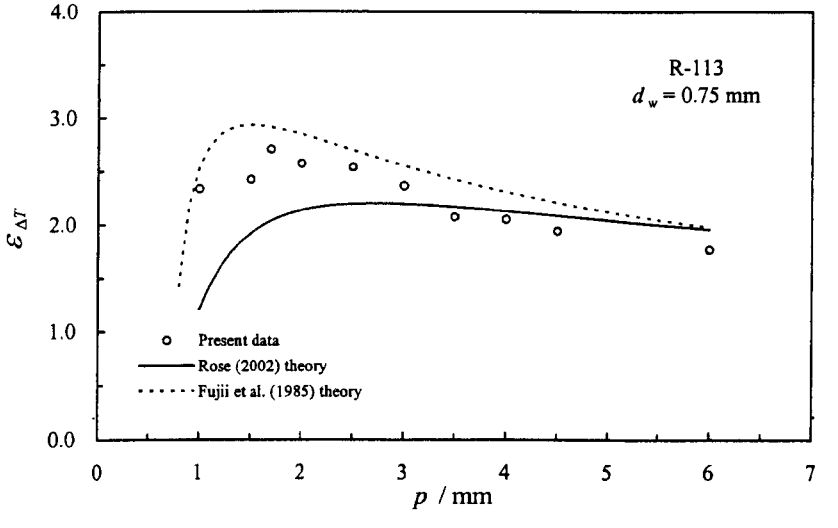

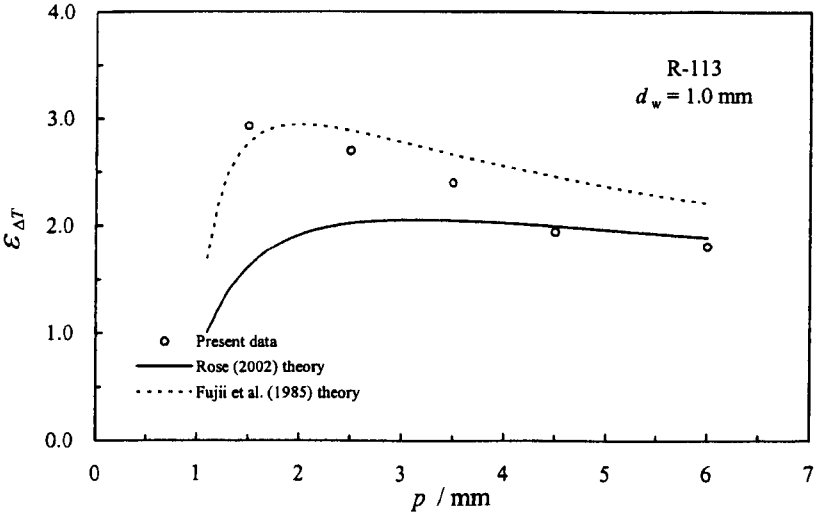

Fig. 4.11. (continued).

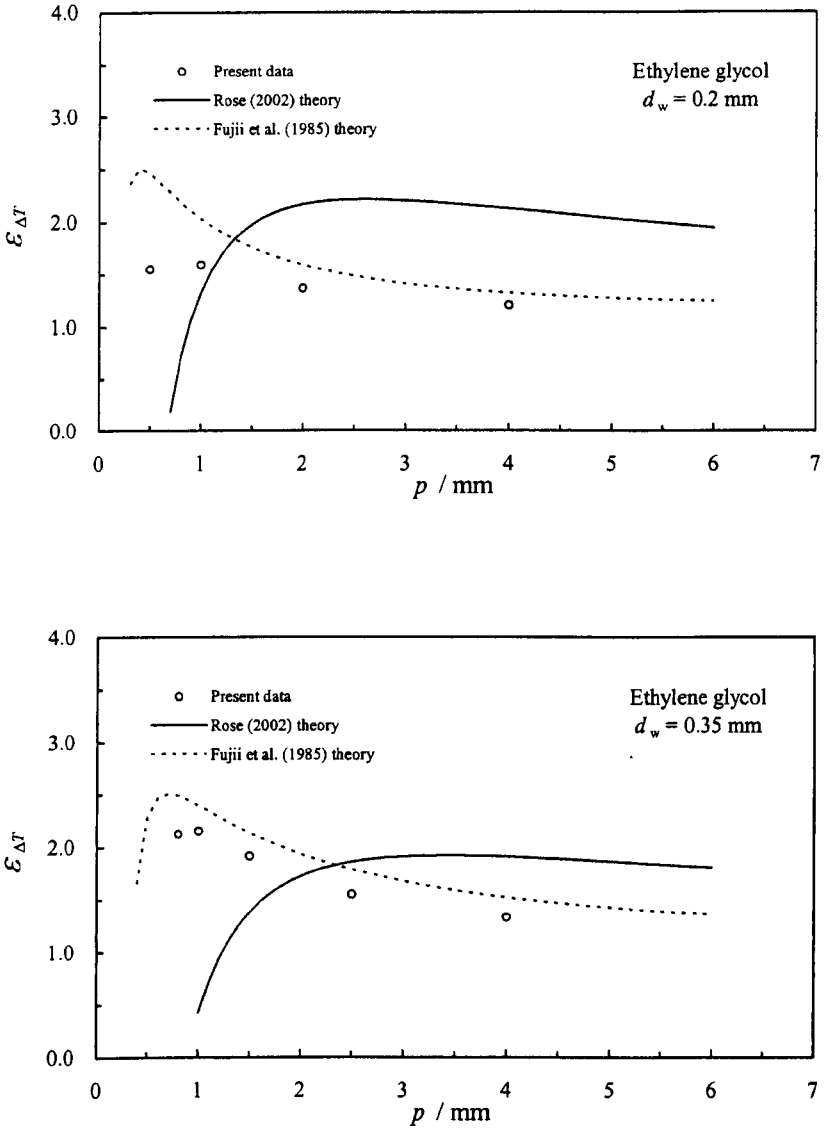

Fig. 4.12. Dependence of enhancement ratio on wire pitch for condensation of ethylene glycol. (B is 0.763 for smooth tube, vapour approach velocity 0.41 m/s).

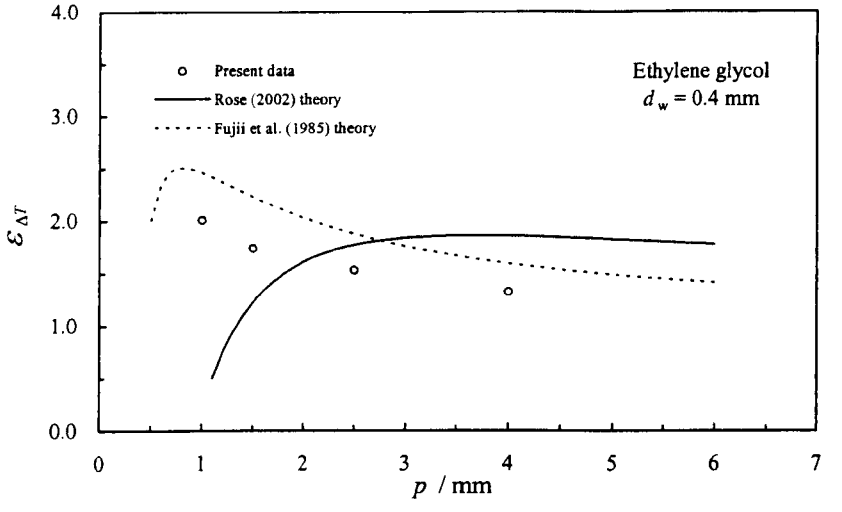

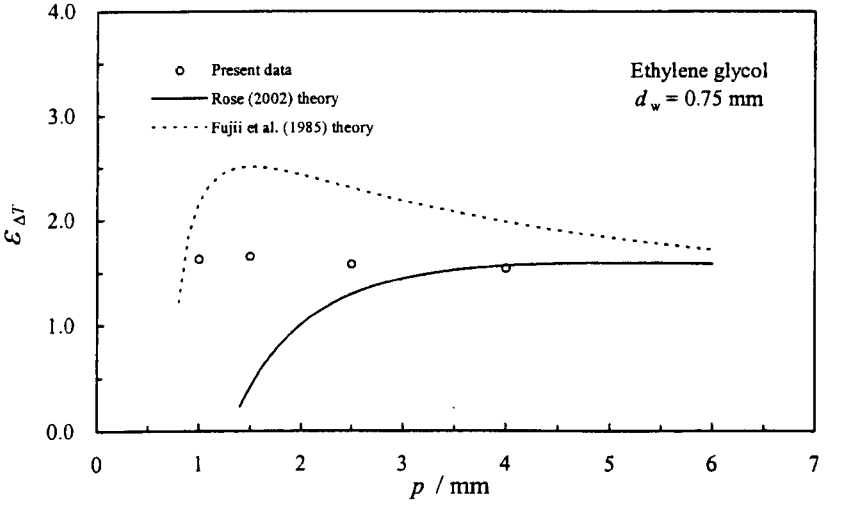

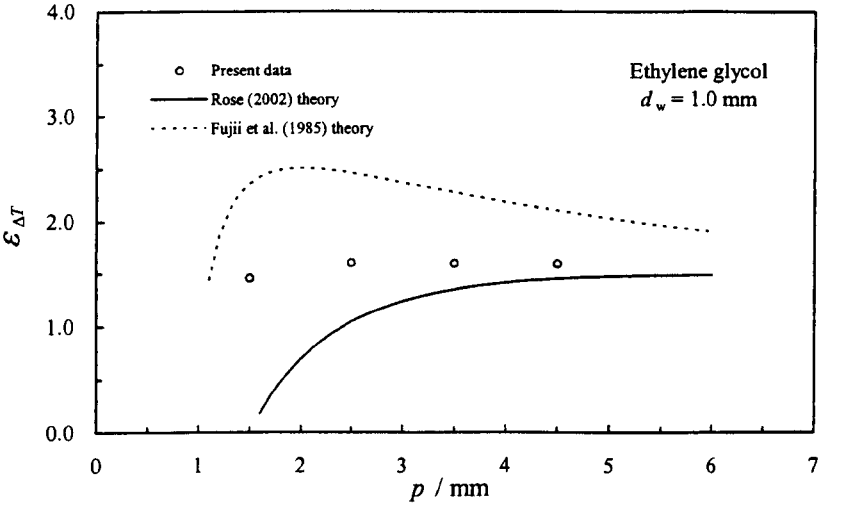

Fig. 4.12. (continued).

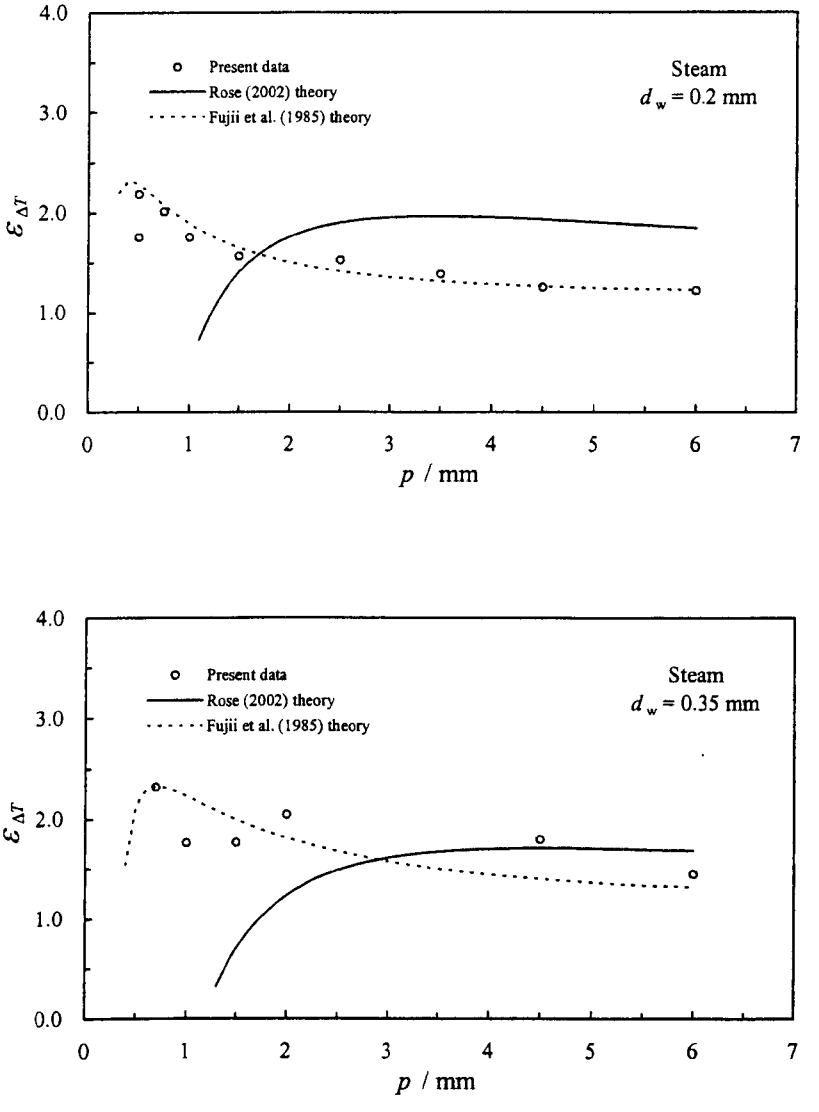

Fig. 4.13. Dependence of enhancement ratio on wire pitch for condensation of steam. (B is 0.837 for smooth tube, vapour approach velocity 0.57 m/s).

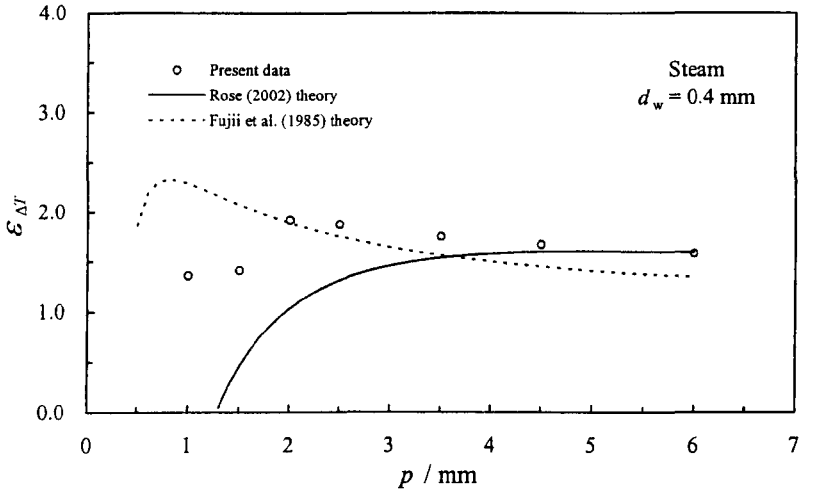

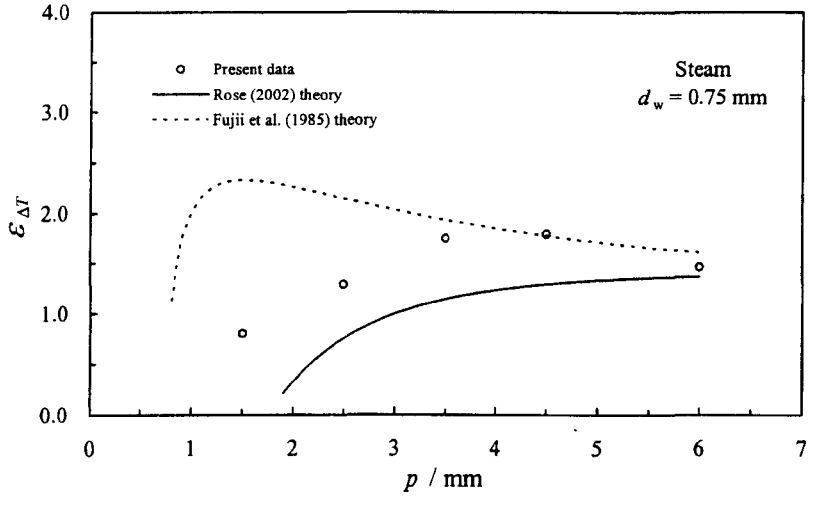

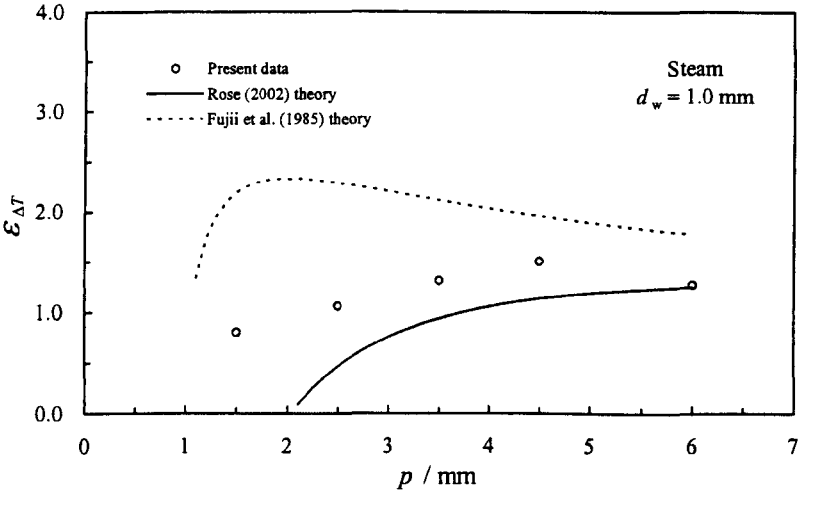

Fig. 4.13. (continued).

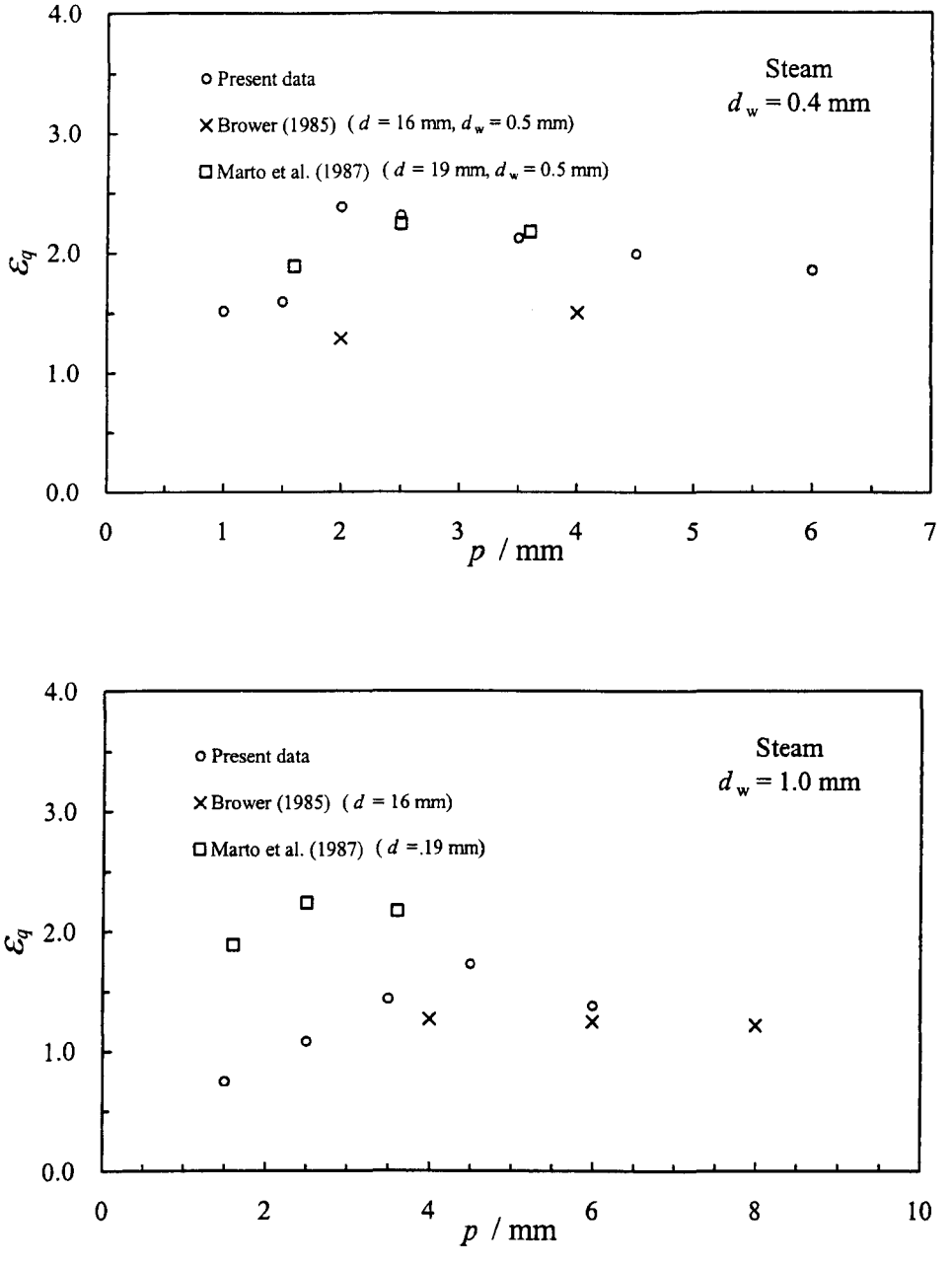

Fig. 4.14. Comparison with experimental data of Marto et al. (1987) and Brower (1985). Dependence of enhancement ratio at the same heat flux on wire pitch for 0.4 mm and 1.0 mm diameter wires.

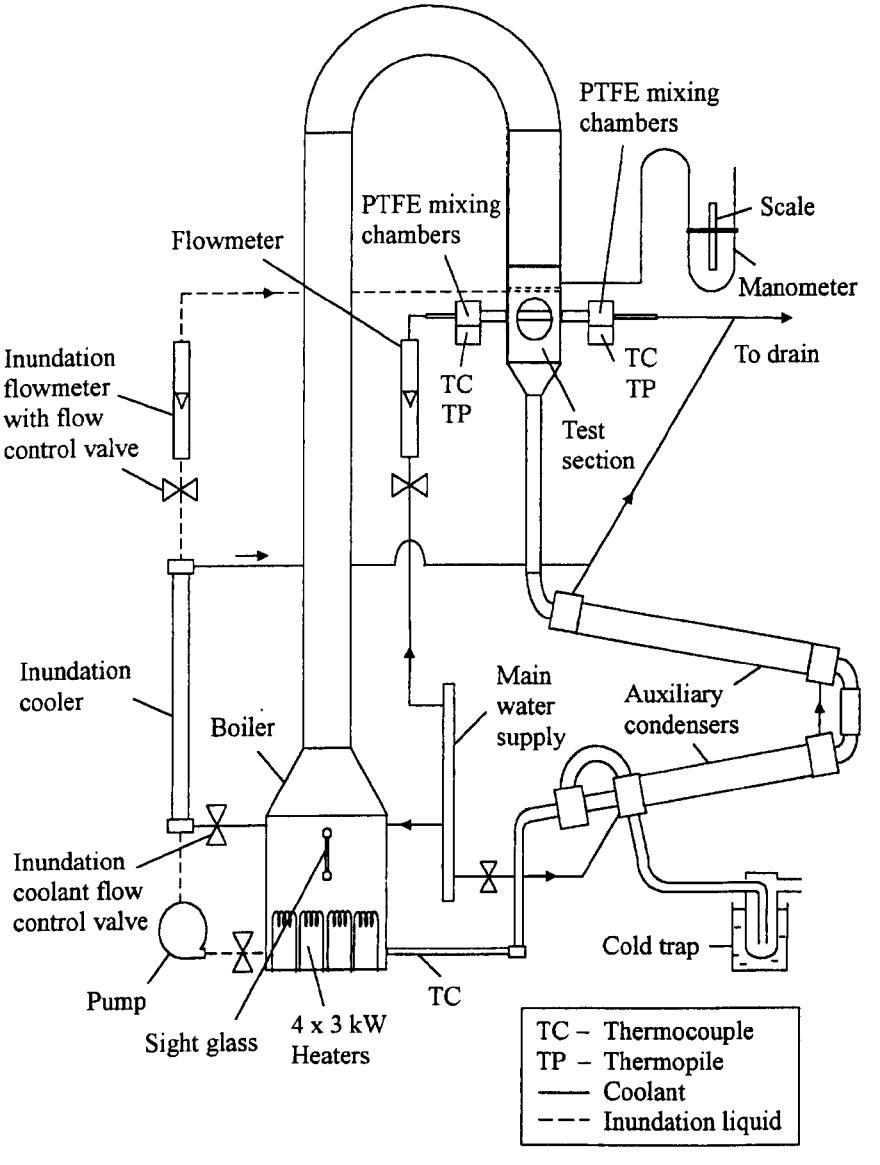

Fig. 4.15. Modified test apparatus for inundation investigation.

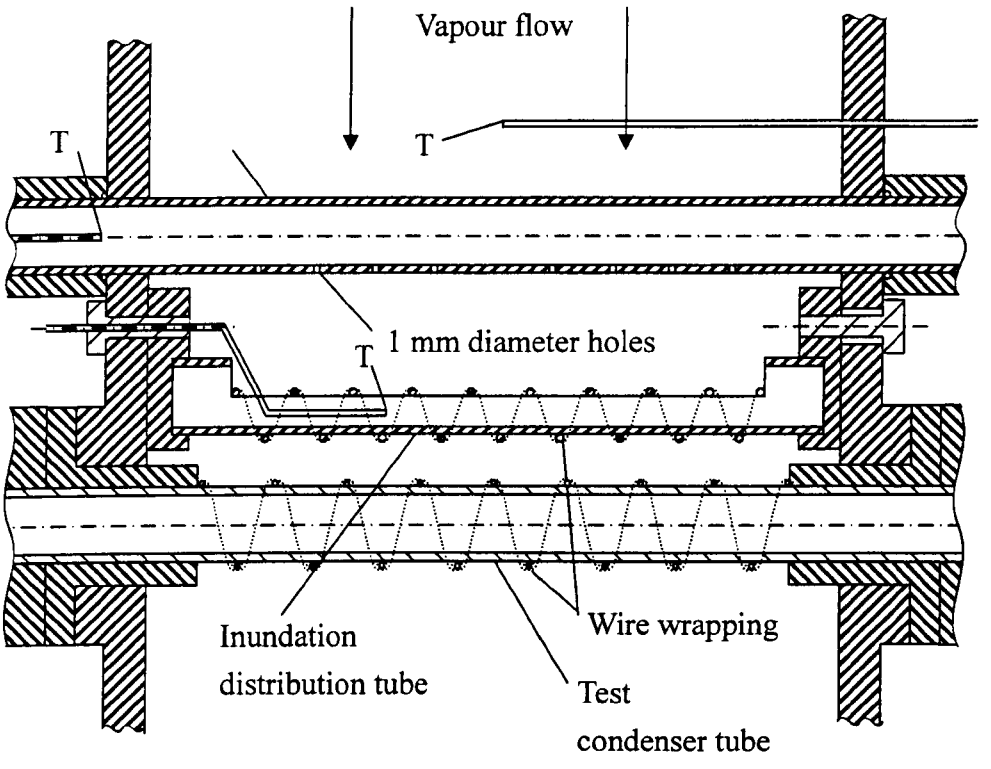

Fig. 4.16. Detail of modified test section showing inundation supply and distribution tubes and positions of thermocouples for vapour temperature and inundation supply temperatures. T denotes thermocouple junction.

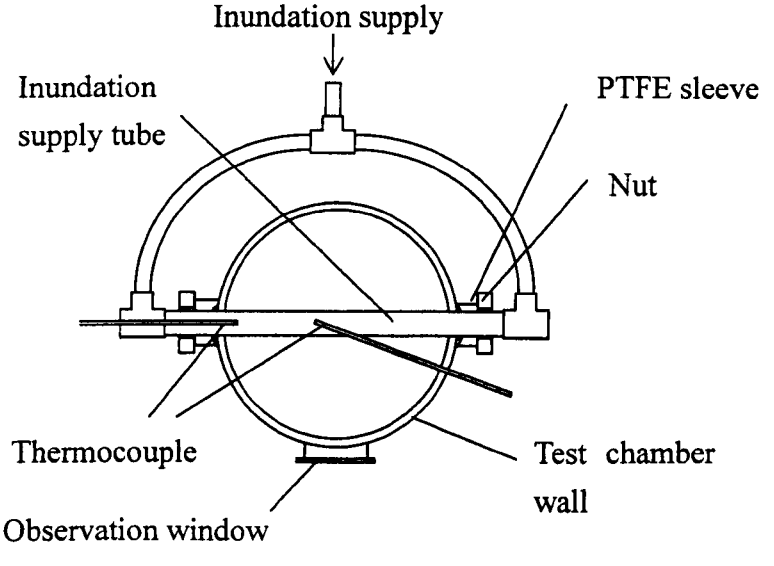

Fig. 4.17. Plan view of connections around test chamber.

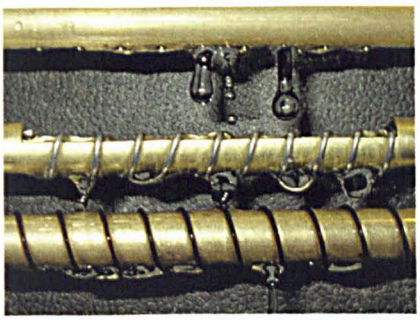

(a) Inundation rate 0.2 l/min

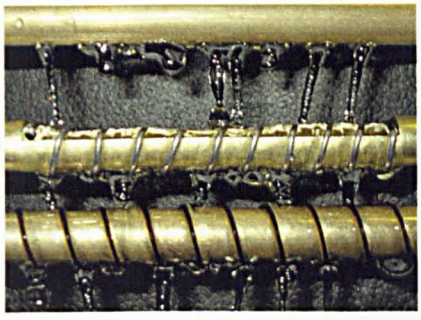

(b) Inundation rate 0.5 l/min

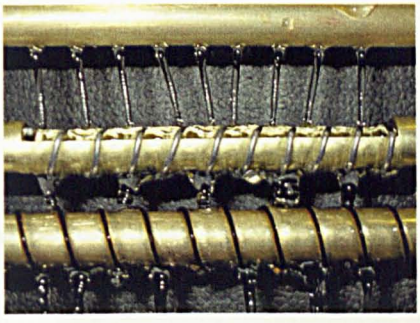

(c) Inundation rate 0.8 l/min

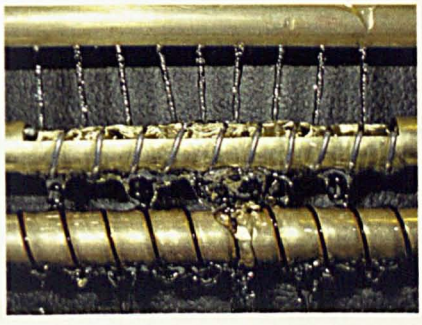

(d) Inundation rate 1.2 l/min

Fig. 4.18. Photographs of preliminary tests to obtain uniform distribution of inundation.

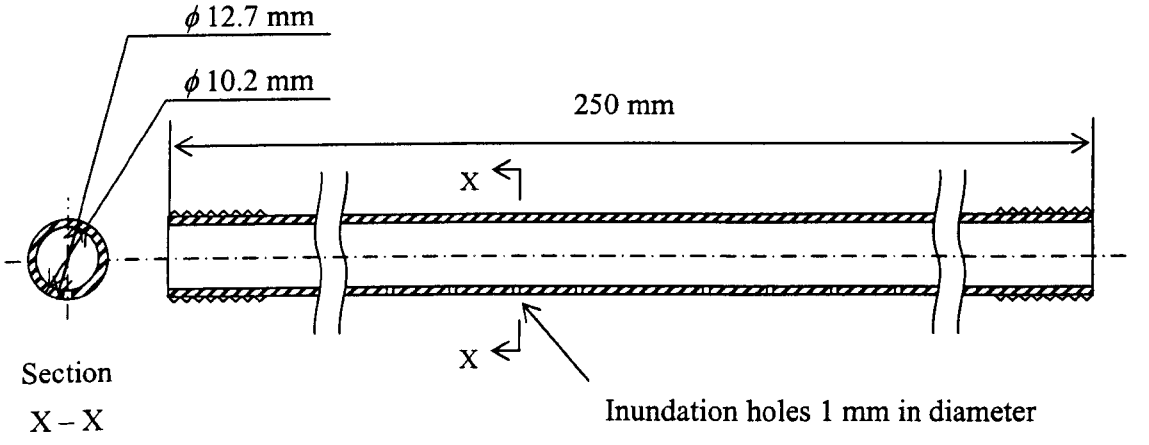

Fig. 4.19. Detail of inundation supply tube.

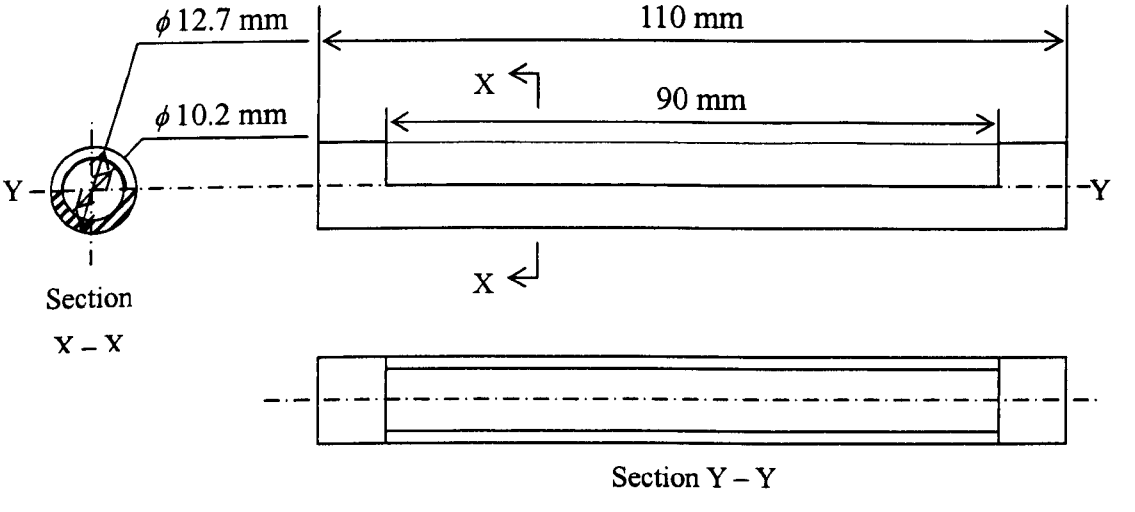

Fig. 4.20. Detail of inundation distribution tube.

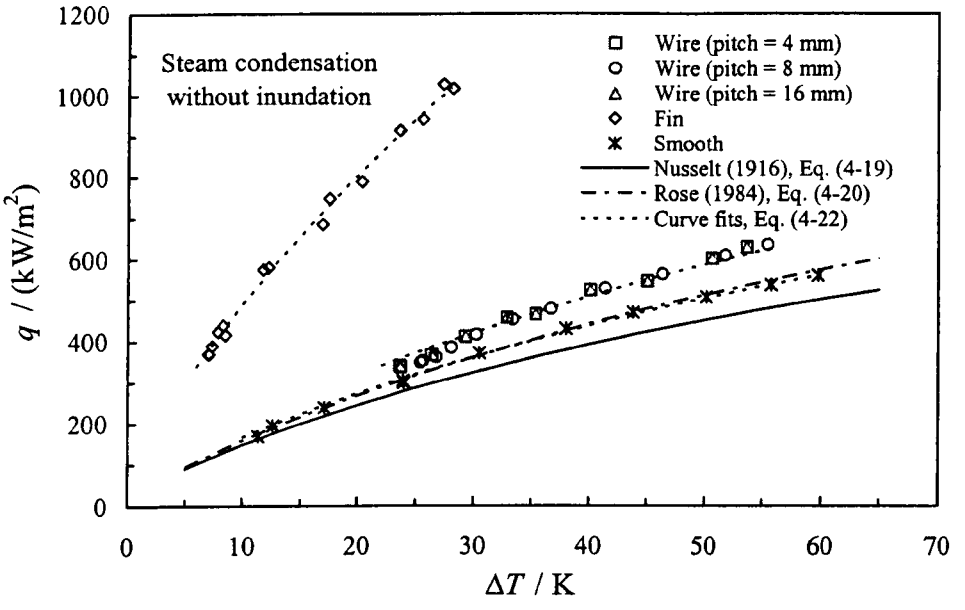

Fig. 4.21. Dependence of heat flux on vapour-to-surface temperature difference for steam condensation without inundation on smooth, wire-wrapped and low integral-finned tubes. (Wire diameter 1.6 mm, vapour approach velocity 0.56 m/s).

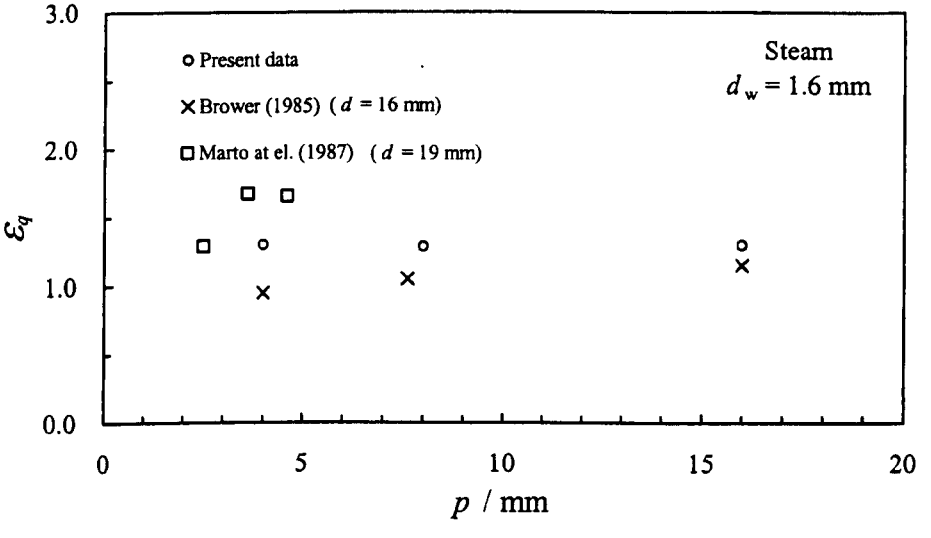

Fig. 4.22. No inundation comparison with experimental data of Marto et al. (1987) and Brower (1985) for wire-wrapped tubes. Dependence of enhancement ratio at the same heat flux on wire pitch for 1.6 mm diameter wire.

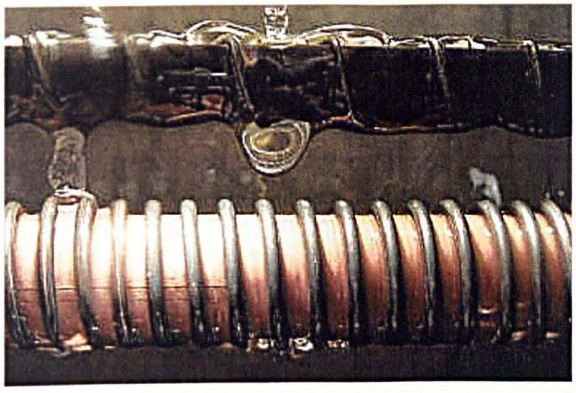

(a) Inundation rate 0.1 l/min

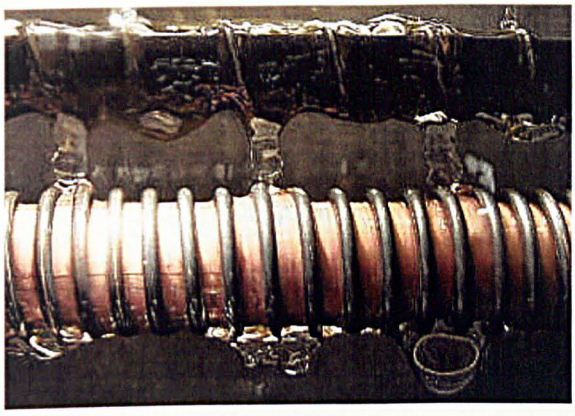

(b) Inundation rate 0.3 l/min

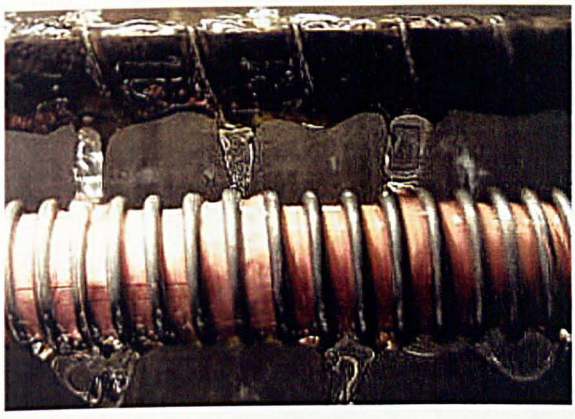

(c) Inundation rate 0.5 l/min

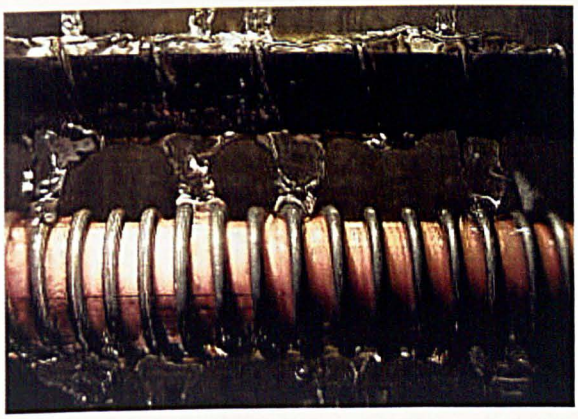

(d) Inundation rate 0.8 l/min

Fig. 4.23. Photographs of inundation during steam condensation on wire-wrapped tube. (Wire diameter 1.6 mm, wire pitch 4 mm.)

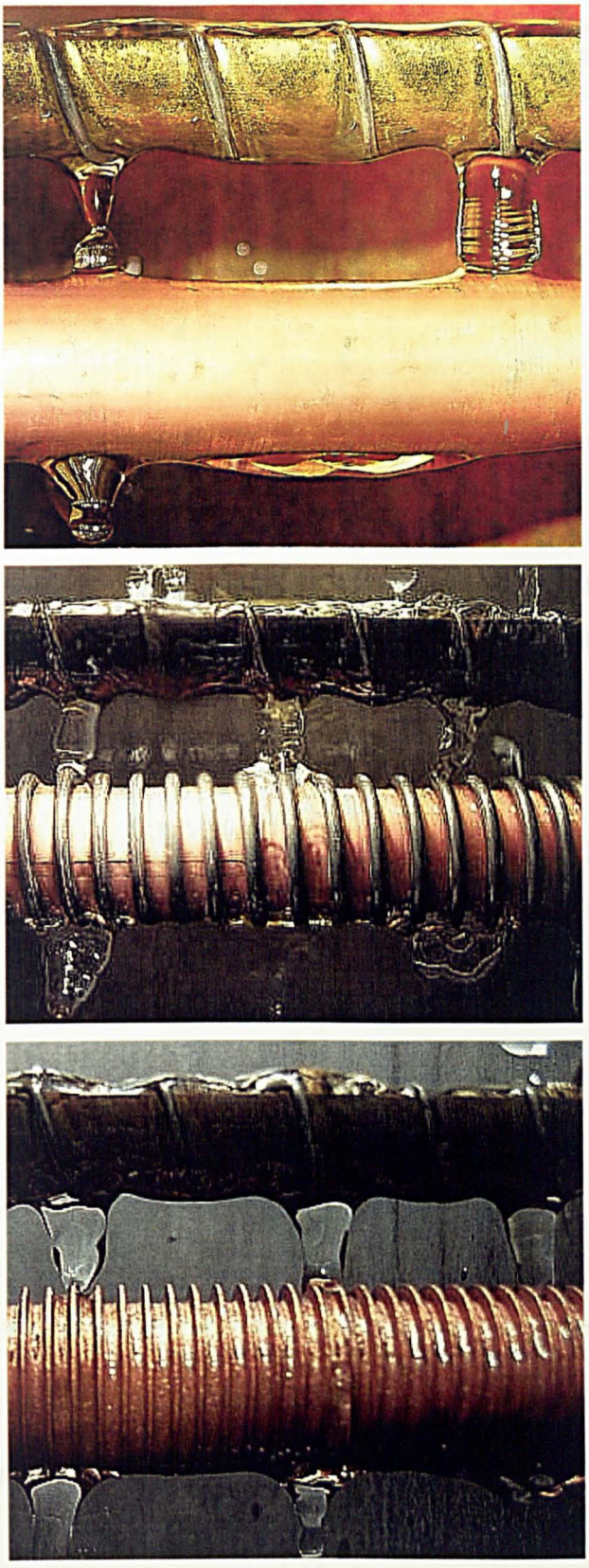

Fig. 4.24. Photographs of inundation during steam condensation on smooth, wire-wrapped and finned tubes. (Inundation rate 0.4 l/min.)

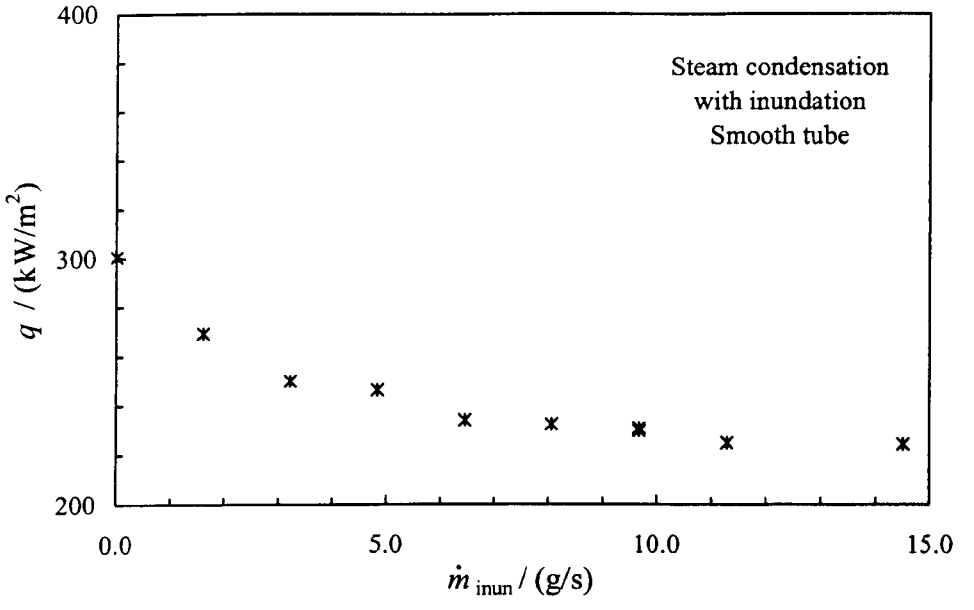

Fig. 4.25. Dependence of heat flux on inundation rate for steam condensation with inundation on smooth tube. (Vapour approach velocity 0.56 m/s, coolant flow rate 2.0 l/min.)

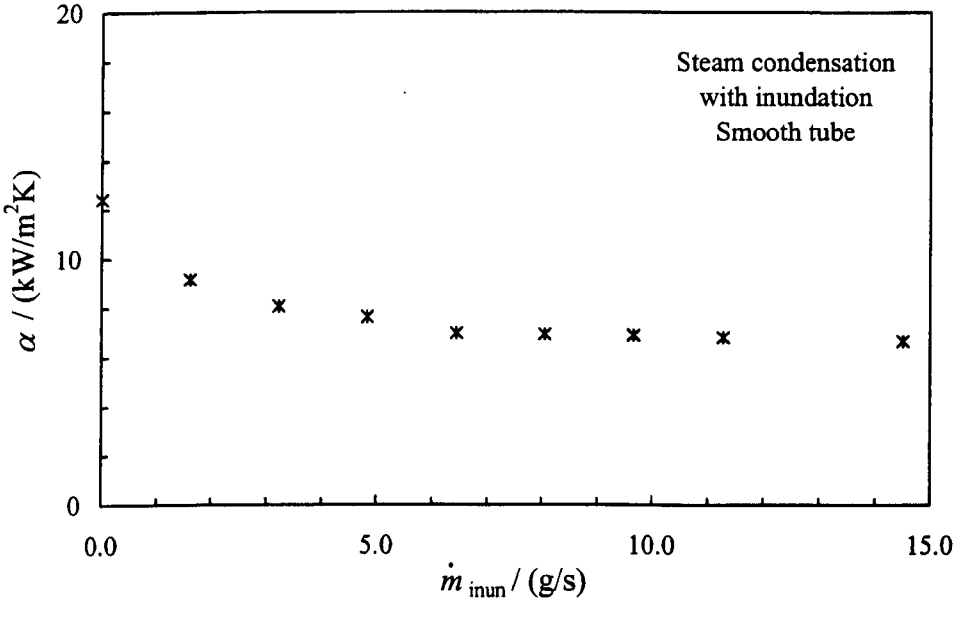

Fig. 4.26. Dependence of vapour-side, heat-transfer coefficient on inundation rate for steam condensation with inundation on smooth tube. (Vapour approach velocity 0.56 m/s, coolant flow rate 2.0 l/min.)

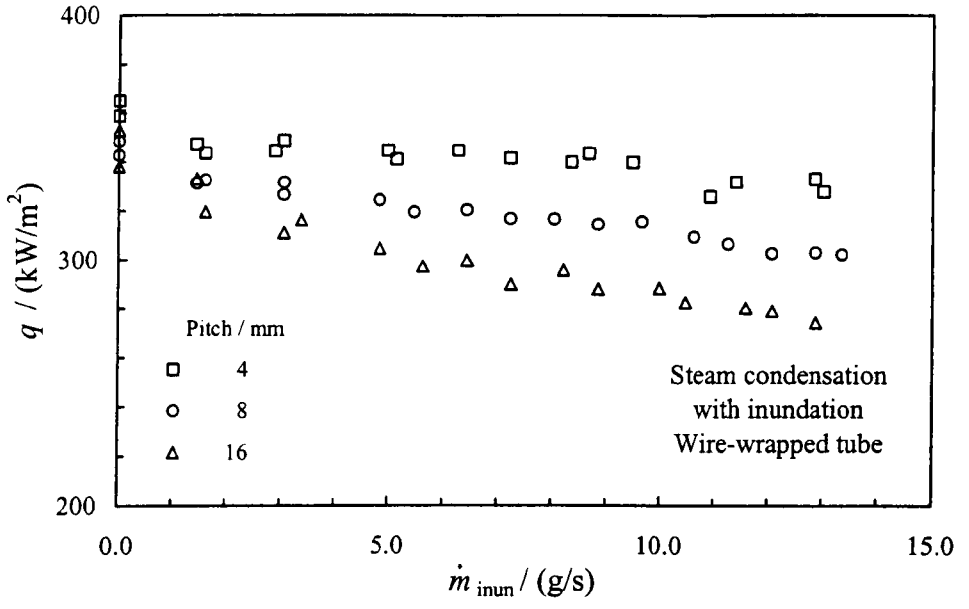

Fig. 4.27. Dependence of heat flux on inundation rate for steam condensation with inundation on wire-wrapped tubes. (Wire diameter 1.6 mm, vapour approach velocity 0.56 m/s, coolant flow rate 2.0 l/min.)

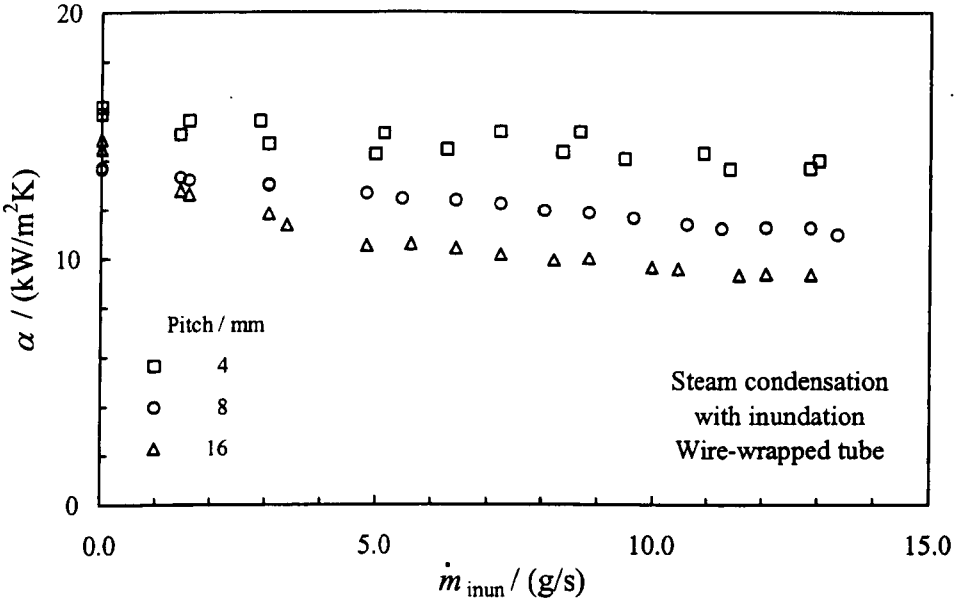

Fig. 4.28. Dependence of vapour-side, heat-transfer coefficient on inundation rate for steam condensation with inundation on wire-wrapped tubes. (Wire diameter 1.6 mm, vapour approach velocity 0.56 m/s, coolant flow rate 2.0 l/min.)

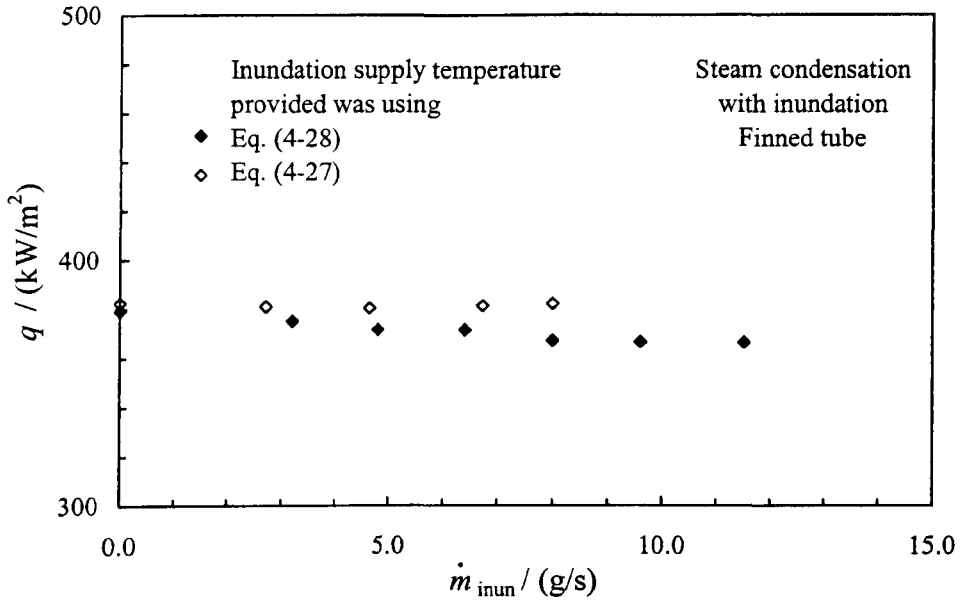

Fig. 4.29. Dependence of heat flux on inundation rate for steam condensation with inundation on low integral-finned tubes. (Fin thickness 0.5 mm, fin height 1.59 mm, interfin space 1.5 mm, vapour approach velocity 0.56 m/s, coolant flow rate 2.0 l/min.)

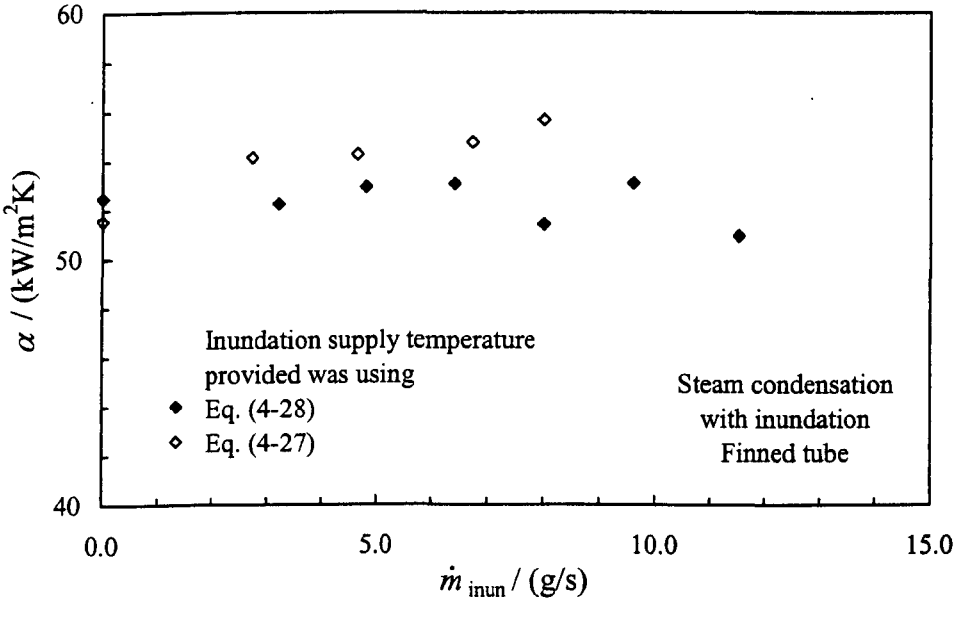

Fig. 4.30. Dependence of vapour-side, heat-transfer coefficient on inundation rate for steam condensation with inundation on low integral-finned tubes. (Fin thickness 0.5 mm, fin height 1.59 mm, interfin space 1.5 mm, vapour approach velocity 0.56 m/s, coolant flow rate 2.0 l/min.)

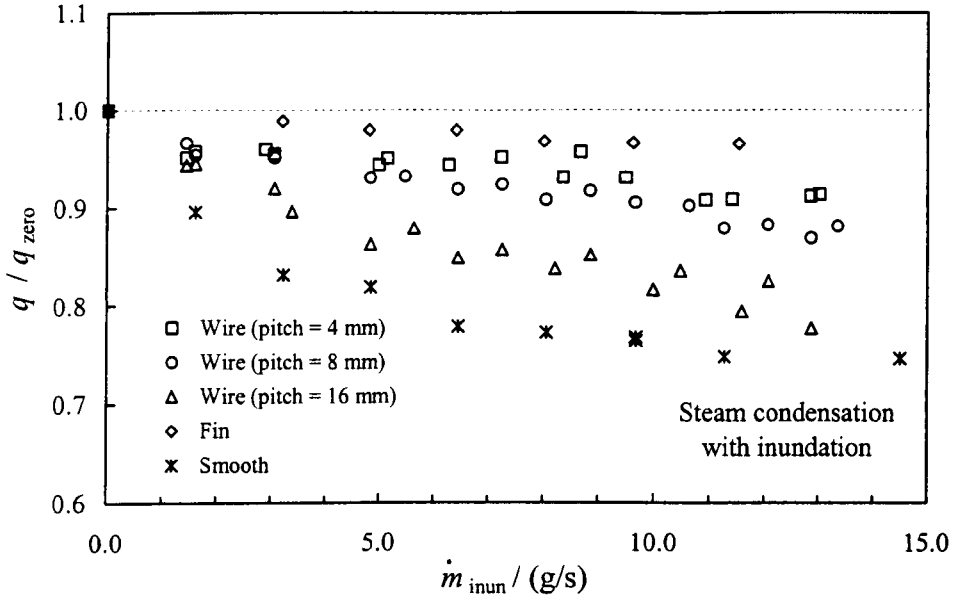

Fig. 4.31. Variation of heat flux ratio on inundation rate for steam condensation with inundation on smooth, wire-wrapped and low integral-finned tubes. q_{zero} denotes the heat flux without inundation. (Vapour approach velocity 0.56 m/s, coolant flow rate 2.0 l/min.)

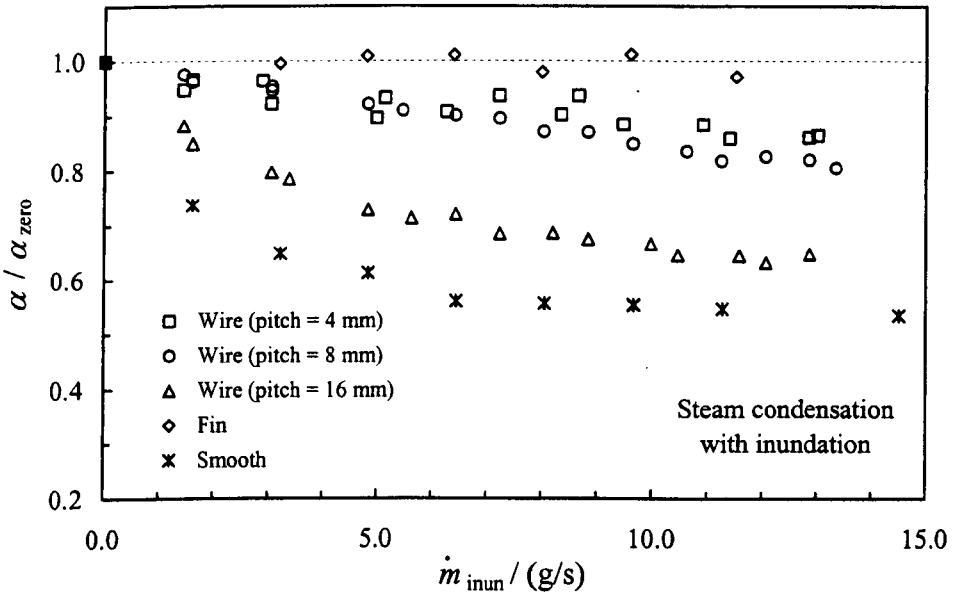

Fig. 4.32. Variation of vapour-side, heat-transfer coefficient ratio on inundation rate for steam condensation with inundation on smooth, wire-wrapped and low integral-finned tubes. α_{zero} denotes the vapour-side, heat-transfer coefficient without inundation. (Vapour approach velocity 0.56 m/s, coolant flow rate 2.0 l/min.)

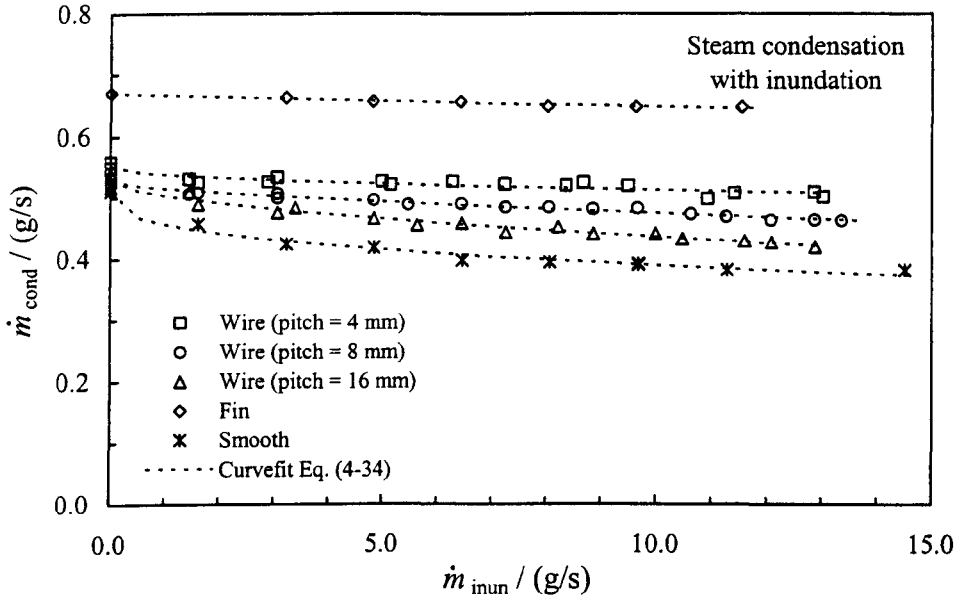

Fig. 4.33. Relation between observed inundation and condensation rates. Curve fits using Eq. (4-34).

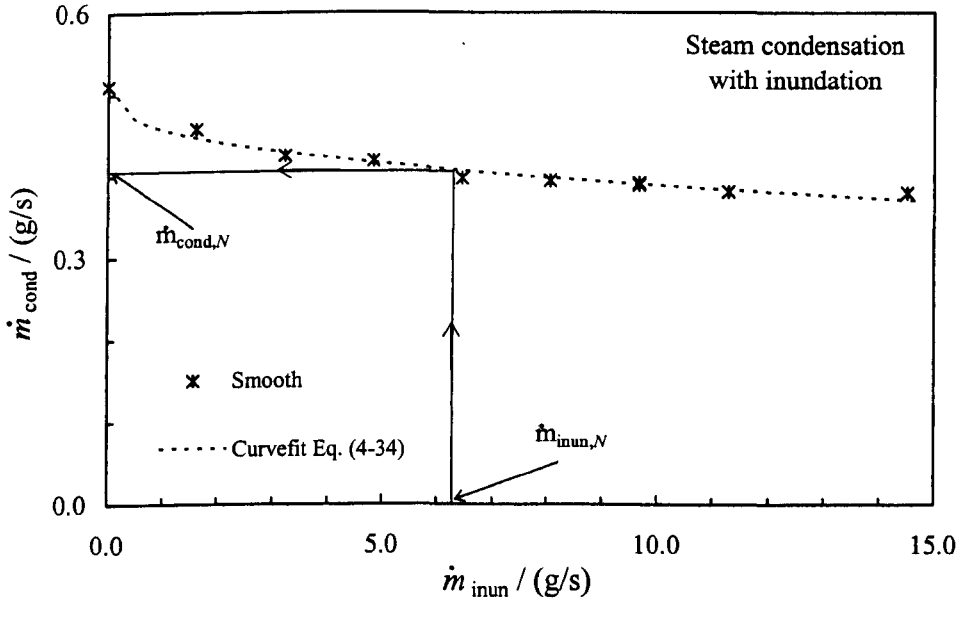

Fig. 4.34. Example of estimation for condensation rate for N^{th} tube in simulated column from relation between observed condensation and inundation rates.

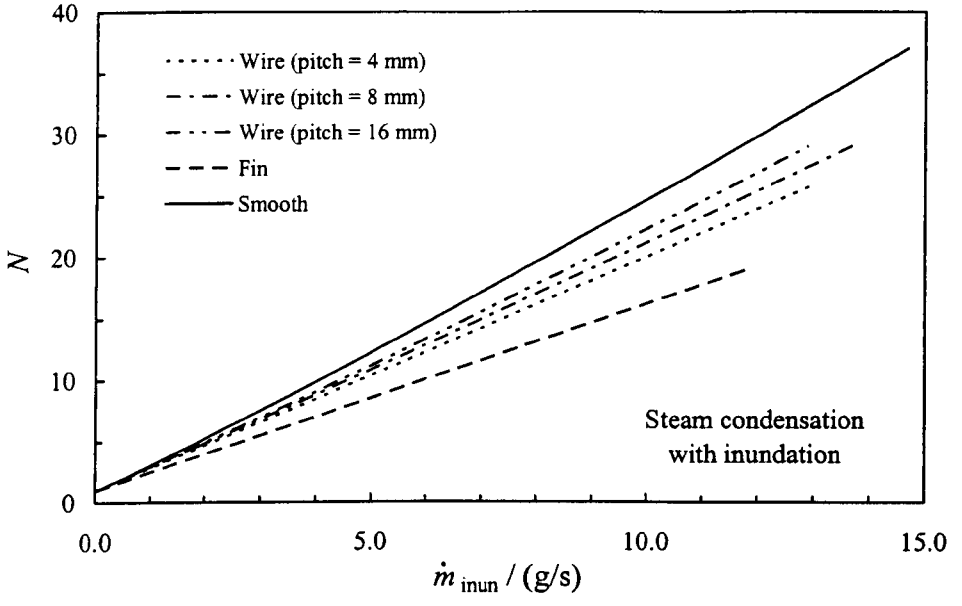

Fig. 4.35. Relation between inundation rate and effective depth of tube in vertical column for smooth, wire-wrapped and finned tubes.

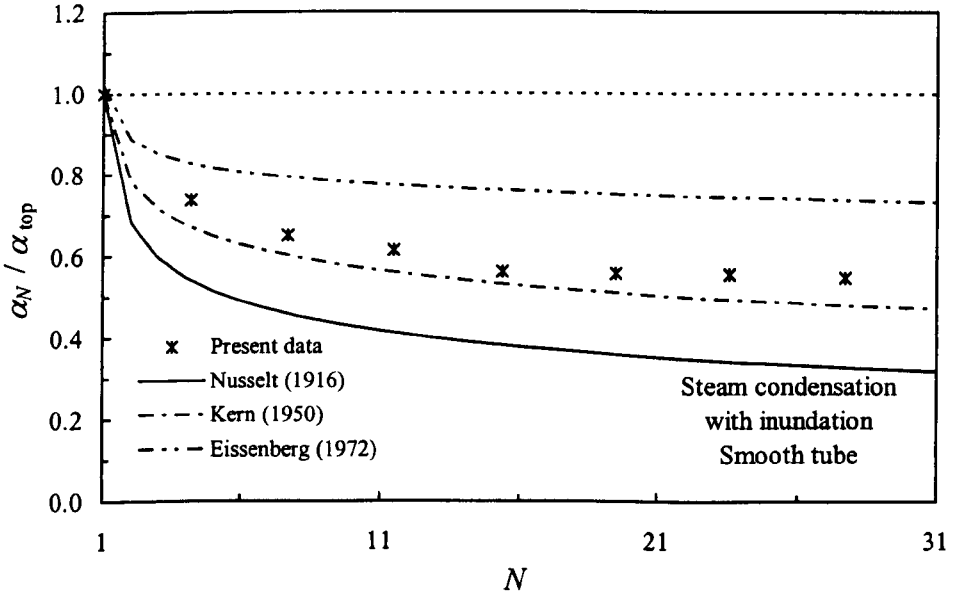

Fig. 4.36. Comparison of smooth tube data under inundation with theories of Nusselt (1916), Kern (1950) and Eissenberg (1972). Ratio α_N/α_{top} plotted against effective number of tubes in simulated column.

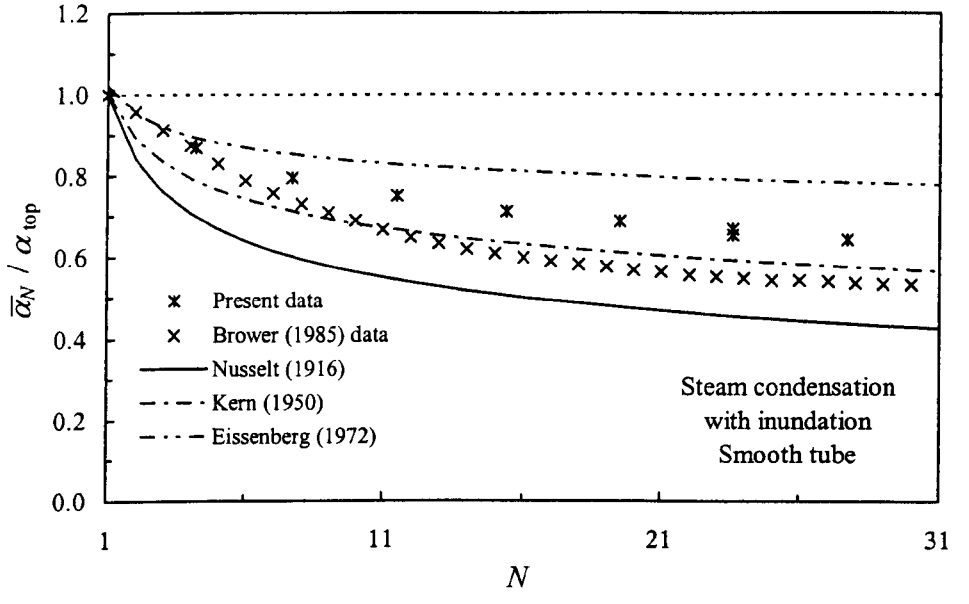

Fig. 4.37. Comparison of smooth tube data under inundation with data of Brower (1985). Ratio $\bar{\alpha}_N/\alpha_{top}$ plotted against effective number of tubes in simulated column.

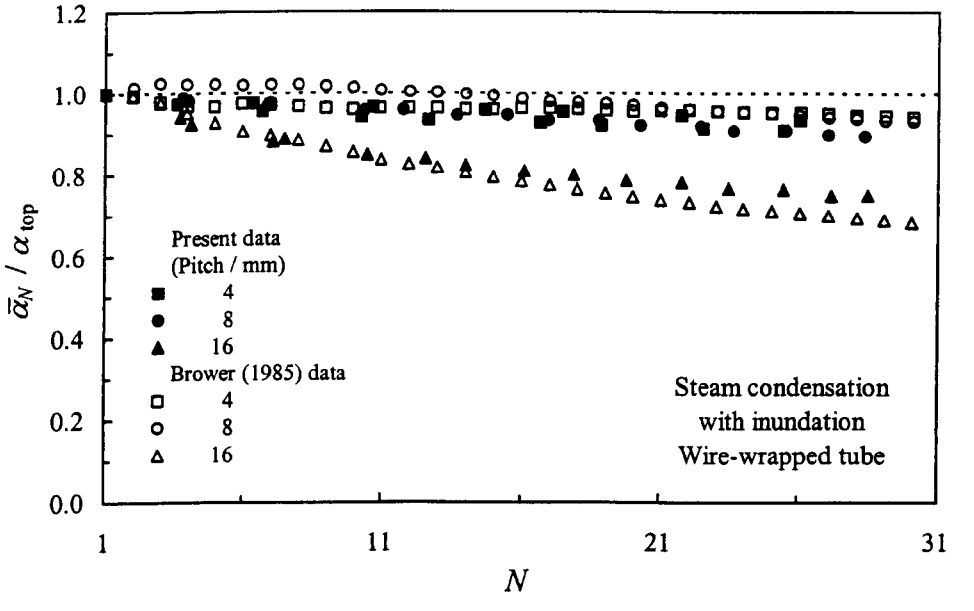

Fig. 4.38. Comparison of wire-wrapped tube data under inundation with data of Brower (1985). Ratio $\bar{\alpha}_N/\alpha_{top}$ plotted against effective number of tubes in simulated column. (Wire diameter 1.6 mm.)

Chapter 5

Marangoni condensation of steam-ethanol mixtures

5.1 Condensation investigation

In order to measure the heat-transfer performance during condensation of steam-ethanol mixtures on a horizontal smooth tube, experiments were conducted using the same apparatus as used in the wire-wrapped tube investigation. Modifications are described below.

5.1.1 Apparatus and instrumentation

All the tests were done using the same copper smooth tube as used for the wire-wrapped tube investigation, having 12.2 mm outside diameter and 100 mm active heat-transfer length with four embedded thermocouples. The manometer to measure the gauge pressure in the test section was filled with distilled water.

5.1.2 Experimental procedure

The experimental procedure was essentially the same as for the wire-wrapped tube investigation. Coolant flow rates of between around 0.2 and 20 l/min were used in order to obtain data covering a wide range of vapour-to-surface temperature difference (the corresponding values of coolant temperature rise were between around 1.2 and 30 K). First the coolant flow rate was set to the maximum and was subsequently reduced in steps to the minimum. The experiments were then repeated in ascending order of the coolant flow rate. At each step, coolant flow rate, vapour temperature, coolant temperatures, coolant temperature rise, test tube wall temperatures, condensate temperature returning to the boiler and chamber gauge pressure were recorded. Visual observations of the condenser tube were also made at each step and the appearance of the condensate film was also recorded.

5.1.3 Determination of experimental parameters

The following variables, namely heat flux, vapour-to-surface temperature difference, various temperatures (tube wall, vapour, coolant-in, coolant-out, coolant temperature rise and condensate returning to the boiler) and various pressures (atmospheric and test section vapour) were calculated using the respective equations for the single wire-wrapped tube investigation (see Section 4.1.3). (Note that ρ_f in Eq. (4-2) used for this case was that for water.)

The ethanol mass fractions in the liquid and vapour phases during experiments were calculated with the assumption of thermodynamic equilibrium, i.e. vapour-liquid equilibrium relation using observed vapour pressure and temperature, as described in Appendix F.

5.1.4 Results

All experiments were done at near atmospheric pressure. Referring to the experimental data of Utaka and co-workers, mass fractions of ethanol in water used were 0.05%, 0.1%, 0.5% and 1.0% as prepared at atmospheric (room) temperature (i.e. initial ethanol liquid mass fraction). Weights of ethanol and water were precisely measured before installation in the test apparatus. For each ethanol mass fraction, vapour approach velocity to the condenser tube was varied by adjusting the boiler heater powers, to give 0.15, 0.24, 0.35, 0.56 and 0.75 m/s. Experiments using pure water were conducted at a vapour approach velocity of 0.56 m/s only. For each condition, experiments were performed twice to confirm repeatability. The coolant inlet temperature was always around 20 °C and the variation during one experiment was less than 1 K. The ranges of vapour temperature, coolant temperature rise, initial ethanol liquid mass fraction, ethanol liquid and vapour mass fraction during experiments, heat flux and vapour-to-surface temperature difference observed are summarized in Table 5.1.

Visual observations

The condensate appearance was observed to change from unstable-filmwise, i.e. filmwise with instability (small ripples) on the condensate film, to pseudo-dropwise and subsequently back to filmwise with increase in vapour-to-surface temperature difference. Between the pseudo-dropwise and filmwise modes, a transition wavy film mode was observed. In the peak heat-transfer region, the pseudo-dropwise mode was usually observed with higher vapour velocity, while only the wavy film mode was seen with low vapour velocity. Complete filmwise mode was only seen with low vapour velocity at high vapour-to-surface temperature difference. It is interesting to note that the condensate appearance at the upper and lower parts of the tube were sometimes different. For instance, the pseudo-dropwise mode was seen at the upper part while the wavy film mode was seen at the lower.

Heat-transfer results

Figs. 5.1 and 5.2 show variations of heat flux and heat-transfer coefficient respectively, plotted against vapour-to-surface temperature difference for different ethanol mass fractions at each vapour approach velocity tested. The ranges of experimental parameters are shown in the legends, namely the initial ethanol liquid mass fraction (C_{iL}), the equilibrium ethanol vapour mass fraction at the observed vapour temperature (C_v) and the range of observed vapour temperature (T_v). The figures also include earlier theoretical lines for pure steam. The solid line represents the Nusselt (1916) equation given by Eq. (4-19) and the dot-and-dashed line the Rose (1984) equation given by Eq. (4-20). The vapour velocity employed in $\tilde{Re}$ and F in Eq. (4-20) is the value shown in each figure. The present data are plotted by closed points. Vertical flat plate data of Wang (2002) and Utaka and Wang (2002) are included in the figures by open points.

With increase in vapour-to-surface temperature difference, the heat-transfer coefficient is first relatively low for the unstable-filmwise mode. The heat-transfer coefficient then begins to increase steeply when the pseudo-dropwise mode was observed for higher vapour velocities of 0.35, 056 and 0.75 m/s. For lower vapour velocities of 0.15 and 0.24 m/s, the lower heat flux was observed due to the wavy

filmwise mode. The heat-transfer coefficient then starts decreasing as the condensation mode changed to relatively steadier pseudo-dropwise or wavy filmwise modes. These trends are thought to be due to the combined effects of diffusion in the vapour phase and changes in condensation modes in the liquid phase, in the same manner as suggested for the vertical flat plate of Utaka and co-workers. Detailed discussion is given in Section 2.4.2 (3). Comparison with the data of Wang (2002) and Utaka and Wang (2002) for a vertical flat plate are discussed in detail later.

For low vapour velocities of 0.15 and 0.24 m/s, the lines in Figs. 5.1 and 5.2 subsequently converge with increase in vapour-to-surface temperature difference. This may reflect insufficient amount of vapour supply to the test tube. In the convergence region, more than 50% of vapour supplied from the boiler (in terms of vapour mass flow rate, $\dot{m}_v$) is condensated on the test tube and vapour velocity just after the test tube was calculated to be less than 0.1 m/s. The insufficient amount of vapour supply and possible accumulation of traces of air and vapour-phase diffusion layer below the test tube due to the very small vapour velocity might significantly reduce the heat-transfer values. This behaviour is not seen for the higher vapour velocities.

Figs. 5.3 and 5.4 show the same data as in Figs. 5.1 and 5.2, but arranged with separate plots for each initial ethanol liquid mass fraction and using different symbols for each vapour velocity. For pure steam, the solid line represents the Nusselt (1916) equation given by Eq. (4-19) while a range of the results by the Rose (1984) equation given by Eq. (4-20) with vapour velocities between 0.15 and 0.75 m/s is shown by dot-and-dashed lines. In contrast with the pure steam case, it is seen from the figures that small changes in vapour velocity have significant influence on the heat transfer for all ethanol mass fractions. Both heat flux and heat-transfer coefficient increase with increase in vapour velocity at the same vapour-to-surface temperature difference. The sensitivity to vapour velocity (also found by Utaka and Kobayashi (2001)) is surprising and presumably due to flow regime changes in the condensate and motion of the condensate film which may not have been obvious to the unaided eye.

With the highest vapour velocity the smallest ethanol mass fraction mixture (C_{iL} = 0.05%) gave the highest heat-transfer coefficient of 70 kW/m^{2}K at a vapour-to-surface temperature difference of 6 K, while the largest ethanol mass fraction mixture (C_{iL} = 1.0%) gave the highest heat flux of 1000 kW/m^2 at a vapour-to-surface temperature difference of 24 K.

For Marangoni condensation of steam-ethanol mixtures, an enhancement ratio may be defined by:

$$\varepsilon_{Ma} = \frac{\text{(water-ethanol)}}{\text{(pure water)}} = \left(\frac{q_{Ma}}{q_{Ro,wa}} \right)_{\Delta T, U_v} \left\{ = \left(\frac{\alpha_{Ma}}{\alpha_{Ro,wa}} \right)_{\Delta T, U_v} \right\} \qquad (5\text{-}1)$$

where q_{Ma} is the observed heat flux for steam-ethanol mixtures and the subscript Ro,wa denotes the Rose (1984) theory for pure water. The Rose (1984) equation with each vapour velocity is employed for the denominator since it has been found to well represent the experimental data for steam in the present investigation, including the effect of vapour shear. (See Figs. 4.9 and 4.21 in Section 4.1.4 and Section 4.2.4 respectively.) As described above, the heat flux and heat-transfer coefficient are strongly dependent on vapour-to-surface temperature difference. Thus the enhancement ratio is also dependent on the vapour-to-surface temperature difference in this case.

Fig. 5.5 shows enhancement ratio (including diffusion resistance in the vapour phase) against vapour-to-surface temperature difference for different ethanol mass fractions at each vapour velocity. The present data are plotted by closed points. Vertical flat plate data of Wang (2002) are also included in the figures plotted as open points. For lower ethanol mass fraction mixtures (C_{iL} = 0.05% and 0.1%) the enhancement ratio exceeds unity over the entire vapour-to-surface temperature difference while higher ethanol mass fraction mixtures (C_{iL} = 0.5% and 1.0%) give deterioration of heat transfer at low vapour-to-surface temperature difference. This is thought to be due to the effect of vapour-phase diffusion. The highest enhancement ratio of around 3.7 was observed for C_{iL} = 0.05% at a vapour-to-surface temperature difference of around 7 K with the highest vapour velocity of 0.75 m/s.

5.1.5 Discussion and comparisons

Referring to Figs. 5.1(c), 5.1(e), 5.2(c), 5.2(e) and 5.5(c), similar trends are seen between the present data for the horizontal tube and the vertical plate data of Wang (2002) and Utaka and Wang (2002). It is seen that the present values of both heat flux and heat-transfer coefficient are lower than those of Wang (2002) and Utaka and Wang (2002). Differences in detail between the present and former results are attributable to (a) difference in geometry – small vertical plate *versus* horizontal tube, (b) variation of vapour velocity around the tube (in view of the sensitivity to vapour velocity seen in Fig. 5.3) and (c) the strong dependence of heat-transfer coefficient on temperature difference which varied appreciably around the tube (see Appendix E). Aspect (c) is discussed in more detail below.

It is interesting to compare the plate and tube cases by using the smallest vapour-to-surface temperature difference rather than the mean. The highest wall surface temperature at the top of the tube, T_w(top) can be estimated using Eq. (E-1) with $\phi = 0$ for each experimental data point, thus:

$$T_w(\text{top}) = T_{wo}(1 + A) \qquad (5\text{-}2)$$

with which vapour-to-surface temperature difference at the top of the tube, ΔT_{top}, is expressed by:

$$\Delta T_{top} = T_v - T_w(\text{top}) \qquad (5\text{-}3)$$

Unfortunately, it is not possible to obtain the local heat flux at the top, thus the average values are used below.

Figs. 5.6 to 5.9 show comparisons between the present data with the estimated vapour-to-surface temperature difference at the top of the tube (horizontal surface) and data of Wang (2002) and Utaka and Wang (2002) for a vertical short flat plate. The present data agree more closely with the results of Wang (2002) and Utaka and Wang (2002) for all cases. Due to lowering the vapour-to-surface temperature difference, the heat-transfer coefficient becomes higher for the present data and

consequently in closer accord with the vertical plate data. It is noteworthy that for a vapour velocity of 0.75 m/s in Figs. 5.7 and 5.9, both heat flux and heat-transfer coefficient are in better agreement with the vertical flat plate data, indicating that the dependence of Marangoni condensation heat transfer on heat-transfer surface geometry (vertical plate or horizontal tube) is essentially the same. Less satisfactorily agreement is seen for a vapour velocity of 0.35 m/s in Figs. 5.6 to 5.8. This is thought to be due to the large difference between actual local heat flux at the top and the average heat flux for the tube. Also separation of the vapour diffusion boundary layer at around $\pi/2$ prevents removal, by velocity, of the ethanol-rich vapour over the lower surface of the tubes. For the same reason, non-condensing gas accumulation, with additional detrimental effect on the heat transfer, will also be greater for the tube in this region.

5.2 Boiling investigation

In case small amounts of ethanol might be used in power plant to enhance the condenser performance it was thought desirable to investigate the effect of the presence of small ethanol concentrations in water on boiling heat transfer. Measurements for water-ethanol mixtures boiling on a horizontal cylindrical heater have therefore been conducted.

5.2.1 Apparatus and instrumentation

Fig. 5.10 shows the test apparatus used for boiling experiments. The test section consisted of a glass boiler with one cylindrical electric heater, to which variable input power was supplied up to a maximum power of 3.6 kW. The dimensions of the heater were an outside diameter of 15.8 mm and a heating length of 234 mm (see Fig. 5.11). The heater was covered by a tightly fitting copper tube sheath instrumented with four K-type (nickel-chromium/nickel-aluminium) thermocouples which were embedded at the centre (lengthwise) of the heater and equally spaced at 90° intervals around the tube with a 22.5° offset from the vertical (see Fig. 5.12). The sheath had an outside diameter of 22.1 mm, an inside diameter of 16.0 mm and a total length of 255 mm. Good thermal contact between the heater and sheath was achieved using an interference fit and high conductance (99.9% silver) paste. The mean surface temperature was taken as the arithmetic average of the temperatures indicated by the embedded thermocouples with a small correction for the depth of the thermocouples below the outside sheath surface. Four thermocouples were used to measure liquid and vapour temperatures in the boiler as shown in Fig. 5.10. From the boiler the vapour flowed up through a 180° bend, vertically down to a condenser and subsequently returned to the boiler by gravity. The apparatus was vented to atmosphere through a second condenser. At the upper part of the boiler, a tube was attached leading to a manometer to measure the gauge pressure in the boiler. The manometer was filled with distilled water.

5.2.2 Experimental procedure

Before measurements, and while boiling, the test apparatus was left for more than an hour in order to achieve a steady operating condition. All tests were done at near atmospheric pressure. Experiments were first performed for natural convection boiling of pure water using power inputs to the heater from 90 to 300 W. For nucleate boiling, pure water was first tested followed by those for mixtures. The same ethanol liquid mass fractions as used in the condensation investigation were tested in the boiling tests, namely 0.05%, 0.1%, 0.5% and 1.0% as prepared at atmospheric temperature. The mixtures were tested in order from smaller to larger ethanol liquid mass fractions by adding the precise amounts of ethanol to give the desired ethanol liquid mass fractions. The range of the power input varied from 500 to 3600 W. After measurement for one power input, the next was set and at least 60 minutes was allowed before the next measurement. The power input was first set to a higher value, i.e. around 3 kW, and subsequently reduced in steps. The consistency of result with increasing and decreasing power input was verified. Tests were performed twice for each ethanol liquid mass fraction on different days.

5.2.3 Determination of experimental parameters

Atmospheric and test section pressure were obtained using Eqs. (4-1) and (4-2). The readings of thermo-e.m.f. for the sheath wall for the heater and liquid temperatures were converted to temperatures using Eq. (4-4). (See Section 4.1.3)

The input power to the heater was obtained by measuring input electric currents and voltages using a voltmeter via a transformer. The readings, both in μV, were converted to the actual values using the following equations which were obtained by a preliminary calibration test:

$$V_{\text{in}} = 201.3 \times E_{\text{Vin}} \tag{5-4}$$

$$I_{\text{in}} = 402.3 \times E_{\text{Iin}} \tag{5-5}$$

where V_{in} (in V) and I_{in} (in A) are the actual voltage input and electric current input to the heater respectively, and E_{Vin} and E_{Iin} are the respective observed output from the transformer in μV.

The input power to the heater, Q_{in} in W, was obtained using the following equation with a predetermined correction for losses in the variac:

$$Q_{in} = 0.9366 V_{in} I_{in} + 0.0059 \tag{5-6}$$

The correction for the depth of the thermocouples below the heating surface for wall temperatures was incorporated in the same manner as in the condensation investigation. The local outside wall surface temperature was obtained by assuming uniform radial heat conduction in the sheath:

$$T_{wo,i} = T_{w,i} + \frac{Q_{in}}{2\pi k_w l_{sb}} \ln\left(\frac{d_{tc}}{d_{sb}}\right) \tag{5-7}$$

where d_{tc} is the pitch diameter of thermocouple junctions in the sheath, d_{sb} is the outside diameter of the sheath, l_{sb} is the active heat-transfer length of the sheath.

The boiling heat flux based on the outside area of the sheath (excluding the circular head area), q^* was calculated using the following equation:

$$q^* = \frac{Q_{in}}{\pi d_{sb} l_{sb}} \tag{5-8}$$

The liquid-to-surface temperature difference, ΔT^*, was given by:

$$\Delta T^* = T_{wo} - T_L \tag{5-9}$$

where T_L is the liquid temperature given by the upper thermocouple.

5.2.4 Results and discussion

Fig. 5.13 shows the relation between heat flux and liquid-to-surface temperature difference for natural convection heat transfer of pure water on a horizontal cylindrical heater where the uncertainty in ΔT^* denotes the typical difference between the two liquid temperature measurements. The solid line is the equations of Churchill and Chu (1977) for natural convection heat transfer on a horizontal cylinder given by:

$$Nu^* = \left[0.60 + \frac{0.387\left(Gr_d Pr\right)^{1/6}}{\left\{1+\left(\frac{0.559}{Pr}\right)^{9/16}\right\}^{8/27}} \right]^2 \tag{5-10}$$

where

$$Nu^* = \frac{q^* d_{sb}}{k\Delta T^*} \tag{5-11}$$

$$Gr_d = \frac{\rho^2 g\gamma \Delta T^* {d_{sb}}^3}{\mu^2} \tag{5-12}$$

$$Pr = \frac{C_p \mu}{k} \tag{5-13}$$

and γ is the volume coefficient of expansion. All properties used in the equations were calculated at the following reference temperature:

$$T^*_{ref} = \frac{1}{2}\left(T_{wo} + T_L\right) \tag{5-14}$$

Good agreement between the present data with the upper liquid temperature and the result of Churchill and Chu (1977) is seen from Fig. 5.13. During the tests there

was a significant vertical temperature gradient in the liquid. Owing to the good agreement with Eq. (5-10) for natural convection, the upper liquid temperature was also used for the data reduction of nucleate boiling results.

Fig. 5.14 shows the relation between boiling heat flux and liquid-to-surface temperature difference during nucleate boiling of water-ethanol mixtures and pure water on a horizontal cylindrical heater. The ranges of boiling heat flux and liquid-to-surface temperature difference during experiments are summarized in Table 5.2.

Focusing on the present data, with increase in ethanol liquid mass fraction, the lines are moving toward the right-hand side; indicating deterioration of boiling heat transfer with increase in ethanol liquid mass fractions. For ethanol liquid mass fractions of 0.05% and 0.1%, boiling heat flux was found to be almost the same as for pure water and the deterioration by adding ethanol in water is negligible. Significant reduction is seen for 0.5% and 1.0% mixtures, which is thought to be due to the additional mass transfer resulting from the composition gradient in the liquid as described in Section 2.4.3.

5.3 Conclusions

New data for Marangoni condensation of steam-ethanol mixtures on a horizontal smooth tube have been obtained for relatively low ethanol mass fractions and covering a wide range of vapour-to-surface temperature difference. All experiments were done at near atmospheric pressure with a range of vapour velocities. A total of 663 data points has been obtained.

As found by Utaka and co-workers for a vertical plate, a strong dependence of heat-transfer coefficient on vapour-to-surface temperature difference with fixed vapour composition and vapour velocity due to the combination effects of diffusion in the vapour phase and changes in the condensation mode has been observed. The *average* heat-transfer coefficient and enhancement ratio are found to be significantly lower for the tube than for the vertical flat plate case. This has been shown to be due to the circumferential wall surface temperature distribution, i.e. the variation of vapour-to-surface temperature difference around the tube perimeter, resulting in the variation of condensation mode and heat transfer.

With the highest vapour velocity of 0.75 m/s, the highest heat-transfer coefficient of 70 kW/m^2K was found with the smallest ethanol liquid mass fraction mixture (C_{iL} = 0.05%) at a vapour-to-surface temperature difference of 6 K. The highest heat flux of 1000 kW/m^2 was found with the largest ethanol liquid mass fraction mixture (C_{iL} = 1.0%) at a vapour-to-surface temperature difference of 24 K. The highest enhancement ratio of around 3.7 was observed for C_{iL} = 0.05% at a vapour-to-surface temperature difference of around 7 K.

It has been demonstrated that significant improvement in condenser performance can be obtained by addition of as little as 0.1% by mass fraction of ethanol to the boiler feed. Boiling experiments have also been performed in the course of the present work in which it has been shown that such small concentrations of ethanol do not impair the boiler performance.

Table 5.1 Summary of ranges of experimental parameters for Marangoni condensation of steam-ethanol mixtures on horizontal tube.

C_{iL} / %	T_v / °C	ΔT_c / K	q / (kW/m^2)	ΔT / K
0	100.0 – 100.1	1.5 – 27.9	100 – 520	5 – 50
0.05	99.7 – 100.2	1.3 – 29.1	90 – 880	2 – 49
0.1	99.6 – 100.1	1.4 – 29.8	90 – 960	2 – 45
0.5	99.3 – 99.7	1.3 – 24.3	75 – 980	5 – 48
1.0	98.5 – 98.8	1.3 – 24.2	65 –1020	7 – 50

C_{iL} / %	C_{iV} / %	C_L / %	C_v / %
0	0	0	0
0.05	0.6	0.06 – 0.14	0.7 –1.6
0.1	1.2	0.14 – 0.20	1.6 – 2.3
0.5	5.6	0.43 – 0.54	4.8 – 6.0
1.0	10.5	0.83 – 1.1	9.0 – 11.5

Table 5.2 Summary of ranges of experimental parameters for boiling of water-ethanol mixtures on horizontal cylindrical heater.

C_{iL} / %	q^* / (kW/m^2)	ΔT^* / K
0	30 – 220	7.8 – 18.8
0.05	40 – 200	8.3 – 17.1
0.1	45 – 190	8.7 – 17.2
0.5	35 – 205	9.0 – 18.7
1.0	35 – 205	10.0 – 20.0

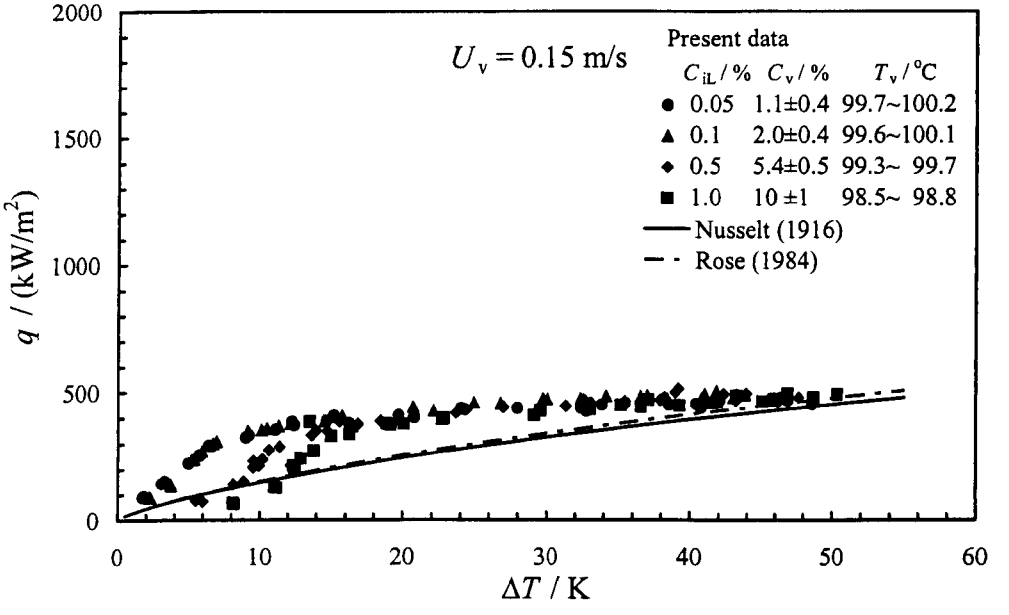

(a) 0.15 m/s

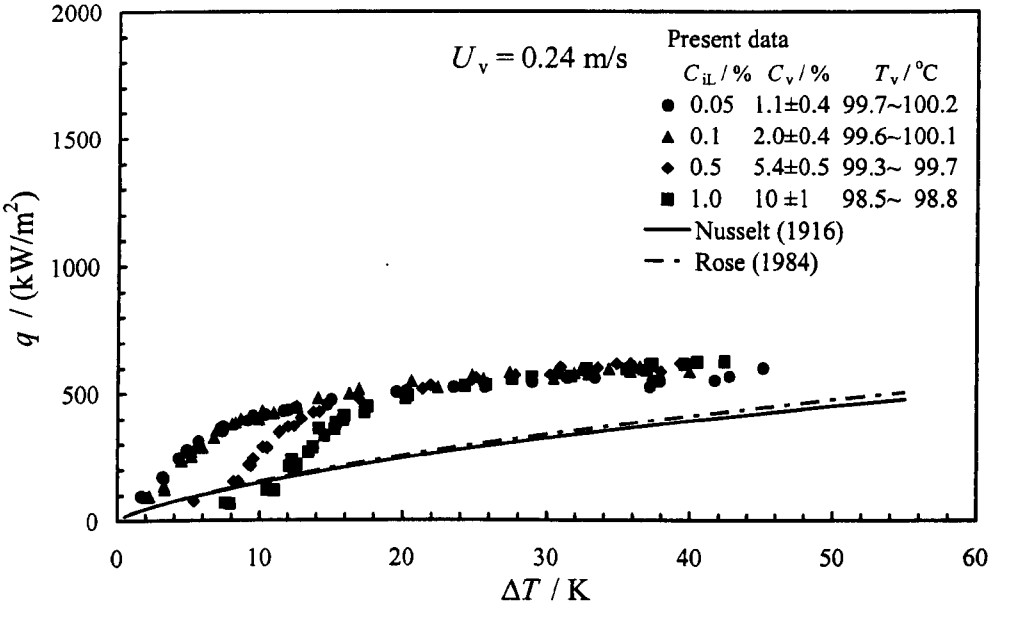

(b) 0.24 m/s

Fig. 5.1. Variation of heat flux with vapour-to-surface temperature difference during Marangoni condensation of steam-ethanol mixtures on horizontal smooth tube for different ethanol mass fractions at each vapour approach velocity. C_{iL} denotes initial ethanol liquid mass fraction as prepared at atmospheric temperature, C_v ethanol vapour mass fraction during experiments.

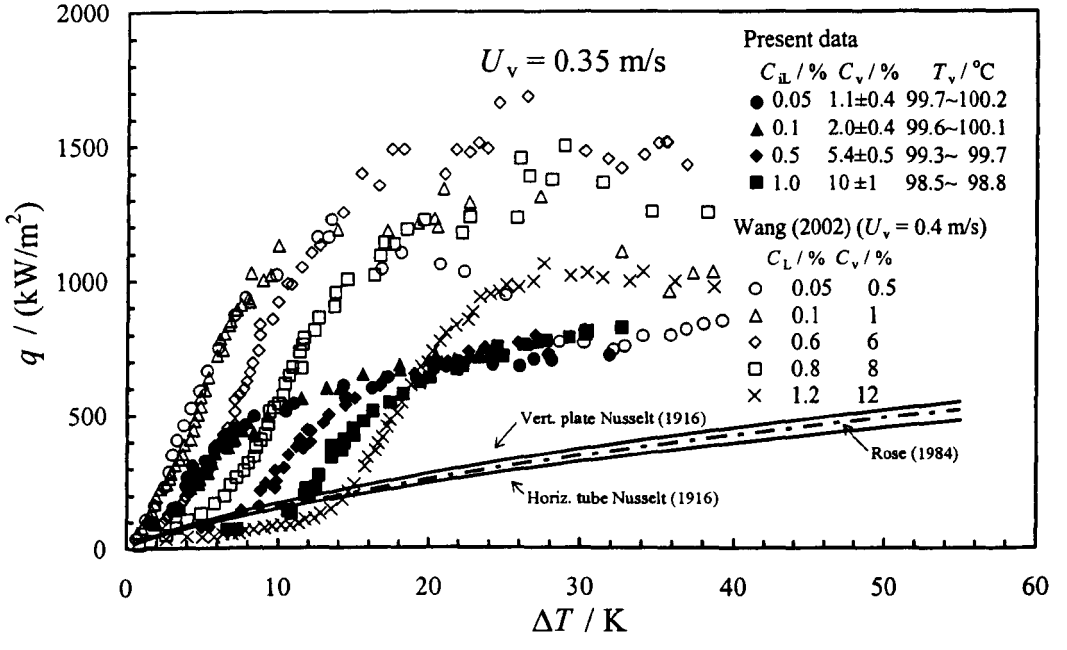

(c) 0.35 m/s

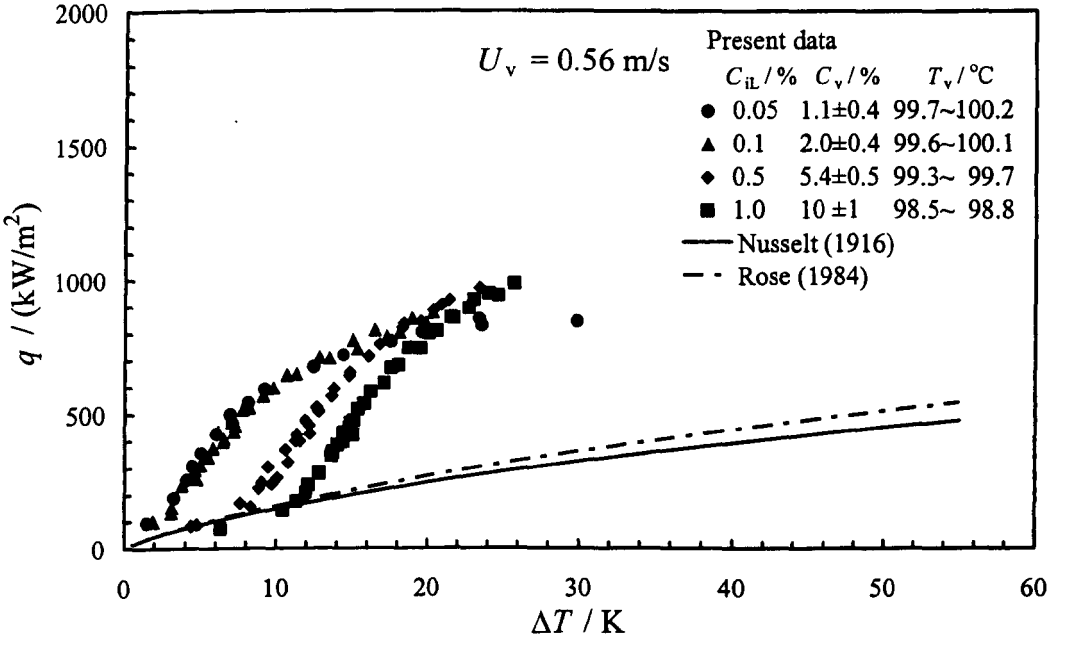

(d) 0.56 m/s

Fig. 5.1 (continued).

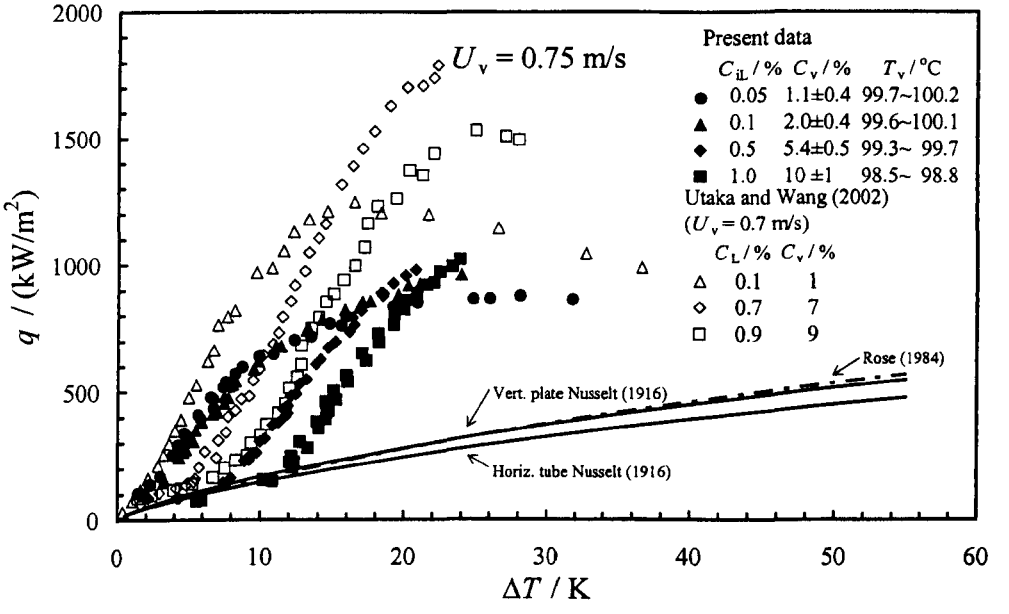

(e) 0.75 m/s

Fig. 5.1 (continued).

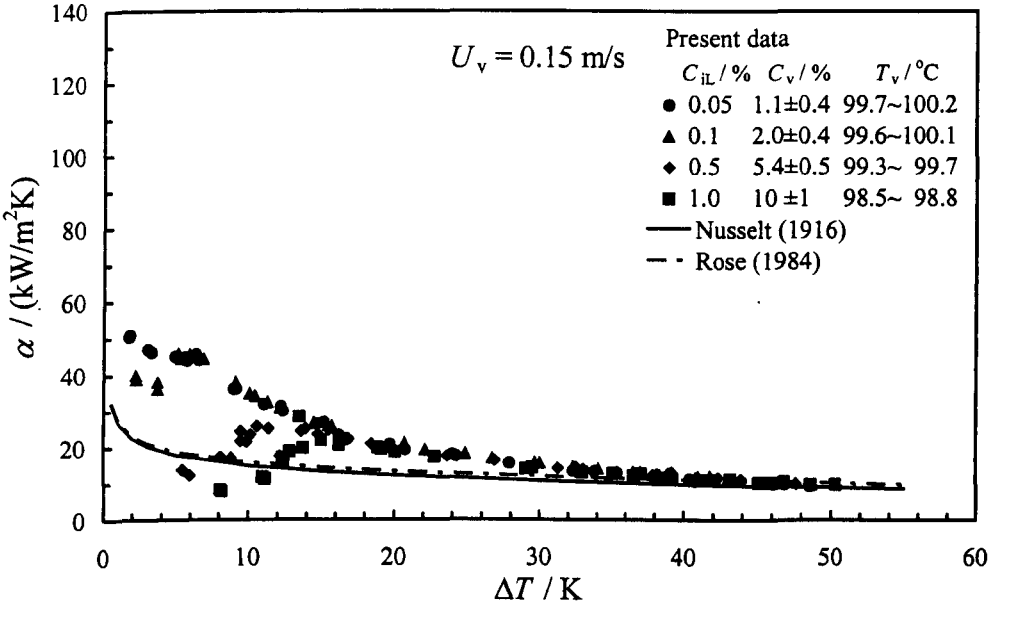

(a) 0.15 m/s

Fig. 5.2. Variation of vapour-side, heat-transfer coefficient with vapour-to-surface temperature difference during Marangoni condensation of steam-ethanol mixtures on horizontal smooth tube for different ethanol mass fractions at each vapour approach velocity. C_{iL} denotes initial ethanol liquid mass fraction as prepared at atmospheric temperature, C_v ethanol vapour mass fraction during experiments.

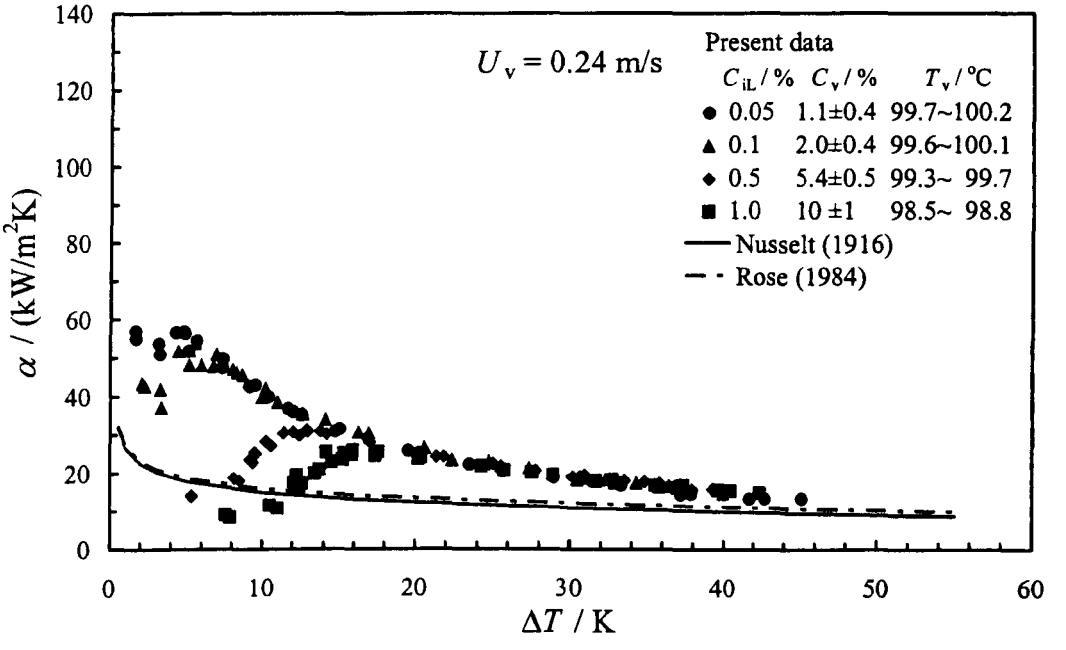

(b) 0.24 m/s

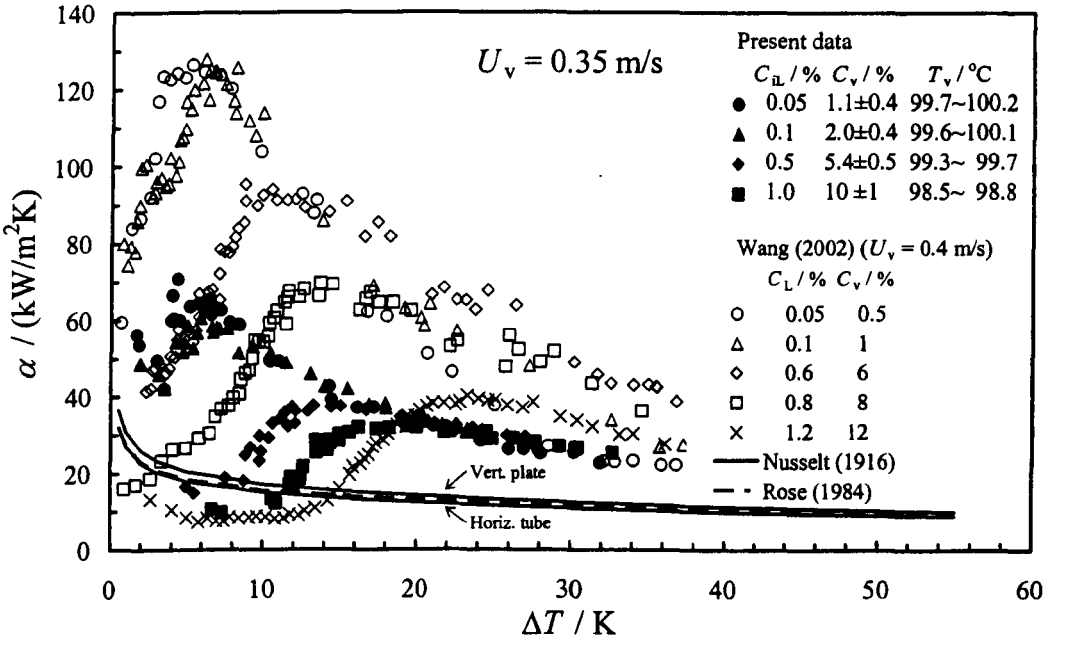

(c) 0.35 m/s

Fig. 5.2 (continued).

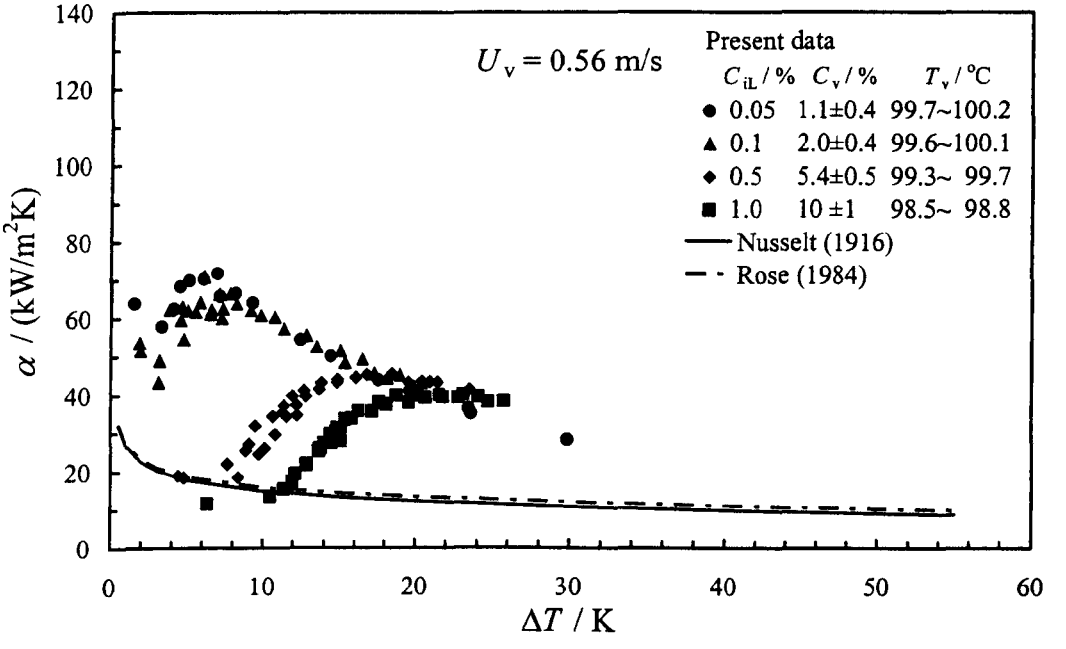

(d) 0.56 m/s

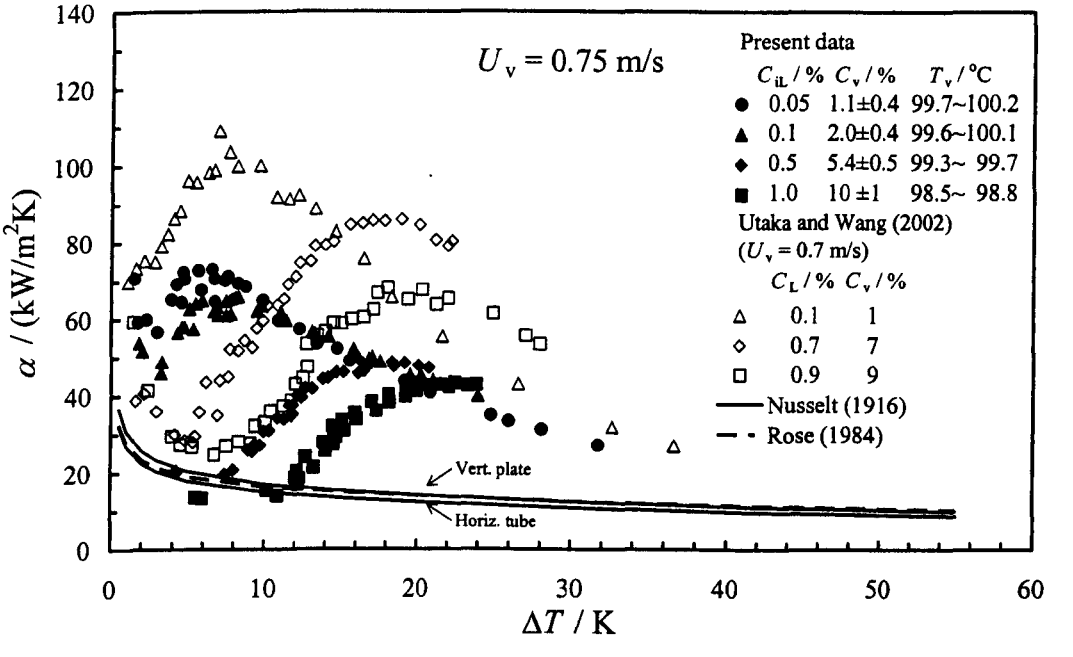

(e) 0.75 m/s

Fig. 5.2 (continued).

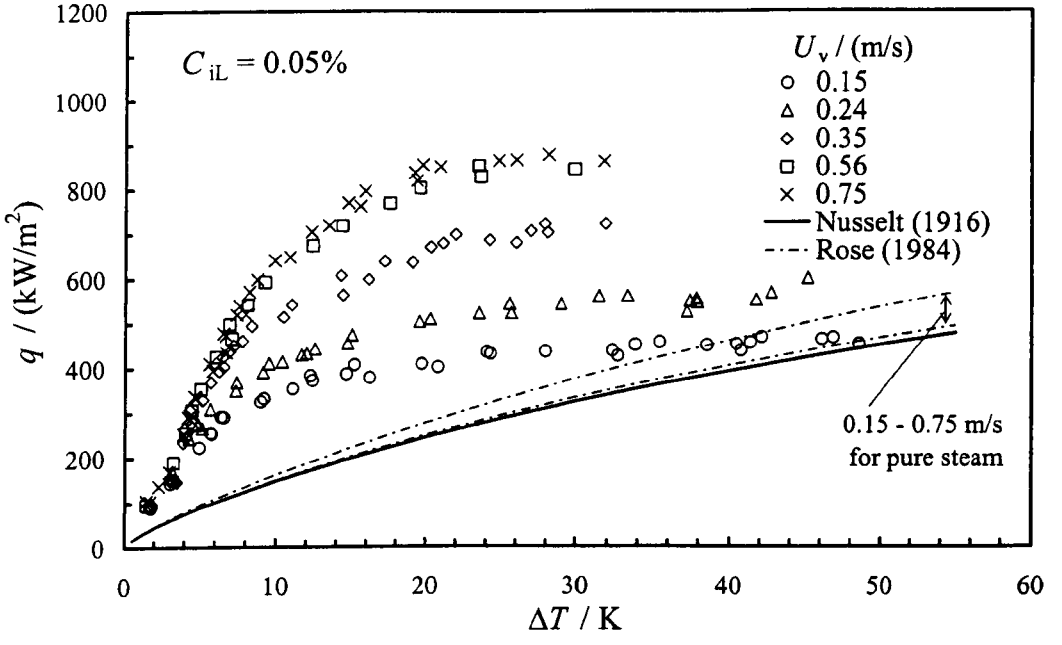

(a) 0.05%

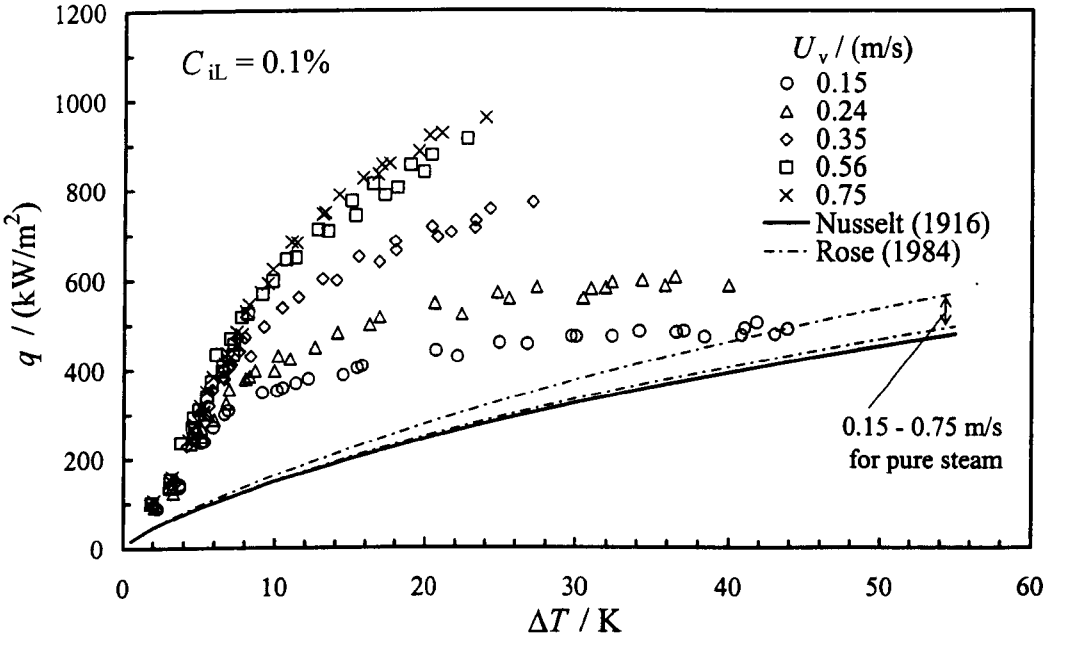

(b) 0.1%

Fig. 5.3. Variation of heat flux with vapour-to-surface temperature difference during Marangoni condensation of steam-ethanol mixtures on horizontal smooth tube for different vapour approach velocities at each ethanol mass fractions. C_{iL} denotes initial ethanol liquid mass fraction as prepared at atmospheric temperature.

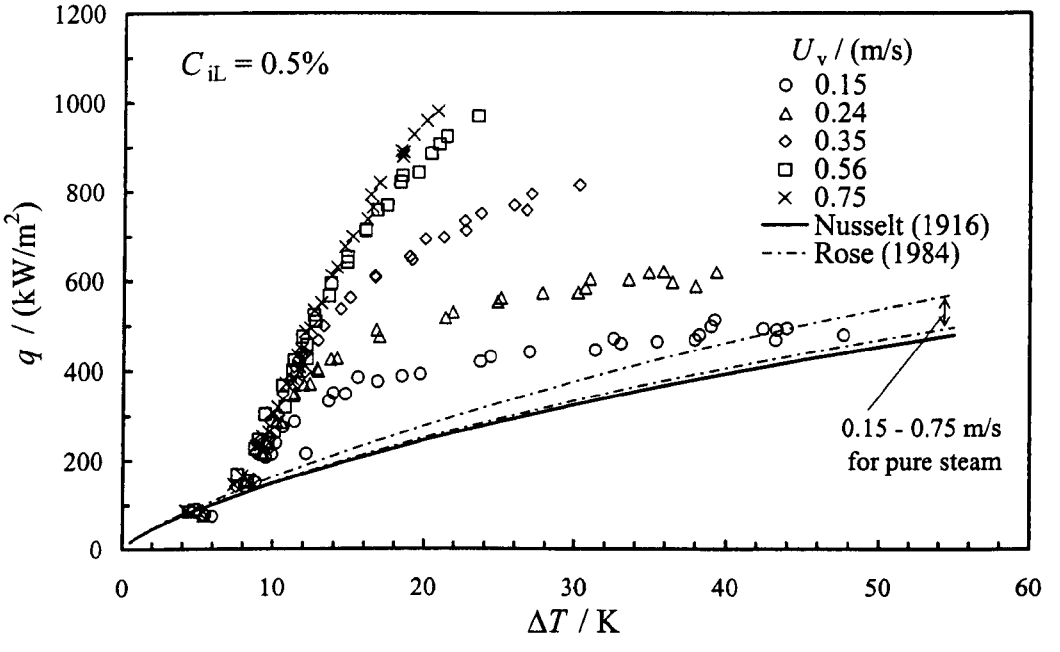

(c) 0.5%

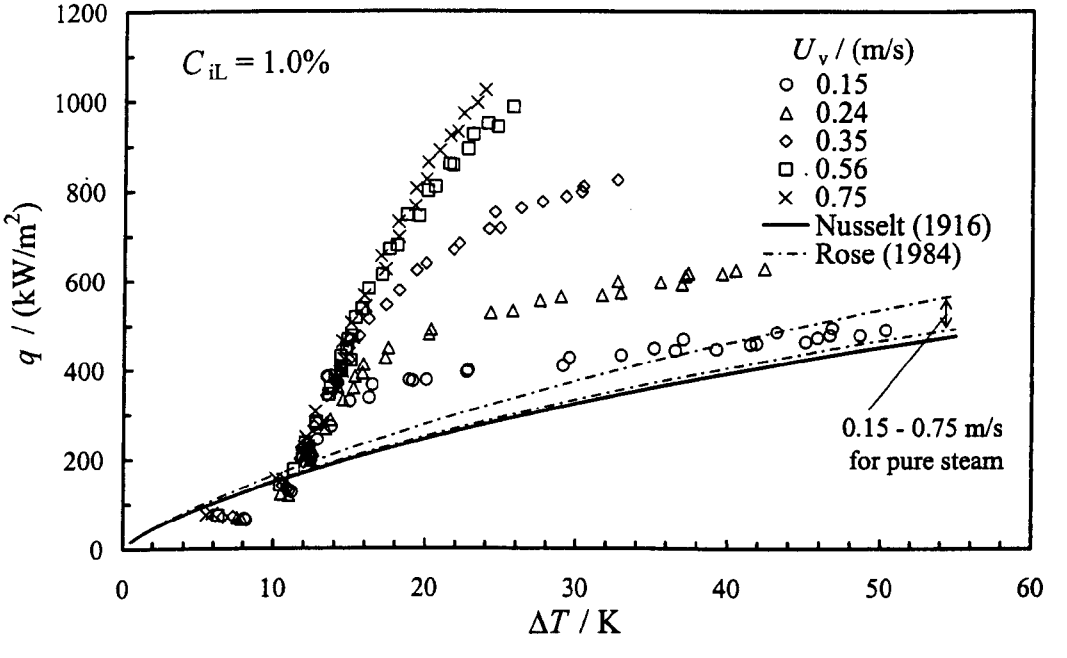

(d) 1.0%

Fig. 5.3 (continued).

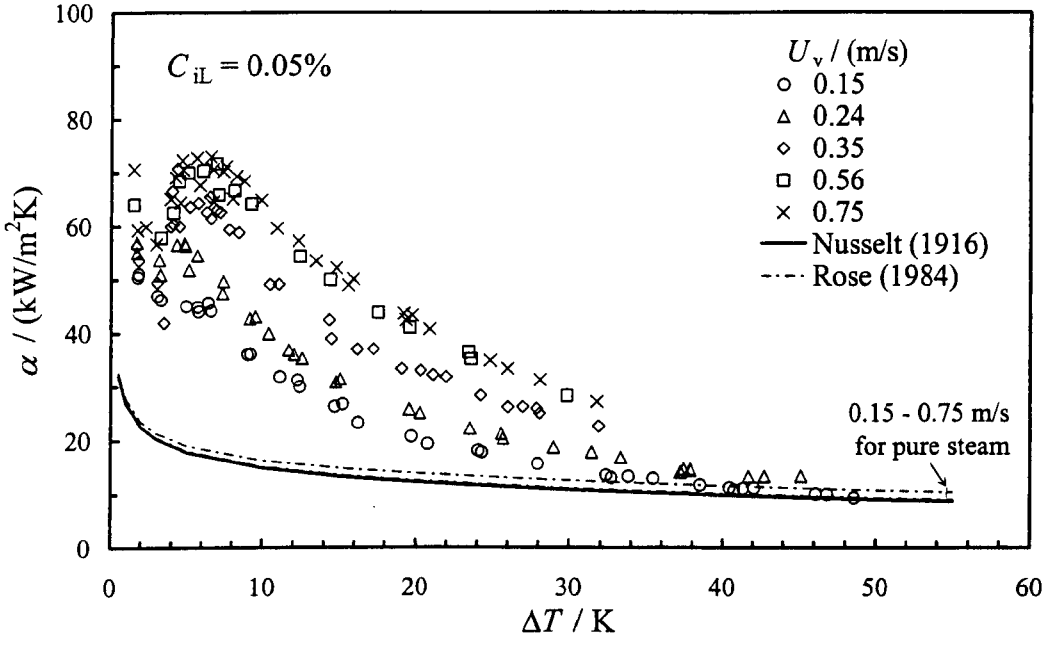

(a) 0.05%

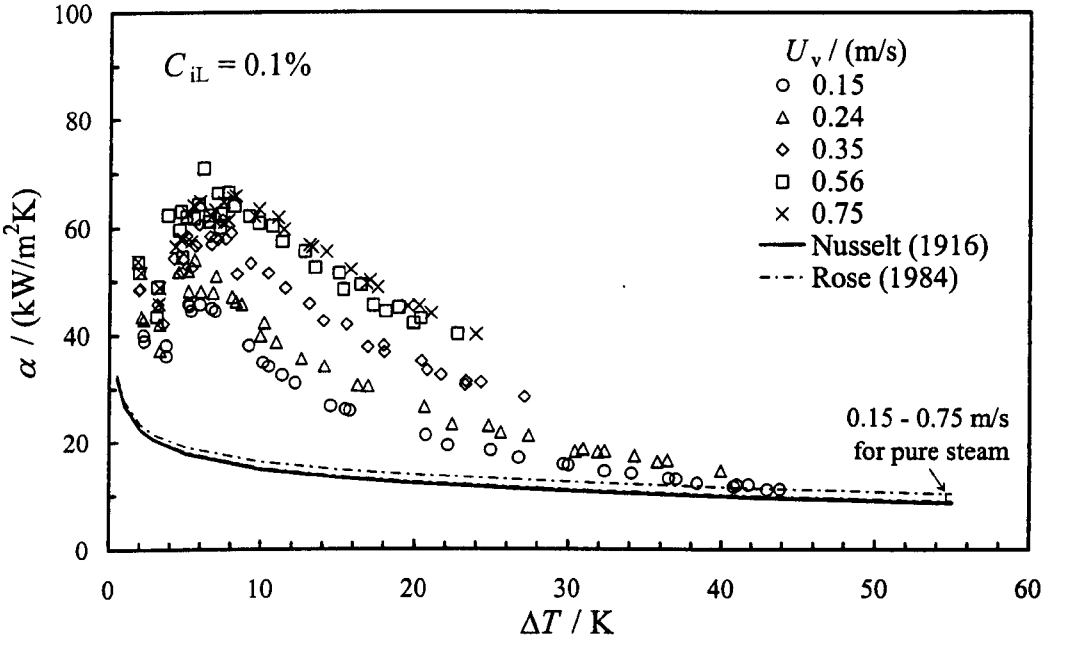

(b) 0.1%

Fig. 5.4. Variation of vapour-side, heat-transfer coefficient with vapour-to-surface temperature difference during Marangoni condensation of steam-ethanol mixtures on horizontal smooth tube for different vapour approach velocities at each ethanol mass fractions. C_{iL} denotes initial ethanol liquid mass fraction as prepared at atmospheric temperature.

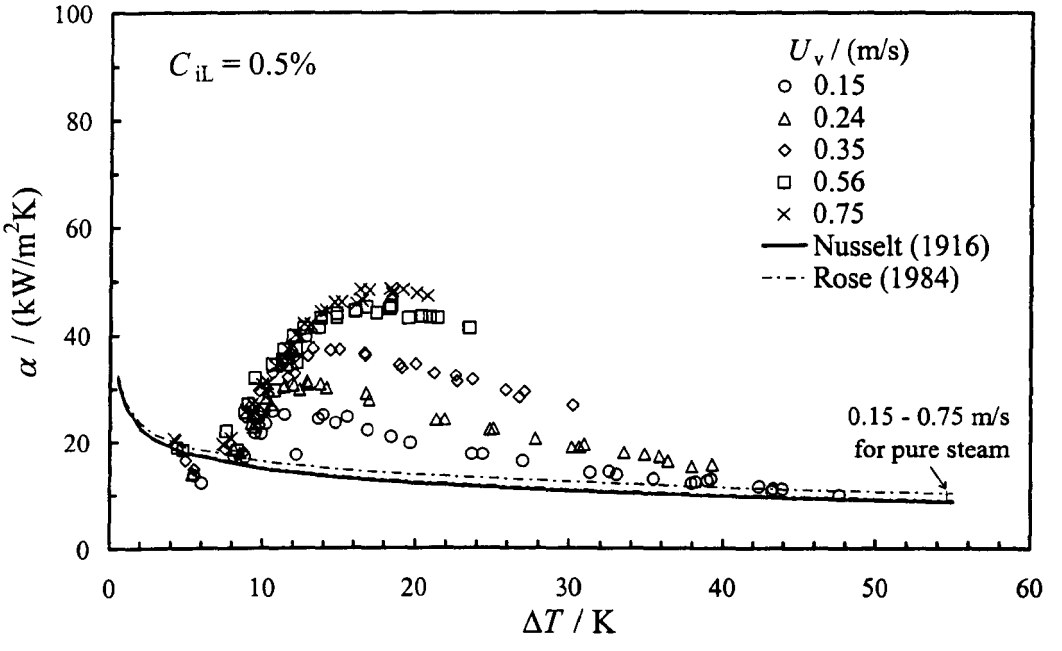

(c) 0.5%

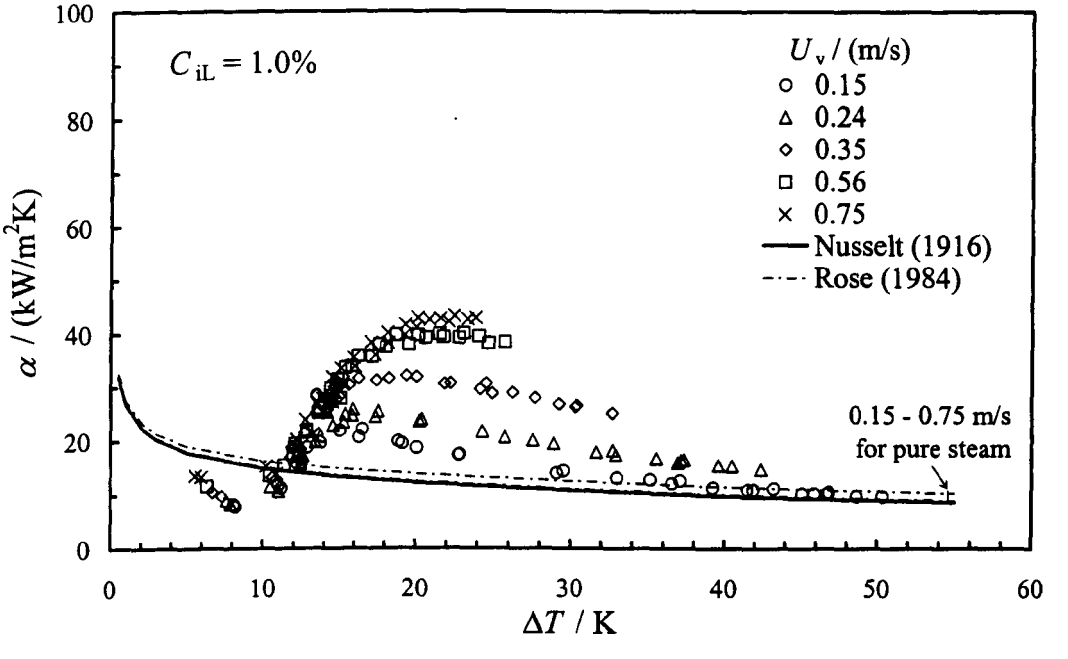

(d) 1.0 %

Fig. 5.4 (continued).

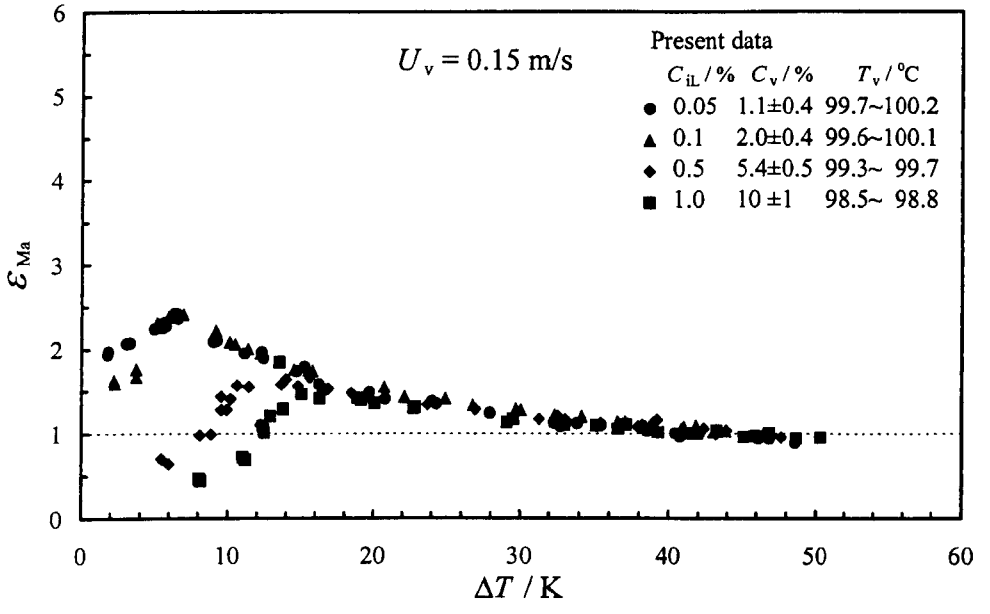

(a) 0.15 m/s

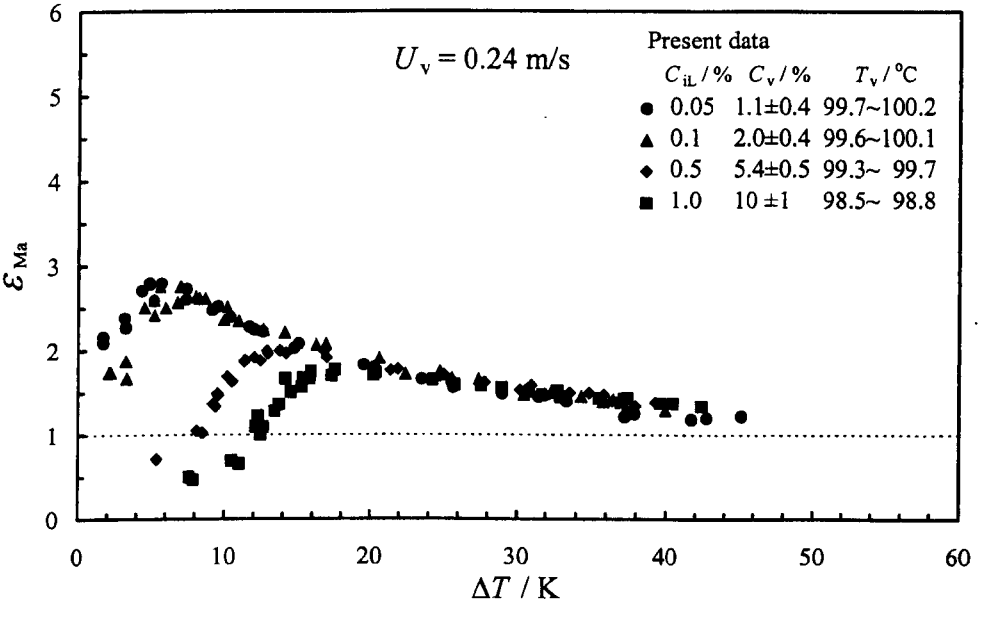

(b) 0.24 m/s

Fig. 5.5. Variation of heat-transfer enhancement with against vapour-to-surface temperature difference during Marangoni condensation of steam-ethanol mixtures on horizontal smooth tube for different ethanol mass fractions at each vapour approach velocity. C_{iL} denotes initial ethanol liquid mass fraction as prepared at atmospheric temperature, C_v ethanol vapour mass fraction during experiments.

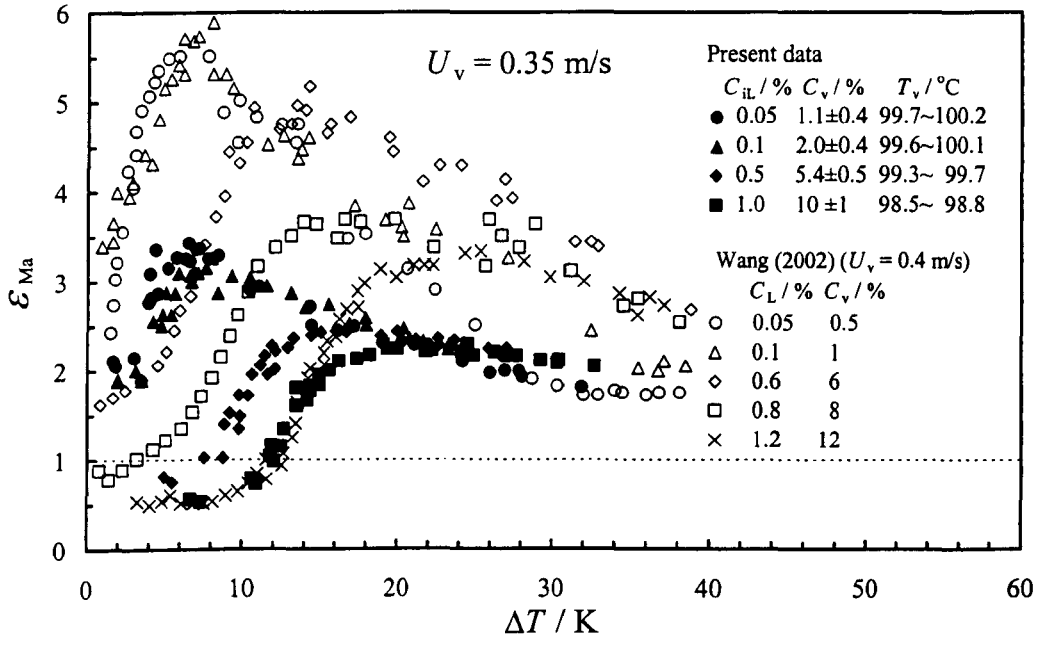

(c) 0.35 m/s

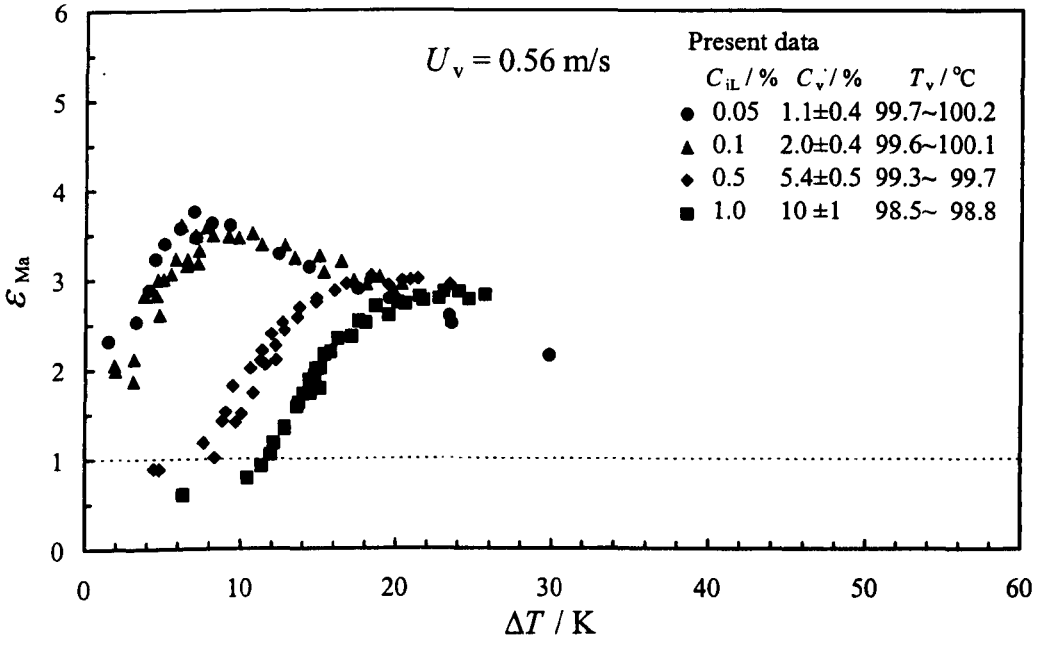

(d) 0.56 m/s

Fig. 5.5 (continued).

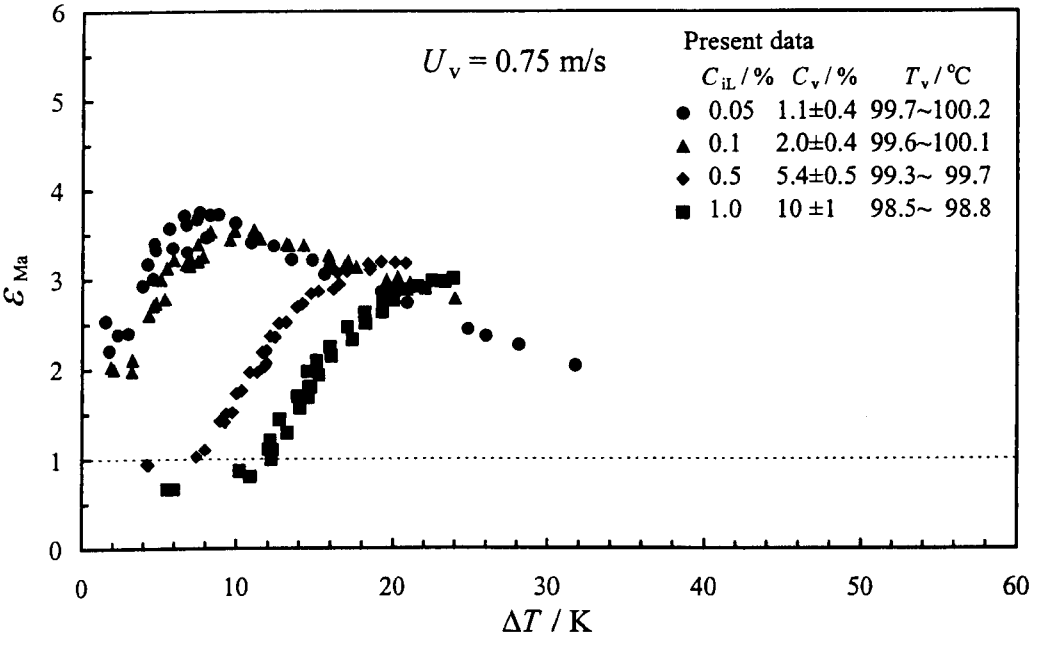

(e) 0.75 m/s

Fig. 5.5 (continued).

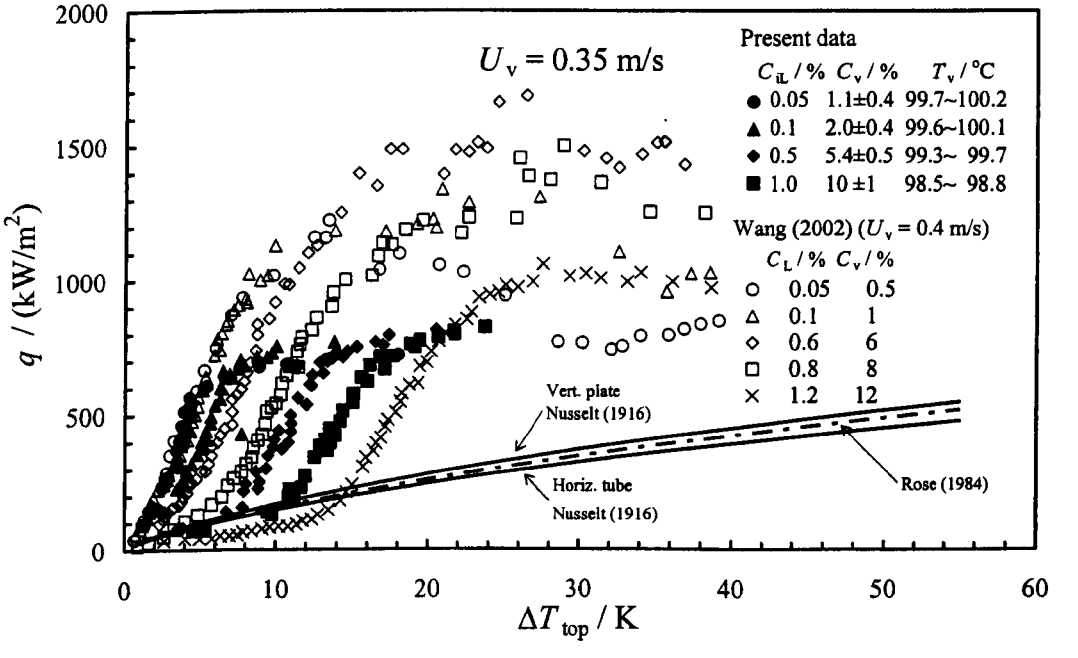

Fig. 5.6. Variation of heat flux with vapour-to-surface temperature difference using estimated wall surface temperature at the top of tube for vapour velocity of 0.35 m/s. Comparison with data of Wang (2002) for short vertical flat plate.

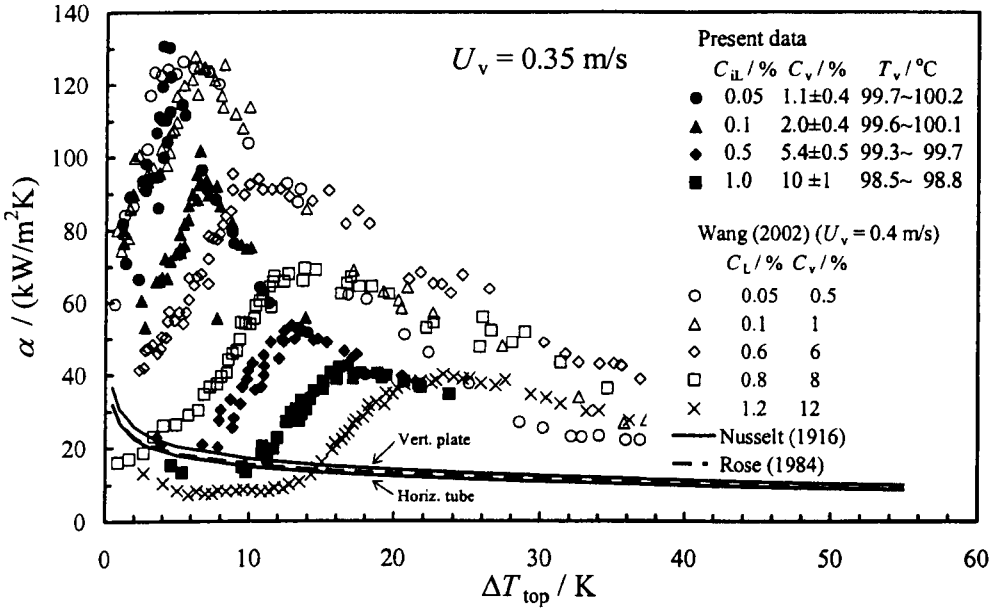

Fig. 5.7. Variation of heat-transfer coefficient with vapour-to-surface temperature difference using estimated wall surface temperature at the top of tube for vapour velocity of 0.35 m/s. Comparison with data of Wang (2002) for short vertical flat plate.

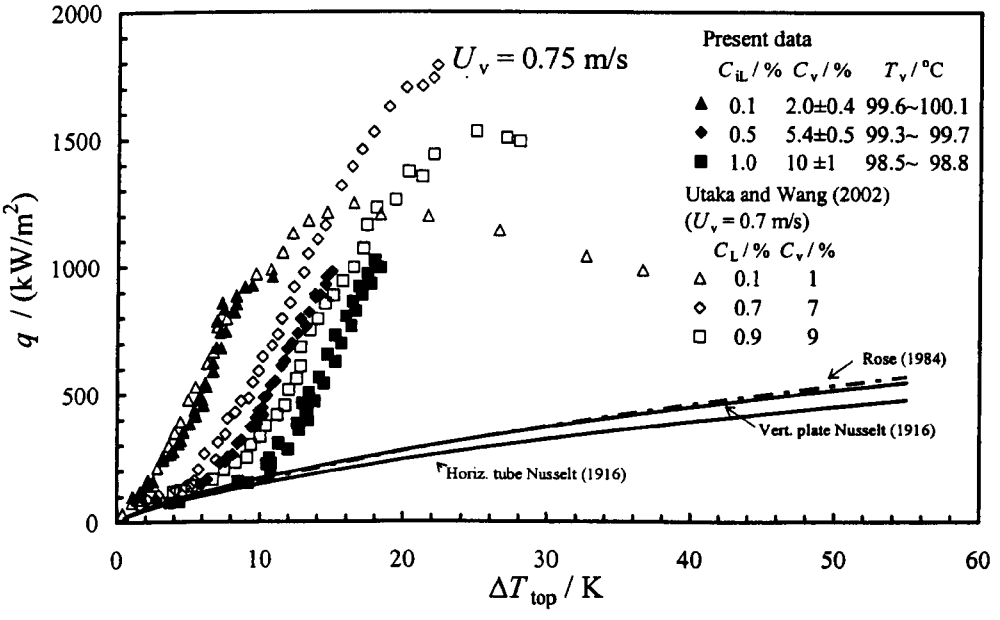

Fig. 5.8. Variation of heat flux with vapour-to-surface temperature difference using estimated wall surface temperature at the top of tube for vapour velocity of 0.75 m/s. Comparison with data of Utaka and Wang (2002) for short vertical flat plate.

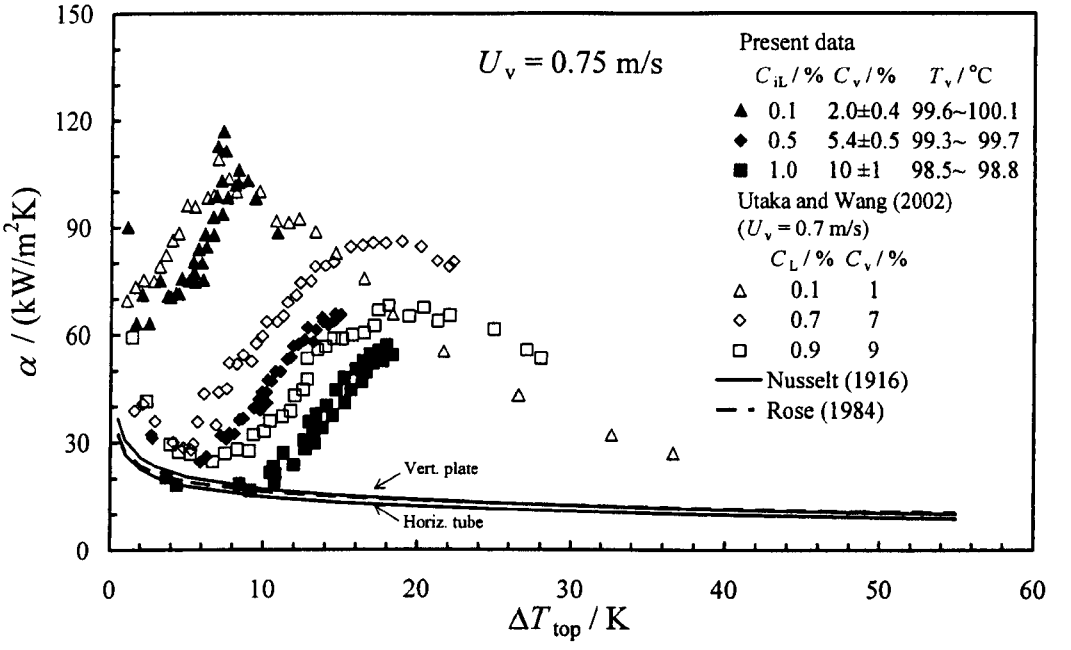

Fig. 5.9. Variation of heat-transfer coefficient with vapour-to-surface temperature difference using estimated wall surface temperature at the top of tube for vapour velocity of 0.75 m/s. Comparison with data of Utaka and Wang (2002) for short vertical flat plate.

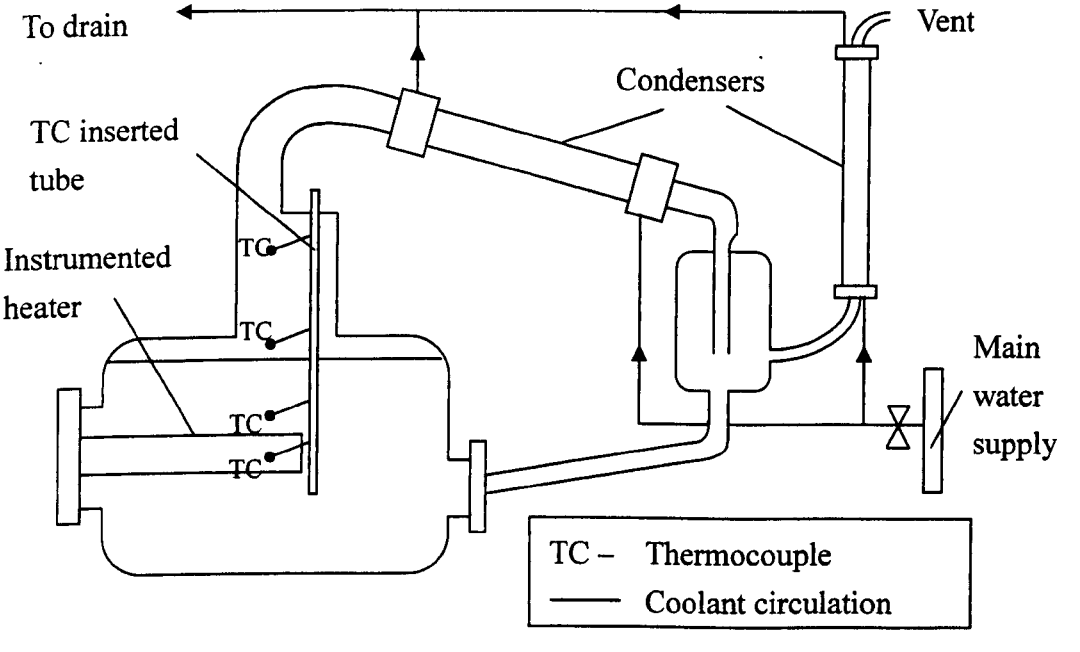

Fig. 5.10. Test apparatus used for boiling investigation and positions of thermocouples for vapour and liquid temperature measurements.

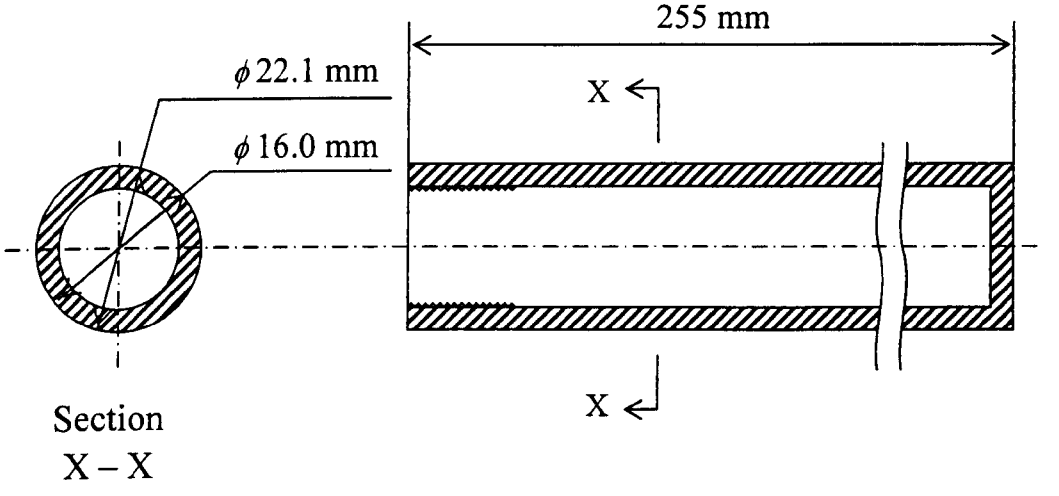

Fig. 5.11. Detail of instrumented sheath for boiling experiments.

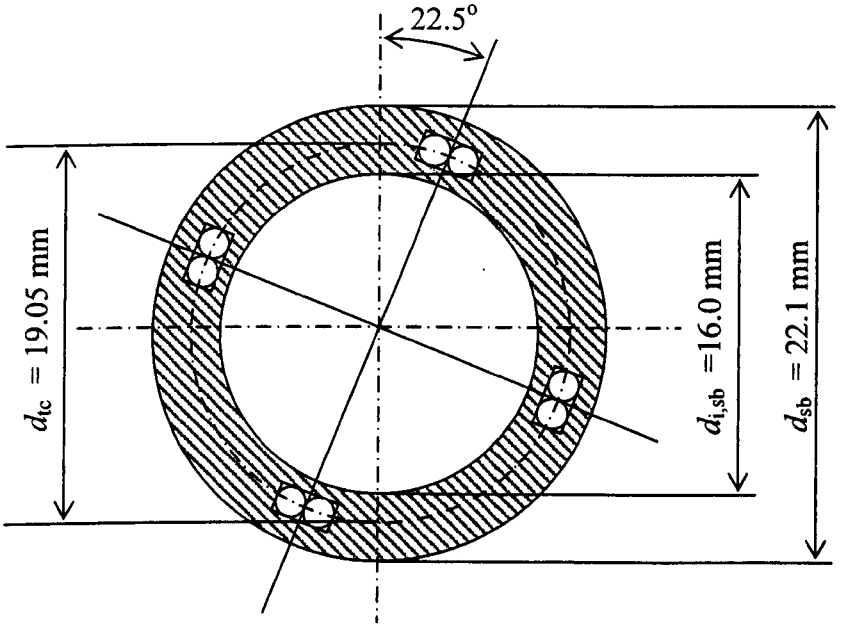

Fig. 5.12. Location of embedded thermocouples in sheath for boiling experiments.

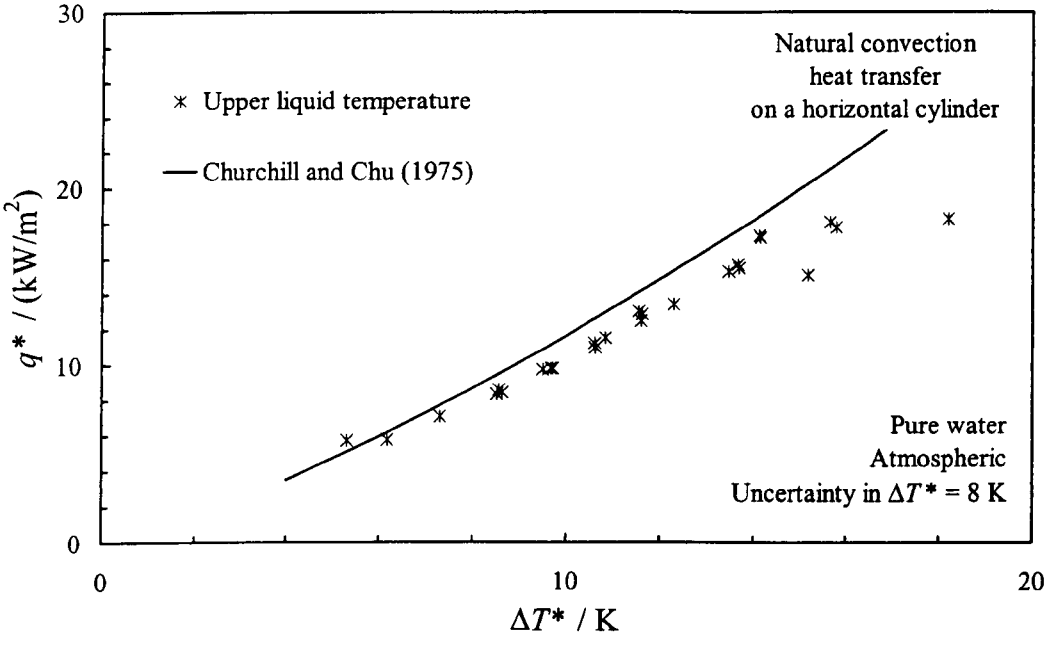

Fig. 5.13. Relation between heat flux and liquid-to-surface temperature difference for pure water during natural convection heat transfer on horizontal cylinder.

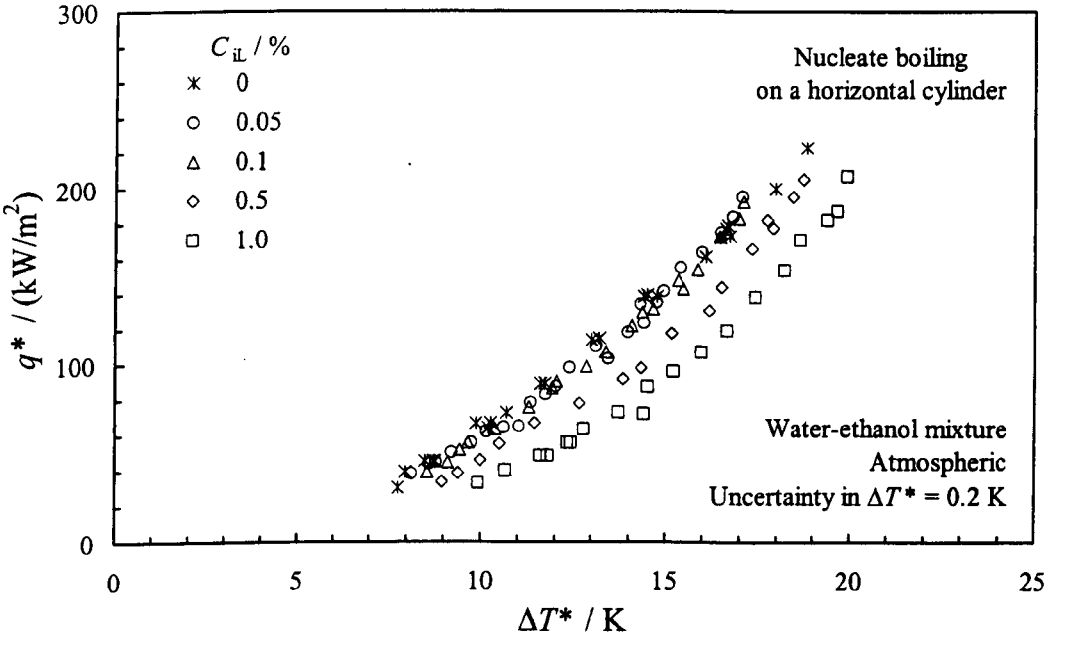

Fig. 5.14. Relation between boiling heat flux and liquid-to-surface temperature difference for small ethanol mass fraction mixtures and pure water during nucleate boiling on horizontal cylinder. C_{iL} denotes initial ethanol liquid mass fraction as prepared at atmospheric temperature.

Chapter 6
Conclusions

6.1 Condensation on wire-wrapped tubes

Incompatibility between sparse pre-existing data and approximate theory has been addressed in this thesis. A large reliable and accurate experimental data base has been generated using three fluids (R-113, ethylene glycol and steam) with widely different properties - notably surface tension. Wire diameters ranging from 0.2 to 1.0 mm have been used with winding pitch ranging from values a little larger than the wire diameter to 6.0 mm. Maximum heat-transfer enhancement ratios of 3.7, 2.2 and 2.3 for R-113, ethylene glycol and steam respectively have been obtained. These may be compared with values of 6.8, 4.8 and 3.0 for condensation on low-finned tubes under similar conditions.

The new data are not adequately explained by existing theory. The theory has been reviewed and carefully examined but time limitation and theoretical complexity has prevented resolution of the problem at the present time. It is considered that the approximation in earlier theories that the condensate film may be treated as having uniform thickness except near the wires is inadequate. However, relaxation of this approximation leads to major complexity resulting from the condensate surface curvature term in the momentum balance for the condensate film. It is considered, however, that the new data base will contribute significantly to the eventual solution of the problem.

Further careful experiments have been conducted on the effect of inundation during condensation of steam on a wire-wrapped tube. A relatively recent report in the literature that wire-wrapped tube is superior in this respect to low-finned tube has been shown to be incorrect. In experiments where condensate from higher tubes falling onto a given tube is simulated, as in the present investigation, by supplying artificial inundation from above the tube in question, the importance of the artificial inundation supply temperature has been highlighted. In particular, attention has been drawn the importance of circumferential wall temperature variation in determining

the correct inundation temperature. It has been verified that the earlier contention that the deterioration in performance with inundation of wire-wrapped tubes is less than for finned tubes is incorrect. Both perform approximately equally well in this respect by channelling inundation columns so that substantial parts of the inundated tube surface are not affected as in the case of smooth tubes.

6.2 Marangoni condensation of steam-ethanol mixtures

Earlier work on this topic has been significantly extended and amplified, in particular for condensation on horizontal tubes. Earlier work with this geometry is relatively sparse and without systematic coverage of the relevant variables. On the other hand detailed, extensive and systematic studies of condensation of steam-ethanol mixtures have recently been made using small plane vertical surfaces. The present work has confirmed that significant enhancement (up to around 3.7) may also be obtained for condensation of steam-ethanol mixtures on horizontal tubes using very small ethanol concentrations. The general trends are the same as those found for small plane surfaces but average heat-transfer coefficients and enhancements for the tube case are significantly smaller. It has been shown that differences between the performances of the two geometries may be attributed largely to the strong dependence of heat-transfer coefficient on vapour-to-surface temperature difference together with the circumferential surface temperature variation of the tube.

It has been demonstrated that significant improvement in condenser performance can be obtained by addition of as little as 0.1% by mass of ethanol to the boiler feed. Boiling experiments have also been performed in the course of the present work in which it has been shown that such small concentrations of ethanol do not impair the boiler performance. It should be noted, however, that both condensation and boiling studies have been performed only at atmospheric pressure. Before attempting to implement this as a means of enhancing the performance of power plants both boiling and condensation measurements at reduced pressure are needed. Time constraint prevented the accomplishment of this in the present investigation.

6.3 Recommendation for future work

Wire-wrapped tube

The present work has demonstrated that existing theory for condensation on wire-wrapped tubes is inadequate and that the problem remains to be solved. A detailed numerical solution of the differential equation (4^{th} order in angle and 1^{st} order in lateral distance) for the condensate film thickness (see Eq. (2-18)) which includes curvature of the condensate in the lateral direction between wires is needed. Despite the assumption of laminar condensate flow this will be a formidable task and at present it is not clear how the boundary conditions should be specified. Such numerical solutions together with the extensive experimental data base provided by the present work would pave the way to development of a satisfactory correlation. A purely empirical approach which would require at least 8 dimensionless parameters is not feasible.

A more refined experimental investigation of inundation for smooth, low integral-finned and wire-wrapped tubes should be undertaken using inundation temperatures as specified in Eq. (4-38).

Marangoni condensation

In view of the different condensate flow regimes resulting from surface instabilities a fully theoretical solution seems prohibitively difficult at this stage. The fact that major enhancement of the vapour-side heat transfer coefficient is possible with very small concentration of ethanol suggests possible application in power plant. This would require further experimental studies of both condensation and boiling of water-ethanol mixtures.

Appendix A

Thermophysical Properties of test fluids

A.1 Nomenclature and units

The symbols, units and subscripts used in property equations are given below:

c_{pf}	specific isobaric heat capacity of saturated liquid / (J/kg·K)
c_{pg}	specific isobaric heat capacity of saturated vapour / (J/kg·K)
D	diffusion coefficient / (m^2/s)
h_{fg}	specific enthalpy of evaporation / (J/kg)
k_f	thermal conductivity of saturated liquid / (W/m·K)
P	pressure / (Pa)
P_{sat}	saturation pressure / (Pa)
R	specific ideal gas constant / (J/kg·K)
T	thermodynamic temperature / (K)
T_{sat}	thermodynamic temperature at saturation / (K)
W_L	liquid mass fraction of mixture
W_v	vapour mass fraction of mixture
Z	compressibility factor
v_f	specific volume of saturated liquid / (m^3/kg)
v_g	specific volume of superheated vapour / (m^3/kg)
γ	coefficient of expansion of superheated liquid / (1/K)
μ_f	dynamic viscosity of saturated liquid / (kg/m·s)
ρ_g	density of saturated liquid / (kg/m^3)
σ_f	Surface tension / (N/m)

Subscripts

e	ethanol
mix	mixture
w	water

A.2 Properties of R-113

Specific volume of saturated liquid (Fujii et al. (1978))

$$v_f = \left\{0.617 + 0.00064(T - 273.15)^{1.1}\right\} \times 10^{-3} \tag{A.2-1}$$

Specific volume of saturated vapour (Fujii et al. (1978))

$$v_g = \frac{8314ZT}{187.39P} \tag{A.2-2}$$

where

$$Z = \frac{1}{1 + 0.636\left(\frac{P}{3413000}\right)^{0.816}} \tag{A.2-3}$$

Saturation pressure (Fujii et al. (1978))

$$P_{sat} = 3.413 \times 10^6 \times 10^A \tag{A.2-4}$$

where

$$A = -A_1\left\{2.8 + 0.1(1 + 185 \times A_1^{5.8})^{0.2}\right\} \tag{A.2-5}$$

and

$$A_1 = \frac{(487.25 - T)}{T} \tag{A.2-6}$$

Saturation temperature

The saturation temperature, T_{sat}, was found from the measured pressure using a

Newton-Raphson iteration to find the relevant root of Eqs. (A.2-4) to (A.2-6).

Specific isobaric heat capacity of saturated liquid (Fujii et al. (1978))

$$C_{pf} = 929 + 1.03(T - 273.15) \tag{A.2-7}$$

Specific isobaric heat capacity of saturated vapour (Fujii et al. (1978))

$$C_{pg} = -101.883 + T\left\{5.81502 - T(1.70256\times10^{-2} - 1.98007\times10^{-5}T)\right\} \tag{A.2-8}$$

Specific enthalpy of evaporation (Fujii et al. (1978))

$$h_{fg} = \left\{1.611 - 0.0031(T - 273.15)\right\}\times10^{5} \tag{A.2-9}$$

Thermal conductivity of saturated liquid (Fujii et al. (1978))

$$k_f = 0.0802 - 0.000203(T - 273.15) \tag{A.2-10}$$

Dynamic viscosity of saturated liquid (Fujii et al. (1978))

$$\mu_f = 1.34\times10^{-5}\times10^{A} \tag{A.2-11}$$

where

$$A = \frac{503}{(T - 2.15)} \tag{A.2-12}$$

Surface tension (Masuda (1985))

$$\sigma_f = 0.0217 - 1.1\times10^{-4}(T - 273.15) \qquad T \geq 293.15\ \text{K} \tag{A.2-13}$$

$$\sigma_f = 0.0217 - 1.3\times10^{-4}(T - 273.15) \qquad T < 293.15\ \text{K} \qquad \text{(A.2-14)}$$

A.3 Properties of ethylene glycol

Specific volume of saturated liquid (Perry and Chilton (1973))

$$v_f = 9.24848\times10^{-4} + 6.2796\times10^{-7}T_B + 9.2444\times10^{-10}T_B^2 + 3.057\times10^{-12}T_B^3 \qquad \text{(A.3-1)}$$

where

$$T_B = T - 338.15 \qquad \text{(A.3-2)}$$

Specific volume of saturated vapour (Perry and Chilton (1973))

$$v_g = \frac{RT}{P} \qquad \text{(A.3-3)}$$

where

$$R = 133.95 \qquad \text{(A.3-4)}$$

Saturation pressure of liquid (Fujii et al. (1978))

$$P_{sat} = 133.32\times10^{A} \qquad \text{(A.3-5)}$$

where

$$A = 9.394685 - \frac{3066.1}{T} \qquad \text{(A.3-6)}$$

Saturation temperature (from Eq. (A.3-3))

$$T_{sat} = \frac{3066.1}{9.394685 - \log_{10}(\frac{P}{133.32})} \tag{A.3-7}$$

Specific isobaric heat capacity of saturated liquid (Perry and Chilton (1973))

$$C_{pf} = 4186.8\left(1.6884\times10^{-2} + 3.35083\times10^{-3}T \right. \\ \left. -7.224\times10^{-6}T^2 + 7.61748\times10^{-9}T^3\right) \tag{A.3-8}$$

Specific isobaric heat capacity of saturated vapour (Perry and Chilton (1973))

$$C_{pg} = 472.433 + 4.6327T - 3.6054\times10^{-3}T^2 + 1.1827\times10^{-6}T^3 \tag{A.3-9}$$

Specific enthalpy of evaporation (Gallant (1970))

$$h_{fg} = 1.35234\times10^{6} - 638.263T - 0.747462T^2 \tag{A.3-10}$$

Thermal conductivity of saturated liquid (Fujii et al. (1978))

$$k_f = 418.68\times10^{-6}(519.442 + 0.32092T) \tag{A.3-11}$$

Dynamic viscosity of saturated liquid (Crume and Johnston (1952))

$$\mu_f = \exp^{A} \tag{A.3-12}$$

where

$$A = -11.0179 + \frac{1.744\times10^{3}}{T} - \frac{2.80335\times10^{5}}{T^2} + \frac{1.12661\times10^{8}}{T^3} \tag{A.3-13}$$

Surface tension (Masuda (1985))

$$\sigma_f = 5.021\times10^{-2} - 8.9\times10^{-5}(T - 273.15) \qquad \text{(A.3-14)}$$

A.4 Properties of water

Specific volume of saturated liquid (Lee (1982))

$$v_f = 0.0012674 - T(2.02915\times10^{-6} - 3.8333\times10^{-9}T) \qquad \text{(A.4-1)}$$

Specific volume of saturated vapour (Le Fevre et al. (1975))

$$v_g = \frac{\left\{1+(1+2T_cT_d)^{1/2}\right\}}{T_d} \qquad \text{(A.4-2)}$$

where

$$T_a = \frac{1500}{T} \qquad \text{(A.4-3)}$$

$$T_b = 2.5\ln\left(1-\exp^{-T_a}\right) \qquad \text{(A.4-4)}$$

$$T_c = \frac{0.0015}{1+0.0001T} - 0.000942\left(\frac{1}{T_a}\right)^{1/2}\exp^{(T_a+T_b)} - 0.0004882T_a \qquad \text{(A.4-5)}$$

$$T_d = \frac{P}{230.755T} \qquad \text{(A.4-6)}$$

Saturation pressure of liquid (Lee (1982))

$$P_{sat} = 10^6\exp^A \qquad \text{(A.4-7)}$$

where

$$A = A_1 + \frac{A_2}{T_f} + A_3 \ln(T_f) + A_4 T_f + A_5 T_f^2 + A_6 T_f^3 + A_7 T_f^4 + A_8 T_f^5 + A_9 T_f^6 + A_{10} T_f^7 + A_{11} T_f^8 \quad \text{(A.4-8)}$$

$$T_f = \frac{T}{1000} \quad \text{(A.4-9)}$$

and

$A_1 = 15.49217901$

$A_2 = -5.6783717693$

$A_3 = 1.4597584637$

$A_4 = 13.877000608$

$A_5 = -80.887673591$

$A_6 = 123.56883468$

$A_7 = -188.31212064$

$A_8 = 660.91763485$

$A_9 = -1382.4740091$

$A_{10} = 1300.1040184$

$A_{11} = -449.39571976$

Saturation temperature

The saturation temperature, T_{sat}, was found from the measured pressure using a Newton-Raphson iteration to find the relevant root of Eqs. (A.4-7) to (A.4-9).

Specific isobaric heat capacity of saturated liquid (Nobbs (1975))

$$C_{pf} = 10768.539 - T\left\{57.216 - T(0.16359 - 1.536 \times 10^{-4} T)\right\} \quad \text{(A.4-10)}$$

Specific isobaric heat capacity of saturated vapour (Nobbs (1975))

$$C_{pg} = 1000\{1.86238 + 5.1713\times10^{-4}(T-273.15) + 2.9015\times10^{-6}(T-273.15)^2 + 9.106027\times10^{-8}(T-273.15)^3\} \quad \text{(A.4-11)}$$

Specific enthalpy of evaporation (Lee (1982))

$$h_{fg} = 3468920 - T(5707.4 - T(11.5562 - 0.0133103T)) \quad \text{(A.4-12)}$$

Thermal conductivity of saturated liquid (Lee (1982))

$$k_f = -0.92407 + T_g\left[2.8395 - T_g\left\{1.8007 - T_g(0.52577 - T_g 0.07344)\right\}\right] \quad \text{(A.4-13)}$$

where

$$T_g = \frac{T}{273.15} \quad \text{(A.4-14)}$$

Dynamic viscosity of saturated liquid (Lee (1982))

$$\mu_f = 0.00002414\times10^{A} \quad \text{(A.4-15)}$$

where

$$A = \frac{247.8}{T - 140.0} \quad \text{(A.4-16)}$$

Surface tension (Masuda (1985))

$$\sigma_f = \frac{75.6 - 0.138(T-273.15) - 0.0003(T-273.15)^2}{1000} \quad \text{(A.4-17)}$$

Coefficient of expansion of superheated liquid (Perry and Chilton (1973))

$$\gamma = \frac{\rho_{g1}^2 - \rho_{g2}^2}{2(T_2 - T_1)\rho_{g1}\rho_{g2}} \tag{A.4-18}$$

where ρ_{gn} is the density of saturated liquid obtained using Eq. (A.4-2) to (A.4-6) at the temperature T_n (n = 1, 2).

A.5 Properties of ethanol

Specific volume of saturated liquid (Fujii et al. (1983))

$$v_f = \frac{1}{-0.90055T + 807.44} \tag{A.5-1}$$

Specific volume of saturated vapour (Fujii et al. (1983))

$$v_g = \frac{ZRT}{P} \tag{A.5-2}$$

where

$$R = 197.63 \tag{A.5-3}$$

$$\frac{1}{Z} = 1 + 0.09\left(\frac{P}{T}\right) \tag{A.5-4}$$

Saturation pressure of saturated liquid (Fujii et al. (1983))

$$\log P_{sat} = 8.21337 - \frac{1652.05}{(T - 273.15) + 231.48} + \log 0.1333 \qquad \text{(A.5-5)}$$

Thus,

$$P_{sat} = 0.1333 \times 10^{8.21337 - \frac{1652.05}{T - 41.67}} \qquad \text{(A.5-6)}$$

Saturation temperature (from Eqs. (A.5-5) and (A.5-6))

$$T_{sat} = 41.67 + \frac{1652.05}{8.21337 - \log \frac{P_{sat}}{0.1333}} \qquad \text{(A.5-7)}$$

Specific isobaric heat capacity of saturated liquid (Fujii et al. (1983))

$$c_{pf} = 2.262 \times 10^3 + 6.53(T - 273.15) + 0.094(T - 273.15)^{1.79} \qquad \text{(A.5-8)}$$

Specific isobaric heat capacity of saturated vapour (Fujii et al. (1983))

$$c_{pg} = 1.52 \times 10^3 + 2.9(T - 273.15)^{1.011} \qquad \text{(A.5-9)}$$

Specific enthalpy of evaporation (Fujii et al. (1983))

$$h_{fg} = 920 - 0.5(T - 273.15) - 5.8 \times 10^{-6}(T - 273.15)^{3.5} \qquad \text{(A.5-10)}$$

Thermal conductivity of saturated liquid (Fujii et al. (1983))

$$k_f = 0.17256 - 2.3412 \times 10^{-4}(T - 273.15) \tag{A.5-11}$$

Dynamic viscosity of saturated liquid (Fujii et al. (1983))

$$\mu_f = 1.545 \times 10^{-7} \times 10^{A} \tag{A.5-12}$$

where

$$A = \frac{1817}{(T - 273.15) + 447.22} \tag{A.5-13}$$

Dynamic viscosity of saturated vapour (Fujii et al. (1983))

$$\mu_g = \{76.33 + 0.33425(T - 273.15)\} \times 10^{-7} \tag{A.5-14}$$

A.6 Properties of water-ethanol mixture

Specific volume of saturated vapour (Fujii et al. (1983))

$$v_{g\,mix} = W_{ve} v_{ge} + W_{vw} v_{gw} \tag{A.6-1}$$

where v_{gw} and v_{ge} were calculated using Eqs. (A.4-2) and (A.5-2) respectively.

Specific isobaric heat capacity of saturated liquid (Fujii et al. (1983))

$$c_{pf\,\mathrm{mix}} = W_{\mathrm{Le}} c_{pf\,\mathrm{e}} + W_{\mathrm{Lw}} c_{pf\,\mathrm{w}} \tag{A.6-2}$$

where $c_{pf\,\mathrm{w}}$ and $c_{pf\,\mathrm{e}}$ were calculated using Eqs. (A.4-11) and (A.5-8) respectively.

Specific isobaric heat capacity of saturated vapour (Fujii et al. (1983))

$$c_{pg\,\mathrm{mix}} = W_{\mathrm{v\,e}} c_{pg\,\mathrm{e}} + W_{\mathrm{v\,w}} c_{pg\,\mathrm{w}} \tag{A.6-3}$$

where $c_{pg\,\mathrm{w}}$ and $c_{pg\,\mathrm{e}}$ were calculated using Eqs. (A.4-12) and (A.5-9) respectively.

Specific enthalpy of evaporation (Wang (2002))

$$h_{\mathrm{fg\,mix}} = W_{\mathrm{Le}} h_{\mathrm{fge}} + W_{\mathrm{Lw}} h_{\mathrm{fgw}} \tag{A.6-4}$$

where $h_{\mathrm{fg\,w}}$ and h_{fge} were calculated using Eqs. (A.4-13) and (A.5-10) respectively.

Diffusion coefficient (Wang (2002))

$$D = \frac{4.58\times10^{-5} T^{1.83}}{P} \qquad 270 < T < 570\ \mathrm{K} \tag{A.6-5}$$

A.7 Thermal conductivity of tube

Thermal conductivity of copper (Niknejad (1979))

$$k_{\mathrm{w}} = 438.643 - 0.130692T + 4.540943\times10^{-5} T^2 \tag{A.7-1}$$

Appendix B

Calibration of thermocouples

All thermocouples used were made from the same reel of wire (nickel-chromium/nickel-aluminium). Two samples were taken from each end of the reel and calibrated using a high-accuracy, constant-temperature bath and a platinum resistance thermometer. The bath contained silicon oil which was heated to the desired temperature and controlled by a thermostat. The fluid was continually circulated around the bath so that the temperature in the measurement zone was kept constant to within 0.005 K.

The temperature in the isothermal bath was measured using the platinum resistance thermometer calibrated with an accuracy of better than 0.005 K. Measurements were taken at 20 K intervals over a range from 0 °C to 200 °C. The results for the two samples agreed to within 0.05 K at all points in the range and an average value was used, with which the following equation was obtained by fitting using the least squares method:

$$T = 273.15 + 2.563\times10^{-2}E - 4.066\times10^{-7}E^2 - 6.973\times10^{-12}E^3 + 1.325\times10^{-14}E^4 - 9.704\times10^{-19}E^5 \quad \text{(B-1)}$$

where E is the thermo-e.m.f. in μV and T is the thermodynamic temperature in K. In the temperature range of interest (0 °C to 200 °C), Eq (B.2-1) fitted the calibration data to within ±0.07 K.

Appendix C

Correction for dissipative temperature rise of coolant

To determine the frictional temperature rise as a function of coolant flow rate, tests were done by running coolant through the test tube without condensation and with the apparatus at room temperature. Measurements for the temperature rise due to the frictional dissipation over the range of coolant flow rates tested in the main tests were performed. The results are shown in Fig. C.1. The frictional dissipation effect was fitted by:

$$\Delta E_{\text{friction}} = \lambda \dot{V}_c^2 \qquad \text{(C-1)}$$

where $\Delta E_{\text{friction}}$ is the thermo-e.m.f. reading using the ten-junction thermopile for temperature rise of coolant in the test tube and the mixing chambers due to frictional dissipation in μV and $\dot{V}_c$ is the coolant flow rate, in l/min. λ was found to be 0.0406 μV/(l/min)^2 using a least square method with the data, as shown in Fig. C.1. The maximum dissipative temperature rise was approximately 0.05 K. This may be compared with the temperature rise of coolant during the condensation tests, which was approximately 0.11 - 30 K.

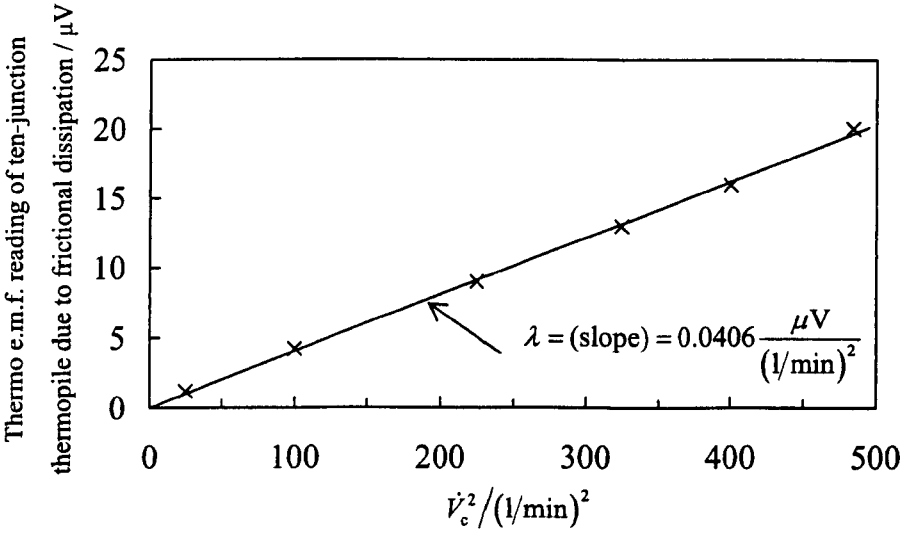

Fig. C.1. Relation between coolant volume flow rate and thermo-e.m.f. reading by ten-junction thermopile due to frictional dissipation.

Appendix D

Inundation supply temperature

The mean temperature of the condensate draining from a tube, T_{cond}, may be determined using the Nusselt (1916) theory for condensation on a horizontal smooth isothermal tube. The coordinate system is shown in Fig. D.1. By definition:

$$T_{cond} = \frac{\int_0^{\delta} \rho u_y T_y \mathrm{d}y}{\int_0^{\delta} \rho u_y \mathrm{d}y} \tag{D-1}$$

where u_y is the tangential velocity and T_y is the temperature in the condensate at coordinate y. From the Nusselt (1916) theory:

$$u_y = \frac{(\rho - \rho_v) g}{\mu} \left(\delta y - \frac{y^2}{2} \right) \sin\phi \tag{D-2}$$

and

$$T_y = \frac{T_v - T_w}{\delta} y + T_w \tag{D-3}$$

The integration of Eq. (D-1) with Eqs. (D-2) and (D-3) may be evaluated to give:

$$T_{cond} = \frac{5}{8} T_v + \frac{3}{8} T_w \tag{D-4}$$

In the inundation experiments described in Chapter 4, the inundation supply temperature, T_{inun}^{*}, was adjusted to T_{cond} in Eq. (D-4) as closely as possible, taking T_w as the mean of the four observed wall surface temperatures.

As discussed in Appendix E, the present measurements show strong dependence of wall surface temperature on angular location around the horizontal tubes. An attempt is made here to take account of the circumferential temperature distribution in the derivation of the mean temperature of condensate. The wall surface temperature at an angle ϕ is given by Eq. (E-1) in Appendix E. Taking Eq. (E-1) for T_w in Eq. (D-3), Eq. (D-1) may be integrated:

$$T_{cond}(\phi) = \frac{5}{8}T_v + \frac{3}{8}T_{wo}(1 + A\cos\phi) \qquad \text{(D-5)}$$

This is the mean condensate temperature at an angle ϕ. The mean temperature of the condensate draining from the bottom of the tube, i.e. $\phi = \pi$, is then given by:

$$T^*_{inun} = \frac{5}{8}T_v + \frac{3}{8}T_{wo}(1 - A) \qquad \text{(D-6)}$$

The values of constant A in Eq. (D-6) may find from experimental data using Eq. (E-1).

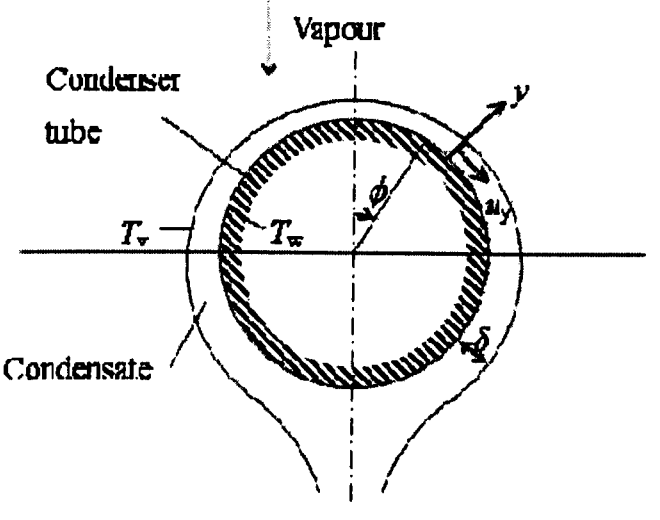

Fig. D.1 Coordinate system for condensation on a smooth tube.

Appendix E

Tube wall surface temperature distribution

Variation of wall temperature around the tube has heat-transfer implications for inundation and for Marangoni condensation. For film condensation of ethylene glycol on a horizontal smooth tube, Memory and Rose (1991) found that the tube surface temperature distribution was closely approximated by:

$$T_w = T_{wo}\left(1 + A\cos\phi\right) \qquad \text{(E-1)}$$

where A is a constant. In the present investigation, the wall surface temperatures were measured by thermocouples in the test tube at angles of 22.5°, 112.5°, -157.5° and -67.5° measured from the top of the tube. The present data for: (1) condensation of steam on horizontal smooth, wire-wrapped and low integral-finned tubes; and (2) Marangoni condensation on a horizontal smooth tube have been fitted with Eq. (E-1) using 'least squares'.

(1) Condensation of steam

Specimens of the cosine curve fits for the present data for condensation of steam on smooth, wire-wrapped and low integral-finned tubes respectively are shown in Figs. E.1 to E.3. The values of the range of A over the range of coolant flow rates used (2.0 to around 20 l/min) are shown in Table E.1. Satisfactory fits using Eq. (E-1) are seen in all cases.

Due to the effect of condensate retention in the lower part of wire-wrapped and finned tubes, it is seen from Table E.1 that the value of A, generally, increases in order of smooth, wire-wrapped and finned tubes. For the wire-wrapped tubes, the range of the values of A decreases with increase in wire pitch of winding and approaches the value for the smooth tube. The finned tube was found to have the largest amplitude of surface temperature variation. This is because the interfin space

for the finned tube used (1.5 mm) is smaller than the distance between the adjacent turns of wire for the wire-wrapped tubes tested (2.4 mm for the wire-wrapped tube with 4 mm pitch) so that the retention angle is greater for the finned tube.

(2) Marangoni condensation of steam-ethanol mixtures

Representative samples of results for the cosine curve fits using Eq. (E-1) with the present data for Marangoni condensation of steam-ethanol mixtures on a horizontal smooth tube are shown in Figs. E.4 to E.7 with values of A for the coolant flow rates of 1.8 and around 20 l/min for each ethanol mass fraction. Quite good fits using Eq. (E-1) are seen in all cases.

The temperature distribution during Marangoni condensation is thought to be due both to thickening of the condensate film and change of mode of condensation due to variation of vapour-to-surface temperature difference around the tube. The temperature difference from the top to bottom could be as large as 30 K. In extreme cases, visual observation showed pseudo-dropwise condensation on the upper part of the tube with film appearance at the lower part.

Table E.1 Ranges of values of constant A in Eq. (E-1) found from the present data for condensation of steam on smooth, wire-wrapped and low integral-finned tubes. (Vapour approach velocity 0.56 m/s, range of coolant flow rates from 2.0 to around 20 l/min.)

Tube / mm	p	A
smooth ($d = 12.2$, $l = 100$)		0.0126 – 0.181
wire-wrapped ($d = 12.2$, $l = 90$, $d_w = 1.6$)	4	0.0214 – 0.326
	8	0.0174 – 0.234
	16	0.0118 – 0.177
low integral-finned ($d = 12.7$, $l = 100$, $h = 1.6$, $t = 0.5$, $s = 1.5$)		0.0156 – 0.451

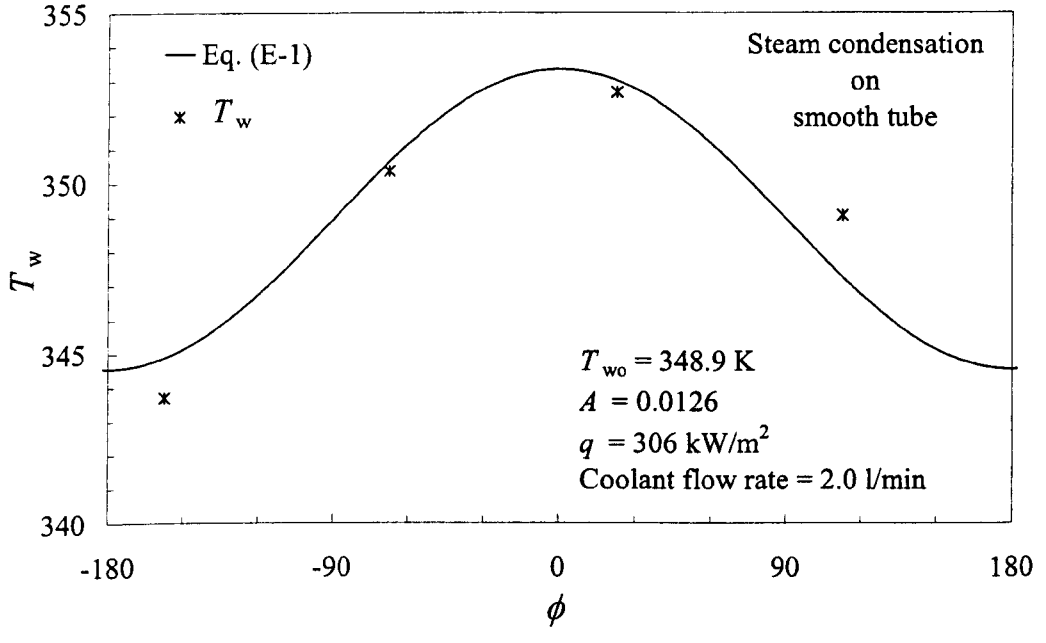

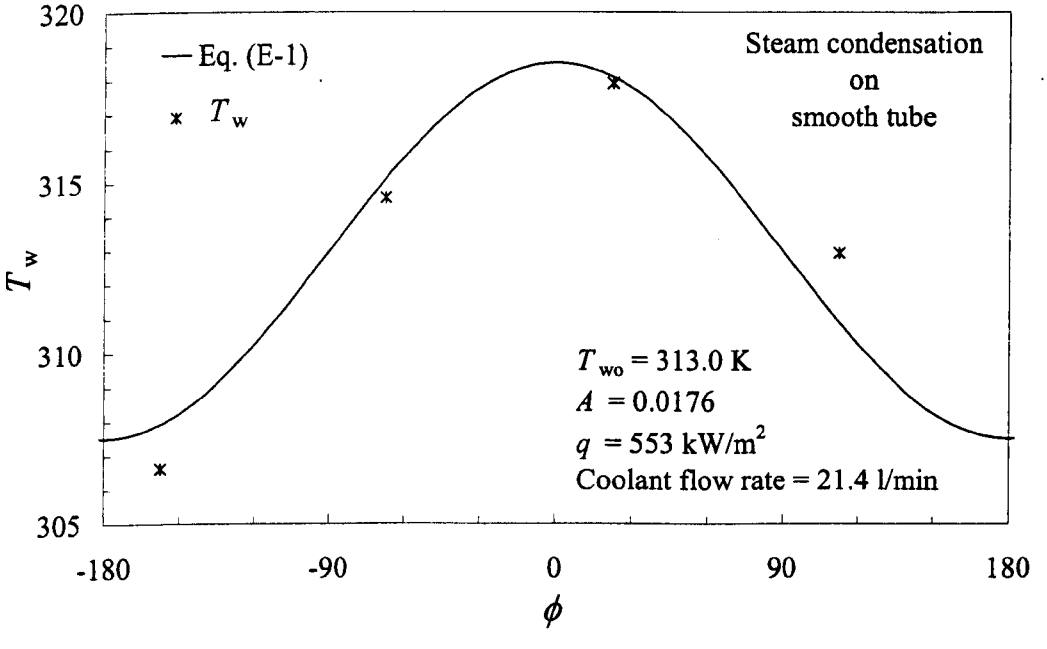

Fig. E.1 Specimens of cosine curve fits using Eq. (E-1) with tube wall surface temperatures during condensation of steam on horizontal smooth tube.

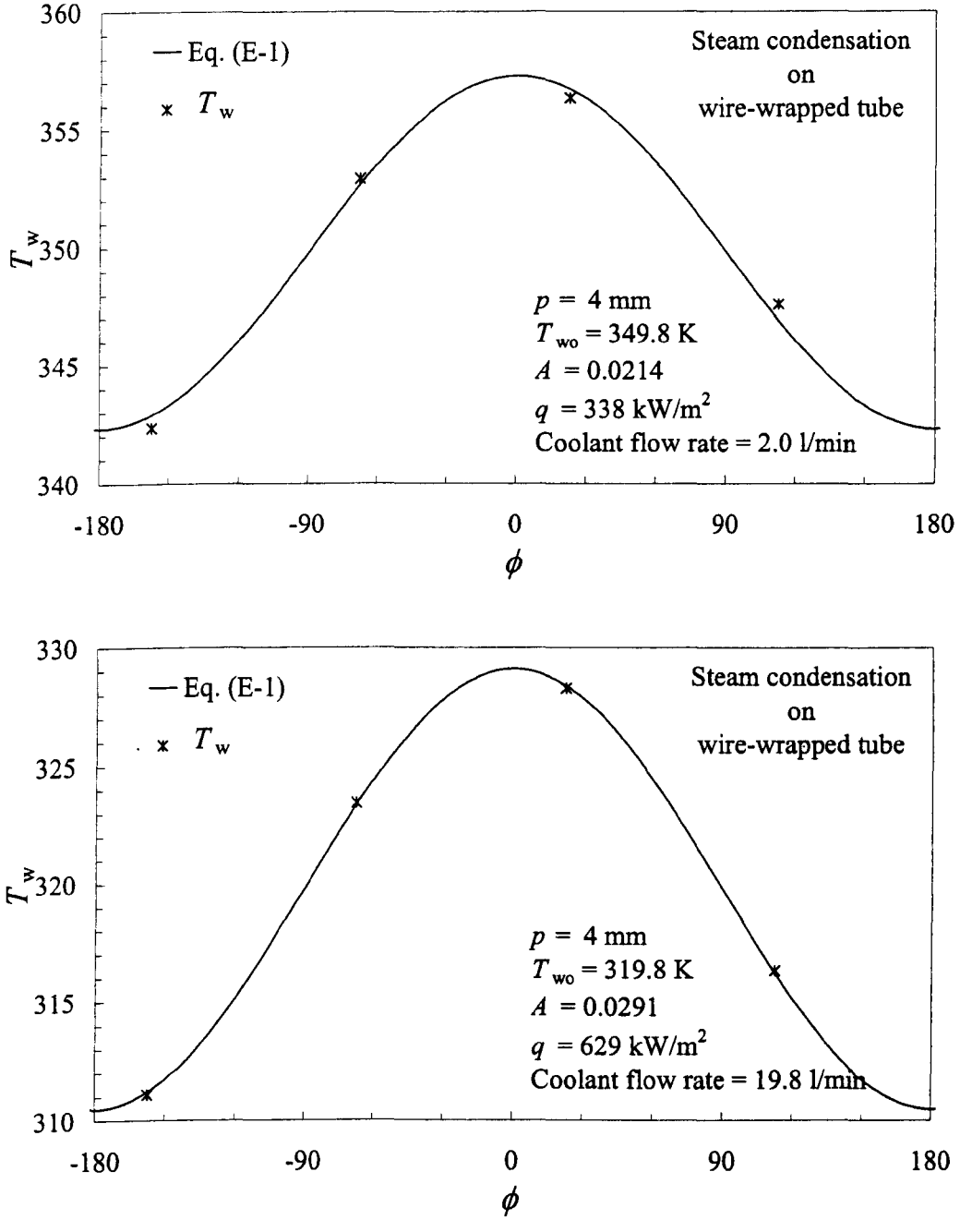

Fig. E.2 Specimens of cosine curve fits using Eq. (E-1) with tube wall surface temperatures during condensation of steam on horizontal wire-wrapped tube.

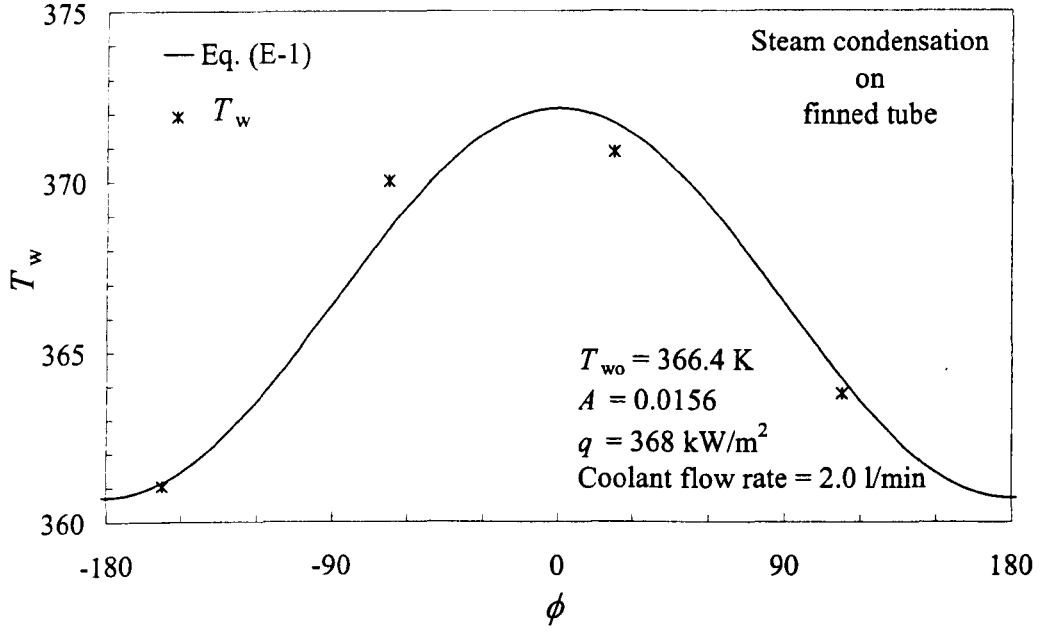

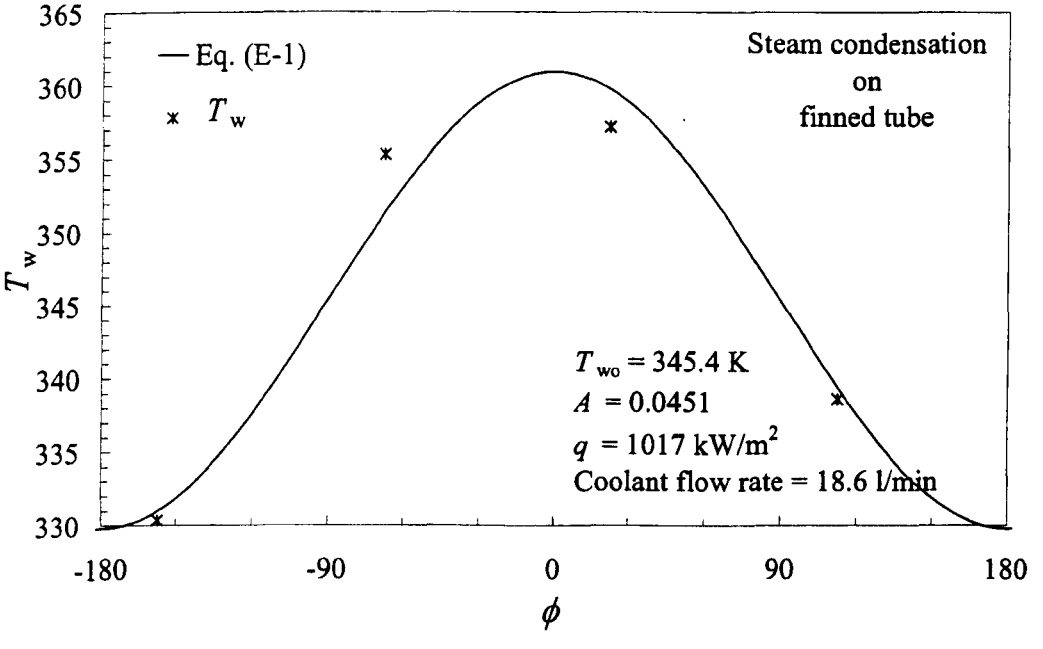

Fig. E.3 Specimens of cosine curve fits using Eq. (E-1) with tube wall surface temperatures during condensation of steam on horizontal low integral-finned tube.

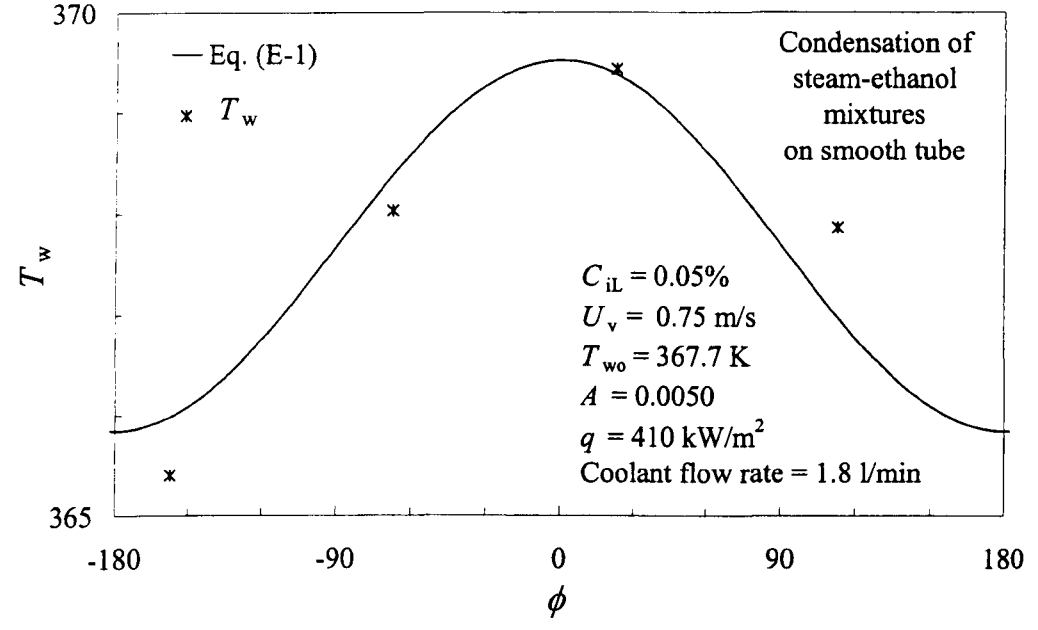

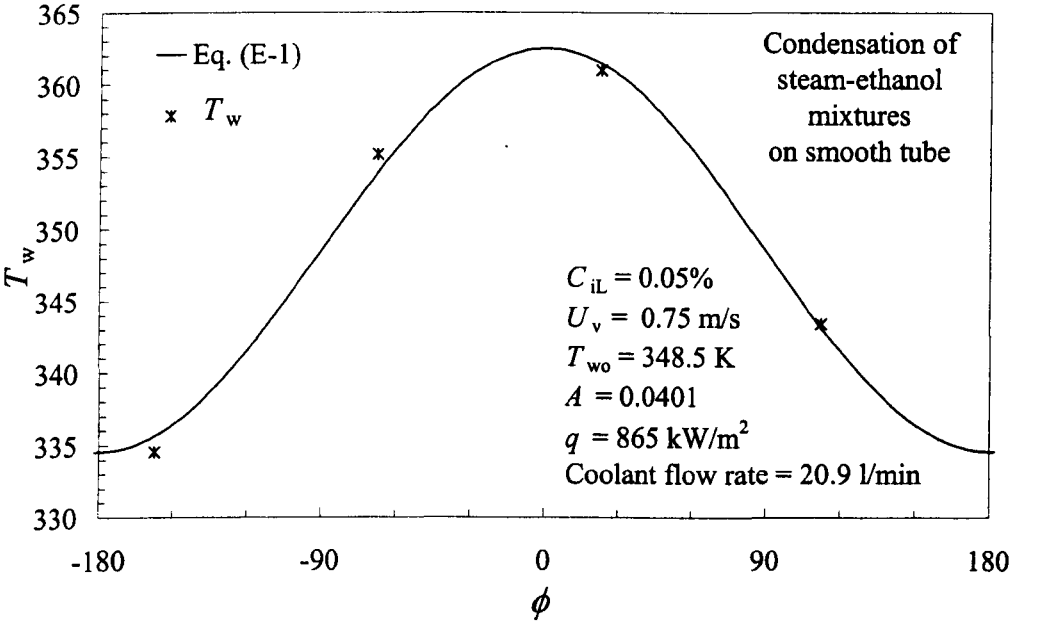

Fig. E.4 Specimens of cosine curve fits using Eq. (E-1) with tube wall surface temperatures during Marangoni condensation of steam-ethanol mixtures on smooth horizontal tube for initial ethanol liquid mass fraction 0.05% mixture.

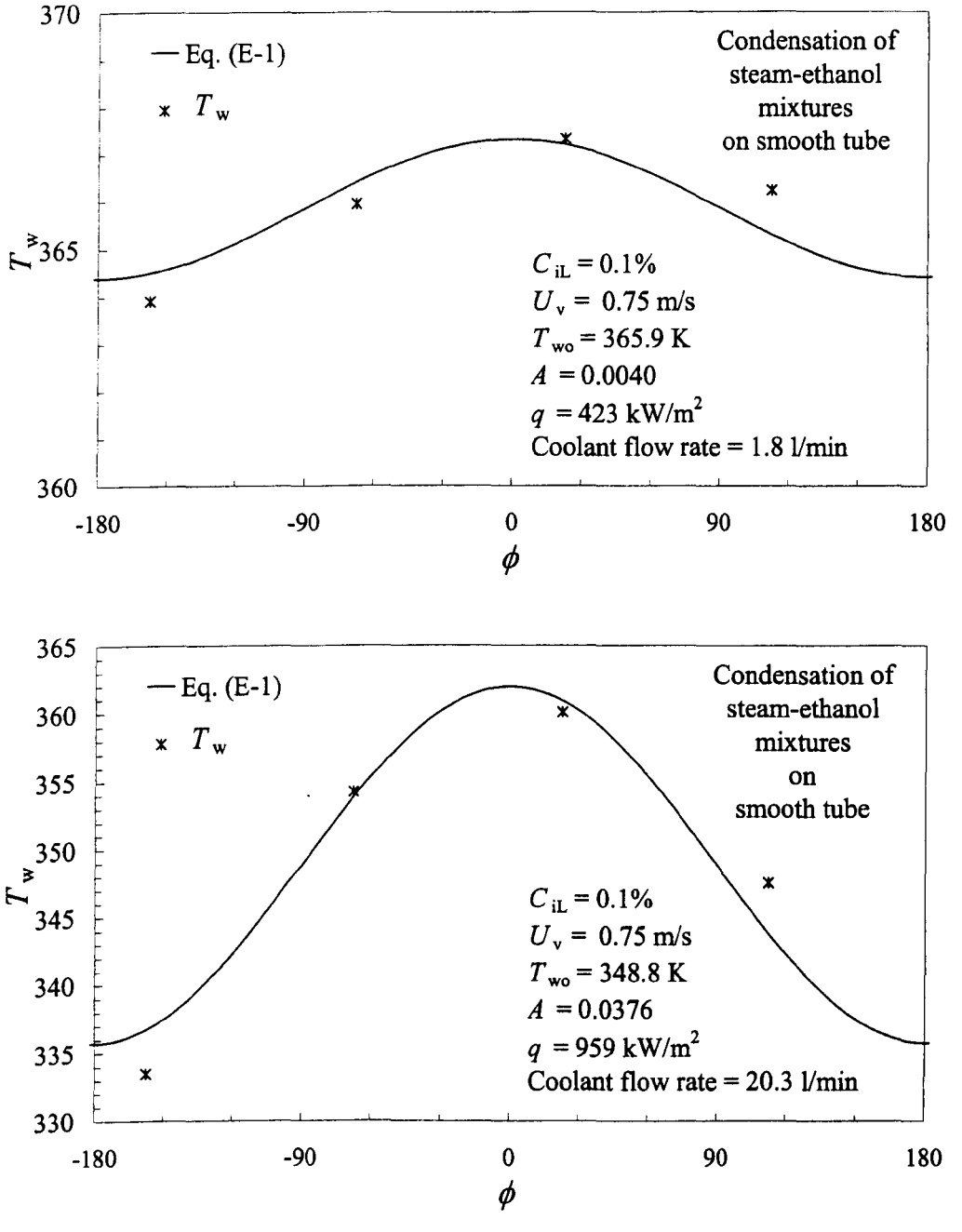

Fig. E.5 Specimens of cosine curve fits using Eq. (E-1) with tube wall surface temperatures during Marangoni condensation of steam-ethanol mixtures on smooth horizontal tube for initial ethanol liquid mass fraction 0.1% mixture.

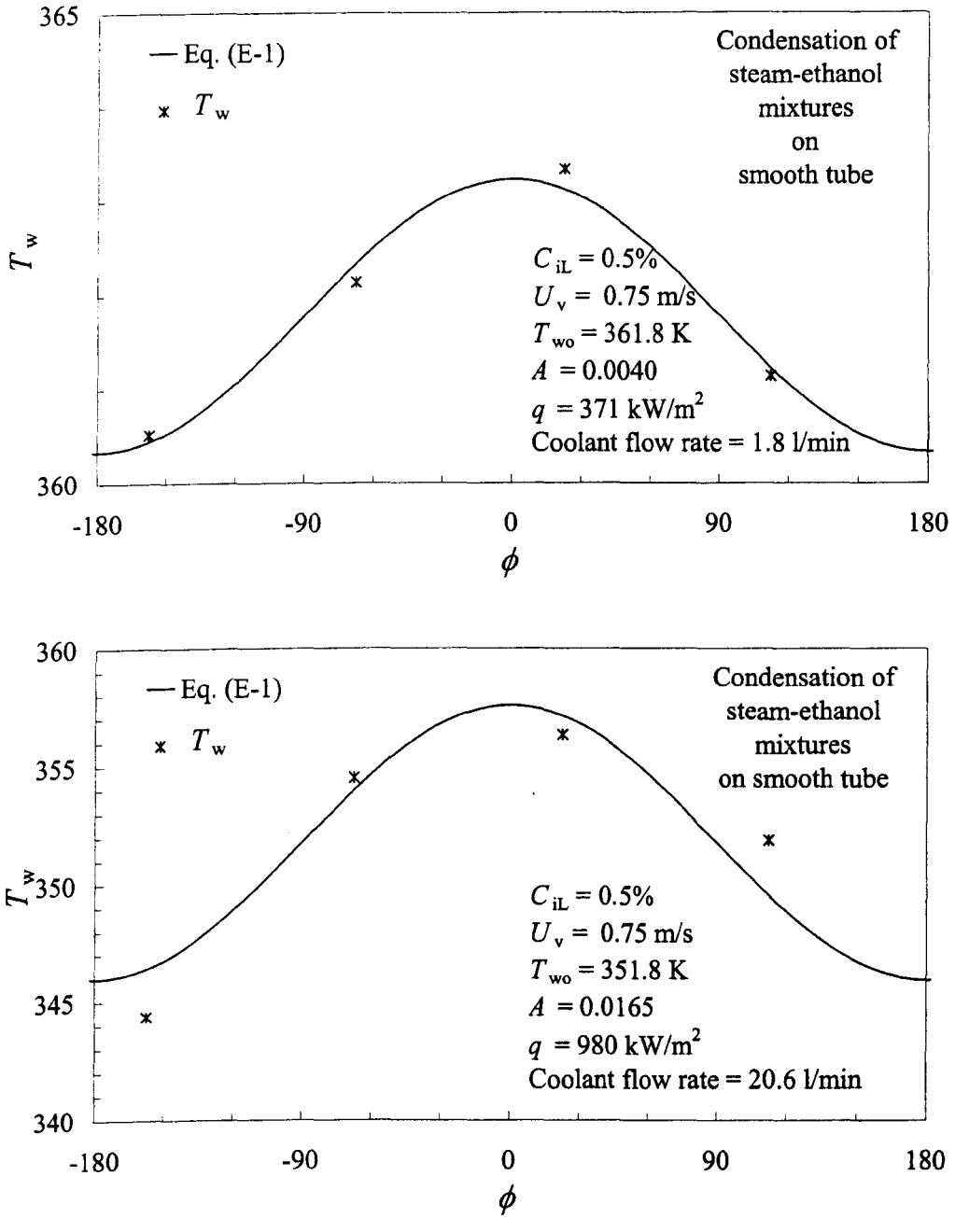

Fig. E.6 Specimens of cosine curve fits using Eq. (E-1) with tube wall surface temperatures during Marangoni condensation of steam-ethanol mixtures on smooth horizontal tube for initial ethanol liquid mass fraction 0.5% mixture.

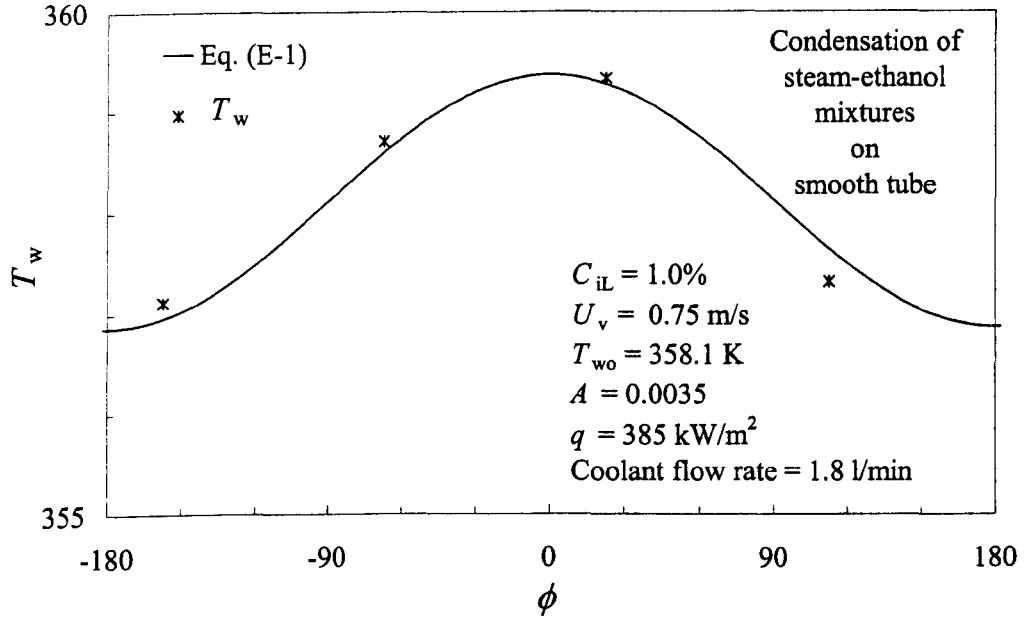

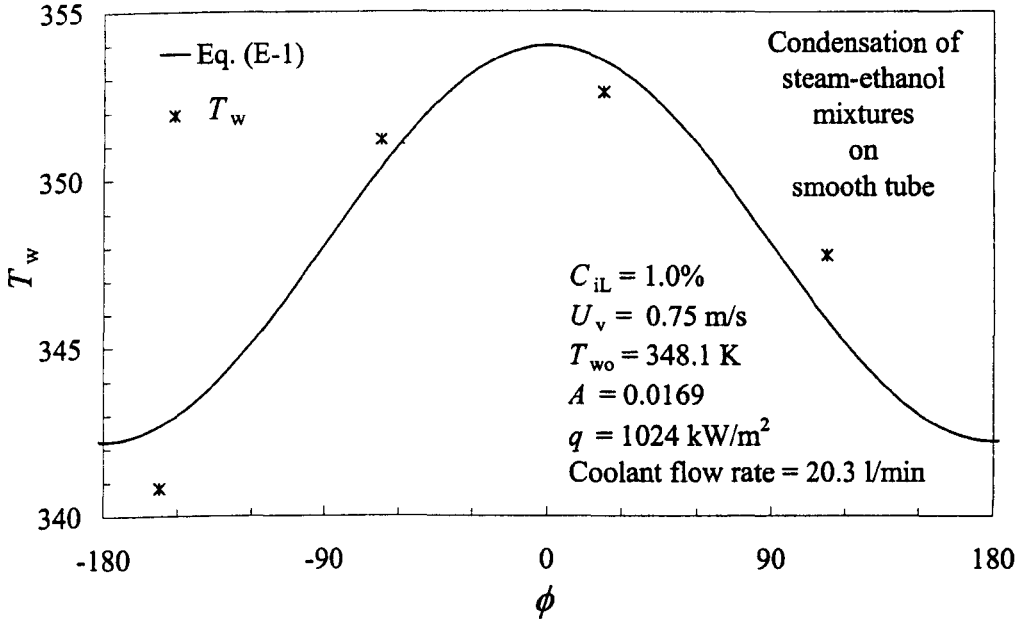

Fig. E.7 Specimens of cosine curve fits using Eq. (E-1) with tube wall surface temperatures during Marangoni condensation of steam-ethanol mixtures on smooth horizontal tube for initial ethanol liquid mass fraction 1.0% mixture.

Appendix F

Phase equilibrium relation for water-ethanol mixtures

Nomenclature

A	constant defined in Eq. (F-7)
B	constant defined in Eq. (F-7)
C	constant defined in Eq. (F-7)
C_L	equilibrium ethanol liquid mass fraction
C_v	equilibrium ethanol vapour mass fraction
$\tilde{g}^E$	molar excess Gibbs energy
$\tilde{M}$	molar mass
P_{mix}	pressure of mixture
P_v	observed vapour pressure in test section
p	partial pressure
$\tilde{R}$	molar ideal-gas constant
T	saturation vapour temperature
T_v	observed vapour temperature in test section
$\tilde{x}$	equilibrium liquid mole fraction
$\tilde{y}$	equilibrium vapour mole fraction
γ	activity coefficient

subscripts

1	ethanol
2	water
mix	mixture

The phase equilibrium relation for water-ethanol mixtures was calculated according to Fujii et al. (1983).

The relation may be given by the molar excess Gibbs energy, $\tilde{g}^E$, with active coefficients (dimensionless), γ, for each component as:

$$\tilde{g}^E = \tilde{R}T\left(\tilde{x}_1 \ln \gamma_1 + \tilde{x}_2 \ln \gamma_2\right) \tag{F-1}$$

$$\gamma_1 = \frac{\tilde{y}_1}{\tilde{x}_1}\frac{P_{\text{mix}}}{p_1} \tag{F-2}$$

$$\gamma_2 = \frac{\tilde{y}_2}{\tilde{x}_2}\frac{P_{\text{mix}}}{p_2} \tag{F-3}$$

where T is the absolute temperature, $\tilde{R}$ is the molar ideal-gas constant, given by:

$$\tilde{R} = 8.3145 \text{ J/mol·K} \tag{F-4}$$

and P_{mix} is the pressure of mixture, p is the partial pressure, $\tilde{x}$ and $\tilde{y}$ are the equilibrium liquid and vapour mole fractions respectively, and the subscripts 1 and 2 denote ethanol and water respectively. In definition,

$$\tilde{x}_1 + \tilde{x}_2 = 1 \tag{F-5}$$

$$\tilde{y}_1 + \tilde{y}_2 = 1 \tag{F-6}$$

The Four-suffix Margules equation gives:

$$\frac{\tilde{g}^E}{(\text{J/mol})} = \tilde{x}_1\tilde{x}_2\left\{A + B\left(\tilde{x}_1 - \tilde{x}_2\right) + C\left(\tilde{x}_1 - \tilde{x}_2\right)^2\right\} \tag{F-7}$$

$$\frac{\tilde{R}T}{(\mathrm{J/mol})}\ln\gamma_1 = (A+3B+5C)\tilde{x}_2^2 - 4(B+4C)\tilde{x}_2^3 + 12\tilde{x}_2^4 \qquad \text{(F-8)}$$

$$\frac{\tilde{R}T}{(\mathrm{J/mol})}\ln\gamma_2 = (A-3B+5C)\tilde{x}_1^2 + 4(B-4C)\tilde{x}_1^3 + 12\tilde{x}_1^4 \qquad \text{(F-9)}$$

where A, B and C are constants. By fitting experimental data in the database of Kogan et al. (1974), Eq. (F-7) was written by:

$$\frac{\tilde{g}^E}{(\mathrm{J/mol})} = \tilde{x}_1\tilde{x}_2\left\{3531.5 - 1197.8(\tilde{x}_1 - \tilde{x}_2) + 449.9(\tilde{x}_1 - \tilde{x}_2)^2\right\} \qquad \text{(F-10)}$$

From Eqs. (F-7) and (F-10), values of constant A, B and C are obtained. The values are then used into Eqs. (F-8) and (F-9), given by:

$$\frac{\tilde{R}T}{(\mathrm{J/mol})}\ln\gamma_1 = 2187.6\tilde{x}_2^2 - 2407.2\tilde{x}_2^3 + 5398.7\tilde{x}_2^4 \qquad \text{(F-11)}$$

$$\frac{\tilde{R}T}{(\mathrm{J/mol})}\ln\gamma_2 = 9374.3\tilde{x}_1^2 - 11989.4\tilde{x}_1^3 + 5398.7\tilde{x}_1^4 \qquad \text{(F-12)}$$

The phase equilibrium diagram can be obtained with Eqs. (F-2), (F-3), (F-11) and (F-12) and the partial pressures, p, for water and ethanol in the vapour given by Eqs. (A.4-7) and (A.5-6) in Appendix A respectively. The resulting values of $\tilde{x}_1$ and $\tilde{y}_1$ was then used in the following equations to obtain the equilibrium ethanol vapour mass fraction, C_v, and the equilibrium ethanol liquid mass fraction, C_L:

$$C_L = \frac{\tilde{M}_1\tilde{x}_1}{(\tilde{M}_1 - \tilde{M}_2)\tilde{x}_1 + \tilde{M}_2} \qquad \text{(F-13)}$$

$$C_v = \frac{\tilde{M}_1\tilde{y}_1}{(\tilde{M}_1 - \tilde{M}_2)\tilde{y}_1 + \tilde{M}_2} \qquad \text{(F-14)}$$

where $\tilde{M}$ is the molar mass and

$\tilde{M}_1 = 46.07$ g/mol $\qquad$ $\tilde{M}_2 = 18.02$ g/mol

For instance, the diagram for 101.325 kPa is shown in Fig. F.1. In the present investigation, the observed test section pressure, P_v, was used into the pressure of the mixture in Eqs. (F-2) and (F-3) and the equilibrium relation was obtained. The equilibrium ethanol vapour and liquid mass fractions, C_L and C_v respectively, were then readily obtained from the diagram with the observed vapour temperature, as shown Fig. F.1

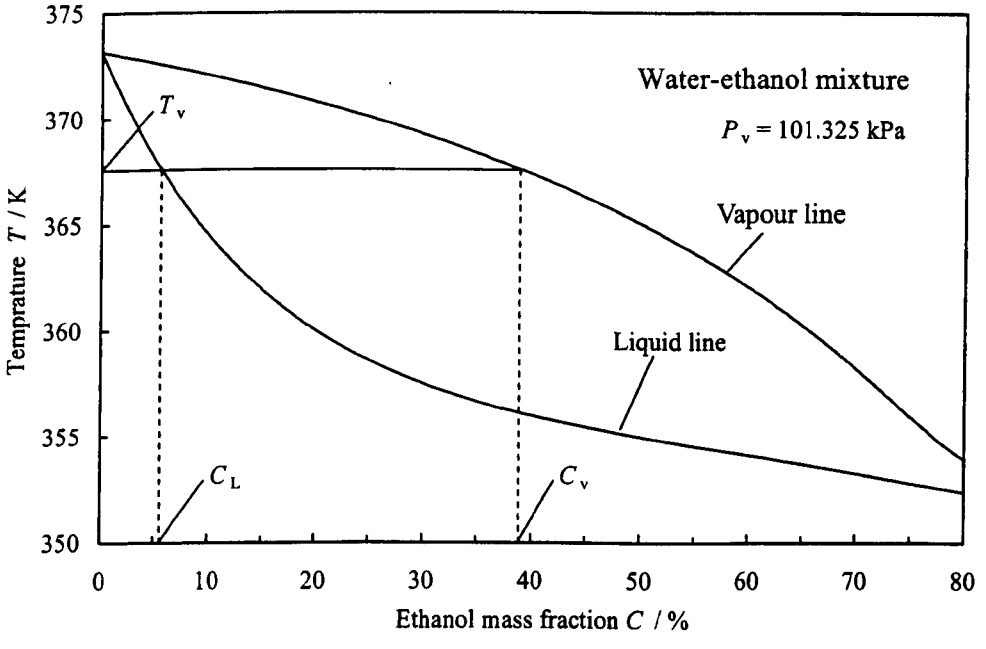

Fig. F.1 Phase equilibrium diagram for water-ethanol binary mixture.

Appendix G

Discussion of errors and uncertainty

Reproducibility

All test runs were repeated, usually on different days, and with coolant flow rate both increasing and decreasing. The results were essentially indistinguishable and have not been shown with different symbols to avoid confusion where different symbols have been used to denote different conditions.

Accuracy

It is not easy to quantify the uncertainty in the enhancement ratio, $\varepsilon_{\Delta T}$. This depends not only on the accuracy of the measured quantities q and ΔT but also uncertainty introduced by forcing the data to fit Eq. (4-22). The standard deviations from the fits are typically less than 1.0% for R-113 and less than 2.0% for steam and ethylene glycol. The error in q is largely determined by that in the temperature rise of the coolant. Using the ten-junction thermopile, coolant mixing arrangements and calibration procedure we estimate the accuracy in coolant temperature rise to be better than 0.01 K. The range of temperature rise measured was 1.00 to 6.98 K for steam, 0.89 to 9.28 K for ethylene glycol and 0.11 to 0.77 K for R-113. The maximum error in q on this basis, and including a maximum coolant flow rate error of 2.0%, would be around 2.5% for steam and ethylene glycol and between 2.5% and 9.0% for R-113, the higher values being at the higher coolant flow rates where the temperature rise is least.

The error estimates in heat flux were calculated as shown below.

The heat flux based on the outside of the test tube was calculated using Eqs. (4-8) and (4-9), may be expressed as:

$$q = \frac{\dot{m}_c C_{pc} \Delta T_c}{\pi d l} \qquad \text{(G-1)}$$

Using the Kline and McClintock (1953) method, the uncertainty of the heat flux is given by:

$$\frac{\delta q}{q}=\left[\left(\frac{1}{\dot{m}_c}\delta\dot{m}_c\right)^2+\left(\frac{1}{\Delta T_c}\delta\Delta T_c\right)^2+\left(-\frac{1}{d}\delta d\right)^2+\left(-\frac{1}{l}\delta l\right)^2\right]^{1/2} \qquad \text{(G-2)}$$

Memory (1989) assumed negligible error in the property equations and went on to show that the uncertainty of C_{pc} due to the uncertainty of measurements for the coolant temperature was negligible. The uncertainty of coolant mass flow rate was estimated of ±2%. For the cooling water temperature rise, the values measured by the ten-junction thermopile were always used, giving the uncertainty of ±0.01 K. The uncertainty of the tube dimensions was estimated the manufacturing tolerances, giving ±0.0001 m for d and ±0.0005 m for l.

The vapour-to-surface temperature difference was calculated from Eq. (4-11),

$$\Delta T = T_v - T_{wo} \qquad \text{(G-3)}$$

where T_{wo} is the arithmetic average of the temperatures measured by the four wall thermocouples fitted in the test tube. Although a correction for the tube wall temperatures to incorporate the depth of the thermocouple in the tube wall was applied, the uncertainty from the correction was small in comparison with the uncertainty of the thermocouple readings. Therefore the uncertainty of the vapour-to-surface temperature difference was expressed as:

$$\frac{\delta\Delta T}{\Delta T}=\left[\left(\frac{1}{\Delta T}\delta T_v\right)^2+\sum_{i=1}^{4}\left(-\frac{1}{4\Delta T}\delta T_{wi}\right)^2\right]^{1/2} \qquad \text{(G-4)}$$

The uncertainty of the thermocouple readings (the vapour temperature) was estimated to be ±0.1 K, of which the corresponding value was ±4 μV. The uncertainty of the tube wall, which had larger fluctuations, was separately estimated to be ±0.5 K.

However, the uncertainty in the vapour-to-surface temperature difference is not primarily due to the accuracy of vapour and wall temperature measurements (each measurement judged to have accuracy better than 0.1 K) but rather to the variation in temperature around the tube perimeter. The temperatures were highest near the top of the tube and lowest near the bottom as discussed in Appendix E. The surface temperature used to calculate the vapour-to-surface temperature difference was arithmetic mean of the four measurements. The largest difference between the highest and lowest of these was around 30 K, 23 K and 6 K for steam, ethylene glycol and R-113 respectively.

End effects

The ends of the condenser tube were internally insulated with PTFE bushes at inlet and exit (see Fig. 4.2) so that the internally-cooled part of the tube was the same as that exposed to vapour. The ends of the tube outside the test chamber passed directly into the PTFE mixing boxes so that no part of the tube was in contact with metal of the chamber. The tube was thus extremely well insulated from all except the condensing side. Under these conditions end effects are negligible (see Memory (1989)) and the surface temperature at the centre position of the tube is representative of the whole tube surface.

Appendix H

Tables of results

H.1 Condensation on wire-wrapped tubes with R-113

Test fluid – R-113
d_w = 0.2 mm, p = 0.5 mm
$\varepsilon_{\Delta T}$ = 3.210, B = 2.433, U_v = 0.236 m/s

T_v / K	T_{wo} / K	T_{w1} / K	T_{w2} / K	T_{w3} / K	T_{w4} / K	q / (kW/m^2)	α / (kW/m^{2}K)	A
320.50	300.16	300.77	300.08	299.70	300.10	83.57	4.11	0.0017
320.50	301.08	301.73	300.97	300.56	301.04	82.37	4.24	0.0018
320.50	302.52	303.13	302.41	302.04	302.49	79.44	4.42	0.0017
320.50	304.67	305.27	304.51	304.14	304.75	72.28	4.56	0.0019
320.50	303.79	304.44	303.65	303.26	303.82	74.48	4.46	0.0019
320.50	301.99	302.61	301.87	301.49	301.97	79.95	4.32	0.0018
320.50	300.89	301.42	300.80	300.48	300.87	83.82	4.27	0.0015
320.50	299.89	300.41	299.82	299.50	299.84	86.24	4.18	0.0014
320.50	299.37	299.90	299.30	298.98	299.30	87.75	4.15	0.0014
320.50	299.08	299.51	299.04	298.77	298.99	90.36	4.22	0.0011

Thermocouple angles : T_{w1} = 22.5°, T_{w2} = 112.5°, T_{w3} = -157.5°, T_{w4} = -67.5°

d_w = 0.2 mm, p = 0.75 mm
$\varepsilon_{\Delta T}$ = 3.042, B = 2.306, U_v = 0.236 m/s

321.11	300.80	301.65	300.74	299.84	300.98	80.88	3.98	0.0029
321.11	301.44	302.24	301.39	300.53	301.59	78.45	3.99	0.0027
321.11	302.25	303.12	302.33	301.26	302.28	76.64	4.06	0.0028
321.11	303.47	304.53	303.64	302.21	303.50	72.82	4.13	0.0034
321.11	305.40	306.19	305.55	304.29	305.57	68.10	4.33	0.0029
321.11	304.65	305.65	304.64	303.43	304.88	68.57	4.16	0.0035
321.11	303.05	304.02	303.28	301.84	303.05	73.42	4.06	0.0032
321.11	302.13	303.00	302.23	301.14	302.13	77.59	4.09	0.0028
321.11	301.30	302.15	301.23	300.44	301.38	80.41	4.06	0.0027
321.11	300.83	301.66	300.74	300.03	300.89	82.76	4.08	0.0026

Thermocouple angles : T_{w1} = 22.5°, T_{w2} = 112.5°, T_{w3} = -157.5°, T_{w4} = -67.5°

d_w = 0.2 mm, p = 1.0 mm
$\varepsilon_{\Delta T}$ = 2.227, B = 1.688, U_v = 0.236 m/s

320.63	298.08	298.58	297.98	297.68	298.08	65.51	2.91	0.0015
320.63	298.57	299.02	298.45	298.18	298.63	64.71	2.93	0.0014
320.63	299.06	299.83	298.94	298.46	299.01	61.63	2.86	0.0022
320.63	299.79	300.56	299.66	299.19	299.74	57.90	2.78	0.0021
320.63	301.04	301.80	300.88	300.42	301.05	58.01	2.96	0.0022
320.63	303.01	303.79	302.77	302.31	303.17	55.61	3.16	0.0025
320.63	302.19	302.90	302.09	301.65	302.11	56.89	3.09	0.0019
320.63	300.58	301.28	300.44	300.01	300.59	59.48	2.97	0.0020
320.63	299.76	300.49	299.62	299.17	299.74	59.55	2.85	0.0021
320.63	298.87	299.48	298.68	298.32	298.98	61.17	2.81	0.0020
320.63	298.43	298.92	298.32	298.03	298.47	62.77	2.83	0.0015

Thermocouple angles : T_{w1} = 22.5°, T_{w2} = 112.5°, T_{w3} = -157.5°, T_{w4} = -67.5°

Test fluid – R-113

d_w = 0.2 mm, p = 1.5 mm

$\varepsilon_{\Delta T}$ = 2.172, B = 1.646, U_v = 0.233 m/s

T_v / K	T_{wo} / K	T_{w1} / K	T_{w2} / K	T_{w3} / K	T_{w4} / K	q / (kW/m^2)	α / (kW/m^{2}K)	A
320.92	297.55	298.06	297.46	297.15	297.53	64.92	2.78	0.0015
320.94	297.73	298.25	297.66	297.34	297.68	64.48	2.78	0.0014
320.94	298.10	298.72	298.02	297.64	298.02	62.98	2.76	0.0017
320.94	298.58	299.18	298.49	298.12	298.54	61.61	2.76	0.0017
320.92	299.26	299.92	299.15	298.75	299.23	60.66	2.80	0.0019
320.92	300.41	301.13	300.29	299.85	300.36	59.20	2.89	0.0020
320.94	302.33	303.09	302.13	301.67	302.43	55.34	2.97	0.0024
320.94	301.50	302.31	301.32	300.83	301.56	55.97	2.88	0.0024
320.94	300.03	300.73	299.87	299.44	300.09	59.01	2.82	0.0021
320.94	299.17	299.82	299.03	298.63	299.18	60.75	2.79	0.0019
320.94	298.40	299.01	298.29	297.92	298.39	61.96	2.75	0.0018
320.94	298.01	298.62	297.93	297.55	297.95	63.73	2.78	0.0017
320.94	297.84	298.37	297.78	297.45	297.78	63.41	2.75	0.0014

Thermocouple angles : T_{w1} = 22.5°, T_{w2} = 112.5°, T_{w3} = -157.5°, T_{w4} = -67.5°

d_w = 0.2 mm, p = 2.5 mm

$\varepsilon_{\Delta T}$ = 2.000, B = 1.516, U_v = 0.233 m/s

321.06	296.81	297.26	296.74	296.46	296.77	60.50	2.49	0.0013
321.06	297.09	297.49	296.97	296.72	297.16	60.46	2.52	0.0013
321.06	297.43	297.90	297.33	297.05	297.46	58.71	2.48	0.0014
321.06	297.89	298.40	297.80	297.49	297.85	58.80	2.54	0.0014
321.06	298.53	299.11	298.42	298.06	298.54	56.80	2.52	0.0017
321.06	299.63	300.25	299.51	299.13	299.63	56.40	2.63	0.0018
321.06	301.44	302.07	301.30	300.92	301.48	53.09	2.71	0.0019
321.06	300.67	301.28	300.54	300.17	300.71	53.56	2.63	0.0018
321.06	299.26	299.88	299.13	298.76	299.28	56.30	2.58	0.0018
321.06	298.47	299.02	298.35	298.01	298.50	57.74	2.56	0.0016
321.06	297.78	298.28	297.68	297.38	297.78	59.56	2.56	0.0015
321.06	297.44	297.88	297.36	297.09	297.41	59.91	2.54	0.0013
321.06	297.25	297.69	297.16	296.90	297.26	60.41	2.54	0.0013

Thermocouple angles : T_{w1} = 22.5°, T_{w2} = 112.5°, T_{w3} = -157.5°, T_{w4} = -67.5°

d_w = 0.2 mm, p = 3.5 mm

$\varepsilon_{\Delta T}$ = 1.759, B = 1.333, U_v = 0.233 m/s

320.97	297.82	298.12	297.83	297.56	297.75	52.61	2.27	0.0009
320.97	298.00	298.30	298.00	297.77	297.95	52.19	2.27	0.0008
320.97	298.29	298.61	298.31	298.02	298.21	50.88	2.24	0.0010
320.97	298.69	299.00	298.68	298.44	298.63	49.52	2.22	0.0009
320.97	299.25	299.62	299.25	298.95	299.17	48.77	2.25	0.0011
320.97	300.15	300.53	300.16	299.83	300.06	47.83	2.30	0.0012
320.97	301.69	302.13	301.64	301.37	301.64	45.44	2.36	0.0012
320.94	301.08	301.49	301.02	300.77	301.02	46.21	2.33	0.0011
320.94	299.87	300.26	299.84	299.58	299.81	47.58	2.26	0.0011
320.94	299.14	299.52	299.12	298.84	299.07	48.57	2.23	0.0011
320.94	298.58	298.91	298.59	298.31	298.51	50.58	2.26	0.0010
320.94	298.26	298.59	298.27	297.99	298.19	51.18	2.26	0.0010
320.94	298.11	298.44	298.12	297.85	298.05	52.07	2.28	0.0010

Thermocouple angles : T_{w1} = 22.5°, T_{w2} = -67.5°, T_{w3} = -157.5°, T_{w4} = 112.5°

Test fluid – R-113
d_w = 0.2 mm, p = 4.5 mm
$\varepsilon_{\Delta T}$ = 1.670, B = 1.266, U_v = 0.235 m/s

T_v / K	T_{wo} / K	T_{w1} / K	T_{w2} / K	T_{w3} / K	T_{w4} / K	q / (kW/m^2)	α / (kW/m^{2}K)	A
320.80	297.34	297.54	297.32	297.20	297.32	50.41	2.15	0.0005
320.80	297.51	297.74	297.49	297.35	297.47	50.28	2.16	0.0006
320.80	297.79	298.06	297.76	297.59	297.73	49.19	2.14	0.0007
320.80	298.17	298.43	298.13	297.97	298.15	48.13	2.13	0.0007
320.77	298.69	298.97	298.64	298.47	298.67	46.73	2.12	0.0008
320.80	299.53	299.86	299.49	299.29	299.51	46.23	2.17	0.0009
320.80	300.97	301.31	300.91	300.71	300.96	43.43	2.19	0.0010
320.77	300.38	300.72	300.32	300.11	300.37	44.11	2.16	0.0010
320.77	299.23	299.56	299.16	298.96	299.24	46.24	2.15	0.0010
320.77	298.58	298.87	298.52	298.34	298.57	47.37	2.13	0.0008
320.77	298.01	298.23	297.98	297.84	297.98	48.18	2.12	0.0006
320.77	297.74	297.96	297.71	297.57	297.71	49.28	2.14	0.0006
320.77	297.60	297.84	297.59	297.44	297.54	49.96	2.16	0.0006

Thermocouple angles : T_{w1} = 22.5°, T_{w2} = 112.5°, T_{w3} = -157.5°, T_{w4} = -67.5°

d_w = 0.2 mm, p = 6.0 mm
$\varepsilon_{\Delta T}$ = 1.534, B = 1.163, U_v = 0.237 m/s

320.65	296.57	296.83	296.59	296.35	296.51	48.22	2.00	0.0008
320.65	296.71	297.00	296.71	296.48	296.66	47.28	1.98	0.0009
320.65	296.99	297.30	297.00	296.74	296.92	45.78	1.93	0.0009
320.65	297.33	297.64	297.34	297.08	297.27	45.33	1.94	0.0009
320.65	297.82	298.16	297.81	297.55	297.76	43.98	1.93	0.0010
320.65	298.60	298.97	298.60	298.30	298.53	43.03	1.95	0.0011
320.65	299.99	300.48	299.98	299.61	299.91	40.93	1.98	0.0014
320.65	299.42	299.84	299.41	299.08	299.34	41.41	1.95	0.0012
320.65	298.37	298.73	298.38	298.09	298.30	43.08	1.93	0.0010
320.65	297.77	298.09	297.76	297.52	297.71	44.37	1.94	0.0009
320.65	297.26	297.57	297.27	297.01	297.20	45.78	1.96	0.0009
320.65	296.99	297.32	296.98	296.72	296.93	46.43	1.96	0.0010
320.65	296.86	297.13	296.88	296.64	296.80	46.80	1.97	0.0008

Thermocouple angles : T_{w1} = 22.5°, T_{w2} = -67.5°, T_{w3} = -157.5°, T_{w4} = 112.5°

d_w = 0.35 mm, p = 0.8 mm
$\varepsilon_{\Delta T}$ = 3.678, B = 2.788, U_v = 0.235 m/s

321.04	301.83	302.48	301.74	301.34	301.76	94.06	4.90	0.0018
321.04	302.70	303.38	302.57	302.15	302.71	91.14	4.97	0.0020
321.04	304.07	304.74	303.90	303.49	304.13	86.20	5.08	0.0020
321.04	306.22	306.90	306.04	305.63	306.31	78.24	5.28	0.0021
321.04	305.33	305.95	305.18	304.81	305.38	80.13	5.10	0.0018
321.04	303.60	304.26	303.44	303.04	303.64	88.02	5.05	0.0020
321.06	302.51	303.14	302.40	302.01	302.50	92.19	4.97	0.0018
321.04	301.62	302.33	301.49	301.05	301.59	94.33	4.86	0.0020

Thermocouple angles : T_{w1} = 22.5°, T_{w2} = 112.5°, T_{w3} = -157.5°, T_{w4} = -67.5°

Test fluid – R-113

d_w = 0.35 mm, p = 1.0 mm

$\varepsilon_{\Delta T}$ = 3.012, B = 2.283, U_v = 0.235 m/s

T_v / K	T_{wo} / K	T_{w1} / K	T_{w2} / K	T_{w3} / K	T_{w4} / K	q / (kW/m^2)	α / (kW/m^{2}K)	A
320.99	299.96	300.97	300.36	298.15	300.36	84.32	4.01	0.0044
320.99	300.34	301.51	300.86	298.18	300.81	81.76	3.96	0.0051
320.99	300.86	302.14	301.40	298.40	301.50	79.18	3.93	0.0058
320.99	301.53	302.83	302.16	298.74	302.38	77.78	4.00	0.0064
320.99	302.56	304.19	303.47	299.04	303.55	73.65	4.00	0.0079
320.99	304.25	306.21	305.60	299.66	305.55	68.12	4.07	0.0099
320.99	303.62	305.48	304.77	299.50	304.72	70.10	4.03	0.0091
320.99	302.29	303.80	303.13	299.07	303.16	74.81	4.00	0.0072
320.99	301.40	302.70	302.04	298.74	302.14	78.22	3.99	0.0061
320.99	300.66	301.78	301.11	298.50	301.23	81.24	4.00	0.0051
320.99	300.36	301.42	300.87	298.39	300.77	83.16	4.03	0.0046
320.99	300.13	301.14	300.52	298.31	300.55	82.55	3.96	0.0044

Thermocouple angles : T_{w1} = 22.5°, T_{w2} = 112.5°, T_{w3} = -157.5°, T_{w4} = -67.5°

d_w = 0.35 mm, p = 1.2 mm

$\varepsilon_{\Delta T}$ = 3.110, B = 2.357, U_v = 0.236 m/s

320.70	298.95	298.98	298.93	298.93	298.95	87.12	4.01	0.0001
320.70	299.23	299.25	299.22	299.21	299.22	86.69	4.04	0.0001
320.70	299.70	299.78	299.71	299.64	299.69	84.42	4.02	0.0002
320.67	300.32	300.40	300.37	300.23	300.27	82.80	4.07	0.0003
320.67	301.17	301.28	301.25	301.04	301.10	80.09	4.11	0.0005
320.67	302.56	302.70	302.65	302.40	302.48	78.17	4.32	0.0006
320.67	303.80	303.99	303.92	303.58	303.70	73.51	4.36	0.0008
320.67	302.04	302.18	302.13	301.88	301.96	78.07	4.19	0.0006
320.67	300.97	301.11	301.03	300.83	300.91	80.73	4.10	0.0005
320.67	300.07	300.18	300.10	299.97	300.03	83.75	4.06	0.0004
320.67	299.59	299.64	299.59	299.56	299.59	84.80	4.02	0.0001
320.67	299.36	299.37	299.37	299.34	299.35	86.04	4.04	0.0001

Thermocouple angles : T_{w1} = 22.5°, T_{w2} = -67.5°, T_{w3} = -157.5°, T_{w4} = 112.5°

d_w = 0.35 mm, p = 1.5 mm

$\varepsilon_{\Delta T}$ = 2.768, B = 2.098, U_v = 0.227 m/s

320.75	298.31	299.06	298.12	297.66	298.39	78.69	3.51	0.0023
320.75	299.14	299.92	298.91	298.43	299.28	76.88	3.56	0.0025
320.75	300.44	301.28	300.18	299.68	300.61	74.25	3.66	0.0027
320.75	302.61	303.51	302.34	301.80	302.76	69.82	3.85	0.0029
320.77	301.74	302.60	301.48	300.97	301.90	70.91	3.73	0.0028
320.75	299.99	300.79	299.74	299.27	300.17	75.47	3.64	0.0026
320.77	298.92	299.73	298.71	298.22	299.01	77.82	3.56	0.0025
320.77	298.01	298.75	297.80	297.36	298.12	79.85	3.51	0.0024
320.77	297.55	298.28	297.38	296.95	297.61	81.11	3.49	0.0022
320.77	297.21	297.89	297.07	296.66	297.24	82.79	3.51	0.0020

Thermocouple angles : T_{w1} = 22.5°, T_{w2} = 112.5°, T_{w3} = -157.5°, T_{w4} = -67.5°

Test fluid - R-113

d_w = 0.35 mm, p = 2.5 mm

$\varepsilon_{\Delta T}$ = 2.460, B = 1.865, U_v = 0.239 m/s

T_v / K	T_{wo} / K	T_{w1} / K	T_{w2} / K	T_{w3} / K	T_{w4} / K	q / (kW/m^2)	α / (kW/m^{2}K)	A
320.70	299.42	299.93	299.31	298.77	299.69	68.12	3.20	0.0020
320.70	299.67	300.18	299.58	299.01	299.93	67.22	3.20	0.0020
320.67	300.10	300.67	300.02	299.38	300.35	66.29	3.22	0.0022
320.70	300.62	301.18	300.56	299.84	300.88	64.32	3.20	0.0023
320.70	301.36	301.92	301.32	300.55	301.64	62.77	3.25	0.0023
320.70	302.47	303.13	302.44	301.57	302.76	62.72	3.44	0.0026
320.70	304.25	304.93	304.33	303.17	304.56	56.24	3.42	0.0028
320.70	303.59	304.27	303.60	302.61	303.87	57.97	3.39	0.0027
320.70	302.11	302.75	302.11	301.26	302.30	61.16	3.29	0.0024
320.72	301.24	301.77	301.20	300.48	301.50	63.05	3.24	0.0022
320.72	300.48	300.96	300.42	299.80	300.74	65.07	3.21	0.0020
320.72	300.09	300.55	300.00	299.50	300.30	66.47	3.22	0.0018
320.72	299.89	300.33	299.78	299.34	300.11	67.91	3.26	0.0017

Thermocouple angles : T_{w1} = 22.5°, T_{w2} = 112.5°, T_{w3} = -157.5°, T_{w4} = -67.5°

d_w = 0.35 mm, p = 3.5 mm

$\varepsilon_{\Delta T}$ = 2.026, B = 1.536, U_v = 0.230 m/s

320.67	297.01	297.42	297.04	296.67	296.92	61.06	2.58	0.0012
320.67	297.40	297.74	297.44	297.11	297.31	60.32	2.59	0.0011
320.67	297.77	298.15	297.80	297.45	297.68	58.70	2.56	0.0012
320.67	298.26	298.64	298.29	297.94	298.17	57.38	2.56	0.0012
320.67	298.95	299.33	298.98	298.63	298.86	56.23	2.59	0.0012
320.67	299.99	300.42	300.05	299.61	299.87	55.18	2.67	0.0013
320.67	301.74	302.14	301.74	301.43	301.67	52.07	2.75	0.0011
320.67	301.01	301.40	301.03	300.70	300.93	53.25	2.71	0.0011
320.67	299.55	300.00	299.65	299.13	299.40	55.39	2.62	0.0015
320.67	298.78	299.14	298.82	298.47	298.69	57.13	2.61	0.0011
320.67	298.10	298.45	298.15	297.79	298.00	58.74	2.60	0.0011
320.67	297.72	298.00	297.83	297.44	297.61	58.93	2.57	0.0010
320.67	297.44	297.74	297.51	297.16	297.34	60.46	2.60	0.0010

Thermocouple angles : T_{w1} = 22.5°, T_{w2} = -67.5°, T_{w3} = -157.5°, T_{w4} = 112.5°

d_w = 0.35 mm, p = 4.5 mm

$\varepsilon_{\Delta T}$ = 1.799, B = 1.364, U_v = 0.234 m/s

321.11	297.46	297.79	297.41	297.22	297.44	55.37	2.34	0.0009
321.14	297.77	298.10	297.70	297.50	297.78	53.52	2.29	0.0010
321.14	298.21	298.57	298.07	297.86	298.32	52.41	2.29	0.0013
321.14	298.85	299.25	298.68	298.44	299.01	50.09	2.25	0.0015
321.14	299.78	300.18	299.73	299.49	299.73	50.95	2.39	0.0011
321.14	301.38	301.87	301.23	300.94	301.50	47.25	2.39	0.0016
321.14	300.67	301.13	300.51	300.24	300.80	47.17	2.30	0.0016
321.14	299.42	299.80	299.28	299.05	299.55	49.45	2.28	0.0013
321.14	298.74	299.21	298.59	298.31	298.86	50.43	2.25	0.0016
321.14	298.07	298.42	297.93	297.72	298.23	53.06	2.30	0.0013
321.14	297.77	298.04	297.71	297.55	297.79	55.07	2.36	0.0008

Thermocouple angles : T_{w1} = 22.5°, T_{w2} = 112.5°, T_{w3} = -157.5°, T_{w4} = -67.5°

Test fluid – R-113

d_w = 0.35 mm, p = 6.0 mm

$\varepsilon_{\Delta T}$ = 1.701, B = 1.289, U_v = 0.229 m/s

T_v / K	T_{wo} / K	T_{w1} / K	T_{w2} / K	T_{w3} / K	T_{w4} / K	q / (kW/m^2)	α / (kW/m^{2}K)	A
320.80	296.18	296.53	296.21	295.87	296.09	53.43	2.17	0.0011
320.77	296.47	296.85	296.50	296.15	296.38	51.87	2.13	0.0012
320.77	296.88	297.27	296.90	296.56	296.80	51.06	2.14	0.0012
320.77	297.47	297.89	297.47	297.14	297.39	50.16	2.15	0.0012
320.77	298.38	298.80	298.35	298.04	298.30	48.75	2.18	0.0012
320.92	300.01	300.45	299.96	299.69	299.96	46.56	2.23	0.0012
320.94	299.28	299.74	299.24	298.93	299.21	46.62	2.15	0.0013
320.94	298.07	298.50	298.03	297.74	298.01	49.06	2.15	0.0012
320.94	297.36	297.74	297.34	297.06	297.29	50.51	2.14	0.0011
320.94	296.74	297.15	296.75	296.40	296.65	51.52	2.13	0.0012
320.94	296.44	296.80	296.43	296.16	296.38	52.26	2.13	0.0010
320.94	296.23	296.59	296.26	295.92	296.14	53.85	2.18	0.0011

Thermocouple angles : T_{w1} = 22.5°, T_{w2} = -67.5°, T_{w3} = -157.5°, T_{w4} = 112.5°

d_w = 0.4 mm, p = 0.7 mm

$\varepsilon_{\Delta T}$ = 3.104, B = 2.353, U_v = 0.239 m/s

320.41	300.98	301.50	300.90	300.59	300.95	79.31	4.08	0.0014
320.41	302.30	302.80	302.21	301.90	302.28	77.28	4.27	0.0014
320.41	304.24	304.77	304.13	303.81	304.26	71.64	4.43	0.0015
320.41	303.49	304.02	303.40	303.08	303.47	73.03	4.32	0.0015
320.41	301.79	302.33	301.71	301.38	301.76	76.91	4.13	0.0015
320.41	300.74	301.22	300.68	300.38	300.68	79.30	4.03	0.0013

Thermocouple angles : T_{w1} = 22.5°, T_{w2} = 112.5°, T_{w3} = -157.5°, T_{w4} = -67.5°

d_w = 0.4 mm, p = 1.0 mm

$\varepsilon_{\Delta T}$ = 2.607, B = 1.976, U_v = 0.231 m/s

320.26	297.39	297.73	297.43	297.10	297.31	75.11	3.28	0.0011
320.26	298.45	298.84	298.47	298.13	298.37	73.36	3.36	0.0012
320.26	299.84	300.20	299.70	299.63	299.85	71.85	3.52	0.0008
320.26	299.06	299.36	298.94	298.87	299.06	72.99	3.44	0.0007
320.26	297.89	298.25	297.93	297.59	297.80	74.65	3.34	0.0011
320.26	298.60	298.94	298.62	298.31	298.52	73.35	3.39	0.0010
320.26	297.40	297.75	297.46	297.10	297.31	75.11	3.29	0.0011
320.16	297.65	298.19	297.75	297.17	297.50	73.57	3.27	0.0017
320.16	300.25	300.81	300.09	299.86	300.22	70.79	3.55	0.0014
320.14	298.14	298.71	298.22	297.65	297.99	72.70	3.31	0.0018

Thermocouple angles : T_{w1} = 22.5°, T_{w2} = -67.5°, T_{w3} = -157.5°, T_{w4} = 112.5°

d_w = 0.4 mm, p = 1.5 mm

$\varepsilon_{\Delta T}$ = 2.615, B = 1.982, U_v = 0.235 m/s

320.99	300.15	300.93	299.92	299.45	300.31	69.88	3.35	0.0025
320.99	301.27	302.06	301.00	300.53	301.49	68.13	3.46	0.0027
320.97	302.49	303.27	302.21	301.74	302.73	66.89	3.62	0.0027
321.01	302.51	303.32	302.23	301.75	302.73	66.53	3.59	0.0027
321.01	301.41	302.16	301.15	300.70	301.62	68.12	3.47	0.0025
321.01	300.31	301.08	300.09	299.62	300.43	69.25	3.34	0.0025

Thermocouple angles : T_{w1} = 22.5°, T_{w2} = 112.5°, T_{w3} = -157.5°, T_{w4} = -67.5°

Test fluid – R-113

d_w = 0.4 mm, p = 2.0 mm

$\varepsilon_{\Delta T}$ = 2.561, B = 1.941, U_v = 0.231 m/s

T_v / K	T_{wo} / K	T_{w1} / K	T_{w2} / K	T_{w3} / K	T_{w4} / K	q / (kW/m^2)	α / (kW/m^{2}K)	A
321.11	298.30	298.82	298.22	297.90	298.27	73.33	3.21	0.0014
321.09	298.95	299.43	298.88	298.59	298.88	72.26	3.26	0.0013
321.09	299.87	300.36	299.79	299.49	299.82	70.16	3.31	0.0014
321.09	301.27	301.77	301.22	300.91	301.17	68.14	3.44	0.0013
321.09	303.26	303.73	303.14	302.85	303.31	64.47	3.62	0.0014
321.09	301.84	302.38	301.71	301.38	301.88	66.56	3.46	0.0016
321.09	300.36	300.86	300.29	299.98	300.31	69.76	3.37	0.0014
321.09	299.65	300.09	299.60	299.32	299.57	70.49	3.29	0.0012
321.06	298.67	299.16	298.61	298.31	298.59	72.52	3.24	0.0013

Thermocouple angles : T_{w1} = 22.5°, T_{w2} = 112.5°, T_{w3} = -157.5°, T_{w4} = -67.5°

d_w = 0.4 mm, p = 2.5 mm

$\varepsilon_{\Delta T}$ = 2.472, B = 1.874, U_v = 0.237 m/s

321.01	300.11	300.55	300.03	299.61	300.26	67.99	3.25	0.0016
321.01	300.61	300.99	300.62	300.12	300.72	66.42	3.26	0.0014
320.99	301.31	301.70	301.45	300.76	301.33	64.42	3.27	0.0014
320.99	302.32	302.95	302.36	301.61	302.38	61.50	3.29	0.0021
321.01	303.98	304.53	304.16	303.23	303.99	56.98	3.34	0.0019
321.01	303.25	303.75	303.43	302.56	303.28	57.96	3.26	0.0017
320.99	302.03	302.55	302.18	301.32	302.06	61.60	3.25	0.0018
320.99	301.21	301.60	301.36	300.71	301.18	64.85	3.28	0.0013
320.99	300.53	300.90	300.48	300.10	300.65	67.47	3.30	0.0013
320.99	300.14	300.48	300.09	299.72	300.29	69.33	3.33	0.0013

Thermocouple angles : T_{w1} = 22.5°, T_{w2} = 112.5°, T_{w3} = -157.5°, T_{w4} = -67.5°

d_w = 0.4 mm, p = 3.5 mm

$\varepsilon_{\Delta T}$ = 2.220, B = 1.683, U_v = 0.238 m/s

320.33	296.77	297.09	296.74	296.54	296.72	65.79	2.79	0.0008
320.33	297.13	297.46	297.09	296.88	297.09	65.55	2.82	0.0009
320.33	297.54	297.90	297.48	297.26	297.53	63.88	2.80	0.0010
320.33	298.08	298.49	298.02	297.77	298.05	63.07	2.83	0.0011
320.33	298.89	299.31	298.84	298.58	298.84	61.82	2.88	0.0011
320.33	300.13	300.54	300.07	299.82	300.12	59.25	2.93	0.0011
320.33	301.98	302.36	301.86	301.64	302.06	56.39	3.07	0.0012
320.31	301.24	301.59	301.22	301.00	301.17	56.31	2.95	0.0009
320.31	299.67	300.02	299.62	299.41	299.65	59.51	2.88	0.0010
320.31	298.72	299.11	298.67	298.42	298.67	62.62	2.90	0.0011
320.31	297.85	298.25	297.78	297.53	297.83	63.62	2.83	0.0011
320.31	297.42	297.78	297.36	297.14	297.41	64.72	2.83	0.0010
320.31	297.11	297.44	297.07	296.86	297.07	66.05	2.85	0.0009

Thermocouple angles : T_{w1} = 22.5°, T_{w2} = 112.5°, T_{w3} = -157.5°, T_{w4} = -67.5°

Test fluid – R-113

d_w = 0.4 mm, p = 4.5 mm

$\varepsilon_{\Delta T}$ = 1.888, B = 1.431, U_v = 0.232 m/s

T_v / K	T_{wo} / K	T_{w1} / K	T_{w2} / K	T_{w3} / K	T_{w4} / K	q / (kW/m^2)	α / (kW/m^{2}K)	A
320.87	297.05	297.30	296.97	296.82	297.10	56.40	2.37	0.0008
320.84	297.39	297.67	297.32	297.15	297.42	56.11	2.39	0.0009
320.84	297.82	298.09	297.74	297.58	297.87	55.96	2.43	0.0009
320.82	298.41	298.73	298.31	298.12	298.48	55.11	2.46	0.0011
320.80	299.33	299.69	299.22	299.01	299.42	53.15	2.48	0.0012
320.77	300.94	301.34	300.79	300.55	301.06	49.79	2.51	0.0014
320.77	300.30	300.70	300.18	299.94	300.38	51.12	2.50	0.0013
320.75	299.04	299.39	298.95	298.73	299.07	53.56	2.47	0.0011
320.72	298.23	298.58	298.16	297.94	298.23	54.09	2.40	0.0010
320.70	297.61	297.91	297.56	297.38	297.59	55.50	2.40	0.0008
320.67	297.28	297.59	297.24	297.05	297.24	55.09	2.35	0.0008
320.67	297.02	297.31	296.99	296.81	296.96	54.90	2.32	0.0008

Thermocouple angles : T_{w1} = 22.5°, T_{w2} = 112.5°, T_{w3} = -157.5°, T_{w4} = -67.5°

d_w = 0.4 mm, p = 6.0 mm

$\varepsilon_{\Delta T}$ = 1.710, B = 1.296, U_v = 0.239 m/s

320.21	296.98	297.29	296.96	296.77	296.89	49.25	2.12	0.0008
320.21	297.44	297.74	297.41	297.23	297.39	49.60	2.18	0.0008
320.21	298.09	298.43	298.08	297.87	297.98	48.46	2.19	0.0008
320.21	298.97	299.32	298.87	298.66	299.02	47.51	2.24	0.0011
320.21	300.54	300.92	300.43	300.20	300.62	45.77	2.33	0.0012
320.21	299.90	300.28	299.78	299.56	299.98	45.99	2.26	0.0012
320.21	298.65	299.02	298.55	298.32	298.70	47.66	2.21	0.0012
320.21	297.97	298.28	297.96	297.77	297.88	49.25	2.21	0.0008
320.21	297.26	297.56	297.24	297.05	297.19	49.85	2.17	0.0008

Thermocouple angles : T_{w1} = 22.5°, T_{w2} = 112.5°, T_{w3} = -157.5°, T_{w4} = -67.5°

d_w = 0.75 mm, p = 1.0 mm

$\varepsilon_{\Delta T}$ = 2.336, B = 1.771, U_v = 0.239 m/s

320.67	298.91	299.30	298.86	298.56	298.93	66.01	3.03	0.0011
320.67	299.13	299.57	299.10	298.70	299.15	65.38	3.03	0.0013
320.65	299.50	299.94	299.52	299.05	299.47	64.59	3.05	0.0014
320.65	299.95	300.45	299.98	299.44	299.93	62.92	3.04	0.0016
320.65	300.60	301.14	300.67	300.05	300.55	61.12	3.05	0.0018
320.65	301.63	302.22	301.75	300.98	301.58	59.50	3.13	0.0020
320.65	303.38	303.93	303.73	302.55	303.29	54.99	3.18	0.0024
320.65	302.66	303.34	302.80	301.91	302.58	56.17	3.12	0.0023
320.65	301.34	301.90	301.43	300.74	301.28	59.82	3.10	0.0019
320.65	300.52	301.02	300.57	300.00	300.50	61.86	3.07	0.0016
320.65	299.87	300.31	299.89	299.42	299.89	63.46	3.05	0.0014
320.65	299.51	299.89	299.52	299.10	299.52	64.57	3.05	0.0012
320.65	299.35	299.72	299.33	298.95	299.38	65.80	3.09	0.0012

Thermocouple angles : T_{w1} = 22.5°, T_{w2} = -67.5°, T_{w3} = -157.5°, T_{w4} = 112.5°

Test fluid – R-113

d_w = 0.75 mm, p = 1.5 mm

$\varepsilon_{\Delta T}$ = 2.424, B = 1.837, U_v = 0.231 m/s

T_v / K	T_{wo} / K	T_{w1} / K	T_{w2} / K	T_{w3} / K	T_{w4} / K	q / (kW/m^2)	α / (kW/m^{2}K)	A
321.38	297.51	298.29	297.37	296.89	297.47	72.73	3.05	0.0022
321.38	297.84	298.68	297.69	297.17	297.81	71.18	3.02	0.0024
321.38	298.25	299.11	298.09	297.56	298.24	71.58	3.09	0.0025
321.38	298.79	299.69	298.60	298.05	298.80	70.12	3.10	0.0027
321.38	299.52	300.50	299.31	298.72	299.56	67.90	3.11	0.0029
321.38	300.66	301.68	300.40	299.77	300.77	66.09	3.19	0.0032
321.38	302.61	303.67	302.33	301.69	302.73	62.17	3.31	0.0033
321.38	301.76	302.88	301.50	300.82	301.84	62.95	3.21	0.0034
321.38	300.22	301.26	299.97	299.34	300.30	66.30	3.13	0.0032
321.38	299.33	300.31	299.14	298.54	299.32	68.66	3.11	0.0028
321.38	298.52	299.42	298.35	297.80	298.50	70.06	3.07	0.0026
321.38	298.13	299.01	297.99	297.45	298.09	71.42	3.07	0.0025
321.38	297.84	298.69	297.72	297.20	297.75	73.80	3.14	0.0023

Thermocouple angles : T_{w1} = 22.5°, T_{w2} = 112.5°, T_{w3} = -157.5°, T_{w4} = -67.5°

d_w = 0.75 mm, p = 1.7 mm

$\varepsilon_{\Delta T}$ = 2.706, B = 2.051, U_v = 0.238 m/s

320.46	299.60	300.40	299.38	298.90	299.73	72.37	3.47	0.0025
320.46	300.23	301.04	299.98	299.49	300.40	72.17	3.57	0.0027
320.46	301.04	301.93	300.76	300.23	301.23	70.62	3.64	0.0029
320.46	302.24	303.13	301.94	301.41	302.48	68.05	3.74	0.0030
320.46	303.30	304.37	303.16	302.50	303.16	65.01	3.79	0.0029
320.46	301.83	302.66	301.55	301.06	302.07	68.97	3.70	0.0028
320.46	300.79	301.63	300.54	300.04	300.94	71.01	3.61	0.0027
320.46	299.92	300.67	299.70	299.25	300.05	72.42	3.53	0.0024
320.46	299.34	300.20	299.23	298.70	299.23	71.35	3.38	0.0023

Thermocouple angles : T_{w1} = 22.5°, T_{w2} = 112.5°, T_{w3} = -157.5°, T_{w4} = -67.5°

d_w = 0.75 mm, p = 2.0 mm

$\varepsilon_{\Delta T}$ = 2.574, B = 1.951, U_v = 0.238 m/s

320.38	298.51	299.18	298.28	297.89	298.70	70.73	3.23	0.0023
320.38	299.18	299.90	298.93	298.51	299.40	70.83	3.34	0.0024
320.38	299.97	300.73	299.71	299.26	300.18	68.47	3.35	0.0026
320.41	301.16	301.93	300.87	300.41	301.41	66.50	3.45	0.0027
320.38	302.26	303.04	301.97	301.52	302.52	64.78	3.58	0.0027
320.38	300.65	301.37	300.36	299.93	300.93	68.59	3.48	0.0026
320.38	300.24	300.44	300.37	300.22	299.92	70.49	3.50	0.0001
320.38	298.82	299.47	298.58	298.19	299.03	70.89	3.29	0.0023
320.38	298.38	299.01	298.16	297.79	298.56	71.43	3.25	0.0021

Thermocouple angles : T_{w1} = 22.5°, T_{w2} = 112.5°, T_{w3} = -157.5°, T_{w4} = -67.5°

Test fluid – R-113

d_w = 0.75 mm, p = 2.5 mm

$\varepsilon_{\Delta T}$ = 2.537, B = 1.923, U_v = 0.233 m/s

T_v / K	T_{wo} / K	T_{w1} / K	T_{w2} / K	T_{w3} / K	T_{w4} / K	q / (kW/m^2)	α / (kW/m^{2}K)	A
321.06	298.31	298.72	298.40	297.93	298.18	74.89	3.29	0.0014
321.06	298.52	298.94	298.59	298.14	298.39	73.55	3.26	0.0014
321.06	298.95	299.38	299.01	298.58	298.84	72.41	3.27	0.0014
321.06	299.50	299.92	299.52	299.14	299.40	70.79	3.28	0.0013
321.06	300.24	300.70	300.23	299.88	300.16	68.42	3.29	0.0013
321.06	301.36	301.83	301.33	301.00	301.29	65.65	3.33	0.0013
321.06	303.28	303.74	303.22	302.93	303.22	60.87	3.42	0.0012
321.06	302.55	302.98	302.48	302.25	302.51	62.61	3.38	0.0011
321.04	301.03	301.46	301.02	300.68	300.94	66.71	3.33	0.0013
321.04	300.09	300.53	300.11	299.72	299.99	69.21	3.30	0.0013
321.04	299.27	299.73	299.33	298.88	299.16	71.63	3.29	0.0014
321.04	298.84	299.28	298.93	298.45	298.71	72.34	3.26	0.0014
321.04	298.62	299.04	298.74	298.22	298.47	73.32	3.27	0.0014

Thermocouple angles : T_{w1} = 22.5°, T_{w2} = -67.5°, T_{w3} = -157.5°, T_{w4} = 112.5°

d_w = 0.75 mm, p = 3.0 mm

$\varepsilon_{\Delta T}$ = 2.365, B = 1.793, U_v = 0.238 m/s

320.99	299.53	299.98	299.46	298.94	299.75	66.98	3.12	0.0018
320.99	299.76	300.22	299.70	299.16	299.97	66.34	3.13	0.0018
320.99	300.10	300.64	300.09	299.35	300.31	64.54	3.09	0.0021
320.99	300.57	301.13	300.61	299.71	300.83	63.58	3.11	0.0023
320.99	301.20	301.84	301.32	300.18	301.47	61.62	3.11	0.0026
320.99	302.12	302.89	302.34	300.81	302.42	59.06	3.13	0.0032
320.99	303.70	304.60	304.13	302.00	304.08	54.95	3.18	0.0039
320.97	303.02	303.81	303.37	301.51	303.37	55.83	3.11	0.0035
320.97	301.86	302.55	302.05	300.72	302.13	60.22	3.15	0.0029
320.97	301.11	301.74	301.20	300.18	301.32	62.42	3.14	0.0025
320.97	300.49	301.00	300.53	299.74	300.68	63.42	3.10	0.0020
320.94	300.13	300.64	300.09	299.47	300.31	64.52	3.10	0.0019
320.94	299.98	300.44	299.90	299.43	300.17	65.62	3.13	0.0017

Thermocouple angles : T_{w1} = 22.5°, T_{w2} = 112.5°, T_{w3} = -157.5°, T_{w4} = -67.5°

d_w = 0.75 mm, p = 3.5 mm

$\varepsilon_{\Delta T}$ = 2.074, B = 1.572, U_v = 0.232 m/s

321.40	298.32	298.64	298.36	298.05	298.24	61.38	2.66	0.0010
321.38	298.65	298.98	298.66	298.38	298.58	60.34	2.65	0.0010
321.38	299.11	299.44	299.12	298.85	299.05	58.72	2.64	0.0010
321.38	299.75	300.08	299.74	299.48	299.69	57.83	2.67	0.0010
321.38	300.72	301.09	300.67	300.44	300.67	55.92	2.71	0.0010
321.38	302.38	302.76	302.29	302.13	302.36	52.26	2.75	0.0009
321.38	301.69	302.07	301.62	301.41	301.65	53.18	2.70	0.0010
321.38	300.38	300.75	300.35	300.10	300.33	56.22	2.68	0.0010
321.38	299.62	299.96	299.59	299.35	299.57	58.27	2.68	0.0010
321.38	298.94	299.25	298.95	298.69	298.88	59.47	2.65	0.0009
321.38	298.61	298.91	298.63	298.35	298.53	60.78	2.67	0.0009
321.38	298.36	298.64	298.39	298.13	298.29	62.61	2.72	0.0009

Thermocouple angles : T_{w1} = 22.5°, T_{w2} = -67.5°, T_{w3} = -157.5°, T_{w4} = 112.5°

Test fluid – R-113

d_w = 0.75 mm, p = 4.0 mm

$\varepsilon_{\Delta T}$ = 2.055, B = 1.558, U_v = 0.239 m/s

T_v / K	T_{wo} / K	T_{w1} / K	T_{w2} / K	T_{w3} / K	T_{w4} / K	q / (kW/m^2)	α / (kW/m^{2}K)	A
320.29	298.94	299.39	298.82	298.55	299.01	57.12	2.68	0.0014
320.31	299.80	300.32	299.63	299.32	299.95	55.38	2.70	0.0017
320.29	300.64	301.13	300.46	300.17	300.78	53.43	2.72	0.0017
320.31	301.91	302.38	301.71	301.44	302.11	51.30	2.79	0.0017
320.31	301.26	301.72	301.05	300.78	301.47	52.63	2.76	0.0017
320.31	300.24	300.74	300.07	299.78	300.39	54.35	2.71	0.0017
320.31	299.25	299.75	299.08	298.79	299.38	56.21	2.67	0.0017
320.31	298.59	299.06	298.44	298.16	298.69	57.35	2.64	0.0016

Thermocouple angles : T_{w1} = 22.5°, T_{w2} = 112.5°, T_{w3} = -157.5°, T_{w4} = -67.5°

d_w = 0.75 mm, p = 2.5 mm

$\varepsilon_{\Delta T}$ = 1.942, B = 1.472, U_v = 0.239 m/s

320.84	297.73	298.04	297.82	297.43	297.62	56.38	2.44	0.0011
320.84	298.00	298.34	298.09	297.69	297.89	56.46	2.47	0.0011
320.84	298.38	298.74	298.46	298.05	298.26	56.05	2.49	0.0012
320.87	298.83	299.18	298.88	298.52	298.73	55.20	2.50	0.0011
320.87	299.55	299.92	299.64	299.20	299.42	53.94	2.53	0.0012
320.87	300.61	300.97	300.68	300.29	300.50	51.89	2.56	0.0012
320.87	302.29	302.67	302.32	301.97	302.20	49.24	2.65	0.0011
320.87	301.64	302.06	301.59	301.33	301.59	50.16	2.61	0.0011
320.87	300.28	300.68	300.31	299.94	300.18	52.60	2.55	0.0012
320.87	299.41	299.74	299.50	299.10	299.30	54.04	2.52	0.0011
320.87	298.68	299.06	298.76	298.33	298.56	55.45	2.50	0.0012
320.87	298.30	298.66	298.36	297.97	298.19	56.00	2.48	0.0012
320.87	297.98	298.29	298.04	297.71	297.89	55.96	2.44	0.0010

Thermocouple angles : T_{w1} = 22.5°, T_{w2} = -67.5°, T_{w3} = -157.5°, T_{w4} = 112.5° .

d_w = 0.75 mm, p = 6.0 mm

$\varepsilon_{\Delta T}$ = 1.770, B = 1.342, U_v = 0.232 m/s

321.28	296.60	296.84	296.62	296.40	296.54	55.34	2.24	0.0007
321.28	296.87	297.14	296.89	296.65	296.81	54.39	2.23	0.0008
321.26	297.21	297.48	297.21	296.99	297.16	53.54	2.23	0.0008
321.26	297.63	297.92	297.63	297.40	297.58	52.43	2.22	0.0009
321.26	298.23	298.54	298.19	298.00	298.19	51.23	2.22	0.0008
321.26	299.17	299.50	299.13	298.93	299.13	50.33	2.28	0.0009
321.26	300.83	301.20	300.78	300.55	300.78	48.03	2.35	0.0010
321.28	300.10	300.43	300.04	299.85	300.06	47.79	2.26	0.0009
321.28	298.87	299.18	298.81	298.64	298.83	50.38	2.25	0.0008
321.28	298.16	298.42	298.12	297.96	298.12	52.28	2.26	0.0007
321.28	297.52	297.80	297.50	297.31	297.48	53.08	2.23	0.0008
321.28	297.20	297.46	297.19	297.00	297.16	54.14	2.25	0.0007
321.28	296.96	297.21	296.96	296.76	296.92	54.91	2.26	0.0007

Thermocouple angles : T_{w1} = 22.5°, T_{w2} = -67.5°, T_{w3} = -157.5°, T_{w4} = 112.5°

Test fluid - R-113
d_w = 1.0 mm, p = 1.5 mm
$\varepsilon_{\Delta T}$ = 2.924, B = 2.216, U_v = 0.230 m/s

T_v / K	T_{wo} / K	T_{w1} / K	T_{w2} / K	T_{w3} / K	T_{w4} / K	q / (kW/m^2)	α / (kW/m^{2}K)	A
321.23	299.15	299.85	298.93	298.51	299.28	83.12	3.76	0.0023
321.23	299.57	300.30	299.35	298.92	299.73	82.36	3.80	0.0024
321.21	300.06	300.86	299.81	299.34	300.24	80.10	3.79	0.0026
321.21	300.68	301.52	300.40	299.91	300.90	78.52	3.83	0.0028
321.21	301.54	302.42	301.21	300.69	301.83	76.16	3.87	0.0031
321.18	302.79	303.75	302.41	301.85	303.15	73.70	4.01	0.0034
321.21	304.91	305.87	304.54	303.97	305.26	69.18	4.24	0.0033
321.21	304.07	304.99	303.71	303.16	304.40	70.76	4.13	0.0032
321.18	302.33	303.20	301.99	301.48	302.64	73.96	3.92	0.0030
321.18	301.30	302.15	301.01	300.50	301.53	75.24	3.78	0.0029
321.18	300.39	301.19	300.13	299.65	300.60	78.07	3.75	0.0027
321.18	299.91	300.66	299.69	299.25	300.06	79.97	3.76	0.0024
321.18	299.55	300.26	299.34	298.92	299.67	80.39	3.72	0.0023

Thermocouple angles : T_{w1} = 22.5°, T_{w2} = 112.5°, T_{w3} = -157.5°, T_{w4} = -67.5°

d_w = 1.0 mm, p = 2.5 mm
$\varepsilon_{\Delta T}$ = 2.695, B = 2.043, U_v = 0.228 m/s

321.14	297.66	298.08	297.59	297.33	297.66	81.67	3.48	0.0012
321.14	297.95	298.38	297.85	297.60	297.98	80.74	3.48	0.0013
321.14	298.41	298.86	298.26	297.99	298.51	77.66	3.42	0.0015
321.14	299.00	299.55	298.83	298.50	299.12	75.84	3.43	0.0018
321.14	299.79	300.35	299.73	299.38	299.69	73.52	3.44	0.0015
321.14	300.97	301.51	300.82	300.49	301.07	71.80	3.56	0.0017
321.14	303.02	303.54	302.85	302.54	303.15	67.03	3.70	0.0017
321.14	302.16	302.71	301.99	301.67	302.29	68.16	3.59	0.0018
321.14	300.51	301.04	300.37	300.05	300.57	71.82	3.48	0.0016
321.14	299.57	300.06	299.44	299.14	299.62	74.77	3.47	0.0015
321.14	298.76	299.28	298.61	298.30	298.86	76.59	3.42	0.0017
321.14	298.27	298.74	298.15	297.86	298.34	79.16	3.46	0.0015
321.14	298.04	298.37	297.97	297.77	298.02	79.79	3.45	0.0010

Thermocouple angles : T_{w1} = 22.5°, T_{w2} = 112.5°, T_{w3} = -157.5°, T_{w4} = -67.5°

d_w = 1.0 mm, p = 3.5 mm
$\varepsilon_{\Delta T}$ = 2.397, B = 1.817, U_v = 0.229 m/s

321.14	297.56	297.99	297.47	297.21	297.57	72.64	3.08	0.0013
321.14	297.98	298.43	297.88	297.61	298.01	70.77	3.06	0.0013
321.14	298.51	298.97	298.45	298.17	298.47	68.75	3.04	0.0013
321.14	299.21	299.63	299.14	298.88	299.21	67.40	3.07	0.0012
321.14	300.32	300.76	300.24	299.98	300.32	65.33	3.14	0.0013
321.14	302.22	302.70	302.10	301.82	302.28	60.70	3.21	0.0015
321.14	301.44	301.94	301.32	301.02	301.47	62.39	3.17	0.0015
321.14	299.93	300.37	299.85	299.58	299.92	65.90	3.11	0.0013
321.14	298.23	298.62	298.18	297.94	298.20	69.30	3.03	0.0011
321.14	297.90	298.35	297.83	297.55	297.86	70.31	3.03	0.0013
321.14	297.61	297.97	297.54	297.33	297.62	72.52	3.08	0.0010

Thermocouple angles : T_{w1} = 22.5°, T_{w2} = 112.5°, T_{w3} = -157.5°, T_{w4} = -67.5°

Test fluid - R-113

d_w = 1.0 mm, p = 4.5 mm

$\varepsilon_{\Delta T}$ = 1.942, B = 1.472, U_v = 0.228 m/s

T_v / K	T_{wo} / K	T_{w1} / K	T_{w2} / K	T_{w3} / K	T_{w4} / K	q / (kW/m^2)	α / (kW/m^{2}K)	A
321.04	297.02	297.38	296.94	296.71	297.04	59.45	2.47	0.0011
321.01	297.35	297.75	297.26	297.01	297.38	58.70	2.48	0.0012
321.01	297.81	298.27	297.64	297.37	297.94	56.68	2.44	0.0016
321.01	298.39	298.68	298.29	298.11	298.46	55.68	2.46	0.0010
321.01	299.29	299.72	299.10	298.85	299.49	53.57	2.47	0.0016
321.01	300.92	301.37	300.72	300.47	301.14	51.07	2.54	0.0017
321.01	300.29	300.78	300.08	299.80	300.50	52.05	2.51	0.0018
321.01	298.98	299.40	298.80	298.56	299.18	54.48	2.47	0.0015
321.01	298.23	298.59	298.06	297.86	298.41	55.92	2.45	0.0014
321.01	297.60	298.02	297.43	297.18	297.77	57.94	2.47	0.0015
321.01	297.27	297.66	297.08	296.86	297.48	58.94	2.48	0.0015
320.99	296.99	297.39	296.87	296.63	297.09	60.47	2.52	0.0013

Thermocouple angles : T_{w1} = 22.5°, T_{w2} = 112.5°, T_{w3} = -157.5°, T_{w4} = -67.5°

d_w = 1.0 mm, p = 6.0 mm

$\varepsilon_{\Delta T}$ = 1.806, B = 1.369, U_v = 0.229 m/s

320.72	296.85	297.20	296.82	296.61	296.77	56.42	2.36	0.0009
320.72	297.16	297.53	297.11	296.88	297.11	54.41	2.31	0.0010
320.72	297.61	297.90	297.53	297.35	297.65	53.14	2.30	0.0009
320.72	298.16	298.59	298.00	297.74	298.32	51.79	2.30	0.0015
320.72	299.05	299.55	298.93	298.63	299.10	49.53	2.29	0.0015
320.72	300.62	301.10	300.43	300.15	300.80	47.28	2.35	0.0017
320.72	299.94	300.31	299.79	299.57	300.09	48.11	2.31	0.0013
320.70	298.80	299.28	298.66	298.37	298.91	49.94	2.28	0.0016
320.70	298.07	298.42	297.92	297.72	298.22	51.68	2.28	0.0013
320.70	297.47	297.78	297.41	297.22	297.46	53.90	2.32	0.0009
320.70	297.16	297.49	297.12	296.91	297.12	55.10	2.34	0.0009

Thermocouple angles : T_{w1} = 22.5°, T_{w2} = 112.5°, T_{w3} = -157.5°, T_{w4} = -67.5°

d_w = 0.0 mm, p = 0.0 mm

$\varepsilon_{\Delta T}$ = 1.0, B = 0.758, U_v = 0.23 m/s

T_v / K	T_w / K	q / (kW/m^2)	α / (kW/m^{2}K)
320.69	294.96	31.93	1.24
320.74	295.34	30.91	1.22
320.74	295.86	30.50	1.23
320.19	298.60	28.33	1.31
320.46	295.13	31.91	1.26
320.14	295.39	31.02	1.25
319.96	295.73	30.52	1.26
319.68	296.33	29.52	1.26
319.35	298.06	28.22	1.33

H.2 Condensation on wire-wrapped tubes with ethylene glycol

Test fluid – ethylene glycol
d_w = 0.0 mm, p = 0.0 mm
$\varepsilon_{\Delta T}$ = 1.000, B = 0.763, U_v = 0.420 m/s

T_v / K	T_{wo} / K	T_{w1} / K	T_{w2} / K	T_{w3} / K	T_{w4} / K	q / (kW/m^2)	α / (kW/m^{2}K)	A
471.02	309.32	312.07	309.00	306.57	309.62	310.38	1.92	0.0086
470.97	312.76	315.84	312.70	309.54	312.97	308.58	1.95	0.0095
470.95	318.40	321.93	318.52	314.32	318.84	303.05	1.99	0.0112
470.95	327.53	331.83	327.99	322.48	327.82	296.13	2.06	0.0131
470.92	339.49	343.89	340.18	334.30	339.60	275.63	2.10	0.0127
470.92	352.81	356.32	353.63	348.29	353.00	270.37	2.29	0.0102
470.90	342.52	345.16	343.55	338.91	342.44	281.04	2.19	0.0078
470.87	336.75	341.15	337.54	331.34	336.96	293.04	2.18	0.0131
470.87	322.76	326.56	323.21	318.17	323.09	300.97	2.03	0.0119
470.87	316.16	319.61	316.15	312.23	316.64	301.92	1.95	0.0111
470.85	311.87	314.81	311.62	308.77	312.26	308.02	1.94	0.0093
470.85	309.97	312.48	309.78	307.17	310.44	307.81	1.91	0.0083
471.07	309.66	312.67	309.24	306.85	309.88	307.42	1.90	0.0091
471.07	351.88	356.00	352.64	346.87	352.03	274.47	2.30	0.0117
471.07	359.96	363.69	360.76	355.03	360.37	261.42	2.35	0.0109
471.07	331.92	336.26	332.35	326.79	332.28	293.72	2.11	0.0131
471.07	309.94	312.95	309.49	307.12	310.20	308.24	1.91	0.0091

Thermocouple angles : T_{w1} = 22.5°, T_{w2} = 112.5°, T_{w3} = -157.5°, T_{w4} = -67.5°

d_w = 0.2 mm, p = 0.5 mm
$\varepsilon_{\Delta T}$ = 1.552, B = 1.184, U_v = 0.409 m/s

469.34	327.23	334.77	329.55	318.55	326.06	440.48	3.10	0.0249
469.34	335.99	344.19	338.87	326.26	334.65	439.45	3.30	0.0271
469.34	345.83	354.30	349.05	335.53	344.44	450.74	3.65	0.0276
469.34	358.79	367.20	361.69	348.10	358.17	424.62	3.84	0.0265
469.34	356.76	365.78	359.57	345.74	355.94	430.11	3.82	0.0279
469.34	349.68	358.50	352.13	339.43	348.69	449.03	3.75	0.0271
469.34	334.64	349.13	343.31	330.54	315.59	443.02	3.29	0.0415
469.34	332.29	339.90	334.81	323.27	331.19	438.48	3.20	0.0252
469.34	321.39	329.78	322.48	313.26	320.02	438.32	2.96	0.0252

Thermocouple angles : T_{w1} = 22.5°, T_{w2} = -67.5°, T_{w3} = -157.5°, T_{w4} = 112.5°

d_w = 0.2 mm, p = 1.0 mm
$\varepsilon_{\Delta T}$ = 1.592, B = 1.215, U_v = 0.407 m/s

470.90	318.45	324.02	320.08	312.63	317.08	461.58	3.03	0.0183
470.90	330.97	338.70	333.92	322.15	329.11	465.37	3.33	0.0259
470.90	339.78	347.92	342.44	330.11	338.63	455.71	3.48	0.0264
470.90	348.99	356.35	351.32	340.04	348.27	461.99	3.79	0.0233
470.87	355.27	361.60	358.09	347.53	353.86	438.00	3.79	0.0206
470.87	358.17	364.41	360.70	350.57	356.99	429.82	3.81	0.0198
470.87	353.01	360.02	356.17	344.17	351.67	459.31	3.90	0.0232
470.85	343.76	350.82	347.21	334.89	342.11	453.21	3.57	0.0242
470.85	336.49	344.32	339.56	326.68	335.39	458.26	3.41	0.0266
470.87	324.41	330.64	327.15	317.28	322.57	461.26	3.15	0.0217

Thermocouple angles : T_{w1} = 22.5°, T_{w2} = -67.5°, T_{w3} = -157.5°, T_{w4} = 112.5°

d_w = 0.2 mm, p = 2.0 mm
$\varepsilon_{\Delta T}$ = 1.371, B = 1.046, U_v = 0.408 m/s

470.60	314.32	318.35	314.37	309.38	315.20	413.76	2.65	0.0127
470.60	324.80	329.65	325.49	318.46	325.61	410.37	2.81	0.0158
470.60	332.22	337.62	333.11	325.32	332.85	404.92	2.93	0.0173
470.57	340.90	346.42	342.04	333.41	341.73	401.44	3.10	0.0178
470.57	351.97	357.73	353.11	344.34	352.70	371.27	3.13	0.0178
470.57	350.97	356.23	351.97	344.11	351.59	368.95	3.08	0.0162
470.55	344.98	350.35	345.95	337.98	345.64	387.64	3.09	0.0167
470.57	336.06	341.48	336.86	328.96	336.95	400.32	2.98	0.0172
470.55	329.57	334.77	330.31	322.89	330.31	404.62	2.87	0.0167
470.55	319.42	323.83	319.74	313.86	320.25	408.97	2.71	0.0141

Thermocouple angles : T_{w1} = 22.5°, T_{w2} = -67.5°, T_{w3} = -157.5°, T_{w4} = 112.5°

Test fluid – ethylene glycol
d_w = 0.2 mm, p = 4.0 mm
$\varepsilon_{\Delta T}$ = 1.208, B = 0.922, U_v = 0.403 m/s

T_v / K	T_{wo} / K	T_{w1} / K	T_{w2} / K	T_{w3} / K	T_{w4} / K	q / (kW/m^2)	α / (kW/m^{2}K)	A
470.65	309.00	312.95	308.85	304.48	309.71	362.03	2.24	0.0121
470.62	319.06	324.15	319.28	313.13	319.67	362.28	2.39	0.0157
470.65	325.84	331.37	326.26	319.34	326.38	357.85	2.47	0.0170
470.65	334.26	340.13	335.10	327.02	334.81	364.37	2.67	0.0183
470.62	346.03	352.63	347.08	337.99	346.43	331.46	2.66	0.0199
470.70	347.66	353.58	348.96	340.23	347.86	332.42	2.70	0.0183
470.67	338.93	344.75	339.75	331.64	339.58	358.63	2.72	0.0180
470.62	329.27	334.83	329.90	322.61	329.76	353.85	2.50	0.0172
470.65	323.71	329.38	324.03	317.19	324.22	362.70	2.47	0.0173
470.72	313.85	318.36	313.84	308.76	314.43	363.68	2.32	0.0138

Thermocouple angles : T_{w1} = 22.5°, T_{w2} = -67.5°, T_{w3} = -157.5°, T_{w4} = 112.5°

d_w = 0.35 mm, p = 0.8 mm
$\varepsilon_{\Delta T}$ = 2.127, B = 1.623, U_v = 0.404 m/s

471.20	340.04	349.79	343.89	329.01	337.46	608.93	4.64	0.0318
471.17	351.42	361.71	355.72	338.74	349.50	591.14	4.94	0.0336
471.20	361.91	371.83	366.40	349.24	360.18	592.50	5.42	0.0321
471.20	365.83	375.52	369.96	353.80	364.05	584.54	5.55	0.0305
471.20	367.96	377.23	371.79	356.85	365.99	556.49	5.39	0.0286
471.17	356.37	366.67	360.86	343.72	354.22	588.84	5.13	0.0333
471.20	347.28	357.33	351.42	335.08	345.29	592.13	4.78	0.0330
471.20	331.98	339.96	334.82	322.66	330.50	601.87	4.32	0.0266

Thermocouple angles : T_{w1} = 22.5°, T_{w2} = -67.5°, T_{w3} = -157.5°, T_{w4} = 112.5°

d_w = 0.35 mm, p = 1.0 mm
$\varepsilon_{\Delta T}$ = 2.157, B = 1.646, U_v = 0.406 m/s

470.77	336.54	345.39	339.57	327.20	333.99	620.78	4.62	0.0281
470.77	355.08	364.69	359.45	344.06	352.11	610.41	5.28	0.0308
470.77	365.44	375.34	369.90	354.16	362.36	603.71	5.73	0.0307
470.77	359.89	369.75	364.49	348.42	356.89	597.50	5.39	0.0314
470.77	344.16	353.35	347.96	333.75	341.56	608.83	4.81	0.0299
470.77	332.09	340.33	334.93	323.47	329.63	624.45	4.50	0.0265
470.85	339.80	348.73	342.74	330.39	337.34	598.14	4.56	0.0280
470.82	362.94	372.73	366.86	351.94	360.24	578.05	5.36	0.0299
470.80	351.08	361.51	354.91	339.62	348.28	588.22	4.91	0.0324

Thermocouple angles : T_{w1} = 22.5°, T_{w2} = -67.5°, T_{w3} = -157.5°, T_{w4} = 112.5°

d_w = 0.35 mm, p = 1.5 mm
$\varepsilon_{\Delta T}$ = 1.917, B = 1.463, U_v = 0.409 m/s

471.12	331.50	338.71	333.14	323.50	330.63	552.21	3.95	0.0227
471.12	339.78	347.78	342.03	330.57	338.75	548.99	4.18	0.0252
471.10	349.44	358.15	351.97	339.19	348.43	539.16	4.43	0.0270
471.10	361.35	369.68	364.11	351.57	360.04	519.56	4.73	0.0253
471.10	359.03	367.21	361.69	349.28	357.94	534.18	4.77	0.0251
471.10	354.29	363.09	357.17	343.71	353.18	525.88	4.50	0.0274
471.10	346.58	355.26	349.18	336.49	345.40	539.15	4.33	0.0271
471.07	335.57	343.30	337.55	326.82	334.60	549.33	4.05	0.0244

Thermocouple angles : T_{w1} = 22.5°, T_{w2} = -67.5°, T_{w3} = -157.5°, T_{w4} = 112.5°

d_w = 0.35 mm, p = 2.5 mm
$\varepsilon_{\Delta T}$ = 1.553, B = 1.185, U_v = 0.414 m/s

470.39	316.42	320.64	316.76	312.21	316.07	455.16	2.96	0.0127
470.49	322.55	327.40	323.30	317.43	322.06	458.01	3.10	0.0150
470.49	329.30	334.76	330.51	323.17	328.75	459.37	3.25	0.0173
470.47	337.31	343.80	338.94	330.04	336.46	444.46	3.34	0.0203
470.44	346.25	352.66	348.21	338.71	345.44	449.97	3.62	0.0201
470.42	355.48	361.63	357.39	348.35	354.56	417.91	3.64	0.0188
470.44	350.40	356.68	352.43	342.93	349.54	441.70	3.68	0.0197
470.44	341.39	347.92	343.07	333.96	340.61	445.81	3.45	0.0203
470.42	334.13	340.28	335.65	327.02	333.58	447.56	3.28	0.0195
470.44	355.94	362.25	358.21	348.16	355.13	422.84	3.69	0.0199

Thermocouple angles : T_{w1} = 22.5°, T_{w2} = -67.5°, T_{w3} = -157.5°, T_{w4} = 112.5°

Test fluid – ethylene glycol
d_w = 0.35 mm, p = 4.0 mm
$\varepsilon_{\Delta T}$ = 1.336, B = 1.019, U_v = 0.409 m/s

T_v / K	T_{wo} / K	T_{w1} / K	T_{w2} / K	T_{w3} / K	T_{w4} / K	q / (kW/m^2)	α / (kW/m^{2}K)	A
470.90	314.48	318.25	314.96	310.18	314.54	398.72	2.55	0.0121
470.87	325.93	330.91	327.28	319.89	325.65	398.87	2.75	0.0166
470.85	332.97	338.40	334.62	326.25	332.61	391.41	2.84	0.0180
470.85	340.93	346.78	342.77	333.83	340.36	391.85	3.02	0.0189
470.82	348.56	353.98	350.57	341.79	347.90	373.46	3.05	0.0176
470.77	351.83	356.82	353.62	345.57	351.29	378.38	3.18	0.0160
470.77	345.11	350.59	346.79	338.24	344.81	381.94	3.04	0.0176
470.75	336.03	341.55	337.60	329.29	335.69	378.75	2.81	0.0179
470.75	329.99	335.26	331.30	323.74	329.65	389.28	2.77	0.0171
470.72	320.01	324.25	320.92	315.14	319.71	395.82	2.63	0.0139

Thermocouple angles : T_{w1} = 22.5°, T_{w2} = -67.5°, T_{w3} = -157.5°, T_{w4} = 112.5°

d_w = 0.4 mm, p = 1.0 mm
$\varepsilon_{\Delta T}$ = 2.009, B = 1.533, U_v = 0.407 m/s

469.89	321.98	328.04	323.69	314.50	321.70	584.61	3.95	0.0206
469.89	337.08	344.98	340.14	327.39	335.83	573.19	4.32	0.0266
469.89	346.89	355.43	350.40	336.25	345.48	559.84	4.55	0.0283
469.89	355.53	364.16	359.32	344.60	354.05	552.01	4.83	0.0282
469.89	366.03	374.50	369.74	355.58	364.29	496.11	4.78	0.0267
469.89	365.06	374.18	368.87	353.79	363.39	500.55	4.77	0.0287
469.89	358.87	367.29	362.42	348.35	357.42	546.40	4.92	0.0270
469.89	351.76	360.91	355.48	340.52	350.14	553.87	4.69	0.0297
469.89	344.09	352.73	347.52	333.40	342.71	570.24	4.53	0.0286
469.89	329.98	337.18	332.69	321.15	328.92	584.93	4.18	0.0246

Thermocouple angles : T_{w1} = 22.5°, T_{w2} = -67.5°, T_{w3} = -157.5°, T_{w4} = 112.5°

d_w = 0.4 mm, p = 1.5 mm
$\varepsilon_{\Delta T}$ = 1.741, B = 1.328, U_v = 0.408 m/s

469.87	318.83	323.64	319.97	313.08	318.63	516.09	3.42	0.0161
469.87	331.98	338.40	333.94	324.26	331.31	505.72	3.67	0.0212
469.84	340.24	347.31	342.58	331.63	339.45	490.72	3.79	0.0231
469.84	348.81	356.11	351.30	339.78	348.06	489.32	4.04	0.0234
469.84	359.67	367.05	362.35	350.39	358.88	447.54	4.06	0.0232
469.84	358.69	366.46	361.47	349.16	357.69	455.75	4.10	0.0243
469.84	352.56	359.81	355.10	343.54	351.81	488.66	4.17	0.0231
469.84	344.96	352.47	347.52	335.82	344.03	493.51	3.95	0.0242
469.84	337.88	344.93	340.19	329.35	337.06	505.47	3.83	0.0231
469.84	325.60	331.44	327.25	318.67	325.04	519.02	3.60	0.0194

Thermocouple angles : T_{w1} = 22.5°, T_{w2} = -67.5°, T_{w3} = -157.5°, T_{w4} = 112.5°

d_w = 0.4 mm, p = 2.5 mm
$\varepsilon_{\Delta T}$ = 1.528, B = 1.166, U_v = 0.403 m/s

470.12	315.25	319.56	316.53	310.31	314.62	453.61	2.93	0.0147
470.12	327.24	333.07	329.42	320.35	326.13	449.42	3.15	0.0199
470.12	335.62	342.16	338.31	327.73	334.26	443.99	3.30	0.0222
470.14	344.31	351.12	347.37	335.86	342.92	444.48	3.53	0.0229
470.09	356.11	363.09	359.43	347.22	354.72	400.73	3.52	0.0231
470.12	354.13	361.37	357.38	345.02	352.76	409.14	3.53	0.0238
470.12	348.28	354.88	351.18	340.07	346.97	437.38	3.59	0.0220
470.12	339.53	346.08	342.47	331.34	338.21	437.81	3.35	0.0225
470.09	332.85	338.97	335.62	325.25	331.54	447.20	3.26	0.0214
470.09	321.41	326.48	323.25	315.45	320.43	452.73	3.04	0.0175

Thermocouple angles : T_{w1} = 22.5°, T_{w2} = -67.5°, T_{w3} = -157.5°, T_{w4} = 112.5°

Test fluid – ethylene glycol

d_w = 0.4 mm, p = 4.0 mm

$\varepsilon_{\Delta T}$ = 1.324, B = 1.010, U_v = 0.404 m/s

T_v / K	T_{wo} / K	T_{w1} / K	T_{w2} / K	T_{w3} / K	T_{w4} / K	q / (kW/m^2)	α / (kW/m^{2}K)	A
470.14	312.85	316.81	313.43	308.05	313.11	391.70	2.49	0.0131
470.14	323.59	329.01	324.77	317.15	323.46	391.11	2.67	0.0177
470.14	331.02	337.04	332.43	323.61	331.00	387.64	2.79	0.0196
470.14	339.59	345.67	341.54	331.60	339.54	386.28	2.96	0.0203
470.14	351.33	358.11	353.52	342.63	351.04	361.34	3.04	0.0217
470.14	349.07	355.59	351.48	340.47	348.72	367.74	3.04	0.0215
470.12	343.40	349.68	345.08	335.43	343.40	382.84	3.02	0.0201
470.12	334.83	340.66	336.73	327.09	334.85	383.76	2.84	0.0198
470.09	328.49	334.25	329.80	321.58	328.33	389.67	2.75	0.0187
470.09	318.29	322.76	319.40	312.58	318.40	393.09	2.59	0.0154

Thermocouple angles : T_{w1} = 22.5°, T_{w2} = -67.5°, T_{w3} = -157.5°, T_{w4} = 112.5°

d_w = 0.75 mm, p = 1.0 mm

$\varepsilon_{\Delta T}$ = 1.625, B = 1.240, U_v = 0.415 m/s

469.44	317.06	321.38	318.87	311.58	316.41	495.20	3.25	0.0158
469.44	329.25	334.62	332.13	322.07	328.19	479.82	3.42	0.0199
469.44	337.27	343.18	340.65	329.34	335.91	465.64	3.52	0.0217
469.44	345.59	351.68	349.01	337.39	344.25	462.69	3.74	0.0217
469.44	355.83	362.17	359.26	347.38	354.50	421.31	3.71	0.0218
469.44	354.93	361.44	358.40	346.24	353.64	433.31	3.78	0.0223
469.44	349.36	355.51	352.63	341.18	348.13	453.36	3.78	0.0214
469.44	340.95	347.40	344.18	332.49	339.72	452.09	3.52	0.0227
469.42	334.44	340.42	337.41	326.63	333.31	468.26	3.47	0.0214
469.39	323.31	328.53	325.55	316.61	322.56	486.75	3.33	0.0188

Thermocouple angles : T_{w1} = 22.5°, T_{w2} = -67.5°, T_{w3} = -157.5°, T_{w4} = 112.5°

d_w = 0.75 mm, p = 1.5 mm

$\varepsilon_{\Delta T}$ = 1.653, B = 1.261, U_v = 0.407 m/s

470.07	317.82	322.45	319.89	311.94	316.99	504.34	3.31	0.0170
470.04	330.28	336.50	333.36	322.38	328.89	489.70	3.50	0.0223
470.04	339.14	346.21	342.70	330.21	337.43	476.60	3.64	0.0248
470.04	347.32	354.94	350.97	337.86	345.52	470.53	3.83	0.0257
470.04	357.23	365.07	360.91	347.61	355.33	422.99	3.75	0.0256
470.04	355.55	363.57	359.26	345.70	353.66	431.12	3.77	0.0262
470.04	350.82	358.49	354.45	341.37	348.97	458.01	3.84	0.0255
470.02	343.06	350.81	346.55	333.62	341.26	466.64	3.68	0.0261
470.04	335.87	343.10	338.99	327.08	334.31	475.56	3.54	0.0247
470.04	324.49	330.52	326.77	317.38	323.30	498.07	3.42	0.0208

Thermocouple angles : T_{w1} = 22.5°, T_{w2} = -67.5°, T_{w3} = -157.5°, T_{w4} = 112.5°

d_w = 0.75 mm, p = 2.5 mm

$\varepsilon_{\Delta T}$ = 1.578, B = 1.204, U_v = 0.408 m/s

469.84	315.67	320.97	317.49	309.87	314.36	475.23	3.08	0.0181
469.82	327.79	334.38	330.75	320.08	325.94	465.11	3.27	0.0230
469.79	336.48	343.53	340.00	327.85	334.55	459.36	3.45	0.0246
469.77	344.90	352.46	348.49	335.59	343.05	437.91	3.51	0.0256
469.72	357.24	364.87	361.13	347.57	355.41	414.60	3.69	0.0254
469.72	355.26	363.36	359.15	345.30	353.23	422.42	3.69	0.0267
469.74	349.24	356.70	352.71	340.11	347.47	450.16	3.74	0.0248
469.77	340.64	347.97	344.27	331.47	338.83	446.49	3.46	0.0254
469.72	333.44	340.48	336.50	325.09	331.70	459.02	3.37	0.0241
469.69	321.82	327.70	324.20	314.94	320.46	468.81	3.17	0.0205

Thermocouple angles : T_{w1} = 22.5°, T_{w2} = -67.5°, T_{w3} = -157.5°, T_{w4} = 112.5°

Test fluid – ethylene glycol
d_w = 0.75 mm, p = 4.0 mm
$\varepsilon_{\Delta T}$ = 1.541, B = 1.176, U_v = 0.406 m/s

T_v / K	T_{wo} / K	T_{w1} / K	T_{w2} / K	T_{w3} / K	T_{w4} / K	q / (kW/m^2)	α / (kW/m^{2}K)	A
470.04	316.10	320.77	316.99	310.54	316.11	462.34	3.00	0.0155
470.09	327.78	333.76	329.48	320.43	327.44	455.85	3.20	0.0200
470.07	336.17	342.83	338.38	327.78	335.68	442.89	3.31	0.0222
470.04	344.65	351.56	347.24	335.95	343.87	447.61	3.57	0.0228
470.04	355.23	362.02	358.07	346.27	354.56	408.39	3.56	0.0224
470.12	353.16	360.10	356.01	344.13	352.42	414.61	3.55	0.0228
470.07	348.24	354.87	350.93	339.60	347.58	434.01	3.56	0.0221
470.07	340.09	346.88	342.55	331.48	339.44	438.05	3.37	0.0227
470.07	333.39	339.88	335.44	325.38	332.86	449.24	3.29	0.0216
470.07	322.20	327.53	323.53	315.73	322.00	459.41	3.11	0.0178

Thermocouple angles : T_{w1} = 22.5°, T_{w2} = -67.5°, T_{w3} = -157.5°, T_{w4} = 112.5°

d_w = 1.0 mm, p = 1.5 mm
$\varepsilon_{\Delta T}$ = 1.461, B = 1.115, U_v = 0.407 m/s

470.42	314.99	318.52	315.47	309.88	316.10	456.51	2.94	0.0123
470.42	326.67	331.33	327.68	320.00	327.68	437.81	3.05	0.0160
470.42	334.25	339.52	335.54	326.84	335.11	424.14	3.11	0.0178
470.42	343.20	348.72	344.61	335.27	344.20	426.06	3.35	0.0183
470.44	354.43	360.01	356.28	346.16	355.27	375.47	3.24	0.0186
470.44	353.55	358.40	355.17	346.37	354.26	374.96	3.21	0.0162
470.42	347.39	352.50	348.97	339.95	348.15	410.90	3.34	0.0171
470.42	337.61	341.99	339.34	330.22	338.91	416.06	3.13	0.0164
470.42	331.67	336.95	332.78	324.43	332.51	432.06	3.11	0.0176
470.39	320.84	325.25	321.46	314.92	321.75	448.11	3.00	0.0147

Thermocouple angles : T_{w1} = 22.5°, T_{w2} = -67.5°, T_{w3} = -157.5°, T_{w4} = 112.5°

d_w = 1.0 mm, p = 2.5 mm
$\varepsilon_{\Delta T}$ = 1.604, B = 1.224, U_v = 0.417 m/s

469.34	316.22	321.59	318.30	310.74	314.25	478.09	3.12	0.0183
469.34	328.68	335.26	332.27	321.07	326.12	473.02	3.36	0.0235
469.34	336.66	344.10	340.78	327.99	333.77	457.78	3.45	0.0261
469.32	345.52	353.09	350.11	336.27	342.61	466.26	3.77	0.0266
469.32	356.13	363.88	360.87	346.54	353.22	414.91	3.67	0.0266
469.32	354.36	362.09	359.23	344.73	351.37	430.15	3.74	0.0269
469.29	348.42	355.91	353.04	339.24	345.50	450.41	3.73	0.0262
469.29	340.45	348.12	344.76	331.45	337.46	452.67	3.51	0.0267
469.27	333.85	341.15	337.80	325.50	330.93	464.93	3.43	0.0256
469.27	322.23	328.42	325.08	315.55	319.87	474.32	3.23	0.0215

Thermocouple angles : T_{w1} = 22.5°, T_{w2} = -67.5°, T_{w3} = -157.5°, T_{w4} = 112.5°

d_w = 1.0 mm, p = 3.5 mm
$\varepsilon_{\Delta T}$ = 1.599, B = 1.220, U_v = 0.408 m/s

470.14	316.05	321.84	316.33	309.61	316.45	483.21	3.14	0.0178
470.14	328.64	335.83	329.86	319.89	328.97	475.90	3.36	0.0229
470.14	336.82	344.78	338.53	327.03	336.96	458.81	3.44	0.0252
470.12	346.10	354.47	348.03	335.53	346.37	462.30	3.73	0.0262
470.12	357.17	365.44	359.54	346.46	357.25	418.08	3.70	0.0258
470.12	355.27	362.46	357.24	345.92	355.46	421.23	3.67	0.0225
470.12	349.65	357.93	351.65	339.26	349.78	455.36	3.78	0.0257
470.09	340.91	349.36	342.58	330.59	341.13	454.52	3.52	0.0262
470.09	333.73	341.54	335.04	324.22	334.12	461.21	3.38	0.0245
470.09	322.19	329.01	322.87	314.31	322.58	475.39	3.21	0.0212

Thermocouple angles : T_{w1} = 22.5°, T_{w2} = -67.5°, T_{w3} = -157.5°, T_{w4} = 112.5°

Test fluid – ethylene glycol
d_w = 1.0 mm, p = 4.5 mm
$\varepsilon_{\Delta T}$ = 1.595, B = 1.217, U_v = 0.412 m/s

T_v / K	T_{wo} / K	T_{w1} / K	T_{w2} / K	T_{w3} / K	T_{w4} / K	q / (kW/m^2)	α / (kW/m^{2}K)	A
469.67	316.71	321.97	317.36	310.70	316.80	479.64	3.14	0.0168
469.67	329.08	335.78	330.74	320.94	328.87	471.38	3.35	0.0219
469.67	337.75	345.20	339.93	328.36	337.49	459.69	3.48	0.0244
469.67	346.55	354.43	349.26	336.29	346.21	454.22	3.69	0.0259
469.64	358.29	365.99	361.37	348.14	357.68	407.66	3.66	0.0250
469.64	356.17	364.22	359.00	345.99	355.49	421.59	3.72	0.0255
469.62	350.39	357.88	352.71	340.87	350.11	449.61	3.77	0.0238
469.62	341.78	349.44	343.90	332.19	341.59	450.36	3.52	0.0246
469.62	334.63	341.85	336.31	325.82	334.53	459.88	3.41	0.0232
469.67	322.87	329.10	324.11	315.65	322.62	474.12	3.23	0.0201

Thermocouple angles : T_{w1} = 22.5°, T_{w2} = -67.5°, T_{w3} = -157.5°, T_{w4} = 112.5°

H.3 Condensation on wire-wrapped tubes with steam

Test fluid – steam
d_w = 0.0 mm, p = 0.0 mm
$\varepsilon_{\Delta T}$ = 1.000, B = 0.837, U_v = 0.570 m/s

T_v / K	T_{wo} / K	T_{w1} / K	T_{w2} / K	T_{w3} / K	T_{w4} / K	q / (kW/m^2)	α / (kW/m^{2}K)	A
373.17	332.81	344.62	336.32	319.43	330.86	466.27	11.55	0.0381
373.15	334.89	346.58	337.82	321.80	333.38	446.88	11.68	0.0367
373.13	338.14	348.97	340.60	325.26	337.71	418.30	11.96	0.0340
373.25	342.63	351.81	345.58	331.10	342.02	380.96	12.44	0.0299
373.22	348.48	356.06	350.98	338.55	348.34	328.01	13.26	0.0247
373.22	351.61	358.34	353.68	342.69	351.75	286.08	13.24	0.0216
373.22	356.89	361.99	358.40	349.94	357.25	231.58	14.18	0.0162
373.22	360.12	364.48	361.52	354.23	360.24	188.00	14.35	0.0138
373.22	367.90	369.69	368.50	365.58	367.83	102.55	19.26	0.0055
373.22	363.51	366.75	364.44	359.16	363.67	141.91	14.60	0.0101
373.20	358.45	363.34	360.06	351.81	358.60	211.38	14.34	0.0156
373.20	353.94	360.17	355.51	345.91	354.16	271.28	14.09	0.0193
373.17	350.71	358.00	352.83	341.27	350.72	306.67	13.65	0.0232
373.20	345.80	354.37	348.38	334.81	345.64	352.79	12.88	0.0276
373.20	340.57	350.15	343.44	328.68	340.00	397.81	12.19	0.0311
373.17	336.80	347.61	339.06	323.86	336.68	429.71	11.81	0.0339
373.17	333.89	345.14	336.38	320.91	333.12	448.77	11.42	0.0354

Thermocouple angles : T_{w1} = 22.5°, T_{w2} = -67.5°, T_{w3} = -157.5°, T_{w4} = 112.5°

d_w = 0.2 mm, p = 0.5 mm
$\varepsilon_{\Delta T}$ = 1.756, B = 1.470, U_v = 0.577 m/s

372.79	334.31	341.49	335.20	325.23	335.32	771.69	20.06	0.0224
372.86	337.15	344.52	338.52	328.28	337.29	733.16	20.53	0.0230
372.83	340.77	347.82	342.84	331.77	340.63	677.80	21.14	0.0230
372.83	345.78	351.66	347.72	337.90	345.85	608.63	22.50	0.0194
372.83	352.64	358.32	354.26	345.17	352.81	503.65	24.94	0.0180
372.86	349.14	355.23	350.83	341.33	349.18	553.73	23.35	0.0193
372.81	342.86	349.76	344.81	333.99	342.86	650.32	21.71	0.0223
372.83	339.26	346.59	341.75	329.08	339.61	712.64	21.22	0.0250
372.83	335.67	342.74	336.60	326.39	336.94	755.82	20.34	0.0223

Thermocouple angles : T_{w1} = 22.5°, T_{w2} = -67.5°, T_{w3} = -157.5°, T_{w4} = 112.5°

d_w = 0.2 mm, p = 0.5 mm
$\varepsilon_{\Delta T}$ = 2.183, B = 1.827, U_v = 0.565 m/s

373.20	338.21	345.02	339.91	327.93	339.96	892.64	25.51	0.0234
373.20	340.71	347.41	342.24	331.04	342.16	852.71	26.25	0.0222
373.20	344.86	350.52	346.04	336.29	346.57	780.60	27.54	0.0193
373.20	349.68	355.27	351.95	340.98	350.51	690.05	29.34	0.0181
373.20	354.57	359.04	355.89	347.26	356.08	590.22	31.68	0.0155
373.20	352.52	358.62	355.06	343.02	353.38	620.02	29.99	0.0195
373.20	347.18	352.84	349.21	338.26	348.40	742.98	28.55	0.0190
373.20	343.41	349.59	344.40	334.56	345.07	825.18	27.70	0.0206
373.20	339.45	346.34	341.51	329.77	340.18	882.52	26.15	0.0218

Thermocouple angles : T_{w1} = 22.5°, T_{w2} = 112.5°, T_{w3} = -157.5°, T_{w4} = -67.5°

d_w = 0.2 mm, p = 0.75 mm
$\varepsilon_{\Delta T}$ = 2.013, B = 1.685, U_v = 0.580 m/s

T_v / K	T_{wo} / K	T_{w1} / K	T_{w2} / K	T_{w3} / K	T_{w4} / K	q / (kW/m^2)	α / (kW/m^{2}K)	A
372.57	335.83	343.72	336.78	324.95	337.87	863.06	23.49	0.0264
372.54	339.15	346.04	340.55	328.74	341.25	817.76	24.49	0.0240
372.57	343.39	349.94	344.31	333.83	345.49	733.83	25.15	0.0223
372.54	348.15	354.29	350.06	338.80	349.46	645.89	26.48	0.0202
372.54	353.09	358.20	355.12	345.04	354.01	528.49	27.17	0.0166
372.54	350.73	357.47	352.95	340.78	351.72	583.70	26.75	0.0213
372.54	345.44	351.70	347.30	335.98	346.77	693.14	25.57	0.0207
372.54	341.65	348.87	342.52	331.71	343.48	773.58	25.04	0.0237
372.54	338.08	345.68	339.18	327.87	339.59	833.89	24.20	0.0246

Thermocouple angles : T_{w1} = 22.5°, T_{w2} = 112.5°, T_{w3} = -157.5°, T_{w4} = -67.5°

Test fluid – steam

d_w = 0.2 mm, p = 1.0 mm

$\varepsilon_{\Delta T}$ = 1.756, B = 1.470, U_v = 0.577 m/s

T_v / K	T_{wo} / K	T_{w1} / K	T_{w2} / K	T_{w3} / K	T_{w4} / K	q / (kW/m^2)	α / (kW/m^{2}K)	A
372.86	333.66	341.14	334.90	323.59	335.02	785.09	20.03	0.0244
372.88	335.85	343.00	336.90	326.02	337.50	758.30	20.48	0.0237
372.93	339.16	346.50	340.58	328.92	340.65	709.44	21.01	0.0240
372.93	344.34	351.74	345.68	334.53	345.40	625.79	21.89	0.0229
372.96	351.06	357.42	352.47	342.49	351.89	521.83	23.84	0.0193
372.88	348.10	354.99	349.70	338.35	349.34	579.67	23.39	0.0219
372.93	341.72	348.80	343.15	331.72	343.20	670.82	21.49	0.0231
372.88	337.03	344.48	337.93	326.78	338.94	730.33	20.37	0.0248
372.93	333.92	341.13	335.12	323.67	335.75	781.04	20.02	0.0245

Thermocouple angles : T_{w1} = 22.5°, T_{w2} = 112.5°, T_{w3} = -157.5°, T_{w4} = -67.5°

d_w = 0.35 mm, p = 0.7 mm

$\varepsilon_{\Delta T}$ = 2.317, B = 1.939, U_v = 0.577 m/s

372.69	340.98	347.94	341.90	330.10	343.97	890.09	28.07	0.0253
372.67	343.63	350.24	345.33	333.55	345.41	835.32	28.77	0.0225
372.69	347.37	353.36	349.03	337.55	349.56	760.00	30.02	0.0213
372.67	352.47	356.45	352.56	346.81	354.05	675.62	33.45	0.0134
372.67	357.87	361.27	358.31	352.47	359.42	537.47	36.33	0.0120
372.62	355.29	359.37	355.57	349.82	356.41	608.68	35.13	0.0129
372.62	349.44	354.58	350.18	341.88	351.14	727.63	31.40	0.0173
372.62	345.79	351.74	347.34	337.39	346.69	799.92	29.82	0.0188
372.62	342.35	348.11	343.97	333.44	343.90	842.67	27.85	0.0198

Thermocouple angles : T_{w1} = 22.5°, T_{w2} = 112.5°, T_{w3} = -157.5°, T_{w4} = -67.5°

d_w = 0.35 mm, p = 1.0 mm

$\varepsilon_{\Delta T}$ = 1.759, B = 1.472, U_v = 0.577 m/s

372.86	332.99	340.03	334.32	322.80	334.80	784.30	19.67	0.0236
372.86	336.31	343.24	337.65	326.24	338.11	749.07	20.50	0.0231
372.88	340.00	346.47	341.41	330.51	341.63	691.34	21.03	0.0216
372.86	345.31	351.47	346.95	336.02	346.83	618.09	22.44	0.0207
372.86	351.42	356.50	352.75	343.78	352.67	525.07	24.49	0.0168
372.88	348.94	354.60	350.39	340.60	350.15	572.38	23.90	0.0187
372.86	342.68	349.12	344.14	333.27	344.19	662.37	21.95	0.0213
372.86	338.06	344.73	339.36	328.51	339.65	721.55	20.74	0.0220
372.83	334.79	341.54	335.83	325.40	336.38	761.08	20.00	0.0220

Thermocouple angles : T_{w1} = 22.5°, T_{w2} = -67.5°, T_{w3} = -157.5°, T_{w4} = 112.5°

d_w = 0.35 mm, p = 1.5 mm

$\varepsilon_{\Delta T}$ = 1.761, B = 1.474, U_v = 0.575 m/s

372.93	334.47	343.76	337.45	322.87	333.80	772.74	20.09	0.0309
372.93	337.60	346.95	340.06	326.36	337.03	732.88	20.74	0.0299
372.93	341.37	350.30	344.51	330.35	340.32	678.33	21.49	0.0293
372.93	346.19	355.77	348.51	334.76	345.72	607.71	22.73	0.0296
372.93	352.06	359.92	354.46	342.56	351.29	527.38	25.27	0.0245
372.93	351.08	359.28	353.84	340.71	350.48	533.99	24.44	0.0263
372.93	343.68	353.20	347.58	331.33	342.60	644.69	22.04	0.0322
372.93	339.29	348.71	342.33	327.94	338.17	707.97	21.04	0.0306
372.93	335.82	345.58	337.95	324.28	335.46	739.79	19.93	0.0307

Thermocouple angles : T_{w1} = 22.5°, T_{w2} = -67.5°, T_{w3} = -157.5°, T_{w4} = 112.5°

d_w = 0.35 mm, p = 2.0 mm

$\varepsilon_{\Delta T}$ = 2.041, B = 1.708, U_v = 0.570 m/s

373.05	337.68	348.34	340.69	324.17	337.51	883.39	24.97	0.0349
373.05	340.38	350.88	342.87	327.08	340.68	808.63	24.75	0.0335
373.05	344.19	353.62	347.13	331.46	344.53	735.50	25.48	0.0312
373.05	349.35	357.79	353.01	337.87	348.73	653.96	27.59	0.0287
373.05	354.85	362.12	358.27	344.30	354.69	549.39	30.17	0.0251
373.05	352.06	360.63	355.53	339.87	352.21	591.43	28.18	0.0290
373.13	346.44	355.13	350.18	334.24	346.23	696.84	26.12	0.0300
373.08	342.01	351.41	344.80	329.57	342.25	761.16	24.50	0.0309
373.05	338.24	348.13	341.05	325.56	338.23	816.18	23.45	0.0324

Thermocouple angles : T_{w1} = 22.5°, T_{w2} = -67.5°, T_{w3} = -157.5°, T_{w4} = 112.5°

Test fluid – steam

d_w = 0.35 mm, p = 4.5 mm

$\varepsilon_{\Delta T}$ = 1.796, B = 1.503, U_v = 0.585 m/s

T_v / K	T_{wo} / K	T_{w1} / K	T_{w2} / K	T_{w3} / K	T_{w4} / K	q / (kW/m^2)	α / (kW/m^{2}K)	A
372.21	331.89	337.81	334.69	322.77	332.30	803.29	19.93	0.0223
372.21	335.50	341.54	338.41	326.12	335.95	770.93	21.01	0.0226
372.16	338.82	344.13	341.94	329.92	339.31	706.03	21.18	0.0209
372.18	345.04	350.05	349.16	336.57	344.40	633.59	23.35	0.0207
372.21	351.38	355.68	354.69	343.80	351.35	535.33	25.71	0.0174
372.23	348.16	353.80	352.21	338.79	347.84	571.01	23.72	0.0223
372.21	341.95	346.83	345.65	333.27	342.05	681.90	22.54	0.0203
372.16	337.17	342.36	339.67	328.87	337.79	740.76	21.17	0.0196
372.16	333.21	339.31	336.28	323.68	333.55	774.96	19.90	0.0232

Thermocouple angles : T_{w1} = 22.5°, T_{w2} = -67.5°, T_{w3} = -157.5°, T_{w4} = 112.5°

d_w = 0.35 mm, p = 6.0 mm

$\varepsilon_{\Delta T}$ = 1.447, B = 1.211, U_v = 0.586 m/s

372.45	328.01	335.46	329.00	318.43	329.15	708.79	15.95	0.0239
372.47	330.98	338.95	332.12	321.09	331.74	676.85	16.31	0.0252
372.45	334.22	342.10	335.26	323.95	335.55	622.99	16.30	0.0249
372.45	339.99	347.22	340.99	330.45	341.30	574.40	17.70	0.0226
372.42	347.21	352.75	348.66	338.58	348.86	490.75	19.47	0.0187
372.45	343.46	349.64	345.12	334.35	344.71	525.37	18.12	0.0208
372.42	336.46	342.87	337.81	327.28	337.89	601.78	16.73	0.0214
372.42	331.87	338.48	333.20	322.56	333.25	653.30	16.11	0.0221
372.42	328.52	334.79	329.98	320.07	329.23	668.87	15.23	0.0211

Thermocouple angles : T_{w1} = 22.5°, T_{w2} = -67.5°, T_{w3} = -157.5°, T_{w4} = 112.5°

d_w = 0.4 mm, p = 1.0 mm

$\varepsilon_{\Delta T}$ = 1.366, B = 1.143, U_v = 0.580 m/s

372.59	348.80	342.16	350.93	354.89	347.21	425.71	17.89	0.0189
372.64	343.17	335.23	345.73	350.46	341.28	495.94	16.83	0.0230
372.67	338.86	330.41	341.65	346.68	336.71	545.48	16.14	0.0250
372.67	335.65	328.28	338.28	342.64	333.39	583.55	15.76	0.0226
372.64	332.89	325.37	335.51	339.97	330.71	610.31	15.35	0.0230
372.74	330.62	322.99	333.70	338.18	327.60	646.99	15.36	0.0247
372.76	333.22	325.77	336.30	340.66	330.14	617.97	15.63	0.0242
372.79	339.50	332.13	342.11	346.48	337.29	546.42	16.42	0.0222
372.88	349.59	342.75	351.74	355.82	348.04	422.76	18.15	0.0193

Thermocouple angles : T_{w1} = -157.5°, T_{w2} = -67.5°, T_{w3} = 22.5°, T_{w4} = 112.5°

d_w = 0.4 mm, p = 1.5 mm

$\varepsilon_{\Delta T}$ = 1.417, B = 1.186, U_v = 0.560 m/s

373.85	330.85	322.14	336.70	341.55	322.99	673.75	15.67	0.0350
373.76	330.56	322.31	335.51	340.18	324.26	657.32	15.22	0.0315
373.73	333.00	324.54	337.97	342.76	326.73	640.17	15.72	0.0317
373.78	335.68	325.77	340.87	346.56	329.53	616.51	16.18	0.0351
373.78	339.38	330.70	344.33	349.27	333.24	582.70	16.94	0.0315
373.83	343.48	335.06	348.18	352.98	337.71	531.39	17.51	0.0299
373.88	349.44	341.59	353.85	358.32	343.99	457.98	18.74	0.0275
373.90	351.21	343.66	355.47	359.77	345.95	438.16	19.31	0.0264
373.85	345.64	337.15	350.26	355.12	340.04	514.36	18.23	0.0297
373.80	340.93	332.22	345.84	350.80	334.88	571.04	17.37	0.0313
373.76	337.36	328.77	342.29	347.17	331.19	610.54	16.77	0.0315
373.71	334.46	325.86	339.52	344.39	328.05	637.21	16.23	0.0322
373.73	331.89	323.29	336.84	341.73	325.71	657.56	15.72	0.0321

Thermocouple angles : T_{w1} = -157.5°, T_{w2} = -67.5°, T_{w3} = 22.5°, T_{w4} = 112.5°

Test fluid – steam

d_w = 0.4 mm, p = 2.0 mm

$\varepsilon_{\Delta T}$ = 1.918, B = 1.605, U_v = 0.569 m/s

T_v / K	T_{wo} / K	T_{w1} / K	T_{w2} / K	T_{w3} / K	T_{w4} / K	q / (kW/m^2)	α / (kW/m^{2}K)	A
373.05	355.54	344.59	359.98	366.40	351.20	481.55	27.50	0.0331
373.03	350.57	337.78	355.82	363.32	345.36	571.49	25.45	0.0394
373.03	346.50	332.55	352.20	360.38	340.87	641.12	24.17	0.0434
373.05	343.34	328.95	349.32	357.75	337.33	699.58	23.54	0.0454
373.05	340.97	326.00	347.24	356.00	334.64	744.29	23.20	0.0477
373.05	338.77	323.74	345.10	353.89	332.33	776.33	22.64	0.0483
373.05	341.31	326.25	347.61	356.42	334.96	744.99	23.47	0.0479
373.10	344.22	329.20	350.41	359.22	338.07	701.37	24.29	0.0471
373.17	348.02	333.42	354.01	362.57	342.10	646.56	25.71	0.0452
373.25	352.17	338.90	357.71	365.48	346.60	578.97	27.47	0.0409
373.22	357.36	345.91	362.03	368.74	352.77	482.38	30.41	0.0345

Thermocouple angles : T_{w1} = -157.5°, T_{w2} = -67.5°, T_{w3} = 22.5°, T_{w4} = 112.5°

d_w = 0.4 mm, p = 2.5 mm

$\varepsilon_{\Delta T}$ = 1.875, B = 1.569, U_v = 0.558 m/s

373.85	357.50	348.08	360.95	366.51	354.46	483.69	29.58	0.0273
373.85	351.58	339.95	356.06	362.92	347.41	597.22	26.82	0.0349
373.83	346.90	334.65	351.98	359.16	341.81	661.14	24.55	0.0382
373.83	342.86	330.72	348.19	355.27	337.26	715.31	23.10	0.0392
373.83	339.55	327.68	344.81	351.73	333.97	765.24	22.32	0.0388
373.83	336.33	324.93	341.37	348.01	331.01	801.11	21.36	0.0376
373.83	335.24	323.72	340.17	346.90	330.15	803.97	20.83	0.0377
373.80	336.20	324.67	341.35	348.06	330.73	797.00	21.20	0.0382
373.83	339.17	327.66	344.31	351.02	333.71	760.82	21.95	0.0378
373.83	342.74	330.57	348.17	355.26	336.98	710.87	22.87	0.0395
373.83	346.94	335.35	352.13	358.88	341.42	655.89	24.40	0.0372
373.83	351.56	340.16	356.18	362.86	347.02	591.29	26.55	0.0348
373.83	357.16	347.56	360.81	366.47	353.79	474.38	28.45	0.0282

Thermocouple angles : T_{w1} = -157.5°, T_{w2} = -67.5°, T_{w3} = 22.5°, T_{w4} = 112.5°

d_w = 0.4 mm, p = 3.5 mm

$\varepsilon_{\Delta T}$ = 1.757, B = 1.471, U_v = 0.569 m/s

373.30	350.79	340.82	353.56	359.55	349.23	576.57	25.62	0.0270
373.32	345.21	334.70	348.74	354.98	342.41	635.86	22.62	0.0306
373.32	340.97	330.61	344.55	350.70	338.03	678.02	20.96	0.0309
373.32	337.97	327.43	341.63	347.88	334.93	712.96	20.17	0.0317
373.34	335.26	324.50	339.59	345.91	331.04	760.61	19.97	0.0344
373.27	355.94	346.93	358.83	364.20	353.81	494.33	28.53	0.0251
373.30	355.94	346.93	358.83	364.20	353.81	494.07	28.47	0.0251
373.34	334.02	323.02	338.39	344.86	329.82	757.68	19.27	0.0351
373.34	336.94	326.31	341.05	347.31	333.09	733.52	20.15	0.0333
373.34	340.34	329.77	344.39	350.61	336.58	694.35	21.04	0.0327
373.34	343.63	333.15	347.01	353.25	341.11	641.41	21.59	0.0303
373.34	348.21	338.66	351.29	356.98	345.88	580.48	23.09	0.0273
373.34	353.42	344.76	356.18	361.34	351.38	494.03	24.79	0.0243

Thermocouple angles : T_{w1} = -157.5°, T_{w2} = -67.5°, T_{w3} = 22.5°, T_{w4} = 112.5°

d_w = 0.4 mm, p = 4.5 mm

$\varepsilon_{\Delta T}$ = 1.674, B = 1.401, U_v = 0.569 m/s

373.51	352.36	347.82	352.62	355.46	353.54	478.49	22.62	0.0095
373.49	349.09	341.01	352.20	356.95	346.19	567.55	23.26	0.0244
373.49	343.54	334.60	346.76	352.05	340.75	640.95	21.40	0.0268
373.49	339.44	330.60	342.78	348.00	336.39	690.04	20.27	0.0273
373.49	335.98	326.52	339.57	345.15	332.69	725.97	19.36	0.0295
373.49	333.17	324.44	336.54	341.68	330.02	748.84	18.57	0.0277
373.51	330.98	322.35	334.47	339.53	327.57	770.51	18.12	0.0280
373.51	333.23	324.43	336.77	341.94	329.77	746.73	18.54	0.0283
373.51	336.29	327.45	339.92	345.10	332.70	717.08	19.27	0.0283
373.51	339.74	330.63	343.66	348.98	335.71	671.54	19.89	0.0294
373.51	343.83	334.51	347.52	352.99	340.30	621.69	20.94	0.0288
373.54	348.68	339.78	351.69	356.97	346.28	561.64	22.59	0.0257
373.54	354.89	347.24	357.58	362.11	352.65	457.13	24.52	0.0220

Thermocouple angles : T_{w1} = -157.5°, T_{w2} = -67.5°, T_{w3} = 22.5°, T_{w4} = 112.5°

Test fluid – steam

d_w = 0.4 mm, p = 6.0 mm

$\varepsilon_{\Delta T}$ = 1.585, B = 1.327, U_v = 0.575 m/s

T_v / K	T_{wo} / K	T_{w1} / K	T_{w2} / K	T_{w3} / K	T_{w4} / K	q / (kW/m^2)	α / (kW/m^{2}K)	A
372.93	353.24	345.52	355.72	360.32	351.41	450.52	22.88	0.0217
372.93	346.90	338.56	349.75	354.70	344.58	532.41	20.45	0.0243
372.96	342.66	334.40	345.96	350.81	339.46	597.87	19.73	0.0258
372.93	338.59	329.82	342.01	347.17	335.38	653.36	19.03	0.0274
372.96	335.58	326.84	339.41	344.50	331.57	690.96	18.49	0.0288
372.93	332.29	324.25	336.11	340.77	328.01	708.90	17.44	0.0276
372.96	335.15	326.82	339.14	343.97	330.69	685.42	18.13	0.0285
372.98	342.28	334.38	345.70	350.31	338.72	593.91	19.35	0.0254
373.08	353.21	346.10	355.84	360.04	350.86	445.75	22.44	0.0209

Thermocouple angles : T_{w1} = -157.5°, T_{w2} = -67.5°, T_{w3} = 22.5°, T_{w4} = 112.5°

d_w = 0.75 mm, p = 1.5 mm

$\varepsilon_{\Delta T}$ = 0.802, B = 0.671, U_v = 0.560 m/s

372.98	335.91	332.23	337.54	339.68	334.17	340.43	9.18	0.0122
372.98	329.52	325.64	331.33	333.58	327.53	379.49	8.73	0.0133
372.98	324.91	321.14	326.73	328.90	322.85	406.38	8.45	0.0133
372.98	320.72	316.88	322.73	324.93	318.35	434.07	8.31	0.0142
372.96	318.19	314.48	320.10	322.23	315.95	443.65	8.10	0.0137
372.98	316.39	312.81	318.19	320.25	314.28	454.20	8.03	0.0132
373.00	315.15	311.87	317.01	318.88	312.85	462.00	7.99	0.0128
372.93	333.57	330.33	335.16	337.03	331.78	346.35	8.80	0.0112
372.96	331.35	327.96	333.04	334.99	329.41	357.68	8.60	0.0119
372.93	327.76	324.44	329.53	331.43	325.65	382.64	8.47	0.0121
372.93	322.68	318.99	324.58	326.71	320.45	414.52	8.25	0.0135
372.93	320.15	316.88	322.00	323.86	317.86	433.31	8.21	0.0125
372.93	316.06	312.81	317.83	319.68	313.91	453.68	7.98	0.0124

Thermocouple angles : T_{w1} = -157.5°, T_{w2} = -67.5°, T_{w3} = 22.5°, T_{w4} = 112.5°

d_w = 0.75 mm, p = 2.5 mm

$\varepsilon_{\Delta T}$ = 1.292, B = 1.081, U_v = 0.571 m/s

373.15	347.03	356.02	342.55	337.37	352.17	433.32	16.59	0.0301
373.34	341.03	351.01	335.97	330.23	346.93	495.15	15.33	0.0343
373.22	336.09	346.40	330.90	324.96	342.12	547.55	14.75	0.0358
373.22	331.05	342.52	327.07	320.26	334.33	583.85	13.84	0.0353
373.22	329.32	339.88	324.16	318.06	335.18	611.38	13.93	0.0370
373.20	326.71	337.15	322.14	316.05	331.48	648.09	13.94	0.0353
373.22	324.74	335.21	320.30	314.18	329.28	670.32	13.83	0.0352
373.17	325.12	335.44	320.77	314.74	329.54	668.29	13.91	0.0346
373.13	326.38	336.83	321.94	315.83	330.92	656.95	14.05	0.0350
373.05	328.69	338.83	324.00	318.11	333.81	628.99	14.18	0.0348
373.03	331.88	342.09	326.78	320.90	337.76	595.14	14.46	0.0358
373.00	335.19	345.54	329.99	324.02	341.20	559.04	14.78	0.0361
372.93	339.78	349.81	334.70	328.92	345.68	511.44	15.43	0.0346
372.93	345.38	354.75	340.70	335.30	350.78	444.37	16.13	0.0316

Thermocouple angles : T_{w1} = 22.5°, T_{w2} = 112.5°, T_{w3} = -157.5°, T_{w4} = -67.5°

d_w = 0.75 mm, p = 3.5 mm

$\varepsilon_{\Delta T}$ = 1.741, B = 1.457, U_v = 0.555 m/s

373.15	345.44	345.76	353.94	345.44	336.61	658.46	23.76	0.0251
373.15	332.09	332.36	342.49	332.09	321.44	783.94	19.09	0.0317
373.13	337.15	337.40	347.30	337.15	326.76	725.75	20.18	0.0305
373.13	329.56	330.07	339.97	329.56	318.64	812.42	18.65	0.0324
372.76	352.10	351.94	362.28	352.10	342.08	537.06	25.99	0.0287
372.76	348.88	348.80	359.86	348.88	337.97	586.89	24.57	0.0314
372.74	342.22	342.23	354.25	342.22	330.16	674.70	22.10	0.0352
372.76	339.54	339.47	351.50	339.54	327.64	704.40	21.20	0.0351
372.74	336.24	336.26	348.30	336.24	324.16	739.70	20.27	0.0359
372.76	332.07	332.26	343.83	332.07	320.12	763.02	18.75	0.0357
372.76	330.05	330.64	341.74	330.05	317.76	779.66	18.25	0.0363

Thermocouple angles : T_{w1} = -90°, T_{w2} = 0°, T_{w3} = 90°, T_{w4} = 180°

Test fluid – steam

d_w = 0.75 mm, p = 4.5 mm

$\varepsilon_{\Delta T}$ = 1.796, B = 1.503, U_v = 0.566 m/s

T_v / K	T_{wo} / K	T_{w1} / K	T_{w2} / K	T_{w3} / K	T_{w4} / K	q / (kW/m^2)	α / (kW/m^{2}K)	A
373.39	334.68	321.73	340.85	348.35	327.81	794.04	20.51	0.0442
373.39	339.21	325.63	345.45	353.34	332.41	742.20	21.71	0.0451
373.39	343.34	329.71	348.87	356.87	337.92	679.86	22.62	0.0426
373.42	346.67	333.82	351.63	359.20	342.01	627.91	23.47	0.0391
373.39	349.44	337.24	354.20	361.38	344.94	584.65	24.41	0.0370
373.42	352.77	341.57	357.20	363.79	348.54	530.87	25.72	0.0338
373.37	355.86	345.42	359.85	366.00	352.15	480.20	27.42	0.0308
373.39	353.92	343.35	358.02	364.24	350.08	500.28	25.70	0.0316
373.39	350.39	339.25	354.89	361.42	345.99	551.55	23.98	0.0341
373.37	347.15	335.36	351.73	358.67	342.83	597.13	22.78	0.0359
373.39	344.79	332.64	349.50	356.65	340.36	634.90	22.20	0.0372
373.34	339.40	328.16	344.08	350.67	334.69	712.00	20.97	0.0359
373.37	333.66	322.44	338.06	344.65	329.48	789.30	19.88	0.0357

Thermocouple angles : T_{w1} = -157.5°, T_{w2} = -67.5°, T_{w3} = 22.5°, T_{w4} = 112.5°

d_w = 0.75 mm, p = 6.0 mm

$\varepsilon_{\Delta T}$ = 1.466, B = 1.227, U_v = 0.559 m/s

372.57	351.25	343.88	354.94	359.19	347.01	459.41	21.55	0.0245
372.57	347.74	340.00	351.55	356.01	343.37	506.37	20.39	0.0258
372.59	343.91	335.62	348.14	352.91	338.99	547.92	19.11	0.0283
372.62	338.57	323.02	343.80	353.04	334.40	599.38	17.60	0.0463
372.64	334.15	324.73	338.75	344.20	328.92	653.54	16.98	0.0325
372.69	330.86	321.95	335.52	340.64	325.35	684.71	16.37	0.0320
372.67	327.31	319.31	331.94	336.48	321.51	694.51	15.31	0.0303
372.71	349.83	342.95	353.17	357.15	346.07	465.72	20.35	0.0226
372.69	345.99	338.33	349.63	354.08	341.94	508.24	19.04	0.0253
372.71	342.23	334.20	346.01	350.66	338.06	555.55	18.23	0.0267
372.71	339.29	330.97	343.27	348.09	334.84	588.61	17.61	0.0281
372.76	333.64	325.59	337.93	342.54	328.50	631.47	16.14	0.0289
372.74	329.48	320.93	334.26	339.14	323.60	674.46	15.59	0.0317
372.71	327.34	319.27	331.90	336.49	321.71	685.68	15.11	0.0303

Thermocouple angles : T_{w1} = -157.5°, T_{w2} = -67.5°, T_{w3} = 22.5°, T_{w4} = 112.5°

d_w = 1.0 mm, p = 1.5 mm

$\varepsilon_{\Delta T}$ = 0.805, B = 0.674, U_v = 0.569 m/s

373.44	338.65	334.40	340.19	342.70	337.30	313.63	9.01	0.0129
373.44	332.51	328.48	334.16	336.52	330.89	364.47	8.91	0.0131
373.42	327.75	323.31	329.61	332.21	325.86	401.39	8.79	0.0147
373.46	324.39	320.22	326.44	328.85	322.05	417.90	8.52	0.0149
373.49	321.91	318.23	323.71	325.83	319.86	434.92	8.43	0.0132
373.51	319.82	316.44	321.56	323.51	317.79	444.75	8.28	0.0125
373.54	324.49	320.72	326.38	328.55	322.30	419.26	8.55	0.0136
373.61	339.00	334.65	340.56	343.13	337.67	315.54	9.12	0.0132

Thermocouple angles : T_{w1} = -157.5°, T_{w2} = -67.5°, T_{w3} = 22.5°, T_{w4} = 112.5°

d_w = 1.0 mm, p = 2.5 mm

$\varepsilon_{\Delta T}$ = 1.061, B = 0.888, U_v = 0.570 m/s

373.63	342.19	335.13	344.05	348.29	341.28	392.52	12.48	0.0193
373.61	335.58	328.19	337.61	342.05	334.47	459.02	12.07	0.0209
373.63	330.97	323.52	333.09	337.55	329.70	498.83	11.69	0.0215
373.59	327.66	320.24	329.81	334.25	326.32	527.11	11.48	0.0218
373.59	325.16	318.04	327.28	331.54	323.76	552.17	11.40	0.0212
373.61	323.07	316.28	325.17	329.23	321.60	568.59	11.25	0.0206
373.63	327.74	320.49	329.84	334.18	326.47	527.76	11.50	0.0213
373.61	342.12	335.35	343.90	347.98	341.25	387.13	12.29	0.0185

Thermocouple angles : T_{w1} = -157.5°, T_{w2} = -67.5°, T_{w3} = 22.5°, T_{w4} = 112.5°

Test fluid – steam

d_w = 1.0 mm, p = 3.5 mm

$\varepsilon_{\Delta T}$ = 1.315, B = 1.101, U_v = 0.576 m/s

T_v / K	T_{wo} / K	T_{w1} / K	T_{w2} / K	T_{w3} / K	T_{w4} / K	q / (kW/m^2)	α / (kW/m^{2}K)	A
373.15	348.94	339.03	352.74	358.58	345.41	400.80	16.56	0.0299
373.17	342.75	331.66	347.08	353.60	338.65	475.50	15.63	0.0343
373.17	338.64	327.44	343.37	349.92	333.85	531.47	15.39	0.0360
373.15	335.12	323.55	340.35	347.08	329.49	583.42	15.34	0.0386
373.17	332.20	320.44	337.63	344.47	326.27	620.57	15.15	0.0400
373.17	329.85	318.57	335.31	341.83	323.69	640.02	14.77	0.0393
373.27	335.12	323.44	340.37	347.16	329.51	586.17	15.36	0.0389
373.44	349.31	339.27	353.22	359.13	345.64	399.16	16.54	0.0304

Thermocouple angles : T_{w1} = -157.5°, T_{w2} = -67.5°, T_{w3} = 22.5°, T_{w4} = 112.5°

d_w = 1.0 mm, p = 4.5 mm

$\varepsilon_{\Delta T}$ = 1.508, B = 1.262, U_v = 0.574 m/s

373.00	353.27	343.70	358.36	363.85	347.18	420.03	21.29	0.0324
373.03	346.80	335.92	352.88	359.08	339.29	509.05	19.40	0.0384
373.05	341.96	331.15	348.13	354.29	334.29	573.66	18.45	0.0390
373.03	338.44	327.26	344.73	351.10	330.65	623.75	18.03	0.0405
373.03	335.14	324.01	341.41	347.75	327.40	654.99	17.29	0.0407
372.98	332.73	321.43	338.98	345.43	325.07	676.46	16.81	0.0413
373.05	338.49	327.26	344.76	351.16	330.77	623.66	18.04	0.0405
373.20	353.65	344.18	358.61	364.04	347.79	420.12	21.50	0.0318

Thermocouple angles : T_{w1} = -157.5°, T_{w2} = -67.5°, T_{w3} = 22.5°, T_{w4} = 112.5°

d_w = 1.0 mm, p = 6.0 mm

$\varepsilon_{\Delta T}$ = 1.274, B = 1.066, U_v = 0.567 m/s

373.39	348.33	339.36	351.72	357.01	345.23	418.90	16.71	0.0270
373.39	341.21	331.41	344.93	350.71	337.80	499.80	15.53	0.0301
373.42	336.78	326.78	341.01	346.85	332.47	547.41	14.94	0.0324
373.39	333.15	323.28	337.41	343.17	328.74	577.47	14.35	0.0326
373.42	330.67	320.35	334.54	340.62	327.16	602.89	14.10	0.0326
373.42	327.39	318.14	331.25	336.67	323.50	625.11	13.58	0.0307
373.42	330.16	320.83	334.29	339.72	325.82	601.13	13.90	0.0313
373.46	337.06	326.89	341.26	347.22	332.89	543.94	14.94	0.0326
373.51	348.53	339.82	351.84	356.98	345.47	414.17	16.58	0.0262

Thermocouple angles : T_{w1} = -157.5°, T_{w2} = -67.5°, T_{w3} = 22.5°, T_{w4} = 112.5°

H.4 Condensate inundation during condensation of steam

(1) Results without inundation

Test fluid – steam

Smooth tube

$\varepsilon_{\Delta T}$ = 1.000, B = 0.813, U_v = 0.566 m/s

T_v / K	T_{wo} / K	T_{w1} / K	T_{w2} / K	T_{w3} / K	T_{w4} / K	q / (kW/m^2)	α / (kW/m^{2}K)	A
372.88	361.55	361.56	360.55	361.10	362.98	169.93	14.99	0.0001
372.86	360.21	360.50	359.20	359.34	361.80	195.80	15.48	0.0001
372.86	348.95	352.66	350.36	343.72	349.06	306.36	12.81	0.0126
372.86	342.42	347.33	344.32	335.56	342.47	374.23	12.29	0.0169
372.91	329.09	334.43	330.71	322.23	328.97	471.99	10.77	0.0181
372.86	317.08	322.28	318.08	310.69	317.28	536.07	9.61	0.0174
372.86	313.01	317.92	314.57	306.63	312.95	553.11	9.24	0.0176
372.83	322.66	327.91	323.83	316.13	322.76	509.05	10.14	0.0175
372.83	334.88	340.00	336.72	328.00	334.79	433.31	11.42	0.0177
372.83	348.85	351.82	349.85	344.27	349.44	301.15	12.55	0.0102
372.81	355.75	358.42	356.68	351.73	356.18	239.90	14.06	0.0090
372.83	348.90	352.71	350.35	343.55	348.98	300.61	12.56	0.0129

Thermocouple angles : T_{w1} = 22.5°, T_{w2} = -67.5°, T_{w3} = -157.5°, T_{w4} = 112.5°

Wire-wrapped tube : d_w = 1.6 mm, p = 4.0 mm

$\varepsilon_{\Delta T}$ = 1.164, B = 0.946, U_v = 0.558 m/s

373.54	349.81	356.35	352.93	342.35	347.62	338.24	14.26	0.0214
373.51	347.11	354.87	351.14	337.74	344.70	366.71	13.89	0.0263
373.49	340.64	349.28	346.13	329.69	337.46	457.96	13.94	0.0314
373.49	333.37	342.37	338.23	322.91	329.97	524.64	13.08	0.0317
373.46	322.80	331.55	327.05	313.65	318.95	601.67	11.88	0.0304
373.46	319.80	328.29	323.46	311.09	316.34	628.73	11.71	0.0291
373.46	328.40	337.60	333.26	318.41	324.34	545.87	12.11	0.0322
373.46	338.06	347.08	343.90	327.38	333.88	466.34	13.17	0.0326
373.44	344.19	352.86	348.80	334.21	340.89	411.94	14.08	0.0294
373.46	349.83	356.50	353.35	341.11	348.35	340.36	14.40	0.0231

Thermocouple angles : T_{w1} = 22.5°, T_{w2} = -67.5°, T_{w3} = -157.5°, T_{w4} = 112.5°

Wire-wrapped tube : d_w = 1.6 mm, p = 8.0 mm

$\varepsilon_{\Delta T}$ = 1.151, B = 0.936, U_v = 0.557 m/s

373.68	345.63	351.20	348.37	338.40	344.57	385.25	13.74	0.0192
373.68	332.28	338.00	336.05	324.70	330.37	528.46	12.76	0.0218
373.68	321.89	327.28	325.02	314.78	320.50	608.83	11.76	0.0206
373.68	318.25	323.32	320.91	311.76	317.00	634.88	11.45	0.0191
373.68	327.30	333.38	330.94	319.46	325.42	563.22	12.14	0.0229
373.68	340.32	346.73	343.90	331.72	338.91	453.79	13.60	0.0232
373.68	346.92	352.61	350.13	338.90	346.02	362.05	13.53	0.0205
373.68	348.05	353.02	350.59	341.26	347.30	352.66	13.76	0.0174
373.68	336.97	343.29	340.84	328.60	335.15	479.77	13.07	0.0234
373.66	343.46	349.81	346.73	335.03	342.28	416.60	13.80	0.0224
373.66	348.26	353.24	350.82	341.51	347.47	348.56	13.72	0.0174

Thermocouple angles : T_{w1} = 22.5°, T_{w2} = -67.5°, T_{w3} = -157.5°, T_{w4} = 112.5°

Test fluid – steam

Wire-wrapped tube : d_w = 1.6 mm, p = 16.0 mm

$\varepsilon_{\Delta T}$ = 1.181, B = 0.960, U_v = 0.558 m/s

T_v / K	T_{wo} / K	T_{w1} / K	T_{w2} / K	T_{w3} / K	T_{w4} / K	q / (kW/m^2)	α / (kW/m^{2}K)	A
373.56	349.75	353.83	350.29	344.95	349.93	354.55	14.89	0.0119
373.56	348.46	353.16	349.12	342.94	348.62	372.10	14.82	0.0138
373.54	341.57	347.33	342.80	334.83	341.31	456.87	14.29	0.0177
373.51	333.53	338.77	335.00	327.29	333.07	531.91	13.30	0.0170
373.51	328.05	332.90	329.44	322.16	327.69	562.13	12.36	0.0161
373.51	319.00	322.48	319.51	314.01	320.00	628.17	11.52	0.0120
373.46	323.49	327.12	324.35	318.39	324.11	600.78	12.02	0.0126
373.49	337.91	342.89	339.47	331.53	337.76	475.55	13.37	0.0165
373.46	344.78	349.67	345.97	338.48	344.98	423.00	14.74	0.0155
373.46	349.08	352.76	350.07	344.18	349.32	352.98	14.48	0.0118
373.61	350.83	354.37	352.19	345.79	350.98	338.16	14.85	0.0120
373.63	351.74	356.10	352.18	346.79	351.89	351.52	16.05	0.0124

Thermocouple angles : T_{w1} = 22.5°, T_{w2} = -67.5°, T_{w3} = -157.5°, T_{w4} = 112.5°

Low integral-finned tube : h = 1.6 mm, t = 0.5 mm, s = 1.5 mm

$\varepsilon_{\Delta T}$ = 3.007, B = 2.445, U_v = 0.555 m/s

373.49	365.59	370.56	362.26	359.98	369.57	423.58	53.63	0.0172
373.51	365.16	370.58	361.68	358.84	369.52	439.15	52.56	0.0190
373.49	356.00	365.38	350.16	344.94	363.53	747.92	42.77	0.0337
373.49	346.16	358.33	338.72	331.79	355.80	1027.81	37.61	0.0449
373.46	349.85	361.20	342.99	336.77	358.45	914.95	38.75	0.0407
373.46	361.21	368.15	357.12	352.87	366.68	580.75	47.37	0.0246

Thermocouple angles : T_{w1} = 22.5°, T_{w2} = 112.5°, T_{w3} = -157.5°, T_{w4} = -67.5°

Low integral-finned tube : h = 1.6 mm, t = 0.5 mm, s = 1.5 mm

$\varepsilon_{\Delta T}$ = 2.897, B = 2.355, U_v = 0.553 m/s

373.51	366.13	370.73	363.40	360.70	369.69	388.39	52.61	0.0159
373.51	356.60	364.59	351.60	346.45	363.77	685.16	40.51	0.0300
373.51	347.93	359.35	341.52	333.42	357.42	941.32	36.79	0.0432
373.49	345.37	357.17	338.60	330.38	355.32	1017.22	36.17	0.0451
373.46	353.16	362.59	347.41	341.37	361.29	788.93	38.86	0.0353
373.51	361.75	368.53	358.18	353.46	366.82	574.53	48.83	0.0238
373.51	366.42	370.86	363.79	361.04	370.01	368.26	51.94	0.0156
373.49	366.44	370.95	363.88	360.99	369.94	368.76	52.34	0.0157
373.46	364.92	369.67	361.89	359.12	369.00	415.33	48.60	0.0171

Thermocouple angles : T_{w1} = 22.5°, T_{w2} = 112.5°, T_{w3} = -157.5°, T_{w4} = -67.5°

(2) Results with inundation

Test fluid – steam
Smooth tube
U_v = 0.576 m/s, $\dot{V}_c$ = 2.0 l/min

$\dot{m}_{inun}$ / (g/s)	T^*_{inun} / K	T_v / K	T_{wo} / K	T_{w1} / K	T_{w2} / K	T_{w3} / K	T_{w4} / K	q / (kW/m^2)	α / (kW/m^{2}K)	A
0.000	372.86	373.08	348.90	352.71	350.35	343.55	348.98	300.61	12.43	0.0129
1.610	363.84	373.05	343.66	346.84	344.39	339.77	343.64	269.38	9.16	0.0099
3.221	361.63	373.03	342.02	344.51	342.73	338.91	341.92	250.03	8.06	0.0080
4.834	361.15	373.00	340.66	343.32	341.25	337.49	340.57	246.34	7.62	0.0083
6.448	360.85	372.98	339.38	341.48	339.55	336.88	339.60	234.12	6.97	0.0062
8.060	360.34	372.96	339.38	341.50	339.28	337.60	339.16	232.35	6.92	0.0054
9.671	359.88	372.96	339.58	342.06	339.24	337.39	339.63	229.75	6.88	0.0061
9.671	360.26	372.96	339.50	341.80	339.47	337.35	339.37	230.85	6.90	0.0061
11.282	360.08	372.93	339.85	342.11	339.73	337.73	339.82	224.86	6.80	0.0059
14.508	360.22	372.93	339.26	341.99	338.76	337.29	338.98	224.35	6.66	0.0063

Thermocouple angles : T_{w1} = 22.5°, T_{w2} = -67.5°, T_{w3} = -157.5°, T_{w4} = 112.5°

Wire-wrapped tube : d_w = 1.6 mm, p = 4 mm
U_v = 0.567 m/s, $\dot{V}_c$ = 2.0 l/min

0.000	373.39	373.44	351.26	357.24	354.23	342.98	350.58	358.80	16.17	0.0207
1.606	365.20	373.44	351.44	356.35	353.25	344.78	351.39	343.53	15.62	0.0162
2.891	365.16	373.44	351.34	356.28	353.18	344.57	351.35	344.47	15.59	0.0164
5.141	364.79	373.44	350.81	355.25	352.73	344.10	351.14	341.12	15.07	0.0156
7.229	365.01	373.44	350.87	355.06	352.03	345.42	350.95	341.63	15.14	0.0133
8.676	364.92	373.42	350.73	354.30	352.24	345.36	351.01	343.47	15.14	0.0124
10.925	364.86	373.42	350.61	354.37	351.70	345.71	350.69	325.83	14.29	0.0120
13.016	364.86	373.42	349.97	353.27	351.42	344.93	350.26	327.79	13.98	0.0116

Thermocouple angles : T_{w1} = 22.5°, T_{w2} = -67.5°, T_{w3} = -157.5°, T_{w4} = 112.5°

Wire-wrapped tube : d_w = 1.6 mm, p = 4 mm
U_v = 0.566 m/s, $\dot{V}_c$ = 2.0 l/min

0.000	373.56	373.66	350.69	357.27	353.25	341.92	350.32	365.10	15.89	0.0218
1.446	364.68	373.68	350.61	355.98	352.40	343.67	350.40	347.24	15.05	0.0173
3.053	364.91	373.68	349.88	355.00	351.76	342.67	350.10	348.79	14.65	0.0172
4.982	364.82	373.71	349.50	354.31	351.16	342.45	350.08	344.68	14.24	0.0163
6.267	364.60	373.66	349.75	354.19	351.42	343.22	350.17	344.64	14.42	0.0152
8.356	364.60	373.59	349.87	354.41	350.99	343.83	350.25	339.88	14.33	0.0144
9.481	364.75	373.63	349.46	353.61	350.15	344.55	349.53	339.82	14.06	0.0123
11.410	364.63	373.63	349.32	353.29	350.21	344.05	349.73	331.78	13.65	0.0125
12.856	364.40	373.66	349.32	353.20	350.12	344.11	349.85	332.96	13.68	0.0122

Thermocouple angles : T_{w1} = 22.5°, T_{w2} = -67.5°, T_{w3} = -157.5°, T_{w4} = 112.5°

Wire-wrapped tube : d_w = 1.6 mm, p = 8 mm
U_v = 0.566 m/s, $\dot{V}_c$ = 2.0 l/min

0.000	373.54	373.66	348.26	353.24	350.82	341.51	347.47	348.56	13.72	0.0174
1.607	364.08	373.66	348.48	351.97	349.85	344.06	348.02	332.54	13.20	0.0115
3.054	364.14	373.63	348.09	351.39	349.37	343.86	347.76	331.62	12.98	0.0109
4.823	364.08	373.63	347.97	351.30	348.83	344.07	347.70	324.43	12.64	0.0102
6.431	363.92	373.63	347.71	350.66	348.71	344.17	347.29	320.38	12.36	0.0094
8.040	363.97	373.63	347.14	349.66	347.73	343.98	347.20	316.59	11.95	0.0078
9.650	363.74	373.61	346.53	348.81	347.01	343.86	346.43	315.57	11.65	0.0069
11.259	363.50	373.63	346.35	348.60	346.68	343.91	346.20	306.41	11.23	0.0065
12.866	363.44	373.63	346.71	348.94	347.29	344.30	346.32	302.97	11.25	0.0067

Thermocouple angles : T_{w1} = 22.5°, T_{w2} = -67.5°, T_{w3} = -157.5°, T_{w4} = 112.5°

Test fluid – steam
Wire-wrapped tube : d_w = 1.6 mm, p = 8 mm
U_v = 0.566 m/s, $\dot{V}_c$ = 2.0 l/min

$\dot{m}_{inun}$ / (g/s)	T^*_{inun} / K	T_v / K	T_{wo} / K	T_{w1} / K	T_{w2} / K	T_{w3} / K	T_{w4} / K	q / (kW/m^2)	α / (kW/m^{2}K)	A
0.000	373.42	373.63	348.52	353.60	350.96	341.70	347.81	342.84	13.65	0.0175
1.447	364.26	373.63	348.75	352.11	350.33	344.36	348.19	331.29	13.31	0.0114
3.054	364.17	373.63	348.53	351.92	349.66	344.51	348.05	326.63	13.01	0.0107
5.466	363.88	373.63	347.90	351.14	348.85	344.12	347.48	319.53	12.42	0.0101
7.235	363.98	373.63	347.70	350.67	348.41	344.25	347.49	316.79	12.22	0.0090
8.844	363.93	373.61	347.12	349.41	347.82	344.24	347.03	314.45	11.87	0.0073
10.615	363.57	373.61	346.48	349.14	346.64	343.76	346.38	309.37	11.40	0.0073
12.062	363.40	373.61	346.77	349.16	347.33	344.25	346.35	302.59	11.27	0.0071
13.351	363.28	373.61	346.13	348.77	347.02	343.84	344.88	302.15	10.99	0.0078

Thermocouple angles : T_{w1} = 22.5°, T_{w2} = -67.5°, T_{w3} = -157.5°, T_{w4} = 112.5°

Wire-wrapped tube : d_w = 1.6 mm, p = 16 mm
U_v = 0.568 m/s, $\dot{V}_c$ = 2.0 l/min

0.000	373.54	373.46	349.08	352.76	350.07	344.18	349.32	352.98	14.48	0.0118
1.447	364.28	373.39	347.31	349.93	347.93	343.43	347.96	333.12	12.77	0.0086
3.379	363.55	373.37	345.50	347.81	345.86	342.39	345.95	316.53	11.36	0.0072
4.828	362.98	373.37	344.45	346.79	344.82	341.47	344.72	304.81	10.54	0.0072
6.438	362.64	373.34	344.58	347.63	344.58	341.43	344.70	299.75	10.42	0.0083
8.210	362.56	373.34	343.60	345.38	343.40	341.29	344.32	295.70	9.94	0.0050
9.981	362.20	373.32	343.43	345.08	343.37	341.11	344.19	288.33	9.65	0.0049
11.592	362.15	373.32	343.25	344.99	343.19	341.21	343.62	280.42	9.33	0.0048
4.162	369.16	372.54	364.93	368.84	362.43	360.12	368.36	398.07	52.31	0.0142
3.842	369.04	372.52	365.01	368.77	362.71	360.11	368.45	397.89	52.99	0.0140
5.443	369.42	372.50	365.01	368.56	362.68	360.34	368.46	395.30	52.80	0.0134
7.204	369.59	372.50	364.98	368.26	362.69	360.62	368.36	393.76	52.41	0.0126
8.804	369.79	372.47	365.05	368.21	362.91	361.01	368.07	389.93	52.55	0.0118
10.405	369.83	372.47	364.99	367.92	362.97	361.12	367.96	388.12	51.90	0.0112
12.327	370.29	372.45	364.92	367.49	363.23	361.47	367.49	385.77	51.24	0.0099

Thermocouple angles : T_{w1} = 22.5°, T_{w2} = 112.5°, T_{w3} = -157.5°, T_{w4} = -67.5°

Low integral-finned tube : h = 1.6 mm, t = 0.5 mm, s = 1.5 mm
U_v = 0.586 m/s, $\dot{V}_c$ = 2.0 l/min $\left(T^*_{inun} = \frac{5}{8}T_v + \frac{3}{8}T_{wo}\right)$

0.000	372.64	372.40	364.98	369.57	362.24	359.16	368.95	382.50	51.57	0.0167
2.721	368.36	372.40	365.36	369.06	362.89	360.86	368.65	380.94	54.15	0.0134
4.642	369.23	372.40	365.39	368.91	363.15	360.74	368.77	380.40	54.28	0.0133
6.723	369.71	372.37	365.41	368.65	363.23	361.2	368.55	381.39	54.75	0.0122
8.003	369.71	372.37	365.51	368.80	363.30	361.33	368.61	382.27	55.68	0.0122

Thermocouple angles : T_{w1} = 22.5°, T_{w2} = 112.5°, T_{w3} = -157.5°, T_{w4} = -67.5°

Low integral-finned tube : h = 1.6 mm, t = 0.5 mm, s = 1.5 mm
U_v = 0.588 m/s, $\dot{V}_c$ = 2.0 l/min, $\left(T^*_{inun} = \frac{5}{8}T_v + \frac{3}{8}T_{w3}\right)$

0.000	372.67	372.47	365.25	369.89	362.42	359.51	369.17	379.27	52.50	0.0167
3.201	365.80	372.45	365.27	369.00	362.90	360.40	368.78	375.05	52.26	0.0140
4.802	366.09	372.47	365.45	368.91	363.00	361.20	368.69	371.67	52.94	0.0127
6.402	366.77	372.47	365.47	368.89	363.15	361.32	368.52	371.60	53.06	0.0124
8.003	367.27	372.47	365.33	368.89	363.10	361.03	368.31	367.23	51.42	0.0127
9.603	367.25	372.47	365.57	368.52	363.63	361.80	368.33	366.62	53.10	0.0110
11.525	367.61	372.47	365.28	368.11	363.31	361.72	367.99	366.34	50.96	0.0105

Thermocouple angles : T_{w1} = 22.5°, T_{w2} = 112.5°, T_{w3} = -157.5°, T_{w4} = -67.5°

H.5 Marangoni condensation of steam-ethanol mixtures

Test fluid – steam-ethanol mixtures

C_{iL} = 0.05%, C_L = 0.12%, C_v = 1.44%, U_v = 0.154 m/s

T_v / K	T_{wo} / K	T_{w1} / K	T_{w2} / K	T_{w3} / K	T_{w4} / K	q / (kW/m^2)	α / (kW/m^{2}K)	ε_{Ma}	A
372.91	324.32	333.52	327.55	316.34	319.88	453.17	9.33	0.89	0.0282
372.91	326.81	334.49	332.19	318.60	321.94	462.58	10.03	0.94	0.0275
372.91	332.17	337.56	337.20	324.19	329.71	438.52	10.76	0.97	0.0221
372.91	340.20	349.37	344.58	330.85	335.99	426.05	13.03	1.09	0.0290
372.91	352.14	356.64	359.24	345.05	347.63	401.58	19.34	1.41	0.0206
372.91	356.68	361.66	361.20	349.30	354.56	378.08	23.30	1.58	0.0188
372.91	363.90	366.93	366.64	359.22	362.79	324.76	36.04	2.09	0.0114
372.91	367.20	369.27	368.23	364.56	366.76	256.07	44.90	2.32	0.0065
372.91	371.09	371.79	371.55	369.79	371.24	92.77	51.08	1.97	0.0026
372.88	369.60	370.45	369.77	368.18	369.99	152.00	46.26	2.08	0.0026
372.91	366.51	368.69	367.48	363.89	365.99	292.16	45.67	2.43	0.0066
372.91	360.64	366.58	364.72	354.01	357.26	383.11	31.23	1.97	0.0194
372.91	357.70	365.27	362.49	348.93	354.10	407.20	26.77	1.79	0.0247
372.91	348.87	358.60	354.99	338.74	343.14	435.27	18.11	1.38	0.0317
372.91	337.48	346.50	342.13	327.14	334.17	456.22	12.88	1.10	0.0300
372.91	330.83	338.08	335.05	323.01	327.19	468.14	11.13	1.01	0.0247
372.91	326.07	332.48	332.07	318.06	321.67	466.71	9.96	0.94	0.0256

C_{iL} = 0.05%, C_L = 0.09%, C_v = 1.02%, U_v = 0.155 m/s

373.03	331.68	341.57	337.74	320.72	326.70	455.98	11.03	1.00	0.0342
373.03	334.52	342.34	341.11	324.27	330.35	450.01	11.68	1.03	0.0300
373.05	340.70	350.70	347.86	328.63	335.61	437.48	13.52	1.13	0.0355
373.05	348.78	357.53	355.60	337.61	344.37	431.51	17.78	1.35	0.0314
373.05	358.38	366.16	362.76	350.68	353.93	386.32	26.33	1.74	0.0239
373.05	361.95	366.68	365.69	355.44	359.98	353.61	31.84	1.95	0.0167
373.05	366.47	369.09	368.03	362.82	365.95	290.74	44.20	2.36	0.0087
373.05	368.09	369.84	368.97	365.62	367.93	223.39	45.01	2.24	0.0056
373.05	371.29	371.80	371.41	370.49	371.46	88.92	50.47	1.93	0.0015
373.05	369.99	370.51	370.10	369.11	370.27	143.77	47.00	2.07	0.0016
373.05	367.28	369.52	368.51	364.14	366.94	254.04	44.01	2.28	0.0073
373.05	363.85	367.11	367.06	358.97	362.24	332.27	36.10	2.11	0.0124
373.05	360.64	365.92	365.78	353.45	357.42	372.11	29.99	1.89	0.0196
373.05	353.35	360.94	361.59	343.33	347.54	408.87	20.75	1.49	0.0295
373.05	345.12	355.74	350.07	333.05	341.60	436.40	15.62	1.24	0.0339
373.05	339.22	351.52	346.00	327.01	332.36	450.21	13.31	1.12	0.0398
373.05	332.62	342.11	338.71	323.02	326.66	452.80	11.20	1.00	0.0323

Thermocouple angles : T_{w1} = 22.5°, T_{w2} = -67.5°, T_{w3} = -157.5°, T_{w4} = 112.5°

Test fluid – steam-ethanol mixtures

C_{iL} = 0.05%, C_L = 0.14%, C_v = 1.59%, U_v = 0.245 m/s

T_v / K	T_{wo} / K	T_{w1} / K	T_{w2} / K	T_{w3} / K	T_{w4} / K	q / (kW/m^2)	α / (kW/m^{2}K)	ε_{Ma}	A
373.05	327.92	335.39	332.30	320.27	323.72	600.26	13.30	1.22	0.0255
373.05	331.34	338.09	335.94	323.47	327.87	551.70	13.23	1.18	0.0242
373.03	335.83	343.89	340.25	326.73	332.46	524.83	14.11	1.21	0.0271
373.05	347.39	357.13	355.16	335.72	341.55	522.65	20.37	1.56	0.0347
373.05	358.30	363.90	363.20	349.75	356.37	454.98	30.85	2.02	0.0211
373.05	361.38	365.78	364.24	355.84	359.64	430.09	36.84	2.27	0.0146
373.05	365.69	367.90	367.27	362.54	365.05	349.83	47.51	2.60	0.0076
373.05	367.91	369.61	368.52	365.82	367.68	266.64	51.80	2.59	0.0050
373.05	371.36	372.18	371.53	370.30	371.41	93.57	55.11	2.09	0.0023
373.05	369.88	370.75	369.93	369.04	369.81	170.29	53.71	2.37	0.0021
373.05	368.21	369.79	368.63	366.36	368.05	274.98	56.78	2.79	0.0045
373.05	363.53	367.86	365.86	358.49	361.89	410.24	43.06	2.51	0.0135
373.05	360.49	365.36	364.45	353.19	358.96	443.05	35.26	2.21	0.0178
373.05	353.50	361.35	360.58	343.15	348.94	503.11	25.74	1.82	0.0290
373.05	344.08	354.46	351.77	332.00	338.10	543.05	18.74	1.49	0.0365
373.03	335.15	342.66	339.56	326.58	331.81	546.04	14.42	1.24	0.0257
373.03	330.30	338.35	334.30	322.41	326.12	567.94	13.29	1.20	0.0262

C_{iL} = 0.05%, C_L = 0.07%, C_v = 0.79%, U_v = 0.246 m/s

373.27	335.88	343.69	342.61	325.31	331.92	549.61	14.70	1.26	0.0302
373.27	341.84	353.04	348.21	329.92	336.17	559.16	17.79	1.44	0.0368
373.27	347.73	358.24	355.06	335.98	341.62	543.22	21.27	1.62	0.0357
373.32	353.06	361.45	360.10	342.04	348.66	508.86	25.12	1.79	0.0305
373.32	361.30	367.61	365.92	353.14	358.55	433.08	36.04	2.23	0.0216
373.32	364.17	368.40	366.83	358.76	362.66	391.14	42.73	2.47	0.0139
373.32	367.64	369.81	368.43	364.62	367.68	309.79	54.52	2.79	0.0067
373.32	369.01	370.37	369.38	366.99	369.31	243.72	56.58	2.70	0.0041
373.32	371.63	372.03	371.86	370.84	371.79	96.39	57.00	2.15	0.0015
373.32	370.07	371.00	370.32	368.56	370.42	165.52	50.97	2.27	0.0029
373.32	368.43	370.23	368.95	365.67	368.88	275.60	56.38	2.78	0.0056
373.30	365.88	369.09	367.60	362.24	364.60	368.16	49.68	2.72	0.0099
373.30	362.91	367.67	366.68	357.21	360.08	414.88	39.95	2.38	0.0162
373.30	358.25	367.24	362.44	348.16	355.18	473.42	31.48	2.07	0.0276
373.30	349.78	358.33	358.24	337.69	344.87	522.08	22.20	1.65	0.0333
373.30	339.96	351.39	346.99	328.15	333.33	560.10	16.80	1.39	0.0380
373.30	335.46	345.66	341.86	324.37	329.97	554.78	14.66	1.26	0.0349

C_{iL} = 0.05%, C_L = 0.09%, C_v = 1.00%, U_v = 0.353 m/s

373.15	341.29	353.89	347.81	328.08	335.38	721.49	22.65	1.82	0.0406
373.15	346.22	358.28	351.64	331.77	343.20	706.67	26.24	2.00	0.0387
373.15	352.05	362.62	357.69	338.88	348.99	678.51	32.15	2.29	0.0347
373.15	358.85	365.86	363.31	348.13	358.11	606.77	42.44	2.72	0.0247
373.15	364.75	368.06	366.42	359.75	364.76	493.89	58.78	3.29	0.0110
373.15	366.21	368.72	367.03	362.95	366.13	437.35	62.99	3.36	0.0075
373.15	367.97	369.56	368.26	365.75	368.31	329.39	63.59	3.15	0.0046
373.15	369.08	370.31	369.32	367.19	369.51	245.68	60.39	2.82	0.0037
373.15	371.33	371.57	371.57	370.61	371.55	97.71	53.58	2.05	0.0012
373.15	369.66	370.98	370.30	366.70	370.64	146.53	41.95	1.89	0.0050
373.13	369.12	370.33	369.32	367.34	369.51	266.13	66.49	3.10	0.0035
373.13	366.84	368.92	367.57	363.88	367.01	393.07	62.58	3.26	0.0064
373.13	365.93	368.61	366.97	361.95	366.19	450.36	62.59	3.37	0.0085
373.15	362.13	367.32	365.39	353.96	361.87	541.26	49.13	2.94	0.0182
373.15	355.92	364.13	362.03	343.75	353.78	638.16	37.04	2.49	0.0298
373.15	351.21	362.64	357.54	337.48	347.18	697.80	31.80	2.29	0.0375
373.15	345.29	357.63	351.98	331.38	340.19	722.32	25.93	2.00	0.0403

Thermocouple angles : T_{w1} = 22.5°, T_{w2} = -67.5°, T_{w3} = -157.5°, T_{w4} = 112.5°

Test fluid – steam-ethanol mixtures

C_{iL} = 0.05%, C_L = 0.07%, C_v = 0.83%, U_v = 0.352 m/s

T_v / K	T_{wo} / K	T_{w1} / K	T_{w2} / K	T_{w3} / K	T_{w4} / K	q / (kW/m^2)	α / (kW/m^{2}K)	ε_{Ma}	A
373.30	345.25	357.90	353.09	330.39	339.62	702.58	25.05	1.93	0.0428
373.30	349.11	360.66	356.21	335.37	344.21	685.97	28.37	2.10	0.0387
373.30	354.23	364.38	360.19	341.00	351.36	635.88	33.36	2.31	0.0341
373.32	358.88	366.69	364.50	346.96	357.35	563.04	38.99	2.50	0.0282
373.30	365.52	368.75	367.11	360.61	365.62	461.23	59.35	3.26	0.0107
373.30	366.73	369.23	367.64	362.84	367.23	403.02	61.43	3.23	0.0080
373.30	368.94	369.90	368.81	368.18	368.88	307.80	70.73	3.36	0.0021
373.30	369.38	370.71	369.63	367.55	369.65	234.27	59.91	2.77	0.0038
373.30	371.62	372.02	371.80	370.88	371.80	94.07	56.27	2.11	0.0014
373.30	370.26	370.88	370.44	369.02	370.71	150.17	49.47	2.15	0.0021
373.30	368.80	370.18	369.19	366.41	369.40	269.59	59.91	2.87	0.0044
373.30	367.56	369.46	368.23	364.34	368.23	368.63	64.31	3.27	0.0062
373.30	366.80	369.09	367.50	363.13	367.50	424.62	65.43	3.43	0.0072
373.30	362.84	367.98	365.98	354.65	362.73	513.56	49.10	2.90	0.0180
373.30	357.14	365.89	363.21	344.94	354.53	597.72	37.01	2.45	0.0306
373.30	353.01	363.86	358.88	338.94	350.34	669.68	33.01	2.32	0.0360
373.30	347.32	360.05	354.40	332.22	342.62	679.73	26.17	1.97	0.0421
C_{iL} = 0.05%, C_L = 0.09%, C_v = 1.05%, U_v = 0.568 m/s									
373.13	343.27	355.16	350.19	330.71	337.02	844.45	28.28	2.15	0.0389
373.13	349.55	359.93	354.66	335.55	348.07	828.44	35.15	2.50	0.0346
373.13	355.59	363.72	359.90	343.59	355.16	768.97	43.86	2.89	0.0277
373.13	360.72	366.58	363.77	351.14	361.38	673.94	54.32	3.28	0.0203
373.13	365.00	368.14	365.94	360.57	365.34	541.21	66.60	3.62	0.0096
373.13	366.05	368.37	366.61	362.94	366.27	466.06	65.83	3.47	0.0068
373.10	368.04	369.73	368.25	366.20	367.99	353.86	69.95	3.40	0.0044
373.13	369.04	370.50	369.65	366.83	369.19	255.22	62.50	2.88	0.0047
373.13	371.64	372.10	371.76	371.06	371.64	95.38	64.02	2.32	0.0013
373.13	369.85	371.04	370.09	368.16	370.12	189.34	57.82	2.53	0.0035
373.10	368.63	369.84	368.92	366.75	368.99	305.97	68.39	3.23	0.0037
373.10	367.05	368.93	367.38	364.71	367.19	425.62	70.34	3.57	0.0053
373.15	366.21	368.56	366.75	363.04	366.49	497.64	71.72	3.76	0.0069
373.15	363.91	367.60	365.39	358.16	364.49	592.16	64.10	3.60	0.0120
373.15	358.78	365.73	362.65	348.00	358.75	718.50	50.01	3.13	0.0240
373.15	353.58	363.52	356.40	341.01	353.39	803.19	41.04	2.78	0.0301
373.15	349.73	361.08	354.97	335.91	346.96	852.77	36.41	2.58	0.0364
C_{iL} = 0.05%, C_L = 0.14%, C_v = 1.57%, U_v = 0.762 m/s									
373.08	341.33	350.63	348.51	330.72	335.46	862.83	27.18	2.04	0.0331
373.10	347.15	356.97	353.46	334.49	343.65	866.19	33.37	2.37	0.0341
373.10	353.78	361.89	357.92	341.37	353.93	819.49	42.40	2.79	0.0279
373.10	359.65	365.32	361.74	350.24	361.30	719.03	53.46	3.22	0.0189
373.10	364.36	367.22	364.69	360.38	365.13	598.33	68.41	3.72	0.0082
373.10	365.11	367.22	365.34	362.11	365.75	520.47	65.10	3.47	0.0061
373.10	367.27	369.12	367.16	365.04	367.74	394.58	67.63	3.35	0.0047
373.10	368.55	369.80	368.60	367.03	368.79	292.77	64.37	3.01	0.0033
373.10	371.62	372.16	371.68	371.10	371.53	104.74	70.66	2.54	0.0014
373.10	370.81	371.64	370.89	369.95	370.77	137.33	59.93	2.38	0.0021
373.10	368.44	369.77	368.58	366.73	368.68	336.91	72.27	3.40	0.0037
373.08	366.38	368.40	366.42	364.04	366.66	473.02	70.63	3.61	0.0052
373.08	365.50	367.86	365.77	362.37	365.98	539.42	71.16	3.74	0.0066
373.08	363.19	366.36	364.17	357.98	364.26	640.49	64.79	3.63	0.0102
373.08	357.51	364.78	360.93	346.16	358.18	762.47	48.99	3.06	0.0246
373.08	352.20	361.16	357.56	340.24	349.84	850.67	40.75	2.73	0.0306
373.08	344.99	355.29	352.43	333.48	338.74	877.67	31.25	2.26	0.0355

Thermocouple angles : T_{w1} = 22.5°, T_{w2} = -67.5°, T_{w3} = -157.5°, T_{w4} = 112.5°

Test fluid – steam-ethanol mixtures

C_{iL} = 0.05%, C_L = 0.06%, C_v = 0.72%, U_v = 0.761 m/s

T_v / K	T_{wo} / K	T_{w1} / K	T_{w2} / K	T_{w3} / K	T_{w4} / K	q / (kW/m^2)	α / (kW/m^{2}K)	ε_{Ma}	A
373.32	348.53	360.96	355.14	334.56	343.45	864.55	34.87	2.44	0.0401
373.32	354.14	363.58	358.60	339.91	354.47	837.04	43.64	2.86	0.0320
373.32	358.55	365.20	361.88	347.93	359.21	770.15	52.16	3.21	0.0228
373.32	362.43	367.24	364.76	354.77	362.95	648.87	59.59	3.41	0.0163
373.32	365.92	368.52	366.66	361.82	366.68	519.13	70.16	3.67	0.0082
373.32	366.58	368.85	367.06	363.18	367.23	434.79	64.52	3.30	0.0068
373.32	368.58	369.88	368.62	366.93	368.89	334.36	70.53	3.33	0.0035
373.32	369.43	370.71	369.67	367.71	369.62	253.37	65.07	2.93	0.0037
373.32	371.59	371.79	371.69	371.16	371.69	102.78	59.28	2.21	0.0008
373.32	370.34	371.21	370.43	369.08	370.63	169.07	56.67	2.40	0.0025
373.32	369.10	370.30	369.17	367.65	369.29	291.35	69.08	3.17	0.0032
373.32	367.68	369.43	368.03	365.40	367.86	409.86	72.71	3.57	0.0050
373.32	366.77	368.98	367.39	363.51	367.19	478.19	72.97	3.71	0.0068
373.32	365.08	368.13	366.18	360.83	365.17	571.11	69.30	3.72	0.0094
373.32	361.01	366.87	364.10	351.69	361.36	704.68	57.23	3.37	0.0201
373.32	357.43	365.30	361.95	345.41	357.04	796.56	50.12	3.14	0.0273
373.32	353.59	363.81	359.65	339.92	350.99	854.75	43.33	2.86	0.0347
C_{iL} = 0.10%, C_L = 0.20%, C_v = 2.35%, U_v = 0.154 m/s									
372.76	328.91	339.07	334.25	318.90	323.43	488.86	11.15	1.03	0.0335
372.76	331.95	341.64	339.83	322.05	324.29	475.89	11.66	1.05	0.0350
372.76	338.63	349.42	345.19	327.53	332.39	483.70	14.17	1.20	0.0359
372.76	346.00	351.79	353.52	337.89	340.78	455.57	17.02	1.34	0.0246
372.76	357.00	363.75	361.96	349.84	352.44	406.80	25.80	1.74	0.0223
372.76	361.42	364.36	364.39	357.50	359.43	368.21	32.46	2.00	0.0110
372.76	365.82	367.63	366.45	363.84	365.36	308.52	44.45	2.41	0.0052
372.74	367.50	368.58	367.71	366.24	367.47	238.26	45.50	2.30	0.0030
372.74	370.51	371.22	370.81	369.62	370.37	89.32	40.03	1.63	0.0021
372.76	369.04	369.79	369.28	368.07	369.01	134.57	36.14	1.67	0.0022
372.74	367.38	368.78	368.00	365.64	367.09	238.91	44.57	2.26	0.0043
372.74	362.63	365.30	365.32	360.51	359.38	352.26	34.84	2.09	0.0089
372.71	358.22	362.21	363.67	352.94	354.05	386.42	26.66	1.76	0.0164
372.71	352.01	359.76	358.10	343.36	346.80	440.88	21.29	1.55	0.0267
372.71	342.67	350.35	350.23	332.65	337.46	471.65	15.70	1.28	0.0299
372.71	335.70	345.53	340.21	325.13	331.91	484.60	13.09	1.14	0.0318
372.71	329.71	338.99	335.71	319.60	324.51	477.41	11.10	1.02	0.0325
C_{iL} = 0.10%, C_L = 0.17%, C_v = 1.99%, U_v = 0.152 m/s									
373.17	331.37	341.38	339.52	320.57	324.00	503.31	12.04	1.09	0.0366
373.15	334.75	345.23	343.47	324.08	326.24	471.99	12.29	1.08	0.0377
373.15	340.81	350.86	346.24	329.68	336.45	472.51	14.61	1.22	0.0331
373.15	348.24	356.54	354.28	340.07	342.07	458.31	18.40	1.41	0.0276
373.15	357.69	363.82	363.17	352.15	351.62	402.49	26.04	1.74	0.0205
373.15	362.67	366.68	365.18	359.28	359.52	358.02	34.15	2.06	0.0120
373.15	366.46	368.25	367.26	364.65	365.69	300.66	44.94	2.41	0.0052
373.15	367.99	369.10	368.69	366.45	367.73	236.36	45.84	2.30	0.0037
373.15	370.88	371.60	371.19	369.84	370.88	88.42	38.91	1.59	0.0023
373.15	369.43	370.13	369.65	368.56	369.39	141.62	38.11	1.76	0.0020
373.15	367.22	368.71	367.82	365.67	366.66	271.32	45.72	2.38	0.0043
373.15	363.99	366.68	366.10	361.65	361.52	348.45	38.04	2.22	0.0085
373.15	360.96	365.08	364.07	356.70	357.98	377.76	30.99	1.95	0.0135
373.15	351.02	357.53	356.79	344.43	345.34	427.60	19.33	1.43	0.0227
373.15	343.45	350.33	348.05	335.87	339.53	472.56	15.91	1.29	0.0234
373.15	336.61	345.20	344.87	327.09	329.29	481.82	13.19	1.14	0.0325
373.15	332.15	341.99	338.82	322.90	324.87	491.03	11.98	1.08	0.0335

Thermocouple angles : T_{w1} = 22.5°, T_{w2} = -67.5°, T_{w3} = -157.5°, T_{w4} = 112.5°

Test fluid – steam-ethanol mixtures

C_{iL} = 0.10%, C_L = 0.18%, C_v = 2.12%, U_v = 0.246 m/s

T_v / K	T_{wo} / K	T_{w1} / K	T_{w2} / K	T_{w3} / K	T_{w4} / K	q / (kW/m^2)	α / (kW/m^{2}K)	ε_{Ma}	A
372.83	332.88	344.12	338.49	321.79	327.13	586.16	14.67	1.29	0.0363
372.81	337.01	345.97	344.48	325.02	332.58	585.73	16.36	1.39	0.0342
372.81	342.34	354.23	348.75	331.24	335.15	556.62	18.27	1.47	0.0374
372.83	350.43	356.43	357.97	342.27	345.03	521.45	23.27	1.71	0.0247
372.81	360.19	365.19	363.77	354.34	357.44	448.14	35.50	2.23	0.0167
372.81	362.86	365.99	364.28	360.21	360.98	396.02	39.80	2.35	0.0088
372.81	366.03	367.68	366.62	364.04	365.78	324.61	47.86	2.56	0.0049
372.81	367.62	368.56	367.74	366.44	367.74	250.01	48.19	2.41	0.0026
372.81	370.57	371.40	370.84	369.63	370.41	96.08	42.85	1.74	0.0024
372.79	369.46	370.32	369.74	368.26	369.54	123.62	37.22	1.67	0.0026
372.81	366.83	368.35	367.03	365.07	366.86	287.98	48.14	2.50	0.0041
372.81	364.50	366.94	365.55	362.15	363.38	383.99	46.23	2.61	0.0070
372.81	361.85	366.06	364.42	358.41	358.50	422.89	38.58	2.34	0.0125
372.79	356.52	362.46	361.30	348.29	354.04	497.78	30.61	2.06	0.0214
372.79	348.01	357.38	354.63	337.65	342.40	569.93	23.01	1.74	0.0318
372.79	341.80	352.22	348.49	330.63	335.88	578.10	18.66	1.51	0.0350
372.79	336.33	347.48	343.75	323.80	330.30	605.23	16.60	1.42	0.0388
C_{iL} = 0.10%, C_L = 0.17%, C_v = 2.01%, U_v = 0.243 m/s									
373.27	338.97	348.72	346.34	327.31	333.50	597.06	17.41	1.45	0.0352
373.27	341.37	349.24	349.99	330.69	335.54	579.43	18.16	1.48	0.0320
373.27	347.71	356.67	354.89	336.72	342.55	556.87	21.78	1.66	0.0321
373.25	356.31	363.55	361.24	346.74	353.69	515.36	30.42	2.07	0.0249
373.25	363.07	366.65	365.61	359.16	360.85	429.74	42.22	2.51	0.0116
373.25	365.20	367.57	366.32	363.30	363.62	378.53	47.05	2.63	0.0066
373.25	367.67	368.95	367.69	366.66	367.38	301.18	54.00	2.75	0.0030
373.25	368.76	369.59	368.72	367.69	369.01	232.73	51.82	2.50	0.0022
373.25	371.15	371.91	371.30	370.24	371.16	91.19	43.50	1.73	0.0021
373.25	369.98	370.50	369.97	369.44	370.02	137.19	42.01	1.87	0.0013
373.25	368.08	369.11	368.31	366.94	367.95	268.40	51.92	2.59	0.0028
373.25	366.26	368.09	366.86	364.43	365.66	355.97	50.95	2.75	0.0051
373.22	364.54	367.34	366.11	361.22	363.49	397.00	45.73	2.61	0.0088
373.22	359.13	364.98	363.77	352.25	355.50	480.03	34.05	2.20	0.0201
373.22	352.61	361.41	360.23	342.14	346.67	546.29	26.50	1.90	0.0314
373.22	345.83	356.66	353.01	333.48	340.16	581.89	21.24	1.66	0.0368
373.22	340.89	352.60	348.03	328.72	334.21	592.70	18.33	1.50	0.0388
C_{iL} = 0.10%, C_L = 0.19%, C_v = 2.25%, U_v = 0.349 m/s									
373.10	345.98	355.88	354.72	331.09	342.24	769.90	28.39	2.17	0.0385
373.10	349.78	360.72	357.18	334.73	346.48	729.58	31.28	2.29	0.0388
373.10	355.13	363.30	359.90	342.95	354.35	682.88	37.99	2.59	0.0284
373.10	359.99	365.54	363.52	352.33	358.58	599.85	45.76	2.87	0.0189
373.13	365.14	367.35	365.66	362.44	365.11	471.18	59.01	3.26	0.0063
373.10	366.00	367.72	366.18	364.01	366.08	410.22	57.73	3.10	0.0046
373.10	367.47	368.77	367.41	366.11	367.58	319.03	56.64	2.87	0.0032
373.10	368.37	369.36	368.49	367.07	368.56	244.58	51.69	2.51	0.0028
373.15	371.17	371.81	371.52	370.19	371.16	96.33	48.62	1.90	0.0021
373.15	369.63	370.55	369.97	368.21	369.80	148.07	42.11	1.90	0.0029
373.15	367.77	368.84	367.90	366.23	368.11	282.89	52.59	2.63	0.0031
373.15	366.56	368.11	366.66	364.90	366.59	384.49	58.37	3.07	0.0040
373.15	364.77	364.39	366.07	363.01	365.62	429.80	51.30	2.87	0.0018
373.15	362.71	366.57	364.62	357.71	361.92	536.96	51.42	3.04	0.0123
373.15	357.62	364.57	362.25	348.14	355.52	649.89	41.85	2.74	0.0240
373.15	352.74	362.34	359.33	340.60	348.68	715.62	35.06	2.47	0.0331
373.15	348.87	360.96	356.29	334.05	344.20	755.16	31.11	2.30	0.0408

Thermocouple angles : T_{w1} = 22.5°, T_{w2} = -67.5°, T_{w3} = -157.5°, T_{w4} = 112.5°

Test fluid – steam-ethanol mixtures

C_{iL} = 0.10%, C_L = 0.15%, C_v = 1.74%, U_v = 0.351 m/s

T_v / K	T_{wo} / K	T_{w1} / K	T_{w2} / K	T_{w3} / K	T_{w4} / K	q / (kW/m^2)	a / (kW/m^{2}K)	ε_{Ma}	A
373.20	349.92	361.63	356.86	334.82	346.36	712.87	30.62	2.24	0.0397
373.20	352.40	362.84	358.87	349.30	338.61	692.86	33.32	2.36	0.0280
373.20	356.29	364.10	361.72	345.24	354.11	637.65	37.72	2.53	0.0275
373.20	361.68	366.05	364.01	355.78	360.90	560.23	48.66	2.95	0.0143
373.20	365.58	367.72	366.29	363.21	365.09	440.43	57.78	3.16	0.0061
373.20	366.53	368.13	366.80	364.90	366.29	378.79	56.80	3.00	0.0042
373.20	368.15	369.09	368.39	367.13	368.00	295.21	58.52	2.88	0.0026
373.20	368.99	369.86	368.99	368.25	368.87	228.40	54.33	2.56	0.0020
373.20	371.27	371.87	371.53	370.42	371.26	93.46	48.46	1.88	0.0019
373.20	370.06	370.53	370.12	369.56	370.02	143.59	45.75	2.01	0.0012
373.20	368.38	369.34	368.49	367.41	368.30	260.68	54.16	2.64	0.0025
373.17	367.32	368.52	367.34	366.35	367.05	354.94	60.60	3.10	0.0028
373.17	366.24	368.05	366.70	364.21	366.00	402.79	58.07	3.10	0.0050
373.17	363.90	367.00	365.41	359.92	363.27	494.71	53.35	3.06	0.0098
373.17	359.14	365.11	363.50	350.68	357.27	596.68	42.52	2.71	0.0211
373.17	355.15	364.94	361.09	343.15	351.42	662.89	36.77	2.51	0.0324
373.17	351.50	362.64	359.20	335.62	348.53	703.59	32.46	2.33	0.0399

C_{iL} = 0.10%, C_L = 0.18%, C_v = 2.05%, U_v = 0.563 m/s

373.17	350.41	362.10	357.00	334.35	348.20	912.55	40.09	2.83	0.0400
373.15	354.21	363.40	359.09	340.64	353.70	853.76	45.07	3.03	0.0315
373.15	358.11	364.66	361.17	348.40	358.23	772.64	51.39	3.25	0.0218
373.15	362.45	366.02	363.77	357.76	362.26	644.65	60.26	3.51	0.0110
373.15	365.38	367.25	365.49	363.27	365.51	516.36	66.48	3.58	0.0049
373.15	365.92	367.49	365.99	364.09	366.12	433.45	59.98	3.17	0.0041
373.15	367.64	368.79	367.63	366.33	367.80	340.04	61.71	3.06	0.0029
373.15	368.40	369.50	368.65	366.82	368.61	259.08	54.49	2.61	0.0033
373.15	371.27	371.78	371.49	370.57	371.25	100.73	53.69	2.06	0.0016
373.15	370.05	370.87	370.22	369.01	370.10	134.43	43.41	1.87	0.0023
373.15	368.50	369.68	368.55	367.12	368.67	292.63	62.99	3.00	0.0031
373.15	366.59	368.00	366.65	364.84	366.89	407.91	62.21	3.22	0.0037
373.15	365.85	367.52	365.98	363.84	366.05	456.38	62.51	3.32	0.0045
373.15	364.00	366.72	364.69	360.22	364.36	567.95	62.05	3.48	0.0082
373.15	360.35	365.31	362.92	352.60	360.56	709.86	55.45	3.37	0.0169
373.15	356.68	364.31	360.38	345.33	356.68	811.46	49.26	3.19	0.0257
373.15	352.79	363.28	358.30	338.04	351.52	876.04	43.02	2.94	0.0355

C_{iL} = 0.10%, C_L = 0.18%, C_v = 2.04%, U_v = 0.562 m/s

373.22	353.34	363.56	359.44	338.68	351.68	837.58	42.13	2.86	0.0354
373.22	355.94	364.65	360.94	343.48	354.71	786.13	45.50	2.98	0.0297
373.22	359.76	365.65	362.47	350.90	360.02	706.10	52.45	3.23	0.0195
373.22	363.42	366.54	364.63	359.36	363.14	596.02	60.78	3.46	0.0096
373.22	366.15	367.73	366.09	364.81	365.97	469.13	66.33	3.49	0.0037
373.20	366.70	368.14	366.59	365.27	366.81	396.56	61.06	3.15	0.0034
373.20	368.19	369.23	368.12	367.21	368.20	310.55	62.00	3.00	0.0024
373.20	369.41	370.87	369.15	368.40	369.22	235.90	62.28	2.82	0.0030
373.20	371.26	371.78	371.58	370.40	371.29	99.84	51.60	1.99	0.0018
373.20	370.05	370.72	370.14	369.32	370.02	153.93	48.95	2.12	0.0018
373.20	368.64	369.41	368.47	368.06	368.59	271.70	59.55	2.82	0.0016
373.20	367.39	368.54	367.23	366.53	367.26	373.02	64.21	3.22	0.0025
373.20	367.08	370.22	366.55	365.08	366.46	434.16	70.95	3.61	0.0064
373.17	364.98	367.28	365.40	362.34	364.90	523.75	63.94	3.49	0.0063
373.17	361.85	365.91	363.70	356.36	361.43	648.61	57.28	3.38	0.0129
373.17	357.86	365.23	361.69	346.81	357.70	740.31	48.33	3.08	0.0250
373.17	355.06	364.39	360.27	341.94	353.66	802.59	44.32	2.94	0.0316

Thermocouple angles : T_{w1} = 22.5°, T_{w2} = -67.5°, T_{w3} = -157.5°, T_{w4} = 112.5°

Test fluid – steam-ethanol mixtures

C_{iL} = 0.10%, C_L = 0.20%, C_v = 2.32%, U_v = 0.764 m/s

T_v / K	T_{wo} / K	T_{w1} / K	T_{w2} / K	T_{w3} / K	T_{w4} / K	q / (kW/m^2)	a / (kW/m^{2}K)	ε_{Ma}	A
372.81	348.86	360.10	354.26	333.48	347.58	959.41	40.05	2.78	0.0376
372.81	352.57	361.87	357.01	338.03	353.36	919.71	45.44	3.02	0.0321
372.81	357.00	363.52	359.55	346.93	357.99	824.22	52.13	3.26	0.0216
372.81	361.39	364.95	362.69	355.93	361.99	680.75	59.62	3.45	0.0115
372.81	364.73	366.56	364.68	362.13	365.53	529.66	65.52	3.50	0.0050
372.81	365.33	366.80	365.14	363.21	366.17	456.28	61.00	3.20	0.0039
372.81	367.32	368.19	367.30	366.14	367.66	351.34	64.03	3.13	0.0023
372.79	368.20	369.07	368.20	367.04	368.47	265.54	57.85	2.71	0.0023
372.79	370.95	371.72	371.07	370.15	370.85	98.71	53.74	2.03	0.0020
372.79	369.57	370.65	369.87	368.28	369.46	147.83	45.90	1.98	0.0031
372.79	367.45	368.54	367.55	366.20	367.50	306.28	57.34	2.78	0.0029
372.79	365.86	367.32	365.95	363.92	366.24	423.05	61.04	3.15	0.0040
372.79	365.00	366.78	365.19	362.59	365.43	477.71	61.32	3.25	0.0050
372.83	363.32	365.91	363.93	359.77	363.67	590.27	62.02	3.44	0.0077
372.83	359.55	364.23	361.89	352.34	359.75	746.95	56.24	3.38	0.0158
372.81	355.76	363.04	358.99	344.59	356.42	853.94	50.08	3.20	0.0245
372.81	351.77	361.49	356.58	337.55	351.46	925.60	43.99	2.96	0.0330
C_{iL} = 0.10%, C_L = 0.14%, C_v = 1.61%, U_v = 0.755 m/s									
373.27	353.75	362.89	358.65	339.97	353.51	884.69	45.33	2.99	0.0316
373.25	356.43	364.07	360.29	344.52	356.85	832.48	49.51	3.15	0.0262
373.27	360.14	365.13	362.07	352.38	360.99	743.95	56.66	3.39	0.0164
373.27	363.44	366.25	364.42	359.63	363.48	622.62	63.36	3.54	0.0086
373.27	365.80	367.53	366.01	363.72	365.96	482.62	64.63	3.39	0.0047
373.27	366.60	367.91	366.51	365.25	366.75	413.78	62.05	3.17	0.0031
373.27	368.18	368.96	367.99	367.41	368.36	318.97	62.66	3.01	0.0017
373.27	368.97	369.96	369.18	367.59	369.14	243.12	56.49	2.61	0.0029
373.27	371.22	371.56	371.25	370.72	371.37	105.75	51.68	2.00	0.0010
373.27	370.01	370.72	370.12	369.08	370.12	159.15	48.83	2.11	0.0020
373.27	368.51	369.31	368.66	367.46	368.59	276.18	57.96	2.74	0.0023
373.27	367.35	368.42	367.11	366.56	367.33	383.53	64.82	3.22	0.0022
373.27	366.38	367.96	366.42	364.73	366.39	436.16	63.26	3.26	0.0040
373.27	365.01	367.11	365.30	362.66	364.97	543.82	65.83	3.53	0.0057
373.27	362.22	365.88	363.66	357.38	361.95	682.53	61.76	3.55	0.0114
373.27	359.07	365.21	361.57	349.79	359.72	786.71	55.40	3.38	0.0201
373.27	355.69	364.28	359.88	343.16	355.45	857.45	48.78	3.13	0.0288
C_{iL} = 0.50%, C_L = 0.54%, C_v = 5.96%, U_v = 0.149 m/s									
372.71	325.08	331.85	330.25	317.48	320.74	477.61	10.03	0.96	0.0251
372.71	329.52	337.83	333.88	320.82	325.56	466.57	10.80	0.99	0.0278
372.71	334.80	344.92	336.88	326.00	331.42	467.36	12.33	1.08	0.0284
372.71	341.40	349.05	346.04	334.31	336.19	444.42	14.19	1.17	0.0246
372.71	353.02	357.39	355.37	347.39	351.95	391.38	19.88	1.43	0.0144
372.69	357.93	360.00	359.11	355.00	357.60	347.87	23.57	1.56	0.0070
372.69	361.28	362.66	361.48	359.41	361.60	286.83	25.15	1.56	0.0040
372.71	362.80	363.88	362.65	361.52	363.13	213.71	21.55	1.28	0.0027
372.69	366.71	368.41	366.87	365.13	366.43	73.47	12.29	0.64	0.0042
372.69	363.83	364.60	363.57	363.09	364.07	151.70	17.13	0.99	0.0016
372.69	362.52	363.66	362.48	361.23	362.70	238.58	23.45	1.41	0.0029
372.69	359.05	361.04	360.27	356.52	358.37	332.83	24.40	1.58	0.0066
372.67	355.79	359.89	357.58	351.86	353.85	375.20	22.24	1.53	0.0121
372.67	348.31	356.00	351.43	339.26	346.53	429.76	17.64	1.35	0.0241
372.67	340.12	346.88	345.34	330.57	337.69	469.73	14.43	1.21	0.0255
372.67	333.71	341.78	338.80	323.64	330.62	497.35	12.77	1.13	0.0288
372.67	328.75	334.89	332.65	320.55	326.91	492.54	11.22	1.04	0.0227

Thermocouple angles : T_{w1} = 22.5°, T_{w2} = -67.5°, T_{w3} = -157.5°, T_{w4} = 112.5°

Test fluid – steam-ethanol mixtures

C_{iL} = 0.50%, C_L = 0.51%, C_v = 5.63%, U_v = 0.149 m/s

T_v / K	T_{wo} / K	T_{w1} / K	T_{w2} / K	T_{w3} / K	T_{w4} / K	q / (kW/m^2)	α / (kW/m^{2}K)	ε_{Ma}	A
372.52	329.25	336.76	332.46	320.12	327.67	488.85	11.30	1.04	0.0253
372.57	333.39	343.82	336.62	323.63	329.47	511.65	13.06	1.16	0.0312
372.57	337.15	343.31	342.54	328.76	333.99	462.56	13.06	1.12	0.0239
372.57	345.63	352.45	348.98	336.54	344.54	440.66	16.36	1.29	0.0229
372.57	354.11	358.98	356.86	348.30	352.29	386.81	20.96	1.48	0.0158
372.57	358.63	361.22	359.75	355.35	358.21	350.07	25.12	1.64	0.0081
372.57	361.94	363.51	361.95	360.26	362.04	274.39	25.82	1.57	0.0040
372.57	363.04	364.38	362.93	361.78	363.08	206.81	21.71	1.28	0.0032
372.57	367.09	368.64	367.12	365.53	367.07	75.28	13.74	0.70	0.0038
372.57	364.45	365.40	364.05	363.71	364.63	140.85	17.34	0.98	0.0018
372.57	363.04	364.26	362.81	361.73	363.36	231.86	24.33	1.44	0.0029
372.57	360.37	361.31	359.60	359.98	360.58	214.34	17.57	1.11	0.0012
372.57	357.01	361.69	359.02	352.14	355.19	384.35	24.70	1.66	0.0140
372.57	348.89	354.44	352.66	340.83	347.63	418.76	17.68	1.34	0.0200
372.57	339.53	347.38	344.76	330.73	335.27	458.35	13.88	1.17	0.0271
372.57	334.38	342.27	339.38	325.97	329.87	477.77	12.51	1.10	0.0270
372.57	330.22	337.73	335.30	322.56	325.28	491.76	11.61	1.06	0.0261
C_{iL} = 0.50%, C_L = 0.53%, C_v = 5.84%, U_v = 0.239 m/s									
372.50	333.22	343.19	337.34	323.06	329.29	618.50	15.75	1.38	0.0315
372.52	336.12	343.85	339.64	326.21	334.80	595.63	16.37	1.40	0.0261
372.50	342.31	350.29	346.20	333.22	339.51	572.25	18.96	1.53	0.0259
372.52	350.64	357.16	354.18	341.61	349.59	529.26	24.18	1.77	0.0222
372.52	358.34	361.39	359.29	354.55	358.14	427.34	30.14	1.96	0.0091
372.50	360.48	362.22	360.46	358.44	360.80	368.83	30.70	1.91	0.0045
372.50	361.97	363.37	361.76	360.36	362.39	285.35	27.11	1.63	0.0034
372.50	363.11	364.22	362.82	361.91	363.50	213.86	22.79	1.33	0.0025
372.50	367.14	369.12	367.31	365.19	366.92	74.79	13.95	0.71	0.0050
372.50	363.98	365.05	363.84	362.78	364.25	153.15	17.98	1.02	0.0026
372.47	362.91	364.12	362.68	361.59	363.25	239.33	25.03	1.47	0.0028
372.47	361.13	362.71	361.00	359.41	361.41	344.28	30.36	1.86	0.0039
372.50	359.56	361.69	359.95	356.80	359.79	398.99	30.84	1.95	0.0062
372.50	355.70	360.01	357.51	349.77	355.51	489.47	29.15	1.98	0.0139
372.50	347.45	355.24	350.86	338.55	345.17	560.48	22.38	1.70	0.0245
372.50	341.54	349.71	347.04	331.43	337.97	602.74	19.47	1.58	0.0288
372.50	336.67	344.88	341.77	326.32	333.72	619.10	17.28	1.47	0.0290
C_{iL} = 0.50%, C_L = 0.51%, C_v = 5.66%, U_v = 0.238 m/s									
372.54	334.60	344.22	338.68	324.29	331.20	586.42	15.45	1.34	0.0308
372.54	339.01	347.25	344.99	328.25	335.57	601.21	17.93	1.49	0.0301
372.54	344.76	352.24	349.11	335.49	342.18	571.76	20.57	1.62	0.0254
372.57	351.21	358.16	354.43	343.52	348.74	515.84	24.15	1.76	0.0217
372.57	358.81	361.90	359.69	355.17	358.46	424.97	30.88	1.99	0.0090
372.57	360.15	362.44	360.47	357.75	359.94	370.29	29.82	1.87	0.0061
372.57	362.36	363.84	362.04	360.74	362.83	288.00	28.22	1.68	0.0035
372.57	363.34	364.52	363.05	362.04	363.75	216.73	23.49	1.36	0.0027
372.57	367.19	368.86	367.29	365.48	367.15	75.80	14.10	0.71	0.0042
372.57	364.43	365.43	364.27	363.42	364.61	151.84	18.66	1.05	0.0023
372.57	363.04	364.30	362.81	361.55	363.51	241.48	25.35	1.48	0.0030
372.57	361.16	363.04	361.12	359.21	361.28	348.77	30.58	1.87	0.0047
372.57	359.69	362.38	360.14	356.03	360.22	403.54	31.34	1.98	0.0079
372.57	355.57	360.45	357.54	350.30	354.00	474.95	27.95	1.91	0.0146
372.57	347.77	355.13	351.93	339.45	344.57	552.13	22.26	1.69	0.0241
372.57	341.91	350.56	348.44	331.91	336.74	582.70	19.01	1.54	0.0306
372.57	337.72	346.58	342.82	327.45	334.03	617.26	17.71	1.49	0.0301

Thermocouple angles : T_{w1} = 22.5°, T_{w2} = -67.5°, T_{w3} = -157.5°, T_{w4} = 112.5°

Test fluid – steam-ethanol mixtures

C_{iL} = 0.50%, C_L = 0.53%, C_v = 5.86%, U_v = 0.341 m/s

T_v / K	T_{wo} / K	T_{w1} / K	T_{w2} / K	T_{w3} / K	T_{w4} / K	q / (kW/m^2)	α / (kW/m^{2}K)	ε_{Ma}	A
372.76	342.51	351.59	345.86	332.05	340.54	814.46	26.92	2.13	0.0284
372.76	346.89	355.08	350.34	335.71	346.43	769.13	29.73	2.25	0.0270
372.79	351.58	358.47	353.93	341.61	352.32	696.36	32.84	2.35	0.0223
372.79	356.07	360.15	357.02	350.58	356.54	606.29	36.27	2.43	0.0123
372.79	359.86	361.98	359.55	357.19	360.70	466.81	36.10	2.26	0.0054
372.76	360.68	362.21	360.21	358.86	361.44	396.85	32.84	2.02	0.0036
372.79	362.43	363.88	361.83	361.35	362.68	300.96	29.07	1.72	0.0027
372.76	362.99	364.16	362.69	361.75	363.39	226.12	23.15	1.35	0.0026
372.79	367.30	368.84	367.68	365.46	367.22	81.31	14.82	0.75	0.0044
372.79	364.03	365.16	363.84	362.87	364.25	157.69	18.01	1.02	0.0026
372.76	362.90	364.08	362.56	361.70	363.24	251.50	25.49	1.49	0.0026
372.76	361.15	362.58	360.77	359.42	361.83	373.08	32.13	1.96	0.0034
372.76	360.64	362.15	360.01	359.03	361.38	437.16	36.07	2.22	0.0032
372.76	358.33	361.03	358.24	355.59	358.48	536.53	37.18	2.40	0.0067
372.76	353.81	359.09	355.24	346.16	354.76	653.39	34.48	2.39	0.0166
372.76	350.15	356.87	352.61	339.38	351.74	733.65	32.44	2.36	0.0227
372.76	345.72	354.16	349.07	334.01	345.65	794.70	29.39	2.25	0.0279

C_{iL} = 0.50%, C_L = 0.45%, C_v = 5.06%, U_v = 0.342 m/s

372.81	346.10	354.11	350.27	334.23	345.79	757.89	28.38	2.17	0.0280
372.83	350.14	357.24	353.08	339.52	350.73	711.73	31.37	2.28	0.0238
372.83	353.73	359.30	356.05	344.68	354.90	645.94	33.81	2.35	0.0190
372.86	357.81	361.24	358.43	353.14	358.45	561.46	37.31	2.43	0.0101
372.86	360.97	362.85	360.68	358.71	361.65	441.92	37.18	2.28	0.0047
372.86	361.72	363.33	361.29	359.89	362.37	380.22	34.14	2.06	0.0037
372.86	363.07	364.43	362.67	361.64	363.54	289.74	29.59	1.72	0.0030
372.83	364.00	365.20	363.71	362.84	364.26	217.55	24.63	1.40	0.0026
372.83	367.89	369.23	368.14	366.18	367.99	81.74	16.52	0.81	0.0038
372.83	365.28	366.10	365.26	364.22	365.55	141.62	18.75	1.02	0.0022
372.83	363.66	364.99	363.45	362.17	364.05	244.08	26.61	1.53	0.0032
372.83	362.22	363.60	361.77	360.68	362.83	348.98	32.87	1.96	0.0031
372.83	361.42	363.17	360.98	359.30	362.24	408.07	35.76	2.17	0.0042
372.83	359.55	362.01	359.33	356.33	360.51	498.38	37.50	2.36	0.0065
372.81	356.14	360.15	357.21	350.31	356.87	610.82	36.63	2.45	0.0125
372.81	352.81	359.08	354.92	343.76	353.48	692.57	34.63	2.43	0.0202
372.83	349.16	356.22	352.30	338.51	349.61	750.19	31.69	2.33	0.0240

C_{iL} = 0.50%, C_L = 0.52%, C_v = 5.75%, U_v = 0.549 m/s

372.81	349.35	355.53	350.36	339.48	352.02	968.31	41.27	2.94	0.0214
372.81	352.44	357.55	352.96	344.56	354.69	884.77	43.43	2.98	0.0173
372.81	355.37	358.98	355.06	350.11	357.32	768.79	44.08	2.91	0.0123
372.81	357.99	360.51	357.26	354.71	359.47	641.39	43.27	2.74	0.0084
372.81	360.04	361.76	359.12	358.37	360.90	508.07	39.77	2.43	0.0051
372.81	360.59	362.15	359.96	358.83	361.40	426.16	34.86	2.10	0.0049
372.81	362.04	363.41	361.63	360.64	362.47	319.62	29.67	1.73	0.0039
372.81	363.13	364.53	362.91	361.57	363.49	238.79	24.66	1.40	0.0040
372.81	368.39	370.30	368.53	366.53	368.20	83.73	18.94	0.89	0.0044
372.81	364.47	365.99	364.45	362.81	364.62	154.13	18.47	1.01	0.0040
372.81	362.75	364.23	362.40	361.34	363.03	262.87	26.13	1.50	0.0039
372.81	361.26	362.67	360.63	359.98	361.76	398.50	34.49	2.05	0.0039
372.81	360.62	362.12	359.67	359.43	361.26	456.59	37.45	2.26	0.0042
372.79	359.15	361.00	358.25	357.07	360.30	565.45	41.48	2.57	0.0059
372.79	356.75	359.80	356.19	352.83	358.19	712.07	44.41	2.87	0.0098
372.79	354.37	358.52	354.38	348.47	356.12	835.14	45.35	3.03	0.0136
372.81	351.42	356.76	352.10	343.03	353.78	922.89	43.14	3.00	0.0183

Thermocouple angles : T_{w1} = 22.5°, T_{w2} = 112.5°, T_{w3} = -157.5°, T_{w4} = -67.5°

Test fluid – steam-ethanol mixtures

C_{iL} = 0.50%, C_L = 0.43%, C_v = 4.79%, U_v = 0.553 m/s

T_v / K	T_{wo} / K	T_{w1} / K	T_{w2} / K	T_{w3} / K	T_{w4} / K	q / (kW/m^2)	α / (kW/m^{2}K)	ε_{Ma}	A
372.86	351.96	357.28	353.07	343.53	353.94	905.30	43.31	2.99	0.0179
372.86	354.54	358.84	354.95	348.09	356.29	821.39	44.85	2.99	0.0142
372.86	356.81	360.10	356.57	352.50	358.08	714.61	44.53	2.87	0.0103
372.86	359.09	361.51	358.41	356.20	360.24	593.67	43.11	2.68	0.0076
372.86	360.94	362.76	360.21	359.01	361.75	475.05	39.84	2.39	0.0054
372.86	361.61	363.18	360.85	360.24	362.17	399.04	35.47	2.09	0.0043
372.83	363.36	364.78	363.34	361.91	363.41	303.08	31.99	1.81	0.0036
372.86	364.02	365.60	363.89	362.30	364.30	225.47	25.51	1.42	0.0043
372.86	368.07	369.11	368.34	366.75	368.10	88.40	18.47	0.89	0.0028
372.86	365.23	366.73	365.16	363.65	365.38	168.08	22.03	1.18	0.0039
372.86	363.81	365.41	363.67	362.08	364.08	245.72	27.15	1.52	0.0043
372.86	362.25	363.75	361.61	360.96	362.69	366.22	34.52	2.01	0.0040
372.86	361.51	363.15	360.79	359.90	362.21	422.60	37.23	2.20	0.0048
372.86	360.20	362.17	359.35	358.06	361.21	523.05	41.31	2.51	0.0061
372.86	358.01	360.85	357.58	354.31	359.31	652.97	43.98	2.78	0.0091
372.86	356.07	359.61	355.97	351.36	357.34	758.00	45.15	2.95	0.0111
372.86	353.35	358.26	354.15	345.81	355.16	842.41	43.18	2.93	0.0163
C_{iL} = 0.50%, C_L = 0.50%, C_v = 5.61%, U_v = 0.744 m/s									
372.54	351.78	356.33	351.88	344.38	354.53	979.72	47.18	3.17	0.0165
372.54	354.06	357.68	353.67	348.93	355.95	887.81	48.03	3.14	0.0122
372.54	356.06	359.03	355.26	352.49	357.45	764.32	46.36	2.94	0.0093
372.52	358.38	360.57	357.35	356.08	359.51	629.80	44.53	2.72	0.0067
372.54	360.10	361.91	359.14	358.35	361.02	493.12	39.64	2.35	0.0054
372.54	360.67	362.28	359.78	359.27	361.37	417.99	35.22	2.07	0.0046
372.54	362.24	363.82	361.80	360.62	362.74	319.38	31.01	1.76	0.0044
372.54	363.32	364.92	363.11	361.55	363.69	234.98	25.47	1.41	0.0045
372.54	368.26	370.07	368.38	366.42	368.16	86.82	20.26	0.94	0.0043
372.52	365.10	366.70	365.18	363.35	365.18	145.48	19.61	1.03	0.0041
372.52	362.79	364.45	362.62	361.08	363.03	263.13	27.05	1.51	0.0044
372.57	361.30	362.86	360.62	360.04	361.70	381.41	33.86	1.96	0.0041
372.54	360.68	362.36	359.86	359.21	361.28	445.90	37.58	2.20	0.0047
372.57	359.45	361.41	358.40	357.63	360.35	550.42	41.94	2.52	0.0057
372.57	357.39	360.03	356.56	354.26	358.73	698.78	46.05	2.87	0.0083
372.57	355.61	358.74	354.92	351.60	357.18	819.70	48.33	3.09	0.0101
372.54	353.38	357.34	353.15	347.84	355.20	927.29	48.39	3.19	0.0131
C_{iL} = 0.50%, C_L = 0.44%, C_v = 4.96%, U_v = 0.747 m/s									
372.59	352.53	356.88	352.72	345.58	354.96	957.85	47.75	3.18	0.0155
372.59	354.14	357.98	353.94	348.50	356.15	878.25	47.60	3.10	0.0131
372.62	356.49	359.56	356.00	352.44	357.95	737.56	45.73	2.88	0.0099
372.62	358.82	360.99	357.88	356.61	359.78	610.37	44.23	2.69	0.0064
372.62	360.52	362.38	359.68	358.87	361.13	485.58	40.12	2.36	0.0051
372.62	360.88	362.69	360.33	358.74	361.77	407.11	34.70	2.03	0.0056
372.62	362.65	364.17	362.15	361.18	363.09	306.40	30.73	1.73	0.0042
372.62	363.71	365.36	363.55	361.84	364.06	231.27	25.95	1.42	0.0046
372.62	368.41	369.95	368.50	366.71	368.48	86.53	20.56	0.95	0.0039
372.62	364.65	366.31	364.59	362.81	364.91	164.92	20.71	1.11	0.0045
372.62	363.29	364.93	363.15	361.61	363.46	253.12	27.14	1.50	0.0043
372.62	361.78	363.34	361.15	360.52	362.13	370.68	34.22	1.96	0.0040
372.62	361.02	362.72	360.17	359.56	361.63	434.14	37.44	2.18	0.0047
372.59	359.91	361.83	358.73	358.34	360.75	533.47	42.08	2.51	0.0054
372.59	357.91	360.50	356.98	355.08	359.08	675.27	45.99	2.84	0.0078
372.59	356.23	359.36	355.46	352.34	357.77	792.51	48.44	3.07	0.0100
372.59	354.25	358.22	353.80	348.95	356.04	890.42	48.55	3.16	0.0129

Thermocouple angles : T_{w1} = 22.5°, T_{w2} = 112.5°, T_{w3} = -157.5°, T_{w4} = -67.5°

Test fluid – steam-ethanol mixtures

C_{iL} = 1.00%, C_L = 0.96%, C_v = 10.19%, U_v = 0.146 m/s

T_v / K	T_{wo} / K	T_{w1} / K	T_{w2} / K	T_{w3} / K	T_{w4} / K	q / (kW/m^2)	α / (kW/m^{2}K)	ε_{Ma}	A
371.87	321.54	326.78	324.79	315.68	318.90	490.63	9.75	0.95	0.0188
371.87	325.17	332.43	327.72	317.50	323.03	477.96	10.24	0.97	0.0232
371.87	329.97	336.81	332.50	322.93	327.66	459.79	10.98	1.00	0.0216
371.84	336.70	342.50	340.79	330.30	333.22	448.67	12.77	1.10	0.0203
371.87	349.12	353.39	352.83	344.06	346.20	394.38	17.34	1.30	0.0154
371.84	355.36	357.66	355.90	352.20	355.68	365.77	22.19	1.52	0.0070
371.87	358.10	359.34	358.09	356.38	358.59	272.08	19.76	1.29	0.0034
371.87	359.38	360.18	359.09	358.32	359.91	199.12	15.94	1.01	0.0019
371.87	363.70	365.62	363.81	361.95	363.42	64.05	7.84	0.45	0.0047
371.87	360.68	361.38	360.56	359.76	361.02	126.15	11.28	0.70	0.0018
371.84	359.48	360.19	359.23	358.31	360.17	212.85	17.21	1.09	0.0019
371.87	356.87	358.71	356.67	354.34	357.75	329.19	21.95	1.47	0.0049
371.87	352.97	357.01	354.48	347.97	352.44	376.48	19.93	1.42	0.0125
371.87	342.33	346.15	344.69	336.40	342.09	426.94	14.46	1.18	0.0141
371.87	334.78	343.07	338.28	327.58	330.20	468.98	12.65	1.11	0.0252
371.87	328.65	333.84	331.84	322.14	326.76	485.27	11.23	1.04	0.0187
371.84	325.00	330.94	328.20	318.43	322.43	494.18	10.55	1.00	0.0205
C_{iL} = 1.00%, C_L = 0.93%, C_v = 9.87%, U_v = 0.146 m/s									
371.96	323.30	330.79	325.70	316.65	320.06	477.76	9.82	0.95	0.0229
371.94	326.84	334.75	330.26	319.41	322.94	462.87	10.26	0.96	0.0252
371.94	332.69	340.52	334.88	323.96	331.40	446.99	11.39	1.02	0.0242
371.94	338.95	346.76	342.81	332.21	334.04	432.79	13.12	1.10	0.0240
371.94	349.11	353.45	351.07	343.40	348.50	398.39	17.45	1.31	0.0142
371.94	352.81	356.20	353.97	349.13	351.92	374.01	19.55	1.40	0.0100
371.94	358.43	359.71	358.46	356.78	358.78	383.84	28.42	1.84	0.0035
371.94	359.51	360.45	359.27	358.23	360.09	205.49	16.53	1.05	0.0023
371.94	363.86	365.87	363.89	362.06	363.63	66.58	8.24	0.47	0.0049
371.94	360.94	361.51	360.89	360.05	361.30	129.86	11.80	0.72	0.0016
371.94	359.06	360.26	359.03	357.76	359.20	242.66	18.84	1.21	0.0030
371.96	355.70	358.12	356.29	353.10	355.28	336.93	20.72	1.41	0.0069
371.94	351.89	355.23	352.85	346.43	353.06	376.23	18.76	1.36	0.0110
371.96	342.87	347.92	346.53	336.18	340.85	409.12	14.06	1.14	0.0183
371.96	335.41	342.64	340.55	326.86	331.58	443.60	12.13	1.06	0.0259
371.96	330.47	336.81	332.53	322.92	329.61	457.62	11.03	1.00	0.0205
371.96	326.08	333.01	329.96	318.75	322.62	472.14	10.29	0.97	0.0237
C_{iL} = 1.00%, C_L = 0.89%, C_v = 9.46%, U_v = 0.235 m/s									
371.91	329.53	336.19	333.51	320.61	327.80	627.30	14.80	1.34	0.0243
371.91	334.75	342.58	337.71	324.99	333.71	610.86	16.43	1.42	0.0257
371.94	339.01	346.80	342.57	330.05	336.62	572.54	17.39	1.44	0.0253
371.91	346.17	352.05	350.06	338.77	343.78	531.93	20.66	1.59	0.0205
371.94	354.40	357.36	355.56	350.03	354.65	447.98	25.54	1.76	0.0097
371.91	356.56	358.54	356.76	354.04	356.92	384.04	25.02	1.66	0.0056
371.91	358.19	359.84	358.35	357.65	356.91	287.27	20.93	1.35	0.0035
371.91	359.81	360.65	359.47	358.70	360.43	211.92	17.50	1.09	0.0019
371.94	364.34	366.51	364.43	362.38	364.02	68.47	9.01	0.50	0.0053
371.94	361.45	362.34	361.35	360.41	361.71	120.63	11.50	0.69	0.0022
371.94	359.68	360.69	359.37	358.31	360.33	237.78	19.39	1.21	0.0025
371.94	357.77	359.17	357.51	355.57	358.81	361.03	25.47	1.66	0.0039
371.94	356.05	358.52	356.30	353.20	356.16	411.18	25.87	1.74	0.0068
371.94	351.58	356.50	353.62	345.47	350.73	489.98	24.06	1.73	0.0156
371.94	343.01	350.97	346.96	334.34	339.78	563.17	19.47	1.55	0.0256
371.91	336.38	344.48	340.73	327.57	332.72	596.23	16.78	1.43	0.0269
371.94	332.33	338.99	336.24	322.92	331.19	615.94	15.55	1.37	0.0244

Thermocouple angles : T_{w1} = 22.5°, T_{w2} = -67.5°, T_{w3} = -157.5°, T_{w4} = 112.5°

Test fluid – steam-ethanol mixtures

C_{iL} = 1.00%, C_L = 0.94%, C_v = 9.98%, U_v = 0.236 m/s

T_v / K	T_{wo} / K	T_{w1} / K	T_{w2} / K	T_{w3} / K	T_{w4} / K	q / (kW/m^2)	α / (kW/m^{2}K)	ε_{Ma}	A
371.72	331.25	337.75	334.76	322.21	330.28	624.15	15.42	1.37	0.0234
371.72	334.76	342.24	338.39	326.38	332.02	591.24	16.00	1.38	0.0247
371.72	340.05	347.47	343.67	330.36	338.69	566.69	17.89	1.47	0.0252
371.72	347.45	352.71	349.89	340.20	347.01	527.63	21.74	1.65	0.0176
371.72	354.38	356.90	354.93	351.11	354.59	425.57	24.54	1.69	0.0075
371.72	356.47	358.03	356.35	354.30	357.21	358.26	23.49	1.56	0.0042
371.72	358.30	359.24	357.99	357.03	358.93	267.13	19.90	1.28	0.0023
371.72	359.28	360.12	358.94	358.22	359.83	197.16	15.84	1.00	0.0019
371.72	363.83	365.84	364.13	361.77	363.58	65.54	8.30	0.46	0.0053
371.72	360.72	361.58	360.76	359.56	360.98	118.21	10.74	0.65	0.0024
371.72	359.12	360.02	358.84	357.90	359.73	217.42	17.26	1.09	0.0022
371.72	357.19	358.51	357.02	355.67	357.55	332.65	22.89	1.50	0.0033
371.72	355.90	357.63	355.93	353.16	356.86	391.78	24.76	1.66	0.0051
371.75	351.54	355.39	353.37	345.99	351.40	479.01	23.71	1.70	0.0130
371.75	344.19	350.93	347.81	335.48	342.54	554.70	20.13	1.58	0.0229
371.75	339.01	346.37	342.37	329.54	337.77	597.81	18.26	1.51	0.0247
371.75	334.39	343.71	336.95	324.80	332.09	617.31	16.52	1.43	0.0280
C_{iL} = 1.00%, C_L = 1.02%, C_v = 10.69%, U_v = 0.334 m/s									
371.84	339.16	347.27	341.71	328.21	339.45	823.46	25.20	2.05	0.0264
371.84	342.59	350.28	345.18	331.97	342.94	786.51	26.89	2.12	0.0251
371.84	346.96	353.27	349.04	337.49	348.05	716.24	28.79	2.16	0.0208
371.84	352.48	355.67	352.76	347.62	353.87	621.69	32.11	2.25	0.0096
371.84	356.22	357.80	355.76	354.00	357.32	474.94	30.41	2.01	0.0040
371.84	357.51	358.56	356.88	356.20	358.42	394.60	27.54	1.78	0.0022
371.84	358.37	359.18	357.79	357.28	359.21	383.83	28.48	1.81	0.0017
371.87	359.86	361.15	358.96	358.89	360.45	191.59	15.96	0.98	0.0021
371.87	364.55	366.64	364.83	362.49	364.25	71.22	9.74	0.53	0.0054
371.87	361.01	362.15	361.02	359.69	361.18	131.37	12.10	0.73	0.0030
371.87	359.41	360.44	359.00	358.30	359.89	229.99	18.46	1.15	0.0022
371.87	357.69	358.77	357.04	356.46	358.50	366.92	25.89	1.67	0.0022
371.87	356.90	358.35	356.16	355.15	357.94	422.24	28.22	1.84	0.0031
371.87	354.48	357.00	354.13	351.13	355.67	544.21	31.31	2.13	0.0066
371.87	350.05	354.30	350.98	343.69	351.22	667.70	30.60	2.21	0.0134
371.87	345.60	351.96	348.19	336.03	346.22	761.08	28.98	2.21	0.0216
371.87	341.46	349.42	344.08	330.98	341.34	809.32	26.61	2.12	0.0256
C_{iL} = 1.00%, C_L = 0.83%, C_v = 8.97%, U_v = 0.341 m/s									
371.82	341.49	349.36	343.83	331.07	341.71	797.06	26.29	2.09	0.0251
371.82	347.31	352.54	348.34	340.93	347.45	750.97	30.65	2.29	0.0155
371.82	349.61	354.96	351.26	341.74	350.49	681.73	30.70	2.23	0.0173
371.82	353.59	356.59	353.83	349.21	354.74	576.41	31.63	2.18	0.0089
371.82	356.88	358.54	356.31	354.86	357.82	447.65	29.97	1.96	0.0039
371.82	357.65	358.96	357.09	356.05	358.48	372.68	26.30	1.69	0.0029
371.82	359.16	360.16	358.62	358.06	359.80	272.34	21.51	1.34	0.0020
371.82	360.07	361.19	359.72	358.83	360.54	199.46	16.98	1.04	0.0025
371.82	365.16	367.34	365.45	362.95	364.90	70.24	10.55	0.56	0.0057
371.82	361.22	362.41	361.20	359.83	361.44	140.26	13.23	0.79	0.0031
371.82	359.97	361.09	359.69	358.77	360.34	223.73	18.89	1.16	0.0026
371.82	358.34	359.54	357.88	357.08	358.84	341.07	25.30	1.61	0.0026
371.79	357.49	358.98	356.79	356.02	358.16	406.49	28.41	1.83	0.0030
371.79	355.56	357.67	355.05	352.98	356.54	513.36	31.62	2.11	0.0052
371.79	351.79	355.86	352.69	346.12	352.50	636.51	31.82	2.25	0.0125
371.79	347.66	354.06	349.97	338.35	348.29	714.24	29.60	2.20	0.0211
371.79	344.11	351.19	346.86	333.51	344.86	775.19	28.00	2.17	0.0240

Thermocouple angles : T_{w1} = 22.5°, T_{w2} = -67.5°, T_{w3} = -157.5°, T_{w4} = 112.5°

Test fluid – steam-ethanol mixtures

C_{iL} = 1.00%, C_L = 1.11%, C_v = 11.52%, U_v = 0.534 m/s

T_v / K	T_{wo} / K	T_{w1} / K	T_{w2} / K	T_{w3} / K	T_{w4} / K	q / (kW/m^2)	α / (kW/m^{2}K)	ε_{Ma}	A
371.84	346.14	351.33	346.71	337.01	349.50	986.29	38.37	2.82	0.0199
371.82	348.75	353.26	348.98	341.69	351.07	924.89	40.09	2.86	0.0159
371.82	351.22	354.67	350.92	345.60	353.71	808.62	39.26	2.72	0.0129
371.82	354.24	356.21	353.23	351.50	356.01	669.10	38.06	2.53	0.0074
371.79	356.43	357.69	355.33	355.00	357.69	517.18	33.65	2.16	0.0046
371.79	357.04	358.09	355.97	355.97	358.14	448.57	30.41	1.93	0.0038
371.79	357.40	358.35	356.48	356.45	358.31	407.15	28.28	1.79	0.0033
371.77	358.16	359.15	357.41	357.22	358.86	344.75	25.33	1.58	0.0031
371.77	360.43	361.90	360.26	358.79	360.77	175.84	15.50	0.92	0.0041
371.75	358.93	360.01	358.40	357.75	359.56	277.91	21.69	1.33	0.0034
371.75	357.74	358.73	356.88	356.76	358.59	384.63	27.46	1.72	0.0033
371.72	356.66	358.87	355.36	354.95	357.45	420.17	27.90	1.78	0.0060
371.70	356.86	358.03	355.74	355.67	358.01	466.41	31.44	2.00	0.0041
371.70	355.48	357.00	354.14	353.70	357.07	580.67	35.80	2.33	0.0056
371.67	352.98	355.40	352.16	349.23	355.12	744.63	39.83	2.69	0.0093
371.67	350.16	354.04	350.02	343.94	352.67	859.07	39.94	2.80	0.0142
371.67	347.64	352.55	347.89	339.66	350.46	949.50	39.51	2.86	0.0179
C_{iL} = 1.00%, C_L = 0.86%, C_v = 9.25%, U_v = 0.548 m/s									
371.82	347.15	352.09	347.52	339.48	349.52	942.41	38.21	2.77	0.0173
371.82	350.07	353.90	349.93	344.33	352.10	856.08	39.36	2.76	0.0133
371.82	352.29	355.15	351.72	348.37	353.90	742.57	38.02	2.59	0.0097
371.82	354.70	356.69	353.68	352.36	356.06	611.91	35.74	2.35	0.0067
371.79	356.70	358.12	355.69	355.26	357.76	474.88	31.47	2.01	0.0047
371.82	357.38	358.64	356.43	356.24	358.21	396.52	27.46	1.73	0.0039
371.82	359.00	360.20	358.57	357.72	359.51	282.41	22.03	1.35	0.0036
371.82	359.89	361.35	359.74	358.20	360.29	208.34	17.47	1.05	0.0042
371.82	365.48	367.35	365.83	363.45	365.30	73.88	11.66	0.60	0.0045
371.82	361.38	362.97	361.40	359.50	361.64	141.64	13.57	0.79	0.0044
371.82	359.72	361.21	359.48	358.13	360.03	235.82	19.49	1.18	0.0041
371.82	358.11	359.35	357.43	356.99	358.68	357.39	26.07	1.62	0.0036
371.82	357.42	358.85	356.44	356.01	358.39	430.01	29.87	1.88	0.0046
371.82	356.04	357.75	354.89	354.31	357.20	535.56	33.94	2.19	0.0055
371.82	353.76	356.27	353.00	350.48	355.28	677.46	37.51	2.51	0.0085
371.82	351.73	354.84	351.19	347.58	353.33	799.28	39.80	2.73	0.0103
371.82	349.06	353.30	349.17	341.90	351.86	893.10	39.24	2.79	0.0160
C_{iL} = 1.00%, C_L = 0.86%, C_v = 9.18%, U_v = 0.732 m/s									
371.94	348.10	352.59	347.78	340.82	351.19	1023.52	42.93	3.00	0.0169
371.94	350.38	353.89	349.81	344.78	353.05	921.62	42.76	2.92	0.0133
371.94	352.66	355.27	351.57	349.12	354.67	803.85	41.69	2.76	0.0094
371.94	354.90	356.78	353.68	352.67	356.47	653.40	38.35	2.46	0.0066
371.94	356.87	358.26	355.73	355.47	358.02	504.97	33.51	2.09	0.0047
371.94	357.36	358.62	356.24	356.31	358.26	423.19	29.02	1.80	0.0039
371.94	359.21	360.24	358.44	357.79	360.36	305.74	24.01	1.44	0.0040
371.94	359.91	361.38	359.72	358.18	360.37	225.65	18.77	1.11	0.0043
371.96	366.02	367.86	366.36	364.10	365.76	79.12	13.31	0.67	0.0043
371.96	361.78	363.52	361.90	359.73	361.95	156.01	15.31	0.87	0.0047
371.96	359.81	361.25	359.44	358.31	360.26	248.01	20.41	1.21	0.0041
371.99	358.12	359.33	357.31	357.12	358.71	384.82	27.75	1.69	0.0035
371.99	357.50	358.88	356.47	356.26	358.37	462.70	31.93	1.97	0.0043
371.96	356.04	357.67	354.66	354.57	357.24	564.92	35.47	2.24	0.0052
371.96	353.82	356.27	352.74	350.84	355.43	729.40	40.20	2.62	0.0083
371.96	351.88	354.84	350.95	347.85	353.88	862.08	42.93	2.87	0.0104
371.96	349.50	353.48	349.13	343.42	351.96	971.48	43.24	2.98	0.0143

Thermocouple angles : T_{w1} = 22.5°, T_{w2} = 112.5°, T_{w3} = -157.5°, T_{w4} = -67.5°

Test fluid – steam-ethanol mixtures

C_{iL} = 1.00%, C_L = 0.94%, C_v = 9.95%, U_v = 0.732 m/s

T_v / K	T_{wo} / K	T_{w1} / K	T_{w2} / K	T_{w3} / K	T_{w4} / K	q / (kW/m^2)	α / (kW/m^{2}K)	ε_{Ma}	A
371.77	348.45	352.34	347.89	342.50	351.06	995.58	42.69	2.97	0.0143
371.77	350.92	353.69	351.19	345.93	352.88	888.75	42.63	2.88	0.0107
371.77	352.53	354.92	351.46	349.56	354.18	764.94	39.76	2.63	0.0082
371.77	354.44	356.24	353.33	352.51	355.68	623.58	35.98	2.32	0.0059
371.77	356.54	357.95	355.52	355.45	357.23	470.40	30.88	1.93	0.0040
371.77	357.25	358.44	356.28	356.42	357.87	395.21	27.22	1.68	0.0034
371.77	358.53	359.82	357.99	357.34	358.95	282.54	21.33	1.29	0.0036
371.77	359.55	361.07	359.34	357.99	359.82	205.13	16.79	1.00	0.0041
371.77	366.23	368.62	366.44	364.22	365.62	75.10	13.54	0.67	0.0050
371.77	360.91	362.58	361.09	358.82	361.14	151.88	13.98	0.81	0.0047
371.77	359.47	361.03	359.23	357.86	359.76	227.83	18.52	1.10	0.0042
371.77	357.75	358.97	356.99	356.63	358.41	357.74	25.52	1.56	0.0037
371.77	357.06	358.35	356.02	355.92	357.94	427.47	29.06	1.80	0.0040
371.77	355.76	357.06	354.34	354.65	356.98	541.69	33.83	2.14	0.0044
371.77	353.59	355.59	352.37	351.12	355.28	696.18	38.29	2.50	0.0072
371.77	351.78	354.50	350.77	348.20	353.66	823.81	41.21	2.76	0.0095
371.77	349.71	352.98	348.96	344.56	352.33	931.00	42.20	2.90	0.0125

Thermocouple angles : T_{w1} = 22.5°, T_{w2} = 112.5°, T_{w3} = -157.5°, T_{w4} = -67.5°

References

Adamek, T., 1981, Calculation of condensation rates on fluted condensing surfaces for optimizing the surface design, *Thermo- and Fluid Dynamics*, vol. 15, no. 4, pp. 255-270

Adamek, T. and Webb, R.L., 1990, Predictions of film condensation on horizontal integral fin tubes, *International Journal of Heat and Mass Transfer*, vol. 33, no. 8, pp. 1721-1735

Ali, S.M. and Thome, J.R., 1984, Boiling of ethanol-water and ethanol-benzene mixtures on an enhanced boiling surface, *Heat Transfer Engineering*, vol. 5, no. 3-4, pp. 70-81

Beatty, K.O. and Katz, D.L., 1948, Condensation of vapors on outside of finned tubes, *Chemical Engineering Progress*, vol. 44, no. 1, pp. 55-70

Bella, B., Cavallini, A., Longo, G.A. and Rossetto, L., 1993, Pure vapour condensation of refrigerants 11 and 113 on a horizontal integral finned tube at high vapour velocity, *Journal of Enhanced Heat Transfer*, vol. 1, no. 1, pp. 77-86

Bergles, A.E., 2003, High-flux processes through enhanced heat transfer, *Proc. 5th Int. Conference on Boiling Heat Transfer*, Montego Bay, Jamaica

Briggs, A., 1991, Forced-convection condensation on horizontal integral-fin tubes, Ph.D. Thesis, Univ. of London

Briggs, A. and Rose, J.W., 1994, Effect of fin efficiency on a model for condensation heat transfer on a horizontal, integral-fin tube, *International Journal of Heat and Mass Transfer*, vol. 7, no. SUPPL 1, pp. 57-463

Briggs, A. and Rose, J.W., 1995, Condensation performance of some commercial integral fin tubes with steam and CFC113, *Experimental Heat Transfer*, vol. 8, no. 2, pp. 131-143

Briggs, A., Huang, X.S. and Rose, J.W., 1995, Experimental investigation of condensation on integral-fin tubes: effect of fin thickness, height, and thermal conductivity, *ASME, Heat Transfer Division, (Publication) HTD*, vol. 308, *Basic Aspects of T_{wo} Phase Flow and Heat Transfer*, 1995, pp. 21-29

Briggs, A., Wang, H.S. and Rose, J.W., 2002, Film condensation of steam on a horizontal wire-wrapped tube, *Proc. 12th Int. Heat Transfer Conference*, Grenoble, vol. 4, pp. 123-128.

Briggs, A., Wang, H.S., Murase, T. and Rose, J.W., 2003, Heat transfer measurements for condensation of steam on a horizontal wire-wrapped tube, *Journal of Enhanced Heat Transfer*, vol. 10, no. 4, pp. 355-362

Briggs, A., Wang, H.S., Murase, T. and Rose, J.W., 2003, Enhanced condensation of CFC113 on a horizontal wire-wrapped tube, *Proceedings of 4th Int. Conf. Compact Heat Exchangers and Enhancement Tech. for the Process Industries*, Crete Island, Greece, pp. 357-360

Briggs, A., Wen, X.L. and Rose, J.W., 1992, Accurate heat transfer measurements for condensation on horizontal, integral-fin tubes, *Transactions of the ASME Journal of Heat Transfer*, vol. 114, pp. 719-726

Brower, K.S., 1985, The effect of condensate inundation on steam condensation heat transfer in a tube bundle, Ph.D. Thesis, Naval postgraduate school in Monterey, California

Carnavos, T.C., 1980, An experimental study: condensing R-11 on augmented tubes, *ASME(Paper)*, no. 80-HT-54, *19th National Heat Transfer Conference*, Orlando, Florida

Cavallini, A., Bella, B., Longo, G.A. and Rossetto, L., 1995, Experimental heat transfer coefficients during condensation of halogenated refrigerants on enhanced tubes, *Journal of Enhanced Heat Transfer*, vol. 2, no. 1-2, pp. 115-125

Cheng, W.Y., Wang, C.C., Hu, Y.Z. Robert and Huang, L.W., 1996, Film condensation of HCFC-22 on horizontal enhanced tubes, *International Communications in Heat and Mass Transfer*, vol. 23, no. 1, pp. 79-90

Churchill, S.W. and Chu, H.H.S., 1975, Correlating equations for laminar and turbulent free convection from a horizontal cylinder, *International Journal of Heat and Mass Transfer*, vol. 18, no. 9, pp. 1049-1055

Das, A.K., Meyer, D.W., Incheck, G.A., Marto, P.J. and Memory, S.B., 1995, Effects of fin height and thermal conductivity on the performance of integral-fin tubes for steam condensation, *ASME, Heat Transfer Division, (Publication) HTD*, vol. 308, *Basic Aspects of T_{wo} Phase Flow and Heat Transfer*, pp. 111-122

Eissenberg, D.M., 1972, An investigation of the variables affecting steam condensation on the outside of a horizontal tube bundle, Ph.D. Thesis, Univ. of Tennessee

Ford, J.D. and Missen, R.W., 1968, On the conditions for stability of falling films subject to surface tension disturbances; the condensation of binary vapor, *Canadian Journal of Chemical Engineering*, vol. 46, no. 5, pp. 309-312.

Ford, J.D., and McAleer, J.E., 1971, Non-filmwise condensation of binary vapors: mechanism and droplet sizes, *Canadian Journal of Chemical Engineering*, vol. 49, pp. 157-158

Fujii, T., 1991, Theory of laminar film condensation, Springer-Verlag, New York

Fujii, T. and Oda, K., 1986, Correlation equations of heat transfer for condensate inundation on horizontal tube bundles, *Transactions of the JSME, Series B*, vol. 52, no. 474, pp. 822-826 (in Japanese)

Fujii, T., Koyama, S. and Nishida, S., 1983, Expressions of physical properties concerning condensation of ethanol – water – air mixture, *Report of Institute of Industrial Science, Kyushu University*, no. 75, pp. 63-76 (in Japanese)

Fujii, T., Koyama, S., Simizu, Y., Watabe, M. and Nakamura, Y., 1989, Gravity controlled condensation of an ethanol and water mixture on a horizontal tube, *Transactions of the JSME, Series B*, vol. 55, no. 509, pp. 210-215 (in Japanese)

Fujii, T., Nozu, S. and Honda, H., 1978, Expressions of thermodynamics and transport properties of refrigerants R-11, R-12 and R-113, *Report of Institute of Industrial Science, Kyushu University*, no. 67, pp. 43-59 (in Japanese)

Fujii, T., Osa, N. and Koyama, S., 1993, Free convection condensation of binary vapor mixtures on a smooth tube: condensing mode and heat transfer coefficient of condensate, *Proceedings Engineering Foundation Conference on Condensation and Condenser Design, St Augustine Florida, ASME*, pp. 171-182

Fujii, T., Wang, W.C., Koyama, S. and Shimizu, Y., 1985, Heat transfer enhancement for gravity controlled condensation on a horizontal tube by coiling wires, *Proc 2nd Int. Symp. Heat Transfer, Tsinghua Univ.*, Beijing, Oct. 15-18, 1985, and in Heat Transfer Science and Technology, Bu-Xuan Wang (Ed.), Hemisphere 1987, pp. 773-780, (also in *Transactions of the JSME, Series B*, vol. 51, no. 467, pp. 2436-2441 (in Japanese))

Fujita, Y. and Bai, Q., 1997, Critical heat flux of binary mixtures in pool boiling and its correlation in terms of Marangoni number, *International Journal of Refrigeration*, vol. 20, no. 8, pp. 616-622

Fujita, Y. and Tsutsui, M., 1994, Heat transfer in nucleate boiling of binary mixtures (heat transfer measurement and assessment of available correlations), *Transactions of the JSME, Series B*, vol. 60, no. 577, pp. 3101-3108 (in Japanese)

Gaidarov, S.A. and Kaziev, K.S., 1996, Heat transfer for the transition regime of binary mixture boiling, *Heat Transfer Research*, vol. 27, no. 1, pp. 246-250

Golubnichniy, Yu.A., Klimenkov, Yu.V., Kolykhan, L.I. and Pulyayev, V.F., 1991, Heat transfer in condensation of vapor on a wire rib (fin), *Heat Transfer - Soviet Research*, vol. 23, no. 5, pp. 683-692

Goto, M., Kojima, M., Koyama, S., Fujii, T. and Kashiwagi, T., 1995, Free-convection condensation of ammonia/water vapour mixtures on a horizontal smooth tube, *Transactions of the JSME, Series B*, vol. 61, no. 581, pp. 231-238 (in Japanese)

Gregorig, R., 1954, Film condensation on finely rippled surfaces with consideration of surface tension, *Z. Angew. Math. Phys.*, vol. 5, no. 1, pp. 36-49

Hashimoto, R., Yanagi, K. and Fujii, T., 1994, Effects of condensate flow patterns upon gravity-controlled condensation of ethanol and water mixtures on a vertical surface, *Heat Transfer - Japanese Research*, vol. 23, no. 4, pp. 330-348

Hashimoto, R., Yanagi, K. and Fujii, T., 1996, Condensation of organic binary mixtures flowing downward inside a vertical tube, *Heat Transfer - Japanese Research*, vol. 25, no. 6, pp. 362-381

Hijikata, K., Fukasaku, Y. and Nakabeppu, O., 1996, Theoretical and experimental studies on the pseudo-dropwise condensation of a binary vapor mixture, *Transactions of the ASME Journal of Heat Transfer,* vol. 118, no. 1, pp. 140-147

Honda, H. and Nozu, S., 1987, A prediction method for heat transfer during film condensation on horizontal low integral fin tubes, *Transactions of the ASME Journal of Heat Transfer,* vol. 109, no. 1, pp. 218-225

Honda, H. and Rose, J.W., 1999, Augmentation techniques in external condensation, Handbook of phase change, edited by Kandlikar, S.G., Taylor & Francis, pp. 605-620

Honda, H., Fujii, T., Uchima, B., Nozu, S. and Nakata, H., 1989, Condensation of downward flowing R-113 vapor on bundles of horizontal smooth tubes, *Heat*

Transfer - Japanese Research, vol. 18, no. 6, pp. 31-52 (also in *Transactions of the JSME, Series B*, vol. 54, no. 502, 1988, pp. 1453-1460)

Honda, H., Nozu, S. and Mitsumori, K., 1983, Augmentation of condensation on horizontal finned tubes by attaching a porous drainage plate, *Proc 1st, ASME-JSME Thermal Engineering Joint Conference*, Eds. Mori, Y. and Yang, W.J., vol. 3, pp. 289-296

Honda, H., Nozu, S. and Takeda, Y., 1989, A theoretical model of film condensation in a bundle of horizontal low finned tubes, *Transactions of the ASME Journal of Heat Transfer,* vol. 111, no. 2, pp. 525-532 (also in *Transactions of the JSME, Series B*, vol. 54, no. 504, 1988, pp. 2128-2135 (in Japanese))

Honda, H., Takamatsu, H., Takada, N., and Makishi, O., 1996, Condensation of HCFC-123 in bundles of horizontal finned tubes: effect of fin geometry and tube arrangement, *International Journal of Refrigeration*, vol. 19, no. 1, pp. 1-9

Honda, H., Takata, N., Takamatsu, H., Kim, J.S. and Usami, K., 2002, Condensation of download-flowing HFC134a in a staggered bundle of horizontal finned tubes: Effect of fin geometry, *International Journal of Refrigeration*, vol. 25, no. 1, pp. 3-10

Honda, H., Takata, N., Takamatsu, H., Kim, J.S. and Usami, K., 2003, Effect of fin geometry on condensation of R407C in a staggered bundle of horizontal finned tubes, *Transactions of the ASME Journal of Heat Transfer*, vol. 125, no. 4, pp. 653-660

Honda, H., Uchima, B., Nozu, S., Nakata, H. and Torigoe, E., 1991, Film condensation of R-113 on in-line bundles of horizontal finned tubes, *Transactions of the ASME Journal of Heat Transfer,* vol. 113, no. 2, pp. 479-486

Honda, H., Uchima, B., Nozu, S., Torigoe, E. and Imai, S., 1992, Film condensation of R-113 on staggered bundles of horizontal finned tubes, *Transactions of the ASME Journal of Heat Transfer,* vol. 114, no. 2, pp. 442-449

Huang, X.S., 1995, Experimental investigation of condensation on integral-fin tubes: Effect of fin height, thickness and thermal conductivity, Ph.D. Thesis, Univ. of London

Hui, T.O. and Thome, J.R., 1985, Study of binary mixture boiling: Boiling site density and subcooled heat transfer, *International Journal of Heat and Mass Transfer*, vol. 28, no. 5, pp. 919-928

Jakob, M., 1949, Heat transfer in condensation, Heat Transfer, vol. 1, John Wiley and Sons, Inc., New York, pp. 672-673

Jung, D., Kim, C., Cho, S. and Song, K., 1999, Condensation heat transfer coefficients of enhanced tubes with alternative refrigerants for CFC11 and CFC12, *International Journal of Refrigeration*, vol. 22, no. 7, pp. 548-557

Karkhu, V.A. and Borokov, V.P., 1971, Film condensation of vapour at finely finned horizontal tubes, *Heat Transfer – Soviet Research*, vol. 3, pp. 183-191.

Katz D.L., Hope, R.C. and Datsko, S.C., 1946, Liquid retention on integral-finned tubes, *Department of Engineering Research, Unicersity of Michigan, Ann Arbor, ME, Project No. M592*

Kern, D.Q., 1950, Process heat transfer, McGraw-Hill Book Company, Inc, New York, pp. 266

Kern, D.Q., 1958, Mathematical development of loading in horizontal condensers, *AIChE Journal*, vol. 4, pp. 157-160

Kline, S.J. and McClintock, F.A., 1953, Describing uncertainties in single-sample experiments, *Mechanical Engineering*, vol. 75, pp. 3-8

Kogan, V.B., Fridman, V.M. and Kafarov, V.M., 1974, Vapour-liquid equilibrium database, translated by Hirata, M., published by Kodansya (in Japanese)

Kumar, R., Varma, H.K., Mohanty, B. and Agrawal, K.N., 2000, Condensation of R-134a vapor over single horizontal circular integral-fin tubes with trapezoidal fins, *Heat Transfer Engineering*, vol. 21, no. 2, pp. 29-39

Kumar, R., Varma, H.K., Agrawal, K.N. and Mohanty, B., 2001, A comprehensive study of modified Wilson plot technique to determine the heat transfer coefficient during condensation of steam and R-134a over single horizontal plain and finned tubes, *Heat Transfer Engineering*, vol. 22, no. 2, pp. 3-12

Kutateladze, S.S., Gogonin, I.I., Dorokhov, A.R. and Sosunov, V.I., 1981, Heat transfer in vapor condensation on a horizontal tube bundle, *Heat Transfer - Soviet Research*, vol. 13, no. 3, pp. 32-50

Kutateladze, S.S., Gogonin, I.I. and Sosunov, V.I., 1985, Influence of condensate flow rate on heat transfer in film condensation of stationary vapour on horizontal tube banks, *International Journal of Heat and Mass Transfer*, vol. 28, no. 5, pp. 1011-1018

Kutateladze, S.S. and Gogonin, I.I., 1985, Investigation of heat transfer in film condensation of flowing vapour on horizontal tube banks, *International Journal of Heat and Mass Transfer*, vol. 28, no. 10, pp. 1831-1836

Lee, W.C., 1982, Filmwise condensation on a horizontal tube in the presence of forced convection and non-condensing gas, Ph.D. Thesis, Univ. of London.

Lee, W.C. and Rose, J.W., 1984, Forced-convection film condensation on a horizontal tube with and without non-condensing gases, *International Journal of Heat and Mass Transfer*, vol. 27, pp. 519-528.

Lee, W.C., Rahbar, S. and Rose, J.W., 1984, Film condensation of refrigerant-113 and ethanediol on a horizontal tube – effect of vapour velocity, *Transactions of the ASME Journal of Heat Transfer*, vol. 106, no. 3, pp. 524-530

Leicy, A., 1999, Filmwise condensation heat transfer of steam and R-113 on smooth and finned tubes with simulated inundation, M.Phil Thesis, Univ. of London.

Marto, P.J., 1986, Recent progress in enhancing film condensation heat transfer on horizontal tubes, *Heat Transfer Engineering*, vol. 7, no. 3-4, pp. 53-63

Marto, P. J., 1988, An Evaluation of film condensation on horizontal integral fin tubes, *Transactions of the ASME Journal of Heat Transfer,* vol. 110, no. 4(B), pp. 1287-1305

Marto, P.J. and Wanniarachchi, A.S., 1984, The use of wire-wrapped tubing to enhance steam condensation in tube bundles, *ASME Heat Transfer Division,* vol. 37, pp. 9-16

Marto, P.J., Mitrou, E., Wanniarachchi, A.S. and Katsuta, M., 1987, Film condensation of steam on a horizontal wire-wrapped tube, *Proceedings of the 1987 ASME-JSME Thermal Engineering Joint Conference*, vol. 1, pp. 509-516

Marto, P.J., Zebrowski, D., Wanniarachchi, A.S. and Rose, J.W., 1990, Experimental study of R-113 film condensation on horizontal integral-fin tubes, *Transactions of the ASME Journal of Heat Transfer,* vol. 112, no. 3, pp. 758-767

Marschall, E., Hall, J.A., 1975, Binary, gravity-flow film condensation, *Transactions of the ASME Journal of Heat Transfer,* vol. 97, no. 3, pp. 492-494

Masuda, H., 1985, Film condensation heat transfer on low integral-fin tubes, Ph.D. Thesis, Univ. of London

Masuda, H. and Rose, J.W., 1985, An experimental study of condensation of refrigerant-113 on low integral fin tubes, *Proc. Int. Symp. Heat Transfer*, Beijing, vol. 2. paper no. 32: (also in *Heat Transfer Science and Technology*, pp. 480-487, Hemisphere, Washington, D.C.)

Masuda, H. and Rose, J.W., 1987, Static configuration of liquid films on horizontal tubes with low radial fins, Implications for condensation heat transfer, *Proc. R. Soc. Lond*, A410, pp. 125-139

Masuda, H. and Rose, J.W., 1988, Condensation of ethylene glycol on horizontal integral-fin tubes, *Transactions of the ASME Journal of Heat Transfer*, vol. 110, no. 4, pp. 1019-1022

Memory, S., 1989, Forced convection condensation on a horizontal tube at high vapour velocity, Ph.D. Thesis, Univ. of London

Memory, S. and Rose, J.W., 1991, Free convection laminar film condensation on a horizontal tube with variable wall temperature, *International Journal of Heat and Mass Transfer*, vol. 34, no. 11, pp. 2775-2778

Michael, A.G., Marto, P.J., Wanniarachchi, A.S. and Rose, J.W., 1989, Effect of vapor velocity during condensation on horizontal smooth and finned tubes, *ASME, Heat Transfer Division, (Publication) HTD*, vol. 114, pp. 1-10

Mills, A.F., Hubbard, G.L., James, R.K. and Tan, C., 1975, Experimental study of film condensation on horizontal grooved tubes, *Desalination*, vol. 16, no. 2, pp. 121-133

Mirkovich, V.V. and Missen, R.W., 1961, Non-filmwise condensation of binary vapors of miscible liquids, *Canadian Journal of Chemical Engineering*, vol. 39, no. 2, pp. 86-87.

Mirkovich, V.V. and Missen, R.W., 1963, A study of the condensation of binary vapors of miscible liquids, *Canadian Journal of Chemical Engineering*, vol. 41, pp. 73-78.

Morrison, J.N.A. and Deans, J., 1997, Augmentation of steam condensation heat transfer by addition of ammonia, *International Journal of Heat and Mass Transfer*, vol. 40, no. 4, pp. 765-772

Morrison, J.N.A., Philpott, C. and Deans, J., 1998, Augmentation of steam condensation heat transfer by addition of methylamine, *International Journal of Heat and Mass Transfer*, vol. 41, no. 22, pp. 3679-3683

Murase, T., Briggs, A., Wang, H.S. and Rose, J.W., 2005, Condensation on a horizontal wire-wrapped tube, *6th World Conf. on Exp. Heat transfer, Fluid Mechanics and Thermodynamics,* Matsushima, Miyagi, Japan

Murase, T., Briggs, A., Wang, H.S. and Rose, J.W., 2005, Condensation on a horizontal wire-wrapped tube, *Transactions of the ASME Journal of Heat Transfer,* vol. 127, no. 11, in press

Namasivayam and Briggs, 2004a, Effect of vapour velocity on condensation of atmospheric pressure steam on integral-fin tubes, *Applied Thermal Engineering*, vol. 24, no. 8-9, pp. 1353-1364

Namasivayam and Briggs, 2004b, Forced-convection condensation of ethylene glycol on integral-fin tubes, *Proceedings of ASME International Mechanical Engineering Congress and Exposition, Anaheim, California USA*

Necmi, S., Rose, J.W., 1977, Heat-transfer measurements during dropwise condensation of mercury, *International Journal of Heat and Mass Transfer*, vol. 20, no. 8, pp. 877-881

Nusselt, W., 1916, *Die Oblerflachenkondensation des Wasserdamfes*, Z.Vereines Deutsch. Ing., vol. 60, pp. 541-546, 569-575

Owen, R.G., Sardesai, R.G., Smith, R.A. and Lee, W.C., 1983, Gravity controlled condensation on low integral-fin tubes, *Institution of Chemical Engineers Symposium Series*, no. 75, pp. 415-428

Perry, R.H. and Chilton, C.H., 1973, Chemical Engineers' Handbook, published by McGraw-Hill

Philpott, C. and Deans, J., 2004, The enhancement of steam condensation heat transfer in a horizontal shell and tube condenser by addition of ammonia, *International Journal of Heat and Mass Transfer*, vol. 47, no. 17-18, pp. 3683-3693

Philpott, C. and Deans, J., 2004, The condensation of ammonia-water mixtures in a horizontal shell and tube condenser, *Transactions of the ASME Journal of Heat Transfer*, vol. 126, Issue 4, pp. 527-534

Reddy, R.P. and Lienhard, J.H., 1989, Peak boiling heat flux in saturated ethanol-water mixtures, *Transactions of the ASME Journal of Heat Transfer,* vol. 111, no. 2, pp. 480-486

Rifert, V.G., Trokoz, Y.Y. And Zadiraka, V.Y., 1984, Enhancement of heat transfer in condensation of ammonia vapor on a bundle of wire-finned tubes, *Heat Transfer – Soviet Research*, vol. 16, no. 1, pp. 36-41.

Rohsenow, W.M., 1952, A method of correlating heat transfer data for surface boiling of liquids, Trans. ASME, vol. 74, pp. 969–976

Rose, J.W., 1984, Effect of pressure gradient in forced convection film condensation on a horizontal tube, *International Journal of Heat and Mass Transfer*, vol. 27, pp. 39-47.

Rose, J.W., 1994, Approximate equation for the vapour-side heat-transfer coefficient for condensation on low-finned tubes, *International Journal of Heat and Mass Transfer*, vol. 37, no. 5, pp. 865-875

Rose, J.W., 2002, An analysis of film condensation on a horizontal wire-wrapped tube, *Trans. IChemE, Part A, Chem. Eng. Res. Des.*, vol. 80, pp. 290-294

Rose, J.W., Uehara, H., Koyama, S. and Fujii, T., 1999, Film condensation, Handbook of phase change, edited by Kandlikar, S. G., Taylor & Francis, pp. 523 -580

Rose, J.W., Utaka, Y. and Tanasawa, I., 1999, Dropwise condensation, Handbook of phase change, edited by Kandlikar, S. G., Taylor & Francis, pp. 581-594

Rudy, T.M. and Webb, R.L., 1981, Condensate retention on horizontal integral-fin tubing, *ASME, Heat Transfer Division, (Publication) HTD*, vol. 18, pp. 35-41

Rudy, T.M. and Webb, R.L., 1983, Theoretical model for condensation on horizontal integral-fin tubes, *AIChE Symposium Series*, no. 225, pp. 11-18

Rudy, T.M. and Webb, R.L., 1985, Analytical model to predict condensate retention on horizontal integral-fin tubes, *Transactions of the ASME Journal of Heat Transfer*, vol. 107, no. 2, pp. 361-368

Sethumadhavan, R. and Raja R.M., 1985, Condensation of steam on single start and multistart spiral wire-$_{wo}$und horizontal tubes, *Industrial & Engineering Chemistry, Process Design and Development*, vol. 24, no. 3, pp. 783-787

Shah, R.K, Zhou, S.Q. and Tagavi, K.A., 1999, Role of surface tension in film condensation in extended surface passages, *Journal of Enhanced Heat Transfer*, vol. 6, no. 2-4, pp. 179-216

Shekriladze, I.G. and Gomelauri, V.I., 1966, The theoretical study of laminar film condensation of a flowing vapour, *International Journal of Heat and Mass Transfer*, vol. 9, pp. 581-591.

Stephan, K. and Abdelsalam, M., 1980, Heat-transfer correlations for natural convection boiling, *International Journal of Heat and Mass Transfer*, vol. 23, no. 1, pp. 73-87

Sukhatme, S.P., Jagadish, B.S. and Prabhakaran, P., 1990, Film condensation of R-11 vapor on single horizontal enhanced condenser tubes, *Transactions of the ASME Journal of Heat Transfer*, vol. 112, no. 1, pp. 229-234

Taborek, K., 1974, Design methods for heat transfer equipment – a critical survey of the state-of-the-art, Heat Exchangers Design and Theory Sourcebook, edited by Afgan, N. and Schlunder, E. U., McGraw-Hill, pp. 45-74

Thomas, D.G., 1967, Enhancement of film condensation heat transfer rates on vertical tubes by vertical wires, *Ind. Eng. Chem. Fundamentals*, vol. 6, no. 1, pp. 97-103

Thomas, A., Lorenz, J.J., Hillis, D.L., Yung, D.T. and Sather, N.F., 1979, Performance tests of 1 MWt shell-and tube and compact heat exchangers for OTEC, *Proceedings of 6th OTEC conference*, vol. 2, paper 11-1, pp. 1-12.

Utaka, Y. and Kobayashii, H., 2001, On condensation transfer for water and ethanol vapour mixture (Characteristics over a wide range of vapor velocity), *Transactions of the JSME, Series B*, vol. 67, no. 653, pp. 141-147 (in Japanese)

Utaka, Y. and Nishikawa, T., 2002, Unsteady measurement of condensate film thickness for solutal Marangoni condensation by using laser absorption method (Measurement and discussion), *Transactions of the JSME, Series B*, vol. 68, no. 672, pp. 124-131 (in Japanese)

Utaka, Y. and Nishikawa, T., 2003, Measurement of condensate film thickness for solutal Marangoni condensation applying laser extinction method, *Journal of Enhanced Heat Transfer*, vol. 10, no. 2, pp. 119-129

Utaka, Y. and Terachi, N., 1995, Measurement of condensation characteristic curves for binary mixture of steam-ethanol vapour, *Heat Transfer - Japanese Research*, vol. 24, no. 1, pp. 57-67, (also in *Transactions of the JSME, Series B*, vol. 61, no. 583, pp. 1063-1069 (in Japanese))

Utaka, Y., and Sai, S., 2002, An investigation of vapor concentration during boiling of a liquid mixture: Measurement of temperature and concentration variations of vapor in bubbles, *Heat Transfer - Asian Research*, vol. 31, no. 6, pp. 475-485

Utaka, Y. and Wang, S., 2001, Effect of ethanol mass fraction on condensation heat transfer characteristics for water-ethanol binary vapor mixture, *Transactions of Japan Society of Refrigeration and Air Conditioning Engineers*, vol. 18 no. 1, pp. 127-134

Utaka, Y. and Wang, S., 2002, Promotion of steam condensation heat transfer by using solutal Marangoni condensation, *Transactions of the JSME, Series B*, vol. 68, no. 674, pp. 2818-2826 (in Japanese)

Utaka, Y. and Wang, S., 2004, Characteristic curves and the promotion effect of ethanol addition on steam condensation heat transfer, *International Journal of Heat and Mass Transfer*, vol. 47, no. 21, pp. 4507-4516

Utaka, Y. and Wang, S., 2004, Effect of non-condensable gas mass fraction on condensation heat transfer for water-ethanol vapor mixture, *JSME International Journal, Series B: Fluids and Thermal Engineering,* vol. 47, no. 2, pp. 162-167

Utaka, Y. and Wang, S., 2005, An experimental study on the effect of non-condensable gas for solutal Marangoni condensation heat transfer, *Experimental Heat Transfer*, vol. 18, no. 2, pp. 61-79

Utaka, Y., Kenmotsu, T. and Yokoyama, S., 1998, A study on Marangoni condensation (measurement and observation for water and ethanol vapor mixture), *Proceedings of 11th International Heat Transfer Conference*, vol. 6, pp. 397-402

Utaka, Y., Takahashi, K. and Tsuboi, T., 2002, Study of vapor concentration during boiling process of binary liquid mixtures, *Heat Transfer - Asian Research*, vol. 31, no. 8, pp. 595-605

Utaka, Y., Wang, S. and Kobayashii, H., 2001, Determination of configuration of heat transfer block to realize large heat flux and high precision of measurement for high thermal conductance phenomena, *Transactions of the JSME, Series B*, vol. 67, no. 660, pp. 141-147 (in Japanese)

Vijay, K.D., 1999, Boiling curve, Handbook of phase change, edited by Kandlikar, S. G., Taylor & Francis, pp. 63-69

Vijay, K.D., Satish, G.K., Fujita, Y., Iida, Y. and Heist, R., 1999, Nucleate boiling, Handbook of phase change, edited by Kandlikar, S. G., Taylor & Francis, pp. 71-120

Wallace, J.L. and Davison, A.W., 1938, Condensation of mixed vapors, *Industry and Engineering Chemistry*, vol. 30, no. 8, pp. 948-953

Wang, S., 2002, Promotion of steam condensation heat transfer by using solutal Marangoni phenomena, Ph.D. Thesis, Yokohama National University, Japan (in Japanese)

Wang, S.P., Hijikata, K. and Deng, S.J., 1990, Condensation heat transfer enhancement by ridges on integral fin surfaces, *Experimental Heat Transfer,* vol. 3, no. 4, pp. 341-354

Wanniarachchi, A.S., Marto, P.J. and Rose, J.W., 1986, Film condensation of steam on horizontal finned tubes: Effect of fin shape, *Transactions of the ASME Journal of Heat Transfer,* vol. 108, no. 4, pp. 960-966

Webb, R.L. and Murawski, C.G., 1990, Row effect for R-11 condensation on enhanced tubes, *Transactions of the ASME Journal of Heat Transfer,* vol. 112, no. 3, pp. 768-776

Webb, R.L., Rudy, T.M. and Kedzierski, M.A., 1985, Prediction of the condensation coefficient on horizontal integral-fin tubes, *Transactions of the ASME Journal of Heat Transfer,* vol. 107, no. 2, pp. 369-376

Wen, X.L., 1990, Film condensation on horizontal integral-fin tubes, Ph.D. Thesis, Univ. of London

Yau, K.K., Cooper, J.R. and Rose, J.W., 1985, Effect of fin spacing on the performance of horizontal integral-fin condenser tubes, *Transactions of the ASME Journal of Heat Transfer,* vol. 107, no. 2, pp. 377-383

Yau, K.K., Cooper, J.R. and Rose, J.W., 1986, Horizontal plain and low finned condenser tubes – effect of fin spacing and drainage strips on heat transfer and condensate retention, *Transactions of the ASME Journal of Heat Transfer,* vol. 108, no. 4, pp. 946-950.